



HAL
open science

Fuctional characterization of different candidate effectors from the root rot oomycete *Aphanomyces euteiches*

Laurent Camborde

► To cite this version:

Laurent Camborde. Fuctional characterization of different candidate effectors from the root rot oomycete *Aphanomyces euteiches*. *Vegetal Biology*. Université Paul Sabatier - Toulouse III, 2020. English. NNT : 2020TOU30227 . tel-03208760

HAL Id: tel-03208760

<https://theses.hal.science/tel-03208760>

Submitted on 26 Apr 2021

HAL is a multi-disciplinary open access archive for the deposit and dissemination of scientific research documents, whether they are published or not. The documents may come from teaching and research institutions in France or abroad, or from public or private research centers.

L'archive ouverte pluridisciplinaire **HAL**, est destinée au dépôt et à la diffusion de documents scientifiques de niveau recherche, publiés ou non, émanant des établissements d'enseignement et de recherche français ou étrangers, des laboratoires publics ou privés.

THÈSE

En vue de l'obtention du
DOCTORAT DE L'UNIVERSITÉ DE TOULOUSE

Délivré par l'Université Toulouse 3 - Paul Sabatier

Présentée et soutenue par

LAURENT CAMBORDE

Le 20 novembre 2020

**Caractérisation fonctionnelle de différents effecteurs candidats de
l'oomycete *Aphanomyces euteiches*, parasite racinaire des
légumineuses.**

Ecole doctorale : SEVAB - Sciences Ecologiques, Vétérinaires, Agronomiques et
Bioingenieries

Spécialité : Interactions plantes-microorganismes

Unité de recherche :

LRSV - Laboratoire de Recherche en Sciences Végétales

Thèse dirigée par

Elodie GAULIN

Jury

Mme Claire VENAULT-FOURREY, Rapporteuse

M. Bruno FAVERY, Rapporteur

M. Christophe ROUX, Examineur

Mme Elodie GAULIN, Directrice de thèse

Abstract

Oomycetes are eukaryote pathogens able to infect plants and animals. During host interaction, oomycetes secrete various molecules, named effectors, to counteract plant defence and modulate plant immunity. Two different classes of cytoplasmic effectors have been described to date, Crinklers (CRNs) and RxLR proteins. The translocation process allowing the entrance into the host cells is still unclear, and while extended research gave insight into some molecular targets and role during infection, most of effectors have not been characterized.

In the root rot pathogen of legumes *Aphanomyces euteiches*, only the CRNs are present. Based on a previous study reported by our research group, we published an opinion paper focused on the emergence of DNA damaging effectors and their role during infection.

Previous experiments indicate that one of these Crinklers, AeCRN5, harbours a functional translocation domain and once the protein reaches host nuclei, dramatically disturbs root development. Here we reveal that AeCRN5 binds to RNA and interferes with biogenesis of various small RNAs, implicated in defence mechanisms or plant development.

Furthermore, comparative genetic analyses revealed a new class of putative effectors specific to *Aphanomyces euteiches*, composed by a large repertoire of small-secreted protein coding genes (SSP), potentially involved during root infection. Preliminary results on these SSPs point out that AeSSP1256, which contains a functional nuclear localisation signal, enhances host susceptibility.

Functional characterisation of AeSSP1256 evidenced that this effector binds to RNA, relocalizes a plant RNA helicase and interferes with its activity, causing stress on plant ribosome biogenesis.

This work highlights that various effectors target nucleic acids and reveals that two effectors from distinct family are able to interact with plant RNA in order to interfere with RNA related defence mechanisms and plant development to promote pathogen infection.

Keywords: Oomycetes, nucleus, DNA damage, RNA-binding proteins, CRN, SSP.

Remerciements

Alors par qui commencer... les membres de mon jury bien sûr, à commencer par Claire Veneault-Fourrey et Bruno Favery qui ont accepté d'évaluer mon travail. En ces temps de Covid et à l'heure où j'écris ces lignes, je ne sais pas encore si on se verra masqués, ou par écrans interposés, mais je vous remercie sincèrement pour le temps que vous m'accordez. Merci aussi à Christophe Roux pour avoir gentiment accepté de faire parti de mon jury.

Un grand merci à Bernard Dumas, ancien chef de l'équipe lors de mon arrivée au laboratoire. Merci pour la confiance que tu m'as accordé et pour m'avoir un peu poussé à faire une thèse. Bon pour m'avoir beaucoup poussé à faire une thèse. Beaucoup.

Mention spéciale à la plateforme d'imagerie, pour leur compétence, leur disponibilité et leur gentillesse en commençant par Alain Jauneau, avec qui j'ai passé des heures autour d'un laser, d'un microscope et d'un tableau Velleda, pour apprendre le FRET-FLIM. Il existe des gens qui rendent tout intéressant. Je n'oublie pas bien sûr Cécile Pouzet, avec qui j'ai beaucoup de plaisir à travailler, et qui en plus veut bien me prêter ses jouets à 500 000 euros. Merci aussi à Yves Martinez et Aurélie Le Ru, d'une patience rare, même si Aurélie me coûte plus cher en bières. Heureusement que vous êtes là.

Merci à Jean Philippe Combié pour les discussions et les suggestions apportées. 5 min de discussion avec JP, c'est 5 mois de manips derrière. Faut pas y aller trop souvent non plus...

Merci aux personnes avec qui j'ai travaillé sur ce sujet de thèse, notamment Annelise, Amandine et Marie Alexane que j'ai eu en stage, Chiel Pel et Sarah Courbier qui ont initié le projet sur les SSP et avec qui j'ai passé de très bons moments. Diana Ramirez qui a effectué sa thèse sur les CRNs, ce qui nous a permis de découvrir le monde merveilleux des amphibiens, l'odeur de l'animal, les inséminations de grenouilles femelles, les injections d'ARN dans des centaines d'embryons. En fait on oublie, mais vraiment, travailler sur les plantes, c'est bien.

Là c'est le paragraphe dédié aux gens qui m'ont rendu la vie plus facile. Par exemple David, qui réceptionne mes bons de commandes, donc mes erreurs hebdomadaires, dans une ambiance de zénitude et d'encens qui rappelle que rien n'est jamais grave avec David, c'est reposant. Catherine, notre gestionnaire, qui a su aussi être très patiente, mais sans la musique zen et l'encens. Son "CammmmmBBBOORDEEEE" résonne encore dans ma tête.

Merci aux membres de mon équipe, ancienne et actuelle, à ceux du LabCom, à Thomas et Olivier pour les discussions et conseils, c'est toujours agréable de parler avec vous. Merci à Charlene qui m'a soutenu, surveillé mes réinscriptions et ma phobie administrative, à Malo, à Andreï. Merci EMILIE, oui en majuscule, parce que tu m'as beaucoup aidé dans la gestion des affaires courantes comme on dit, en se partageant les tâches à merveille. En gros tu t'occupais de tout ce qui ne me plaisait pas!

Enfin, un grand merci à ma directrice de thèse, Elodie Gaulin, qui a su me guider et me soutenir durant ce travail. Ta patience et la facilité avec laquelle tu évacues la pression m'ont beaucoup aidé. C'est un vrai plaisir de travailler avec toi!

A ma famille, dont mes parents, éternelle source d'inspiration, à mes enfants, qui vont retrouver leur pôpa, et à ma femme, pour tout ce qu'elle est.

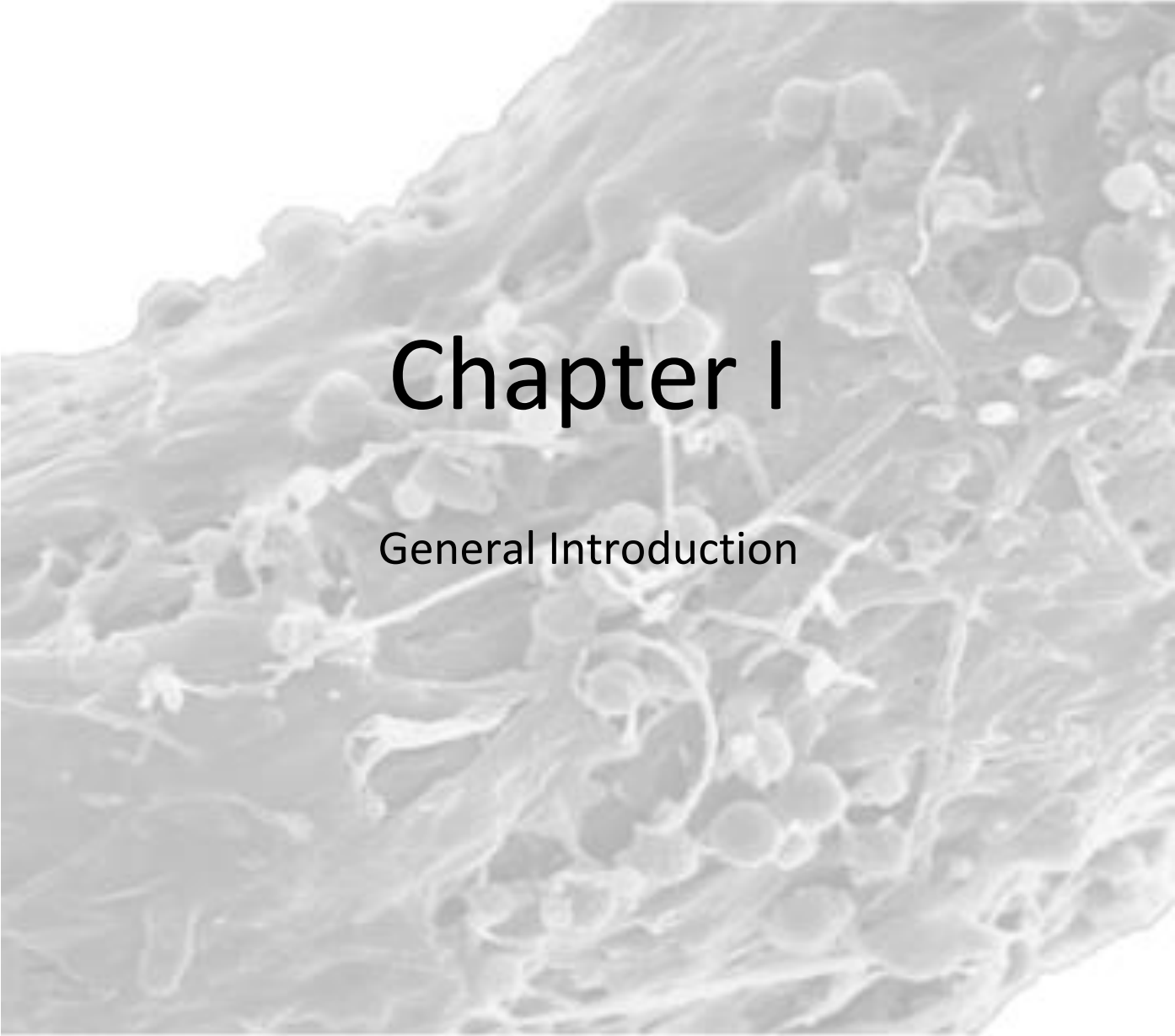
List of abbreviations

Ae	<i>Aphanomyces euteiches</i>
AEPs	Apoplastic Effector Proteins
AM	Arbuscular Mycorrhiza
Avr	Avirulence
Bd	<i>Batrachochytrium dendrobatidis</i>
BIC	Biotrophic Interfacial Complex
CSEPs	Candidate Secreted Effector Proteins
CBEL	Cellulose Binding Elicitor
CRN	Crinkling and Necrosis
CSEPs	Candidate Secreted Effector Proteins
CWDEs	Cell Wall Degrading Enzymes
ECM	Ectomycorrhizal Fungi
ER	Endoplasmic Reticulum
ESTs	Expressed Sequence Tags
ETI	Effector-Triggered Immunity
EVs	Extracellular Vesicles
FLIM	Fluorescence Lifetime Imaging Microscopy
FRET	Fluorescence Resonance Energy Transfer
GFP	Green Fluorescent Protein
GWAS	Genome Wide Association Study
HGT	Horizontal Gene Transfer
HIGS	Host-Induced Gene Silencing
HR	Hypersensitive Response
HRP	HorseRadish Peroxidase
HSP	Heat Shock Protein
JA	Jasmonic Acid
MAMP	Microbe-Associated Molecular Pattern
MAPKKK	Mitogen Activated Protein (MAP) Kinase Kinase Kinase
MAX	<i>Magnaporthe</i> Avr _s and ToX B-like effectors
NES	Nuclear Export Signal
NLPs	Necrosis and Ethylene inducing peptide 1 (Nep1)-like proteins

NLRs	Leucine-Rich Repeat proteins
NLS	Nuclear Localization Signal
PAMP	Pattern-Associated Molecular Pattern
PTGS	Post-Transcriptional Gene Silencing
PTI	PAMPs-Triggered Immunity
PBS	Phosphate-Buffered Saline
PCW	Plant Cell Wall
PR	Pathogenesis Related
PTI	PAMP-Triggered Immunity
QTL	Quantitative Trait Loci
R	Resistance
RALPHs	RnAse-Like Proteins Associated with Haustoria
REase	Restriction Endonuclease (REase) superfamily
RIP	Repeat-Induced Point mutations
RBPs	RNA Binding Protein
rDNA	Ribosomal DNA
ROS	Reactive Oxygen Species
SA	Salicylic Acid
SAR	Systemic Acquired Resistance
SAR	Stramenopiles, Alveolates, and Rhizaria
SDS	Sodium Dodecyl Sulfate
siRNA	Small Interfering RNAs
SSPs	Small-Secreted Proteins
SNPs	Single Nucleotide Polymorphism
TALE	Transcription Activator-Like Effector
TBS	Tris-Buffered Saline
TE	Transposable Element
TFs	Transcription Factors
Ubi	Ubiquitin
WGA	Wheat Germ Agglutinin
Y2H	Yeast-2-Hybrid

Table des matières

Abstract	
List of abbreviations	
I – CHAPTER I: General Introduction	1
I-1. Oomycetes and fungi, The World Is Not Enough	1
I-1.1. The Phantom menace	1
I-1.2. Defence and Resistance against pathogens.....	2
I-2. Oomycetes, so close and yet so far from Fungi	6
I-2.1. The false brothers	6
I-2.2. Lifestyle: oomycete and fungi in front of the mirror	6
I-2.3. Oomycete phylogeny, still a growing tree	8
I-2.4. Oomycetes, origin(s) and evolution	9
I-3. Effectors, the infectious Swiss knife.....	10
I-3.1. Effector genes evolution	11
I-3.2. Apoplastic and intracellular effectors	13
I-3.2 a. Apoplastic effectors: in front of the Wall	13
I-3.2 b. Intracellular effectors: Destroy from within	15
I-3.3. Intracellular effectors targets: hit the defence key players.....	21
I-4. <i>Aphanomyces</i> : an oomycete genus to study effectors and host adaptation	24
I-4.1. <i>Aphanomyces euteiches</i> , the Legume threat.....	25
I-4.2. <i>Aphanomyces euteiches</i> – <i>Medicago truncatula</i> pathosystem	27
I-4.3. Insight into <i>Aphanomyces euteiches</i> intracellular effectors	29
I-5. Scope of the thesis	31
II – CHAPTER II: DNA-Damaging Effectors: New Players in the Effector Arena (Camborde et al. TIPS, 2019).....	33
III – CHAPTER III: AeCRN5 effector from <i>A. euteiches</i> targets plant RNA and perturbs RNA silencing	42
IV – CHAPTER IV: Genomics analysis of <i>Aphanomyces spp.</i> identifies a new class of oomycete effector associated with host adaptation (Gaulin et al. BMC Biol, 2018)	74
V – CHAPTER V: A DEAD-Box RNA helicase from <i>Medicago truncatula</i> is hijacked by an RNA-binding effector from the root pathogen <i>Aphanomyces euteiches</i> to facilitate host infection	97
Complementary results: <i>Aphanomyces euteiches</i> effectors from two different families interact and modulate their activity.	135
General discussion and perspectives	142
References	153



Chapter I

General Introduction

I-1. Oomycetes and fungi, The World Is Not Enough

I-1.1. The Phantom menace

Plants and animals have to face constantly with abiotic stresses, like environmental modifications due to climate change, including higher temperature, pH variation or long drought for instance, but also various biotic stresses due to multiple interactions with other organisms, from bacteria to nematodes, via fungi, oomycetes, viruses or insects. Unlike animals, who can move to find a better environment, plants are rooted in place and must adapt very quickly to changes or attacks. One of the major biotic threats are eukaryotic filamentous microorganisms, represented by oomycetes and fungi, which comprise several of the most devastating plant and animal pathogens, considered as a major threat for agriculture, but also for natural terrestrial or oceanic ecosystems (Beakes et al., 2012).

Even if humans and most mammals are remarkably resistant to invasive fungal diseases, in the same time entire ecosystems are currently devastated by fungal pathogens (Fisher et al., 2012; Casadevall, 2017). Bats or reptiles are threatened with extinction due to pathogenic fungi (Fisher et al., 2012; Casadevall, 2017). Another example of feared fungus is *Batrachochytrium dendrobatidis*, considered as the major threat for amphibians causing a catastrophic loss of biodiversity (Fisher et al., 2012; Scheele et al., 2019). Fungal diseases also impact plant crops, destroying a third of all food crops annually and impacting the most important crops (rice, wheat, maize, potatoes, and soybean) (Fisher et al., 2012; Almeida et al., 2019). For instance, the wheat stem rust caused by the fungus *P. graminei* *sf. tritici*, which has been threatening wheat cultures since 1998, had disastrous impact in the Middle East and West Asia, with reduction in yields up to 40% (Pennisi, 2010). Very recently, researchers warned and reported the re-emergence of this fungus in Western Europe (Saunders et al., 2019; Bhattacharya, 2017). Another example is the rice blast disease agent *Magnaporthe oryzae*, one of the most economically devastating fungus that infect rice as well as other grass

species including wheat. Only on rice, annual yield losses can reach 20% in many production zones but the entire harvest can be lost when significant outbreak occur (Prabhu et al., 2009).

Oomycetes also comprise devastating pathogens and represent the most problematic group of disease-causing organisms in both agriculture and aquaculture (Derevnina et al., 2016b). However, oomycetes stand as notorious plant pathogens with remarkable examples, like *Phytophthora infestans* causing late blight triggering the Irish potato famine in 1840 (Haas et al., 2009). *Phytophthora* species are responsible of serious diseases affecting crop yields. The annual economic loss on tomato and potato due to *P. infestans* was estimated at \$ 6.7 billion (Haas et al., 2009). On soybean, for North America, the average annual yield loss caused by *P. sojae* was estimated at 1.1 million tons, from 2007 to 2014 (Allen et al., 2017). Others notable species are *P. palmivora* and *P. capsici*, causing agents of cocoa black pod causing yield losses of 20–30% annually (Adeniyi, 2019). On legumes, *Aphanomyces euteiches*, the causing agent of root rot, represent one of the major limitations to pea production worldwide (Wu et al., 2018). All those examples highlight the important impact of plant pathogen oomycetes, but some species are also responsible for devastating diseases in natural ecosystems or in aquaculture. For instance, members of the *Saprolegnia* genus, such as *S. parasitica* infecting freshwater fish, are involved in the decline of wild salmon populations around the world (Phillips et al., 2008; van West, 2006). Another example of killing agent is *Aphanomyces astaci*, parasite of fresh-water decapods and causing crayfish plague. Originate from North America, it is now present in Europe and has been nominated among the “100 of the World’s Worst Invasive Alien Species” in the Global Invasive Species Database (GISD).

I-1.2. Defence and Resistance against pathogens

Despite the impact of these diseases and the increase of dedicated research, it is still challenging to control fungal or oomycete attacks. To reach high-quality crops with optimal yields, modern agriculture had resort to intensive use of fungicides that frequently became ineffective due to high adaptation frequency, caused by gene mutations, leading to the emergence of new fungal races (Zhou et al., 2007; Lucas et al., 2015). Same problem occurs

with oomycete diseases control, where complex fungicidal mixtures were used for many years, often inefficient due to wide range of intrinsic sensitivities (Judelson and Senthil, 2005) or because resistance evolved against most single-site inhibitors in many oomycete pathogen species (Gisi and Sierotzki, 2015). Some fungicides are also inefficient because the metabolic pathways or key molecules they target in fungi are absent in some oomycete species. For instance, the class of triazole pesticides, representing the largest class of fungicides which target CYP51 enzymes involved in sterol biosynthesis, should not be used against *Phytophthora* or *Pythium* species since these oomycetes do not possess CYP51 enzymes (Tyler et al., 2006; Sello et al., 2015) and are sterol auxotrophs (Kazan and Gardiner, 2017), leading these fungicides to be inefficient against diseases caused by these pathogens (Gaulin et al., 2010).

Fortunately, chemicals are not the only way to counteract pathogen attacks. Hosts have evolved innate immunity due to their long coevolution with microorganisms. The first layer of plant defence is based on the recognition of essential molecules derived from microorganisms. When the host perceives those molecules that are specific to microorganisms and indispensable for its life cycle and called pathogen-associated molecular patterns (PAMPs), it triggers and activates numerous defence responses. The PAMPs-Triggered Immunity (PTI), comprises a set of responses including callose deposition, oxidative bursts or activation of defence gene (Jones and Dangl, 2006; Nicaise et al., 2009). One of the most famous identified PAMPs is the bacterial flg22, a conserved peptide from the protein flagellin, a major component of the motility organ flagellum, which is recognized by most plants thanks to an LRR Receptor-like Kinase (Gómez-Gómez and Boller, 2000). Numerous eukaryotic PAMPs correspond to cell wall components, like Pep-13, a highly conserved amino acid fragment within the cell wall glycoprotein GP42 from the oomycete *Phytophthora sojae* (Brunner et al., 2002), or NPP1, a cell-wall protein identified in several *Phytophthora* species as eliciting immune responses in plants (Fellbrich et al., 2002), or CBM1 from the cell wall protein CBEL from *P. parasitica* (Gaulin et al., 2006; Larroque et al., 2012). PAMPs are not only proteins as β -Glucans also represent a common fungal and oomycete PAMPs derived from cell wall fractions. Most plants recognize chitin, the main component of fungal cell wall, but also the branched β -Glucans from oomycete cell wall. As example branched glucan-

chitosaccharides from the oomycete *Aphanomyces euteiches* induce defence and calcium signals in *Medicago truncatula* root cells (Nars et al., 2013).

Faced to PTI, microorganisms evolved and secreted hundreds of pathogenesis-related molecules, named effectors, to modulate immunity and facilitate host colonization. In turn, some hosts evolve to detect specifically those molecules, leading to the Effector-Triggered-Immunity (ETI). Perception is mediated by receptors known as resistance proteins (R) that directly or indirectly recognize some secreted effectors, then called avirulence proteins (AVR). This process was previously named gene-for-gene resistance (R/AVR) (Van Der Biezen and Jones, 1998). This recognition is frequently associated to a hypersensitive response (HR), a localized host cell death to confine the pathogen at the infection site (Jones and Dangl, 2006). Then, major R genes have been used by breeding companies to protect crops against fungal plant diseases (Stuthman et al., 2007). However, the strategy using a single resistance gene often turns out to be inefficient due to adaptation of pathogen populations, which have a high evolutionary potential and rapidly evolve by AVR genes mutations to become virulent. For instance, the fungus *Leptosphaeria maculans*, the causing agent of the phoma stem canker disease on oilseed rape (*Brassica napus*), produce new strains by mutations of genes rendering the corresponding major host resistance genes ineffective in only three years (Sprague et al., 2006). Similarly, appearance of new and more virulent pathotypes of the downy mildew (*Plasmopara halstedii*) in sunflower leads researchers to identify new R genes in order to combine them in varieties carrying a wide range of resistance genes (Pecrix et al., 2019, 2018). Nowadays, major R genes are deployed in cultivars in combination with sustainable disease management practices like precise chemical treatments in order to prolong the use of those resistance genes (Mitrousia et al., 2018).

In addition, another aspect of genetic resistance is related to a quantitative resistance with a partial reduction of symptoms and disease severity (Kamoun et al., 1999). This partial resistance is due to quantitative resistance genes localized in genome area named Quantitative Trait Loci (QTLs). Even if this resistance is frequently less efficient than gene-for-gene resistance like R-AVR gene interaction (Hu et al., 2008; Pilet-Nayel et al., 2017), it appeared to be more durable, with a lower selection pressure for pathogens, which limit mutations, and resistance acquired by the expression of different QTLs is more difficult to

circumvent (Poland et al., 2009). For instance, no resistant pea, lentil cultivars are available against the oomycete *Aphanomyces euteiches* that causes the devastating root rot diseases of legumes. However, genome-wide association studies based on the model legume *Medicago truncatula* identified one major and several minors QTLs contributing to the tolerance (Badis et al., 2015; Bonhomme et al., 2014, 2019). Then some *Aphanomyces* resistance QTLs were identified in pea but fine mapping to identify underlying genes is still challenging (Hamon et al., 2013; Desgroux et al., 2016). In lentil, numerous QTLs were recently detected and some genes are under validation (Ma et al., 2020; Marzougui et al., 2019). Similarly, the oilseed rape (*Brassica napus*), threatened by stem rot caused by the fungus *Sclerotinia sclerotiorum*, represents another crop with absence of resistant lines. Currently, breeding for *Sclerotinia* resistance in *B. napus* is only based on germplasms with quantitative resistance genes (Wu et al., 2013) and the identification of new QTLs is still an active research (Qasim et al., 2020). In rice, where many R genes were characterized, QTLs were also identified. Then, the resistance in cultivars to the blast fungus *Magnaporthe oryzae* is controlled by a combination of both major genes and QTLs (Kang et al., 2016).

The use of chemicals to threat animal pathogens invasion triggered also the development of chemical-resistance coupled with negative side-effects on the ecosystem. Then, alternative strategies have to be developed. In aquatic culture for instance, biological control strategies are under development to control zoosporic diseases due to chytrid fungus and oomycetes (Frenken et al., 2019). This include for example a project of immunization against the oomycete *Saprolegnia parasitica* using a serine protease, the identification of stimuli able to increase the production of natural antifungal peptides produced by the skin of amphibians, or the modification of the pathogen fitness using secondary parasites (Frenken et al., 2019). While those projects are promising, much work still needs to be done to implement biological-control applications in aquaculture (Frenken et al., 2019). Biocontrol strategies are also currently develop to protect plant against pathogens (Köhl et al., 2019).

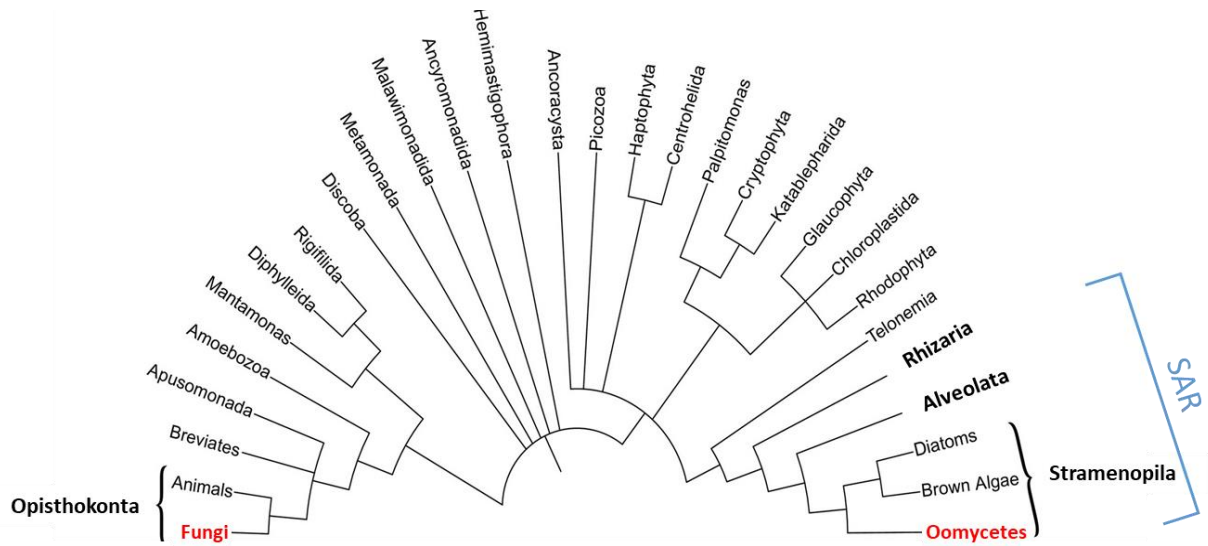


Figure 1: Simplified tree of eukaryotes showing the distant relationship between oomycetes and fungi.

SAR is an acronym of its constituents: Stramenopiles, Alveolates, and Rhizaria. Oomycetes and Fungi are highlight in red. Adapted from (McGowan and Fitzpatrick, 2020).

I-2. Oomycetes, so close and yet so far from Fungi

I-2.1. The false brothers

Oomycetes were originally considered as members of the kingdom of Mycota, in the Opisthokonta clade, with the same classification level as the ascomycetes and basidiomycetes within Fungi (Lévesque, 2011). Even if oomycetes and fungi share common characteristics, as filamentous growth in the form of tip-growing branching hyphae, or similar ecological role and feeding behaviour (Beakes et al., 2012), oomycetes form a phylogenetic lineage distinct from fungi, closely related to brown algae and diatoms among Stramenopiles (Straminipila) (Cavalier-Smith and Chao, 2006). Stramenopiles constitute one of the major eukaryotic clades, branching with Rhizaria and Alveolata within the 'supergroup' SAR (Derelle et al., 2016) (**Figure 1**). Major differences at morphological and molecular levels are now evidenced, as oomycetes are diploid organisms while fungi are haploid during the majority of their life cycle, disseminate mainly asexually with biflagellated zoospores and are mostly auxotrophic for sterols (with few exception like *Aphanomyces euteiches* (Gaulin et al., 2010)). Oomycetes develop mostly non-septate hyphae and unlike true fungi, the main structural polysaccharide of the oomycete cell wall is cellulose and not chitin (Judelson, 2017), with few exception like *A. euteiches* which contains chitin derivate in the cell wall (Badreddine et al., 2008). Then, molecular analysis based on combined protein data and rDNA sequences, and more recently, large-scale genome phylogenetic studies confirmed the distant relation of oomycetes from true fungi (Baldauf et al., 2000; Burki, 2014; Derelle et al., 2016).

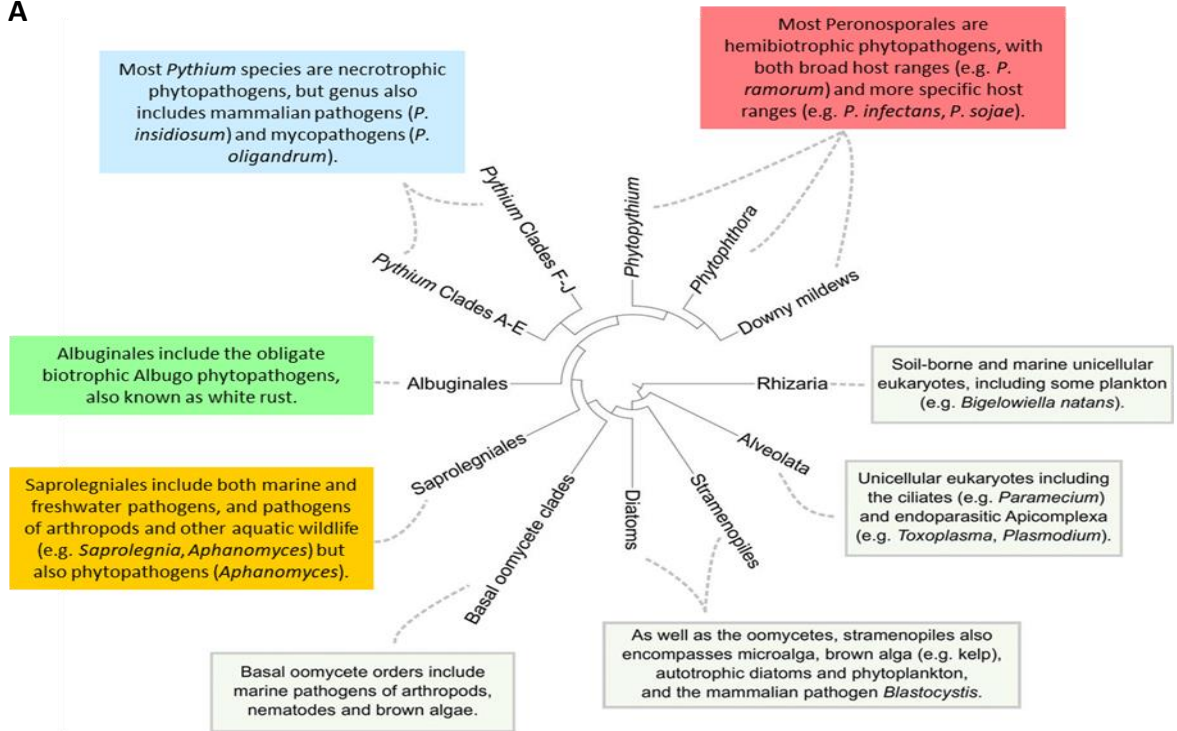
I-2.2. Lifestyle: oomycete and fungi in front of the mirror

Although oomycetes and fungi are evolutionarily very distantly related, both taxa evolved similar lifestyles. The saprophytic species, which represent a large group of fungi but also numerous oomycetes related to *Pythium* and some Saprolegnian species (Lamour and Kamoun, 2009), are able to develop on dead host tissue and perform the initial steps in the decomposition macromolecules, like cellulose or lignin on plant cells (Berg et al., 2014). On the other hand, many fungal and oomycete species are obligate biotrophs, meaning that they

are unculturable on artificial media, and grow only on living cells. Those species require metabolic active tissues to achieve their life cycle and then are highly adapted to their host, such as downy mildew *Plasmopara viticola*, which infects grapevine (*Vitis vinifera*), *Albugo candida*, the causing agent of white rust on crucifers (Kamoun et al., 2015) or the pathogenic fungus *Blumeria graminis* causing powdery mildew on barley (Thomas et al., 2001) and the smut fungus *Ustilago maydis* on corn (Banuett and Herskowitz, 1996). By contrast, many plant pathogenic oomycetes or fungi, especially species of the genus *Phytophthora*, or fungi/Ascomycota like *Colletotrichum* or *Magnaporthe*, display an intermediate lifestyle called hemibiotrophy, starting infections like biotrophs by establishing a transient biotrophic relationship with the host, then switch to necrotrophic phase later in the disease cycle (Latijnhouwers et al., 2003; Lamour and Kamoun, 2009; Thines, 2018). Finally, necrotrophic pathogens kill host tissues to feed during the colonisation like the fungus *Botrytis cinerea*, the causal agent of gray mold, an economically devastating disease, which serves as a model species for plant-necrotroph interactions (Petrasch et al., 2019). *Pythium* represent the largest genus of necrotrophic oomycetes, but some aquatic pathogenic oomycetes like *Lagenisma coscinodisci* are also efficient necrotrophic organisms, able to kill marine diatoms in few days by hijacking the host's alkaloid metabolism (Vallet et al., 2019). However, the classification in hemibiotrophy or necrotrophy is not always clear, as for the oomycete *Aphanomyces euteiches* that causes root rot of legumes (Judelson and Ah-Fong, 2019).

Both oomycetes and fungi share similar traits for host interaction. Dispersal of oomycetes is mediated by water or wind through asexual sporangia or directly by the release of asexual motile zoospores from sporangia (Tyler, 2002). Once oomycete zoospores have reached host surface, they encyst by shedding their flagella and secrete adhesion molecules (Hardham and Shan, 2009; Carzaniga et al., 2001). Asexual spores of fungi as conidies are transported by wind and water, before an adhesion step to the host due to the secretion of adhesion molecules. The germinated cyst produce hyphae able to penetrate inside cell layers, mainly by using a pathogenic structure called appressorium, then vegetative hyphae grow in intercellular space and develop haustoria which penetrated inside host cells (Fawke et al., 2015). Oomycetes and fungi hyphae can also penetrate by natural opening such as stomata

A



B

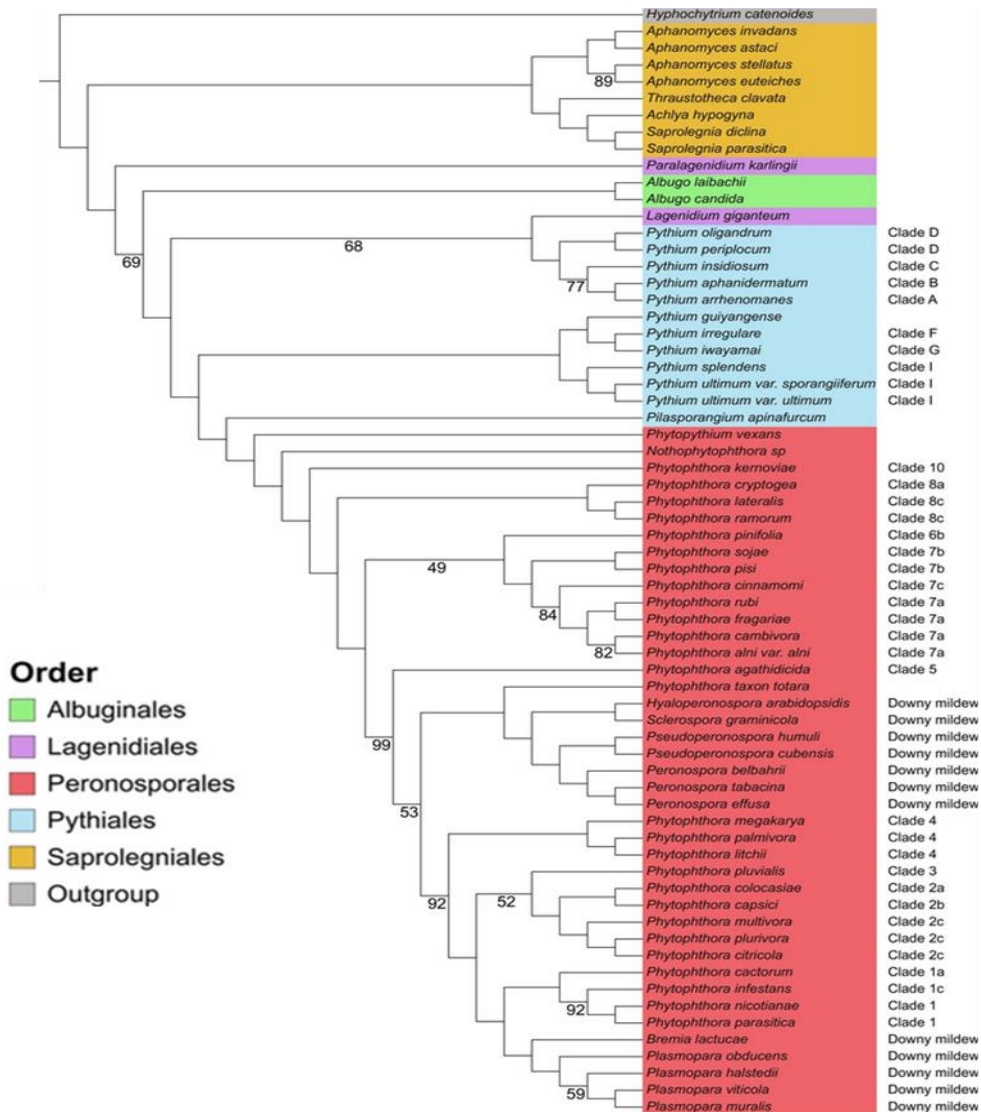


Figure 2: Phylogeny of the Oomycetes.

(A) Consensus phylogeny of the oomycete class within the greater SAR grouping, including information pertaining to various taxa. Adapted from (McCarthy and Fitzpatrick, 2017). (B) Maximum-likelihood phylogeny of the 65 oomycete species based on the concatenation of 102 conserved BUSCO sequences. The stramenopile *Hyphochytrium catenoides* is included as an outgroup. All nodes have 100% bootstrap support except where indicated. Species are colored according to their order. *Phytophthora* clades are indicated as designated by Blair, Coffey, Park, Geiser, and Kang (2008) and *Pythium* clades are as designated by de Cock et al. (2015). From (McGowan and Fitzpatrick, 2020).

(Lucas, 2020). Numerous enzymes to break the host barriers (i.e. cell wall, cutin) are also produced by oomycetes and fungi during the penetration and colonization steps. However, some oomycetes do not form haustoria, like *Pythium ultimum* or neither appressorium, such as *Aphanomyces euteiches* (Gaulin et al., 2008). Finally, they complete their life cycle by producing new asexual spores and/or by making their sexual life cycle/stage.

I-2.3. Oomycete phylogeny, still a growing tree

Oomycete phylogeny is still subject to revision due to new genome availability. To date, 65 oomycete species have publicly available genome sequences deposited in databases (McGowan and Fitzpatrick, 2020) and although many species are yet unsampled, the current consensus phylogeny of the oomycetes split them into a basal order and four major “crown” orders: the Peronosporales, Pythiales, Albuginales, and Saprolegniales (Beakes et al., 2014; McCarthy and Fitzpatrick, 2017; McGowan and Fitzpatrick, 2020) (**Figure 2a**). The basal order of oomycetes includes exclusively marine organisms which are predominantly parasites of seaweeds, nematodes or arthropods (Beakes et al., 2012). The Saprolegniales order is the most basal of the four major crown orders and includes saprophytes and animal parasites, such as the fish pathogen *Saprolegnia* (Hulvey et al., 2007), and also the plant and animal pathogenic *Aphanomyces* genus (Gaulin et al., 2007) (**Figure 2a and b**). The Peronosporales order includes the largest group of terrestrial organisms and represent the best studied order, comprising the well-known oomycete *Phytophthora* genus. It is also composed by the phytopathogenic *Phytopyrium* genus as well as downy mildew such as *Hyaloperonospora*, *Plasmopara* or *Sclerospora* genera (Fletcher et al., 2019; McCarthy and Fitzpatrick, 2017; McGowan and Fitzpatrick, 2020) (**Figure 2a and b**). The Pythiales order contains animal and

plant pathogens, but also comprises some species able to parasitize fungi and other oomycetes, such as *Pythium oligandrum*. These mycoparasites are used as new types of biocontrol agents (Benhamou et al., 2012; Faure et al., 2020). The last member of the four crowns are the Albuginales, which include the plant pathogenic *Albugo* genus (**Figure 2a and b**) which causes “white blister rust” on many valuable crop species. Additionally, few species are members of the Lagenidiales genus, a complex taxon still unclearly defines (Spies et al., 2016). The phylogeny of the 65 available sequenced oomycete species exposed in the recent paper of Mc Gowan and Fitzpatrick is presented in **Figure 2b**.

I-2.4. Oomycetes, origin(s) and evolution

The history and the evolution of oomycetes are still an ongoing research, partially under debate and regularly update due to the increasing number of available genomes. To date, the consensus hypothesis is that Stramenopiles originate from the enslavement of algal ancestors by a biflagellate photosynthetic organism. Then oomycetes evolved by multiple losses of plastids and genes for phototropism (Cavalier-Smith and Chao, 2006), even if some lineages like some *Phytophthora* species still conserve photosynthesis-related genes (Tyler et al., 2006).

Molecular clock studies, based on complete genome analyses, estimated the origin of oomycetes around the mid-Palaeozoic Era, up to 430 million years ago (Matari and Blair, 2014). This is supported by the discovery of preserved oomycete structures in the fossil records from the Carboniferous period (approximately 360 to 300 million years ago during the late Paleozoic Era) (Krings et al., 2011). In addition, fossils from the same period evidenced the parasitic lifestyle of oomycetes towards plants (Strullu-Derrien et al., 2011). By the way, parasitism is widespread in oomycetes lineage, reflecting the radical reconfiguration of lifestyle and trophic mechanism from the oomycetes ancestor, changing from carbon fixation by photosynthesis and/or digests microbes inside the cell, to a cellular form that processes complex substrates in the extracellular environment for transportation into the cell

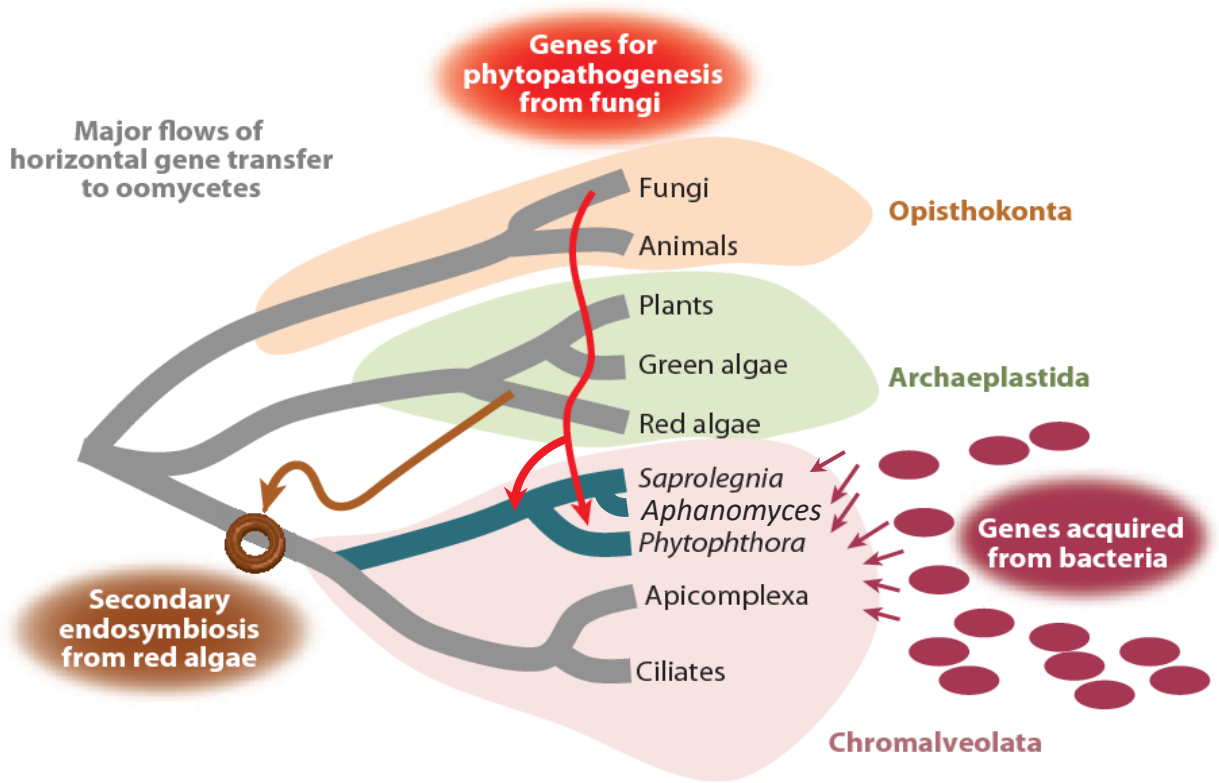


Figure 3: Gene acquisitions from horizontal gene transfer (HGT) in oomycetes.

The three major flows of genes are annotated in ovals. Only three broad group of eukaryotes are drawn schematically on the tree. Arrows indicate the direction of gene transfer. Multiple acquisitions have occurred from different fungal species and bacterial species. Adapted from (Jiang and Tyler, 2012).

(Savory et al., 2015; Beakes et al., 2012). It is thought that horizontal gene transfer (HGT), especially from bacteria and fungi, supported this evolution for pathogenicity and virulence genes (Jiang and Tyler, 2012; Savory et al., 2015; McCarthy and Fitzpatrick, 2016) (**Figure 3**). Notably, HGT had a major impact upon the evolution of the secretomes of oomycetes, which represent all the molecules released out of the cell into the external environment such as hydrolytic enzymes, toxins and effectors (Jiang and Tyler, 2012; Savory et al., 2015).

I-3. Effectors, the infectious Swiss knife

This diversity of lifestyle, coupled with the wide host range and various environment displayed by oomycetes and fungi raised questions about genetic and molecular mechanisms involved in their evolution and rapid adaptation to their hosts and environmental changes (Raffaele and Kamoun, 2012; Judelson, 2012). One answer is that for both oomycetes and fungi, success of infection mainly relies on large repertoires of secreted proteins defining the secretome. The secretome represents all the molecules secreted by the microbe to adapt to new environmental resources or changes in his close environment (McCotter et al., 2016). The estimated size of fungi / oomycete secretome range from 4–15% of the total gene number (Girard et al., 2013; Pellegrin et al., 2015), with a highly variable composition closely related to the niche the microbes reside in (Soanes et al., 2008). This comprises a wide range of proteases, lipases, enzymes and small-secreted proteins (SSPs) to achieve functions such as nutrient acquisition, detoxification or cell wall manufacture (Feldman et al., 2020; Pellegrin et al., 2015). Among secreted proteins, some affect host physiology to neutralize plant defences and promote microorganism colonisation, the so-called effectors. Effectors include mainly proteins, secondary metabolites but also nucleic acids (e.g. small RNAs) (Wang et al., 2019). Therefore, secreted effectors evolved quickly, have different function, localization and may affect various host processes to enhance infection.

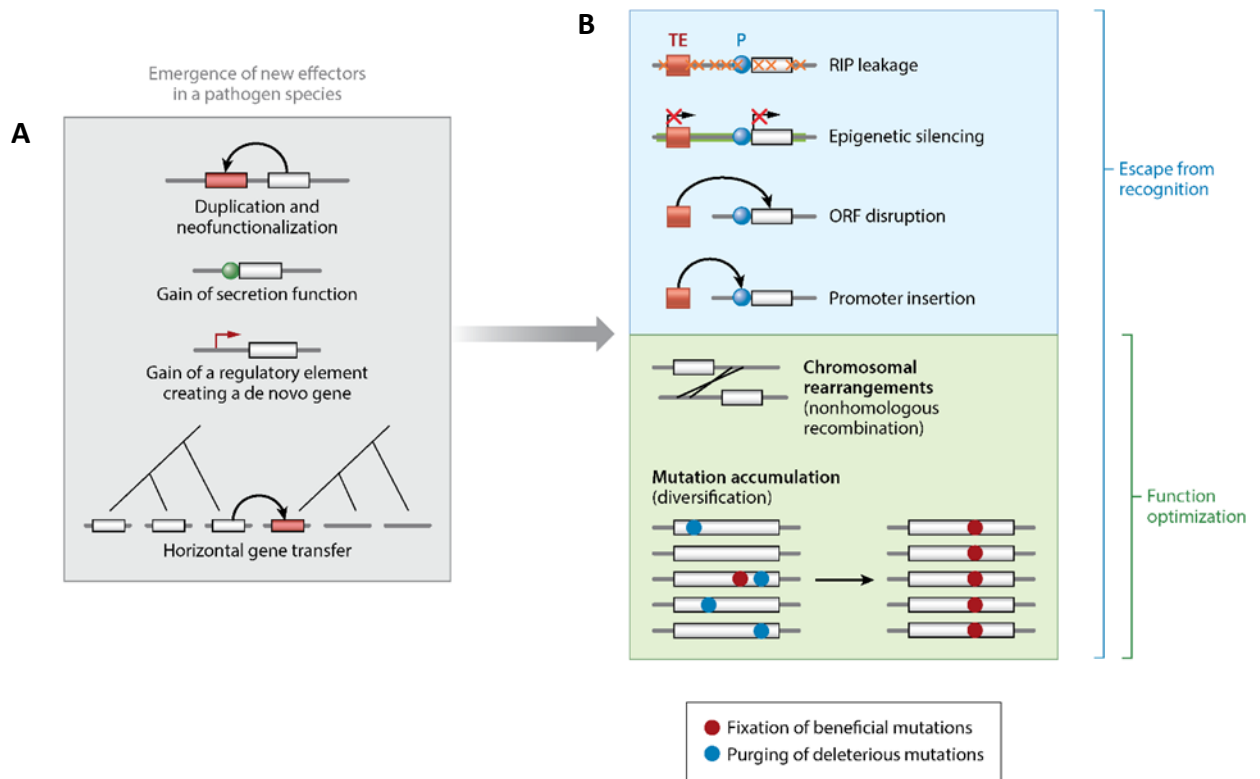


Figure 4: The evolutionary birth and death of effectors.

(A) New effectors can emerge through gene duplication or the gain of a secretion function. Effector genes may also evolve de novo from noncoding sequences through the gain of a regulatory element or be acquired horizontally from a different pathogen species. (B) Effector genes can undergo rapid sequence evolution upon recognition of the encoded effector by the host. The major mechanism leading to the loss of an effector gene is the presence and activity of nearby transposable elements (TEs). The effects of the transposable elements can include repeat-induced point (RIP) mutations, epigenetic silencing or the disruption of the gene sequence. Escape from recognition can also be mediated by chromosomal rearrangements or the fixation of beneficial mutations. Rearrangements and selection for beneficial mutations are also major routes for effectors to optimize their function. Abbreviations: ORF, open reading frame; P, promoter regions. From (Sánchez-Vallet et al., 2018).

I-3.1. Effector genes evolution

Effectors show rapid evolution within a given genome as a result of co-evolution with their hosts and are often associated with transfers to unrelated host (Dong et al., 2015; Raffaele et al., 2010). For instance, protease inhibitors produced by two sisters *Phytophthora* species evolved to target plant proteases of their respective unrelated hosts, linking effector specialization and host diversification (Dong et al., 2014). This close link between effectors and host adaptation was also revealed by comparative fungal genomic studies showing evidences of rapid evolution of effectors in related pathogens with different host ranges (Meerupati et al., 2013; Condon et al., 2013; O'Connell et al., 2012; Richards et al., 2019). Evasion of host recognition and effector functional optimization is achieved by sequence modification, gene deletion, modulation of effector genes expression and the gain of new effectors by horizontal gene transfer (**Figure 4a**) (Lo Presti et al., 2015b).

Some HGT have been evidenced, like for the transfer of *ToxA* between three unrelated wheat pathogens, leading to isolates that are more virulent (Friesen et al., 2006). Another example was reported in the cotton fungal pathogen *Verticillium dahlia* where lineage-specific region that might have originated from *Fusarium oxysporum* increased virulence on cotton but not on other hosts (Chen et al., 2018). Even if the main mechanisms leading to HGT are poorly understood, it seems that necrotrophic pathogens are far more susceptible to the acquisition of effector genes, particularly with host-specific toxin coding genes (Sánchez-Vallet et al., 2018). In oomycetes, gene acquisition by HGT was also evidenced for a cutinase gene from bacteria to *Phytophthora* species (Belbahri et al., 2008), and more extensively reported between fungi and oomycetes, at least in Peronosporales (Richards et al., 2011). In addition, changes in secretome of Saprolegniales oomycetes due to HGT from bacterial and fungal donor lineages were evidenced (Misner et al., 2014).

In addition to HGT, other genetic events occurred to evolve effector genes. For instance, gene duplications combined with mutations were shown to generate new effector genes in the smut fungus *Ustilago maydis* (Dutheil et al., 2016) (**Figure 4a**).

Transposable elements (TEs) were evidenced to play a major role in gene duplication and are significantly associated in the formation of virulence gene clusters through non-homologous recombination (Dutheil et al., 2016). The last generation of sequencing strategies

greatly increased the quality of genome assemblies and gave new insight into effector evolution and genome organization. Firstly, it revealed that TEs content was often underestimated. For example, the last version of *Colletotrichum higginsianum* genome contains 7% TEs whereas it was estimated to only 1.2% in the first assembly (Dallery et al., 2017). Then, it is now clear that many effector genes are not randomly distributed across the genomes and are associated with TEs and repetitive sequences in specific genome compartments. These results have led to the “two-speed genome” model in which some pathogen genomes have a bipartite architecture with essential genes in the core genome, protected from deleterious mutations, and the accessory genome where effector genes take place in a rapid evolutionary compartments (Raffaele and Kamoun, 2012; Croll and McDonald, 2012).

Rapid host adaptation can lead to effector recognition that triggers host defence. Hence, adaptive pressure on effector gene sequence can force mutations in order to modify, modulate or delete a given effector to escape host recognition. The most efficient mechanism leading to the loss of an effector gene is related to the activity of TEs. TEs can drive multiple effects on gene sequence, from gene disruption to repeat-induced point (RIP) mutations (**Figure 4b**). Adaptive loss of function was reported in the fungal pathogen of wheat *Zymoseptoria tritici*, where gene losses affected more than 10% of all genes in the genome, including both effectors and genes with conserved functions such as secondary metabolite gene clusters (Hartmann and Croll, 2017).

In addition to TEs activity, two types of mutations are known to modulate effector genes evolution (**Figure 4b**) (reviewed in (Sánchez-Vallet et al., 2018)). The first type of mutation consists in substitutions, insertions or deletions that change the protein properties of a given effector. The second type of mutation concerns neutral mutations with weak but cumulative effects. Fixation of beneficial mutations leads to optimization of the effector function and can infer the past selective history at the effector locus (Sánchez-Vallet et al., 2018).

Transcriptional silencing of an effector gene is another mechanism involved to escape host recognition, which preserve the effector sequence (Gijzen et al., 2014; Whisson et al., 2012). This was observed for the *Phytophthora sojae* effector gene Avr3a that is recognized in soybean plants carrying the resistance gene Rps3a. Silenced Avr3a alleles were transmitted

and persisted over multiple generations suggesting that transgenerational gene silencing at this locus mediated the gain of virulence phenotype (Qutob et al., 2013).

I-3.2. Apoplastic and intracellular effectors

During eukaryotic filamentous pathogens-plant interactions, two types of effectors can be distinguished depending on their localization. Apoplastic effectors proteins (AEPs) stay in the plant extracellular space (i.e. apoplast) while intracellular effectors proteins traffic into the host cell in various compartments.

I-3.2 a. Apoplastic effectors: in front of the Wall

The apoplast is a hostile environment notably due to secreted basal defence compounds like proteases, secondary metabolites or hydrolytic enzymes like chitinases (Doehlemann and Hemetsberger, 2013; Jashni et al., 2015). The release of PAMPs in the apoplast due to activity of plant chitinases or β -glucanases that disrupt microbial cell wall integrity leads to their perception through cell surface-localized immune receptors, such as Lysin motif (LysM)-containing proteins, which activates plant immune system (Cook et al., 2015; Liu et al., 2012). Thus, to counteract this first recognition process, numerous fungal and some oomycete AEPs have been characterized to evade glycan-triggered immunity or to protect cell wall microorganism from degradation (reviewed in (Rocafort et al., 2020)). *Phytophthora spp.* for instance secrete glucanase inhibitor proteins (GIPs) to inhibit the degradation of pathogen β -1,3/1,6-glucans and the release of defence-eliciting oligosaccharides by host endoglucanases (Rose, 2002; Damasceno et al., 2008). The tomato fungal pathogen *Cladosporium fulvum* secretes two characterized AEPs, the chitin-binding effector protein Avr4, which protects fungal hyphae against hydrolysis by plant chitinases (van den Burg et al., 2006), and Ecp6, an effector which uses LysM domains that competitively sequesters chitin oligomers from host immune receptors leading to the perturbation of chitin-triggered host immunity (Sánchez-Vallet et al., 2013). Other LysM effectors have been shown to contribute to virulence through chitin binding in other plant pathogenic fungi like *Magnaporthe oryzae*, *Colletotrichum higginsianum* and *Verticillium dahlia* (Kombrink et al., 2017; Mentlak et al., 2012; Takahara et al., 2016). Interestingly, AEPs with similar roles to both Avr4 and Ecp6 have been described in the fungal wheat pathogen *Zymoseptoria tritici*

(Marshall et al., 2011; Sánchez-Vallet et al., 2020) but also in the mutualistic fungus *Trichoderma atroviride* and in the arbuscular mycorrhizal fungus *Rhizophagus irregularis* (Zeng et al., 2020; Romero-Contreras et al., 2019). This indicates that both pathogenic and mutualistic microbes use AEPs to evade glycan-triggered immunity.

Thus, many characterized AEPs act to suppress this glycan-triggered immunity (Rocafort et al., 2020) but other families of AEPs have been described. One large group of apoplastic effectors commonly found in fungi and oomycetes are cell wall degrading enzymes (CWDEs), which play a major role in pathogenicity, contributing to plant cell wall degradation. Thus, this family includes hundreds of genes coding for enzymes such as cellulases, hemicellulases, pectinases, β -1,3-glucanases, glyceraldehyde hydrolases, carbohydrate binding molecules and other proteases able to degrade glycoproteins. The aim is to reduce the complexity of the cell wall structure to facilitate entry and colonization of the host. In animal pathogen interaction, those enzymes are absent and replaced by other specific enzymes. For instance, the plant pathogen oomycete *A. euteiches* possesses a large repertoire of CWDEs coding genes that target plant cell wall polysaccharides, absent in *Aphanomyces astaci*, the causing agent of crayfish plague. In turn, *A. astaci* shows an expansion of protease genes predicted to target chitin, the main component of the crayfish shell ((Gaulin et al., 2018) and see **CHAPTER IV**). Recently, it has been shown that a CWDE effector was protected by another AEP, acting as a decoy. Indeed, *Phytophthora sojae* displays an apoplastic effector, called PsXLP1, able to promote infection by protecting PsXEG1, another effector with xyloglucanase activity essential for full virulence but targeted for inhibition by GmGIP1, a soybean protein. Then, PsXLP1 binds to GmGIP1 and functions as a decoy to protect PsXEG1 from the inhibitory action of GmGIP1 (Ma et al., 2017).

Some AEPs are considered as toxins, called necrosis-inducing proteins (NLPs), able to cause cell death. NLPs were first identified from culture filtrate of *Fusarium oxysporum* but have been isolated in oomycetes, fungi and bacteria, and have the ability to induce cell death and ethylene accumulation in plants (Gijzen and Nürnberger, 2006; Cobos et al., 2019). The structure of NLPs is remarkably conserved among long phylogenetic distance, from bacteria to oomycetes (Feng et al., 2014; Ottmann et al., 2009). However, the role of NLPs during infection is unclear. When studies reported evidences that NLPs function as virulence factors that increase pathogen growth in host plants or extend the host range (Veit et al., 2001;

Mattinen et al., 2004; Pemberton et al., 2005), others revealed that mutations in some NLP genes from various fungi like *Fusarium oxysporum* or *Botrytis cinerea* do not reduce their virulence (Cuesta Arenas et al., 2010; Bailey et al., 2002). In addition, most identified NLPs are perceived by the host as PAMPs leading to the stimulation of PTI, such as NLPs from *Phytophthora* species in *Arabidopsis* (Qutob et al., 2006, 2002), or from *Pythium* in various dicotyledonous plants (Veit et al., 2001).

In oomycetes, particularly in *Phytophthora* and *Pythium* species, elicitors represent another family of small AEPs and display similar characteristics with NLPs. Elicitors are structurally conserved and induce a sustained oxidative burst that leads to hypersensitive response (HR) cell death in most case (Derevnina et al., 2016). Plants from different botanical families perceived elicitors as MAMPs, which induce activation of defence through MAMP-triggered immunity (MTI) (Derevnina et al., 2016). Then, like NLPs, the role of elicitors is still unclear. Since elicitors bind sterol and other lipids (Osman et al., 2001) and given the fact that most oomycetes including *Phytophthora* are sterol auxotrophs, elicitors are proposed to act as sterol-carrier proteins (Mikes et al., 1998). As sterols and fatty acids stimulate sexual reproduction and oospore production in *Phytophthora*, elicitors could contribute to the appearance of more virulent strains (Chepsergon et al., 2020).

Finally it is anticipated that some apoplastic effectors, especially cyclic peptides, could play a role in self-defence against competitor antimicrobial compounds, or in manipulating the apoplastic microbiome to promote host colonization (Snelders et al., 2018; Rocafort et al., 2020).

I-3.2 b. Intracellular effectors: Destroy from within

The second class of effectors are secreted proteins translocated to the host cytoplasm or intracellular compartments. In oomycetes, the first (and the largest) family of cytoplasmic effectors, named RxLR effectors, were identified by comparative sequence analysis of predicted secreted avirulence proteins from several oomycete species, leading to the identification of a conserved amino acid motif, namely the RxLR-EER motif (Rehmany et al., 2005). Thus more than 350 RxLRs effectors characterized by their R (arginine) – X (any amino

acid) – L (Lysine) – R (arginine) motif after signal peptide sequence, were predicted in *Phytophthora* species (Tyler et al., 2006). Then presence of RxLR genes was evidenced in numerous *Phytophthora* species, where several hundred putative RxLRs were predicted (Haas et al., 2009; Jiang and Tyler, 2012), but only one in *Saprolegniales* species (Trusch et al., 2018). Finally, RxLR and RxLR-like effectors may also be present in fungi (Kale and Tyler, 2011) as in the endophytic fungus *Piriformospora indica* (named later *Serendipita indica*) in which 5 proteins with a degenerated RxLR motif were predicted to be secreted but none of them were found to be up-regulated during colonization of barley roots (Zuccaro et al., 2011).

RxLR proteins contain a conserved N-terminal motif in addition to a predicted signal peptide and a highly variable C-terminal part that allows biological function (Birch et al., 2006). It was proposed that the RxLR motif acts as a signal for host delivery (Whisson et al., 2007; Dou et al., 2008). In addition, RxLR effectors have been reported to translocate into host cells in the absence of the pathogen, after binding of the RxLR motif to lipids via phospholipid-mediated endocytosis (Kale and Tyler, 2011; Kale et al., 2010). However, studies made on other RxLR effectors could not observe this entry mechanism and finally exclude the phospholipid binding as a general host entry mechanism (Gan et al., 2010; Yaeno and Shirasu, 2013; Wawra et al., 2012). Then, pathogen-independent translocation of effectors into plant cells is controversially discussed and the entry mechanism of effectors is still unclear (Wawra et al., 2013). A recent study demonstrated that the RxLR motif of the *Phytophthora infestans* effector AVR3a was cleaved before secretion (Wawra et al., 2017). Even more recently, in the oomycete *Saprolegnia parasitica*, it was reported that the uptake process of the RxLR protein SpHtp3 is guided by a gp96-like receptor via its C-terminal region, but not by the N-terminal RxLR motif (Trusch et al., 2018). After translocation into host cell, a major part of RxLR effectors target nucleus, but some have a nucleo-cytoplasmic localization when others accumulate in membranes (Sperschneider et al., 2017), as described for the oomycete *Hyaloperonospora arabidopsidis* (Caillaud et al., 2012).

The identification of RxLR effectors with conserved motif and the availability of *Phytophthora infestans* genome lead to the discovery of another family of intracellular effectors named CRNs, for CRinkling and Necrosis effectors. CRNs were first identified in the plant pathogenic oomycete *Phytophthora infestans*. To identify pathogen-secreted proteins potentially involved in the manipulation of host processes, a large screen of cDNA coding for

secreted proteins were expressed in *N. benthamiana* and tomato leaves. Two of which, named CRN1 and CRN2, presenting similarities at the sequence level were found to cause a CRinkling and Necrosis (CRN) phenotype when expressed in plant tissue (Torto et al., 2003). Like RxLR proteins, CRNs present a modular architecture with a conserved N-ter signal characterized by LxLFLAK-derived amino acid sequence (with possible variation) followed by a highly variable C-ter domain (Schornack et al., 2010). With the increasing number of available genomes, many studies performed on other oomycetes revealed that, in contrast to the RxLR protein family, CRN coding genes are widespread in oomycete lineage, and were found in all plant pathogenic oomycetes sequenced to date including Peronosporales (Haas et al., 2009; Tyler et al., 2006; Baxter et al., 2010), Albuginales (Kemen et al., 2011), Pythiales (Adhikari et al., 2013; Lévesque et al., 2010) and Saprolegniales (Gaulin et al., 2008). Some CRN-like coding genes were also predicted in the animal pathogen *Aphanomyces astaci*, the causing agent of the Crayfish plague ((Gaulin et al., 2018) and see **CHAPTER IV**). The identification of hundreds CRNs genes in *Aphanomyces* species, which are early divergent species among the “crown” oomycetes, suggests that CRNs are an ancient class of conserved oomycete effector proteins (Schornack et al., 2010).

CRNs have a modular architecture with two distinct protein regions. The N-terminus domains, composed around 130 amino acids (aa), contains a conserved LxLFLAK or LxLFLAK-derivate motifs (within the first 60 aa) and more diversified DWL domains. Another highly conserved HVLVxxP motif marks the end of the N-terminal region (**Figure 5a**). This N-terminal part is presumed to specify the secretion and the translocation of the protein into the host. The functionality of CRNs N-termini domain was initially tested via an infection-translocation assay ((Schornack et al., 2010) and see P29-30 of this manuscript for more details). In this study, three CRN N-termini of *P. infestans* (CRN2, CRN8 and CRN16) and one *A. euteiches* (AeCRN5) were fused to C-terminal domain of the *P. infestans* Avr3a RxLR protein, and introduced in *Phytophthora capsici*. Those strains were used to infect transgenic *N. benthamiana* leaves expressing the potato resistance protein R3a.

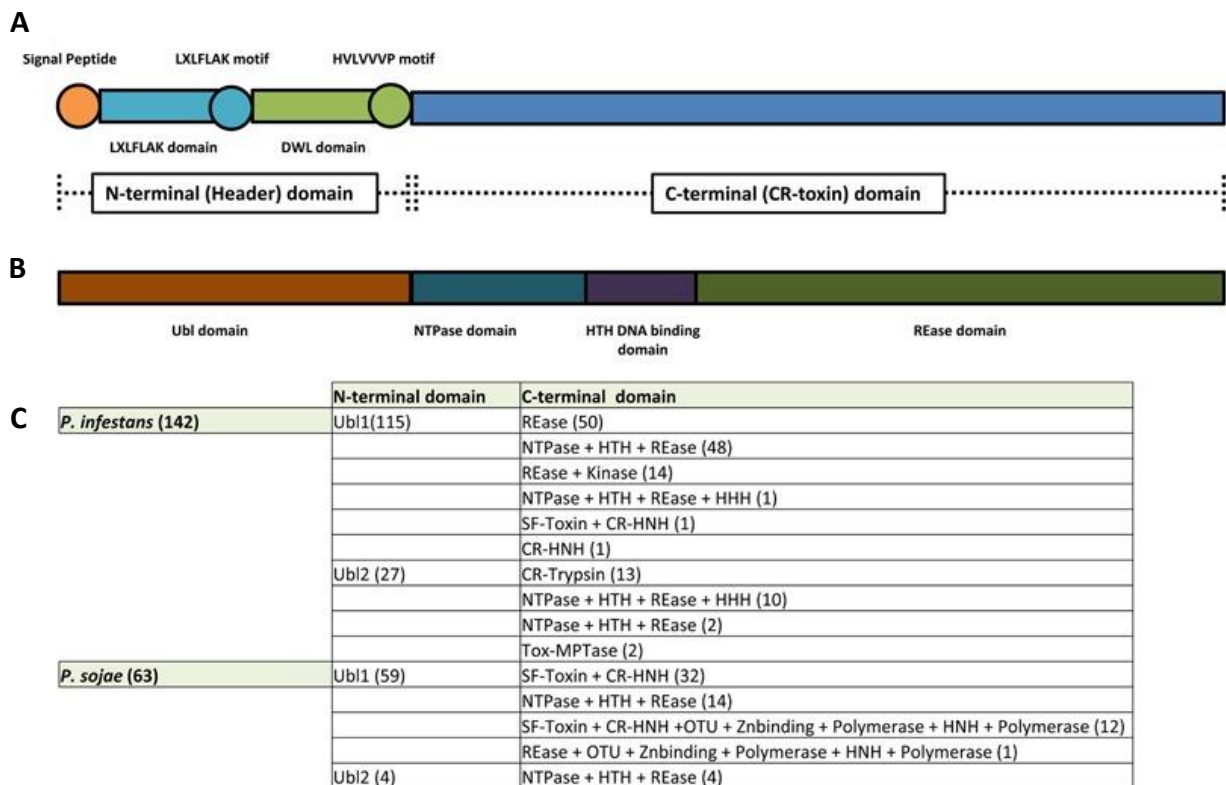


Figure 5: CRNs structure analysis (adapted from (Amaro et al., 2017)) .

(A) Initially CRN N-termini contain a conserved structure featuring: a signal peptide for secretion; an LXLFLAK domain containing the respective LXLFLAK motif connected with translocation; and a DWL domain that ends in a conserved HVLVVVP motif that marks the end of CRN N-terminus. This site is predicted as a hot spot for recombination events. In contrast, CRN C-termini were shown to exhibit a large variety of domain structures (not depicted here). (B) Zhang et al. (2016) redefined CRN structure. CRN N-termini (renamed header domains) from the two *Phytophthora* species analyzed (*P. infestans* and *P. sojae*) all feature an Ubiquitin like (Ubl) domain that is thought to be responsible for secretion and translocation into the host cell. CRN C-termini (also named CR-toxin domains) feature distinct domain architectures, having enzymatic origins. The majority of *Phytophthora* CRN C-termini contained the depicted domain structure (NTPase + HTH + REase). (C) Summary of domain architectures predicted to occur in *Phytophthora* (from Zhang et al., 2016). The number of CRN proteins with each given domain architecture/composition are indicated between brackets. Figure from (Amaro et al., 2017).

As chimera proteins induced avirulence by the recognition of the R3a protein, it was concluded that those N-termini domains allow secretion and translocation of C-termini CRN proteins into host cells. Even more, mutations in the LxLFLAK conserved motif indicate that these motifs are necessary for translocation function. Importantly, N-termini domains of AeCRN5 and CRN16 were demonstrated to be functional, even if no signal peptide were predicted in the first 30 amino acids. These results demonstrate that despite the absence of signal peptide, which was reported for numerous CRNs (Stam et al., 2013b; Voß et al., 2018; Amaro et al., 2017; Adhikari et al., 2013; Gaulin et al., 2018), an unpredictable secretion signal is present in this region and ensure secretion of CRNs in oomycetes (Schornack et al., 2010).

A recent study proposed to reconsider the requirement of LxLFLAK motifs in CRN translocation and challenged the classification of CRNs proteins as members of a larger order of Eukaryotic effectors (Zhang et al., 2016). In this paper, authors performed multiple *in silico* analyses using a combination of sequence alignments and structure prediction programs, coupled to comparative genomics to assess CRN occurrence across the Eukaryote taxon. Results of those analyses ruled out the presence of signal peptides and indicate that the proteins containing the LxLFLAK motif but also numerous proteins lacking this motif were predicted to have an ubiquitin-like structure, similar to those found in the N-terminal region of SSK1 (mitogen activated protein kinase) / Mcs4 (mitotic catastrophe suppressor 4) signalling proteins in fungi. The LxLFLAK motif was located in strand 2 and 3 of this ubiquitin-like domain (Ubl), suggesting that structural features rather than sequence conservation underpin CRN translocation (Zhang et al., 2016). Authors then renamed the N-terminal region as a Header Domain (**Figure 5b**). SSK1 orthologs play important roles in stress responses in various true fungi, such as oxidative and osmotic shock, and in some cases in a phosphorylation-dependent manner, employing an interaction between their N-terminal domains and a MAPKKK heteromer (Morigasaki and Shiozaki, 2013; Yu et al., 2016). From this, the authors suggest that CRN Ubl N-terminal domains could facilitate translocation inside the host by analogous mechanisms (Zhang et al., 2016) but functional studies are required to support this new concept. Similarly, the classification of CRN C-termini was challenged by the study of Zhang and colleagues (Zhang et al., 2016). Initially 36 different conserved subdomains that can assemble in different combinations defining C-terminal subfamilies were identified in *P. infestans* (Haas et al., 2009). Then it has been proposed that the highly variable

organisation of C-termini was the result of recombination events between subdomains. Following studies indicated that among oomycetes, most of these subfamilies are present and that specific subfamilies can also be found. For example, in *P. capsici*, 30 of these subfamilies are present while 7 new subfamilies appear specific to this species (Stam et al., 2013b). Similarly, in *A. euteiches*, 160 CRN gene models have been described, among which 12 C-terminal domains are novel subdomains (Gaulin et al., 2008). In the study of Zhang and colleagues, even if high levels of diversity are still present, the re-classification of CRN C-terminal domains led to a limited set of domain configurations that were found to be prevalent. Numerous CRN C-termini are related to enzymatic activities (**Figure 5c**). For instance, one-fourth of all CRN C-termini analysed contains a P-loop NTPase domain, coupled with a nuclease domain of the restriction endonuclease (REase) superfamily. In the same way, approximately one-sixth of the C-termini domains harbour REase superfamily domain combined with protein kinase domain. Then, those NTPase or Kinase domains, but also other domains like HNH domain, could regulate REase activity or affinity toward nucleic acids (Zhang et al., 2016), suggesting that targeting nucleic acids could be a shared feature among CRNs. This hypothesis is supported by two studies that report the DNA binding activity of CRN proteins in addition to the nuclear localization of numerous CRNs (Song et al., 2015; Ramirez-Garcés et al., 2016; Amaro et al., 2017).

CRN-like proteins were identified outside oomycete lineage, in the fungal pathogen *Batrachochytrium dendrobatidis* (Bd) and in the fungal symbiont *Rhizophagus irregularis* (Sun et al., 2011; Lin et al., 2014). The presence of CRN-like proteins in such different organisms suggests a HGT event or the presence CRN genes in early eukaryote progenitors (Sun et al., 2011; Lin et al., 2014). Bd causes chytridiomycosis and is responsible for the declines of amphibian population worldwide (Fisher et al., 2012; Scheele et al., 2019). Genome analyses of Bd strains revealed 84 CRN-like sequences presenting up to 46.5 % of similarity to CRNs of *P. infestans*, with a conserved modular architecture, comprising both LxLFLAK-derived signal and C-ter domains organization (Sun et al., 2011; Joneson et al., 2011). Comparative analyses of Bd with its closest relative, the non-pathogenic chytrid fungus *Homolaphlyctis polyrhiza*, highlight the absence of CRN-like sequences, suggesting a link between pathogenic processes and CRN effectors (Joneson et al., 2011). However, 42 genes were predicted with high sequence similarity and canonical amino acid motifs of CRNs in the arbuscular

endomycorrhizal (AM) fungus *Rhizophagus irregularis* (Lin et al., 2014). The functional characterization of the RiCRN1 protein evidenced the biological role of this Crinkler in the establishment of the symbiosis, especially on the initiation of arbuscule development (Voß et al., 2018). Furthermore, the study of Zhang *et al.* revealed that CRN effectors are also present in free-living eukaryotes and land plants that are not known to have a pathogenic lifestyle, indicating that CRNs are widespread in Eukaryotes (Zhang et al., 2016). Thus it was proposed that CRN proteins could be firstly involved in inter-organismal conflicts, after which in some host-pathogen interactions, these proteins were co-opted as effectors (Zhang et al., 2016; Amaro et al., 2017).

In contrast to oomycetes, intracellular fungal effector lacks a conserved sequence that facilitate their prediction; therefore, their identification relies on small-secreted proteins (SSPs). Typical fungal pathogens possess several hundreds and sometimes more than a thousand of these SSP effectors. SSPs are defined as proteins of less than 300 amino acids with a signal peptide and devoid of any functional domains. Many SSPs are coded by orphan genes, lacking known domains or similarities to known sequences, and usually are cysteine-rich proteins. Large repertoires of SSPs have been evidenced upon genome annotation of fungi interacting with plants (Duplessis et al., 2011; O'Connell et al., 2012), nematodes (Meerupati et al., 2013), insects (Hu et al., 2014) and human (Vivek-Ananth et al., 2018). Thus, SSPs were initially described as virulence effectors produced by pathogens, but finally large repertoire of SSPs were also predicted in mycorrhizal fungi (Martin and Selosse, 2008; Kamel et al., 2017) and their role in the establishment of symbiosis evidenced, like MiSSP7 from the ectomycorrhizal fungus *Laccaria bicolor* (Plett et al., 2011, 2014). SSPs were also reported in bacteria in the plant pathogen *Pseudomonas syringae* (Shindo et al., 2016), and finally within the scope of this PhD study, SSPs were described in oomycete genomes ((Gaulin et al., 2018) and see **CHAPTER IV**).

Within the fungal kingdom, the proportion of SSPs ranges from 40 to 60% of the secretome across all lifestyles and phylogenetic groups (Feldman et al., 2020; Pellegrin et al., 2015; Kim et al., 2016). However, it seems that this proportion may vary depending on the lifestyle. For instance obligate biotrophs likely encode more and diverse effector-like SSPs to suppress host defence compared to necrotrophs, which generally use cell wall degrading enzymes and phytotoxins to kill hosts (Kim et al., 2016). Comparative analyses of secretomes

also identified shared or lifestyle-specific SSPs between saprotrophic and Ectomycorrhizal (ECM) fungi, indicating that presence of SSPs is not limited to fungi interacting with living plants (Pellegrin et al., 2015).

Some sequence similarity leads to the classification of SSPs in superfamily as in *Blumeria graminis*. Sequence analyses of candidate secreted effector proteins (CSEPs) of the powdery mildew revealed that 25% of those CSEPs, highly expressed in haustoria, contain features resembling catalytically inactive RNases. Thus, they are part of the superfamily of RnAse-Like Proteins associated with Haustoria, the so-called 'RALPH' effectors (Pedersen et al., 2012). Recently, a new family of small fungal effectors, that has particularly expanded in the fungus *Magnaporthe oryzae*, was described (de Guillen et al., 2015) and was called the MAX family for *Magnaporthe* Avrs and ToxB-like effectors. Despite sharing little protein sequence similarity, MAX effectors are characterized by a conserved structure. Those effectors have different shapes and surface properties suggesting that they target different host processes.

How SSPs are addressed within the host cytoplasm is still an opening question, but when transiently express *in planta*, numerous SSPs localized in nucleus or nucleolus, but some can be found in mitochondria or chloroplasts (Petre et al., 2015). Recently, plant Golgi, peroxisomes and microtubules were also reported as targets for fungal SSPs (Robin et al., 2018).

I-3.3. Intracellular effectors targets: hit the defence key players

To promote microbial colonization, effectors could favour microbial growth by manipulating plant defences and/or by enhancing invader nutrition. Thus, functions and targets of intracellular effectors are diverse and range from altering plant cellular metabolic pathways, signalling cascades, RNA silencing, transcription, trafficking and interfering with DNA machinery.

One of the primary mechanism targeted by intracellular effectors is to suppress the host response by targeting crucial compounds. For instance, the two essential defence phytohormones salicylic acid (SA) and jasmonic acid (JA) that act antagonistically in response to pathogen infection (Niki et al., 1998) can be modulated by effectors. Cmu1, from the maize pathogenic fungus *Ustilago maydis*, is secreted into the host cell and acts as a chorismate

mutase to reduce SA levels during infection (Djamei et al., 2011). Similarly, effectors PsIsc1 from *Phytophthora sojae* and VdIsc1 from *Verticillium dahliae* reduce the amount of SA by hydrolyzing isochorismate, a precursor to SA, when expressed within plant cells (Liu et al., 2014). HaRxLR44 from the oomycete *Hyaloperonospora arabidopsidis* degrades Mediator subunit 19a (MED19A) to alter the balance of JA and SA, which affects defence-related transcriptional changes (Caillaud et al., 2013). Other plant metabolites can also be modulated by effectors. The SSP Tin2, from *Ustilago maydis*, prevents the degradation of the maize protein kinase ZmTTK1, which is responsible for the activation of genes involved in anthocyanin biosynthesis. This overproduction of anthocyanins turns to plant defence detriment, since anthocyanin biosynthesis competes with tissue lignification, promoting the pathogen to reach vascular tissue due to a lower content of lignin (Tanaka et al., 2014). Additionally, the RxLR PSE1 from *Phytophthora parasitica* interferes with auxin physiology through the redistribution of auxin efflux carrier proteins, modulating auxin content which enhances pathogen infection (Evangelisti et al., 2013).

Another key point of plant defence response is the reactive oxygen species (ROS) production, which plays a role in MTI, phytoalexin production, callose deposition and systemic acquired resistance (SAR) (O'Brien et al., 2012). Crinkler PsCRN63 from *Phytophthora sojae* interacts and destabilizes plant catalases to promote plant cell death, whilst PsCRN115 inhibits the catalases degradation to maintain the proper H₂O₂ levels and block plant cell death (Zhang et al., 2015).

Plant defence responses are also dependent on signalling pathways like MAPK cascades, which are essential for both MTI and ETI. Then it is not surprising to find effectors that evolved to block these pathways. For instance, the RxLR PexRD2 from *P. infestans* interacts with the kinase domain of MAPKKKε to interrupt plant immunity-related signalling (King et al., 2014).

Some effectors play a role in the disruption of various trafficking pathways that lead to the secretion of defence proteins. In *Blumeria graminis*, BEC4 Interacts with ARF-GAP protein, a key player of membrane vesicle trafficking in eukaryotic cells (Schmidt et al., 2014). Pi03192, an RxLR from *P. infestans* is able to prevent the re-localisation of two plant NAC transcription factors from the endoplasmic reticulum to the nucleus (McLellan et al., 2013). To ended, still in *P. infestans*, PexRD54 stimulate autophagosome formation through binding to the autophagy protein ATG8CL (Dagdas et al., 2016). This activation of autophagy suggests that

the pathogen produce this effector to selectively eliminate some of the molecules that the plant use to defend itself (Dagdaz et al., 2016).

Another major defence mechanism is RNA silencing. This process was firstly described in plant-virus interactions, where viral RNA is recognized as a MAMP and induces small interfering RNAs (siRNAs) which trigger the cleavage of viral RNAs. In response, viruses have developed suppressors of RNA silencing to allow the virus proliferation in the host (Vance, 2001). This defence system is also targeted by other microbes. PSR1 and PSR2, two RxLR effectors from *P. sojae*, suppress RNA silencing and enhance susceptibility to *P. sojae* (Qiao et al., 2013). PSR1 is able to bind with a conserved nuclear protein called PSR1-interacting protein 1 (PINP1), which is involved in small RNA biogenesis. Alteration of small RNA production in plants leads to developmental defects and hyper-susceptibility to *Phytophthora* infections, which is similar to transgenic plants expressing the PSR1 protein (Qiao et al., 2015). A PSR2-like effector was found in the related species *Phytophthora infestans* with the same RNA silencing suppression activity, meaning that PSR2 represents a prevalent effector family conserved within the genus *Phytophthora* (Xiong et al., 2014). Then, in viruses and oomycetes, RNA silencing suppression is a key strategy for infection (Qiao et al., 2013).

Inhibition or alteration of gene transcription in order to down regulate genes involved in defence responses is also a common process shared by various microorganisms to facilitate the association with the plant. In *Rhizophagus irregularis*, SP7 targets nucleus and interacts with the transcription factor ERF19 to block the plant immune system (Kloppholz et al., 2011). The RxLR PsAvh23 from *P. sojae* disrupts the formation of the ADA2-GCN5 subcomplex and subsequently represses the expression of defence genes by decreasing GCN5-mediated H3K9ac levels, suggesting that the pathogen manipulates host histone acetylation to gain virulence (Kong et al., 2017).

Transcription can also be altered by effectors which bind directly to nucleic acids, like PsCRN108 from *P. sojae* which targets HSP promoters to block association with heat shock transcription factors (Song et al., 2015). Furthermore, nucleic acids and especially DNA itself could be targeted, as AeCRN13 from *Aphanomyces euteiches*, where it binds directly to DNA and triggers double strand breaks (Ramirez-Garcés et al., 2016).

Finally, the vast majority of intracellular effectors from different fungal and oomycete families, including RxLR, CRNs and SSPs, localizes in nucleus when expressed in host tissue. Since it was evidenced that plant DNA is altered during infection of various pathogens (Song and Bent, 2014) and regarding the large number of intracellular effectors that target nucleus, we propose that DNA-damaging effectors could be a family of proteins involved in plant-filamentous pathogen interactions and represents the subject of the Chapter II of this thesis (see Chapter II: DNA-Damaging Effectors: New Players in the Effector Arena).

I-4. *Aphanomyces*: an oomycete genus to study effectors and host adaptation

The *Aphanomyces* genus belongs to the Saprolegniales order and has been shown to contain three major lineages, including plant pathogens, aquatic animal pathogens, and saprophytic species (Diéguez-Uribeondo et al., 2009), making this genus an interesting model to understand evolutionary mechanisms involved in adaptation of oomycetes to distantly related hosts and environmental niches (**Figure 6**). It contains around 40 species, but this number is inconsistent due to the difficult culture and identification of some species.

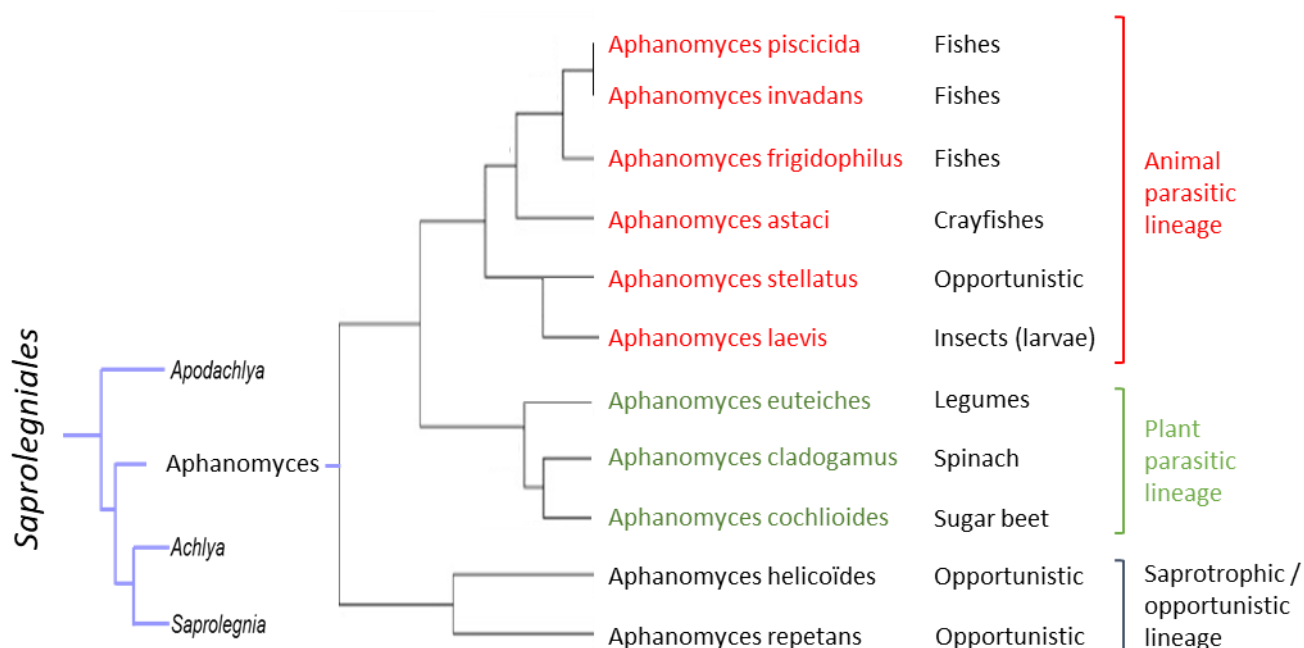


Figure 6: Phylogeny of *Aphanomyces* genus, lifestyle and principal hosts.

This consensus phylogenetic tree is based on analyses of ITS sequences of nuclear rDNA of the principal *Aphanomyces spp* identified. Principal hosts are indicated next to the species name. The phylogenetic tree correlates to the lifestyles species: a plant pathogen lineage, a saprophytic / opportunistic lineage and animal pathogenic lineage. *A. laevis* is generally assigned as saprotroph but one study has reported a larvicidal activity in mosquito larvae (Patwardhan et al., 2005). The position of *A. stellatus* is not yet clearly defined. It has been found as a free-living species but its ITS sequence analyses branched it with *A. laevis* into the animal parasitic lineage (Sarowar et al., 2019). The scheme was performed based on (Diéguez-Urbeondo et al., 2009; Patwardhan et al., 2005; Sarowar et al., 2019; Iberahim et al., 2018).

Most of these species are aquatic animal parasites, such as *A. invadans*, *A. piscicida* and *A. frigidophilus*, which infect a wide range of freshwater and estuarine fishes. *Aphanomyces astaci*, the causing agent of the crayfish plague, has been nominated among the “100 of the World’s Worst Invasive Alien Species” in the Global Invasive Species Database (Gaulin et al., 2018). Two more species are related to animal parasitic lineage with less confident evidences. *A. laevis* is generally assigned as saprotroph but one study has reported a larvicidal activity in mosquito larvae (Patwardhan et al., 2005). Similarly, *A. stellatus* was considered as a saprotroph but one study reported that it can act as opportunistic pathogen on crustaceans (Royo et al., 2004). Furthermore, ITS sequence analyses branched it with *A. laevis* into the animal parasitic lineage (Sarowar et al., 2019).

A second lineage includes species with prevalence for saprophytism as *A. repetans* and *A. helicoïdes* and can exhibit opportunistic parasitism, notably on crayfish (Diéguez-Urbeondo et al., 2009).

The third lineage is related to plant parasitic species that is restricted to *Aphanomyces* genus in the Saprolegniales order. Within, *A. cladogamus* has a broad range of hosts including different families such as Fabaceae (e.g. common bean), Poaceae (e.g. barley), Solanaceae (e.g. tomato) and Chenopodiaceae (e.g. spinach). At the opposite, *A. cochlioides* is confidently reported so far only on sugar beet. In the same way, *A. euteiches* seems to be restricted to Fabaceae species (Diéguez-Urbeondo et al., 2009).

The diversity of lifestyles and hosts in *Aphanomyces* species is in contrast with species of the Peronosporalean lineage that are mainly phytopathogens, giving to *Aphanomyces* genus a special taxonomic position towards Peronosporales, but also among Saprolegniales, mostly composed by aquatic animal pathogens (with few exceptions for *Achlya spp.* (Choi et al., 2019).

I-4.1. *Aphanomyces euteiches*, the Legume threat

Among the most damaging *Aphanomyces* species is the root rot legume pathogen *Aphanomyces euteiches*. *Aphanomyces euteiches* Drechs was firstly described by Jones and

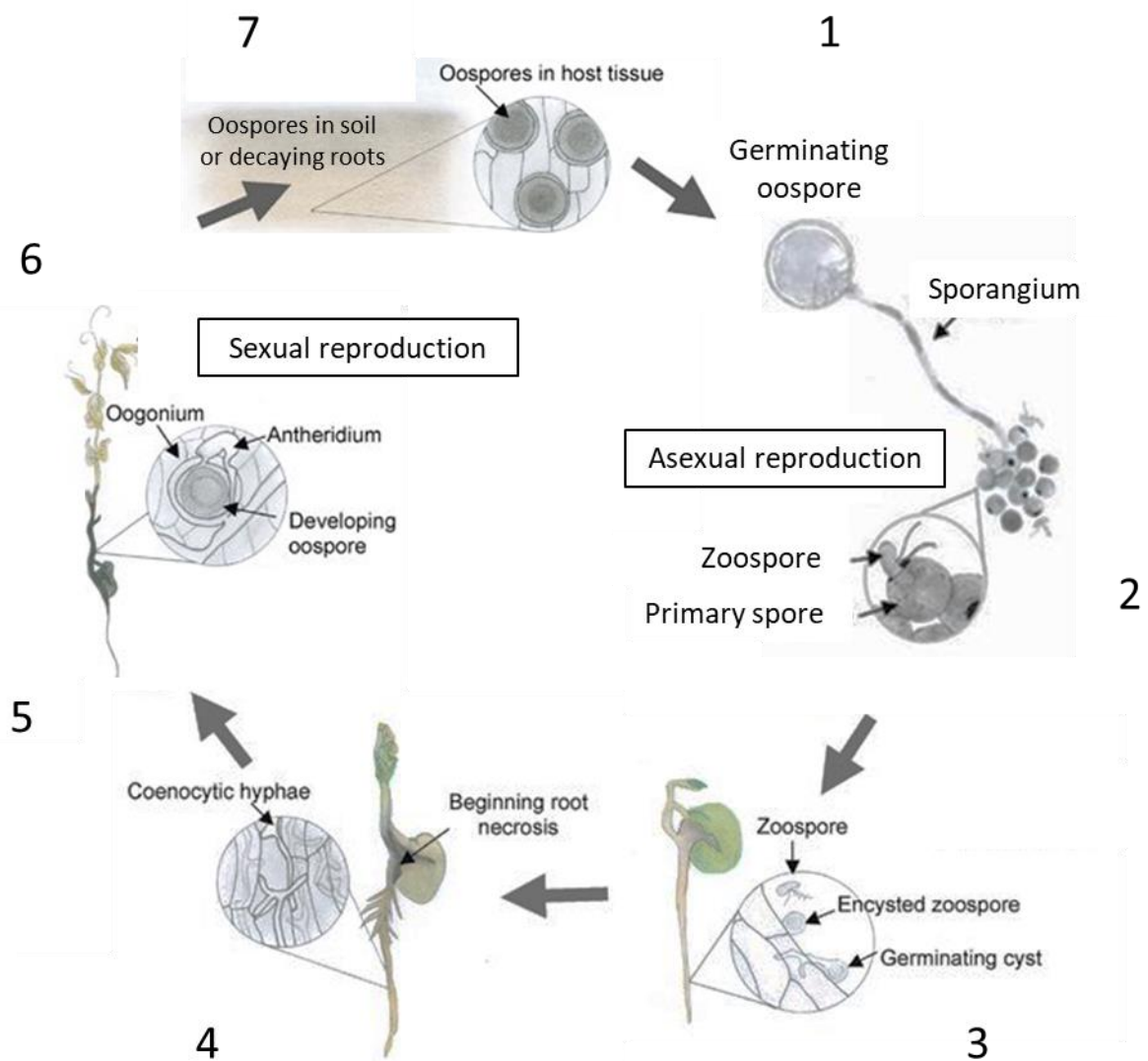


Figure 7: Life cycle of *Aphanomyces euteiches*.

(1) Oospores present in the soil germinate and produce a sporangium. (2) At the sporangium apex, primary spores release hundreds of bi-flagellate motile zoospores through a pore of their cell wall (asexual reproduction). (3) Zoospores produce adhesive molecules and adhere to root cells to encyst, losing their flagella. (4) Germinated cyst produced coenocytic hyphae, which develop between the cells, in the extracellular space. (5) Growing hyphae colonize the root system and subsequently progress to hypocotyls. (6) Differentiation of hyphae into antheridia and oogonia leads to sexual reproduction, where haploid nuclei from antheridia are delivered into oogonia to produce diploid oospores. (7) Decaying tissue release oospores that can remain in soil for many years, ready to infect new hosts. Adapted from (Hughes and Grau, 2007).

Drechsler (1925) after analyses on various pea diseases in the United States. Nowadays, it is reported that *A. euteiches* causes significant damages to various legume crops worldwide (Gaulin et al., 2007), including pea (*Pisum sativum*), alfalfa (*Medicago sativa*), faba bean (*Vicia faba*), common bean (*Phaseolus vulgaris*), lentil (*Lens esculenta puyensis*), the red and white clover (*Trifolium pratense* and *T. repens*) and can also infect the leguminous model plant *Medicago truncatula* (Badis et al., 2015; Bonhomme et al., 2014). However, virulence and symptoms are variable from one host to another. Distinct subspecific groups based on genotype and host preference have been defined resulting in two major pathotypes: pea-infecting strains and alfalfa infecting strains from the USA and from France (Malvick and Grau, 2001; Wicker et al., 2001). Economically, *A. euteiches* is a major concern for pea production and causes devastating root rot disease in many pea-growing countries including Europe (especially in France), Australia, New Zealand, and throughout the USA. Plants can be infected at any age, but germinated seeds are the most susceptible (Pilet-Nayel et al., 2018). *Aphanomyces* life cycle harbours sexual and asexual stages that occur in soil. Sexual reproduction leads to the formation of oospores, which can survive in soil for up to 10 years (Papavizas and Ayers, 1974). The presence of a root triggers oospore germination, leading to a germ tube and a long terminal zoosporangium that can release more than 300 bi-flagellate motile zoospores (Gaulin et al., 2007) (**Figure 7**). The morphology of the zoospores and especially the structure of their two flagella is a common attribute in oomycetes. To target host tissue, it has been shown for various oomycetes that the motile zoospores are chemotactically attracted by compounds from root exudates (reviewed in (Walker and van West, 2007). For instance, zoospores of *Aphanomyces cochlioides* show chemotaxis towards the host derived flavone cochliophilin A (Sakihama et al., 2004). After reaching the host, the zoospores encyst, releasing adhesive chemicals to adhere to the host tissue, leading to the loss of both flagella and the formation of a primary cell wall (**Figure 7**). Zoospore encystment and germination is regulated by calcium ions (Warburton and Deacon, 1998). Unlike other plant pathogenic oomycete such as *Phytophthora infestans*, the presence of appressorium, a specific penetration structure, has never been reported for *A. euteiches*. Once entered inside the root tissue, *A. euteiches* forms extracellular coenocytic hyphae (multiple nuclei) (Gaulin et al., 2007) (**Figure 7**). Then the pathogen colonize the entire root and reach the stem, provoking the disintegration of cortex tissue leading to water-soaked areas of roots, which become brownish. After few days, haploid antheridia (male reproductive structures) and oogonia

(female reproductive structures) are formed. Then antheridia deliver male nuclei to oogonia through fertilization tubes, resulting in the formation of diploid oospores (**Figure 7**).

Efficient chemical controls do not exist, fully resistant pea nor alfalfa cultivars neither. Then, prophylactic measures and crop rotation are preconized, such as cultivating non-host legume like lupin (*Lupinus angustifolius*) or chickpea (*Cicer arietinum*). However, the development of tolerant cultivars appears to be the most effective and promising management available to farmers. Various studies identified several quantitative trait loci (QTLs) that mediated the partial resistance in pea (Hamon et al., 2013; Desgroux et al., 2016; Lavaud et al., 2016). In parallel, whole genome sequencing data combined with genome-wide association studies (GWAS) performed on the model plant *M. truncatula* allowed the identification of promising QTLs involved in the resistance to the parasite (Bonhomme et al., 2014, 2019).

I-4.2. *Aphanomyces euteiches* – *Medicago truncatula* pathosystem

To decipher the molecular interactions between host plants and *A. euteiches*, from mechanisms of partial resistance to the role of effectors in the infection process, our research group developed an *Aphanomyces euteiches* / *Medicago truncatula* pathosystem. *Medicago truncatula* is a well-known legume model plant closely related to the cultivated alfalfa (*M. sativa*), able to engage root symbioses with both nodulating bacteria and arbuscular mycorrhizae fungi (Jones et al., 2007; Parniske, 2008). Furthermore, *Medicago truncatula* is a natural host for various crop legume pathogens, including *A. euteiches*. Additionally, a wide collection of mutants and natural genotypes are available for the scientific community and genomic resources include sequences of almost 300 accessions (Stanton-Geddes et al., 2013). *A. euteiches* reference strain used in the lab is a pea infecting strain (ATCC 201684) and *M. truncatula* genotypes display wide range of tolerance to this strain. Two accessions are commonly used for their opposite resistance degrees to *A. euteiches*, the A17 Jemalong line which is partially resistant, and at the opposite the highly susceptible F83005.5 line.

A clear contrast in tolerance is evidenced with *in vitro* infection assays performed on A17 and F83005.5 lines. In both lines, upon inoculation of roots with zoospores, *A. euteiches*

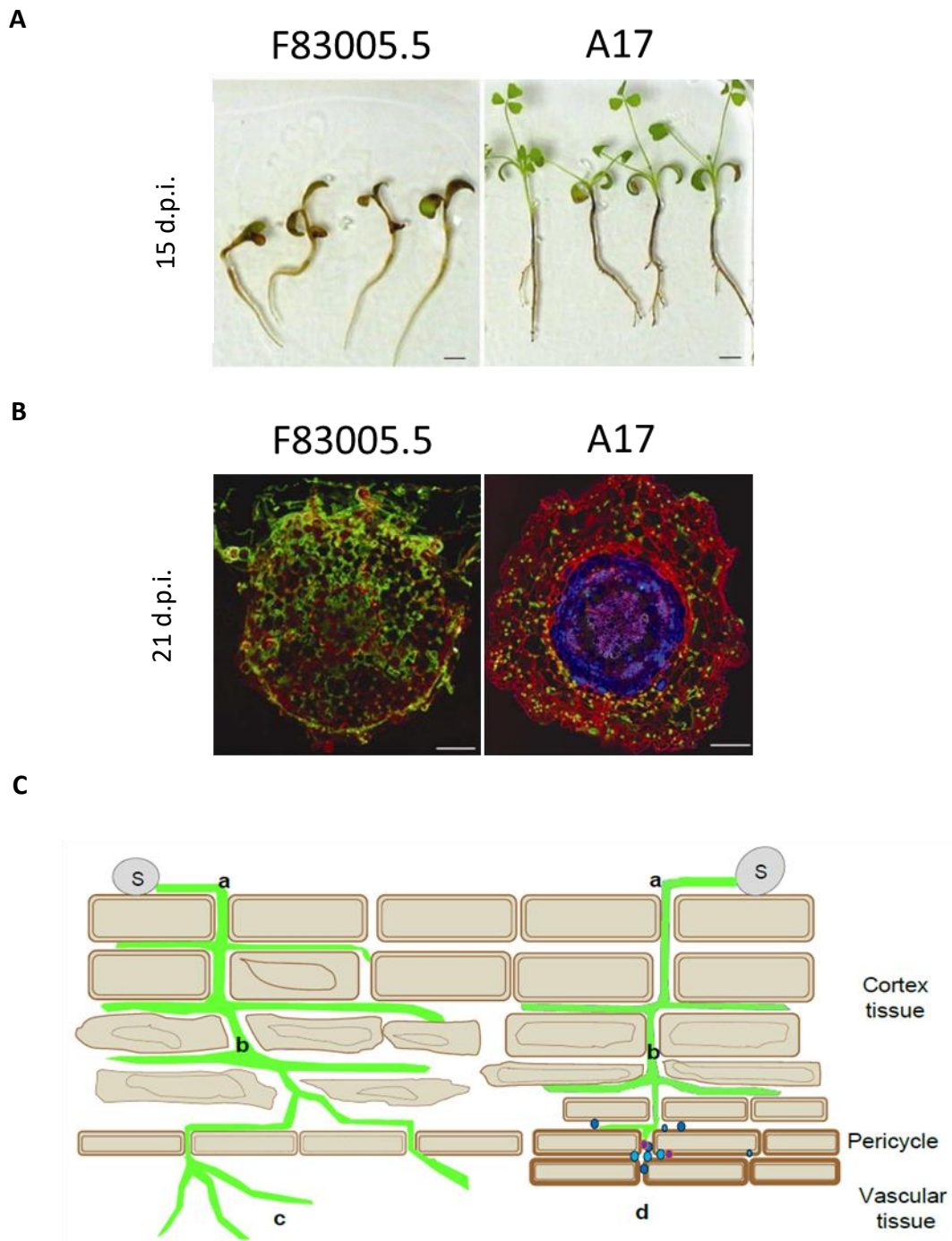


Figure 8: Infection model in the *Aphanomyces euteiches*/*Medicago truncatula* pathosystem.

(A) Macroscopic symptoms of *M. truncatula* susceptible line F83005.5 and partially resistant line A17 infected with *A. euteiches* spores in *in vitro* conditions. Pictures were taken at 15 days post inoculation (dpi). Adapted from (Djébalı et al., 2009). (B) Cross-sections of infected roots showing full invasion (F83005.5) and partial invasion (A17) by *A. euteiches* (in green). Plant cell walls are coloured in red. A17 plants produced antimicrobial phenolic compounds (in blue) in the central cylinder. Pictures were taken at 21 dpi. Adapted from (Djébalı et al., 2009). (C) Scheme of a transversal section of a root infected by *A. euteiches* (in green).

On the left side, the scheme describes infection in F83005.5 where an asexual spore (S) has landed on the rhizoplane and germinated to produce a germ tube giving rise to an infectious hyphae that directly penetrates root cortex tissues (a). Hyphae develops between root cells of cortex which becomes completely colonized 6 days post inoculation. Cortical cells died as *A. euteiches* develops leading to root disassembly and water-soaked symptoms typical of root rot disease (b). The pathogen reaches the vascular cylinder before completion of its cycle (not shown) (c). On the right side, the infection is depicted in the tolerant host (A17) where the plant produces supplementary pericycle cell layers with higher levels of lignin in their cell walls, reinforcing the root stele. In addition to this mechanical barrier, cells produce antimicrobial compounds (in blue) (d). These cytological responses restrain the advance of the pathogen to the vascular cylinder. Scheme from (Ramirez-Garcés, 2014).

hyphae penetrate inside the roots and grow between cells of the outer cortex tissue within 1 day. As mentioned above, no specialized infectious structures as appressoria or haustoria have been reported. The pathogen presents an intercellular development and invades the whole cortex area within 3 to 6 days. 15 days post inoculation (dpi) with *A. euteiches* zoospores, susceptible F83005.5 plants harbour no or few leaves and very few secondary roots, while the tolerant A17 plants still develop aerial part and present branched brownish roots (**Figure 8a**). At 21 dpi, most of susceptible plants are dead (Djébali et al., 2009). While oomycete cell wall is mostly composed by cellulose, *A. euteiches* has an original cell wall containing around 10% of chitosaccharides exposed at the cell wall surface (Badreddine et al., 2008; Nars et al., 2013). This structural characteristic allows the staining of hyphae using wheat-germ agglutinin lectin (WGA) coupled with fluorophore. Confocal analyses performed on cross section of inoculated A17 or F83005 roots revealed a whole colonization of all cell layers in the susceptible lines, indicating that the pathogen reached the central cylinder (**Figure 8b**). Invasion of vascular system in F83005 lines seems to start after 6 dpi and is confirmed at 15 and 21 dpi. In contrast, in the tolerant A17 plants, *A. euteiches* hyphae were restricted to the root cortex, where defence related phenolic compounds are produced (**Figure 8b**) (Djébali et al., 2009). In addition to phenolic compounds production, A17 plants produce supplementary pericycle cell layers coupled with a reinforcement of the cell walls that might act as a physical barrier for the invading hyphae (**Figure 8c**). Furthermore, partial resistance of A17 is correlated to an increase of lateral roots (Djébali et al., 2009).

Genetic approaches coupled to the characterization of infection phenotypes in *M. truncatula* have led to the identification of a major QTL (Djébali et al., 2009). Forward GWAS experiments refined this result and identified several candidate genes and pinpointed two independent major loci (Bonhomme et al., 2014). Within the most significant locus, Single Nucleotide Polymorphisms (SNPs) found in the promoter and coding region of an F-box gene have been spotted out and linked to the variable tolerance of *M. truncatula* against *A. euteiches* (Bonhomme et al., 2014). Additionally, it was shown that basal levels of flavonoids play a significant role in resistance to *A. euteiches*, and could inhibit zoospore germination (Badis et al., 2015). Finally, recently, a local score approach technic improved GWAS resolution, refining the previously reported major locus, underlying a new tyrosine kinase candidate gene involved in resistance, and detected minor QTLs (Bonhomme et al., 2019).

I-4.3. Insight into *Aphanomyces euteiches* intracellular effectors

Before this PhD, previous analyses on *A. euteiches* were performed to gain insights into effectors biology and to unravel the biological functions of identified intracellular effectors. A first transcriptomic analysis on *A. euteiches* revealed the absence of RxLR effectors while more than 160 CRN genes have been detected (Gaulin et al., 2007). Among them, some are induced during plant colonization, such as AeCRN5 and AeCRN13. We then characterized one of these CRNs, AeCRN13, which harbours an N-ter domain containing a characteristic LYLALK motif (derivate of the LxLFLAK motif in *Aphanomyces*) coupled with HVLVxxP motif, followed by a C-ter domain composed by DFA-DDC subdomains reported in *Phytophthora* CRN13s (Ramirez-Garcés et al., 2016) (**Figure 9a**). This work reports that AeCRN13 act as a genotoxin through its binding to plant DNA and activates DNA-damage responses (DDR). It also provides evidences that the effect is conserved among CRN13 family since its closest ortholog from the

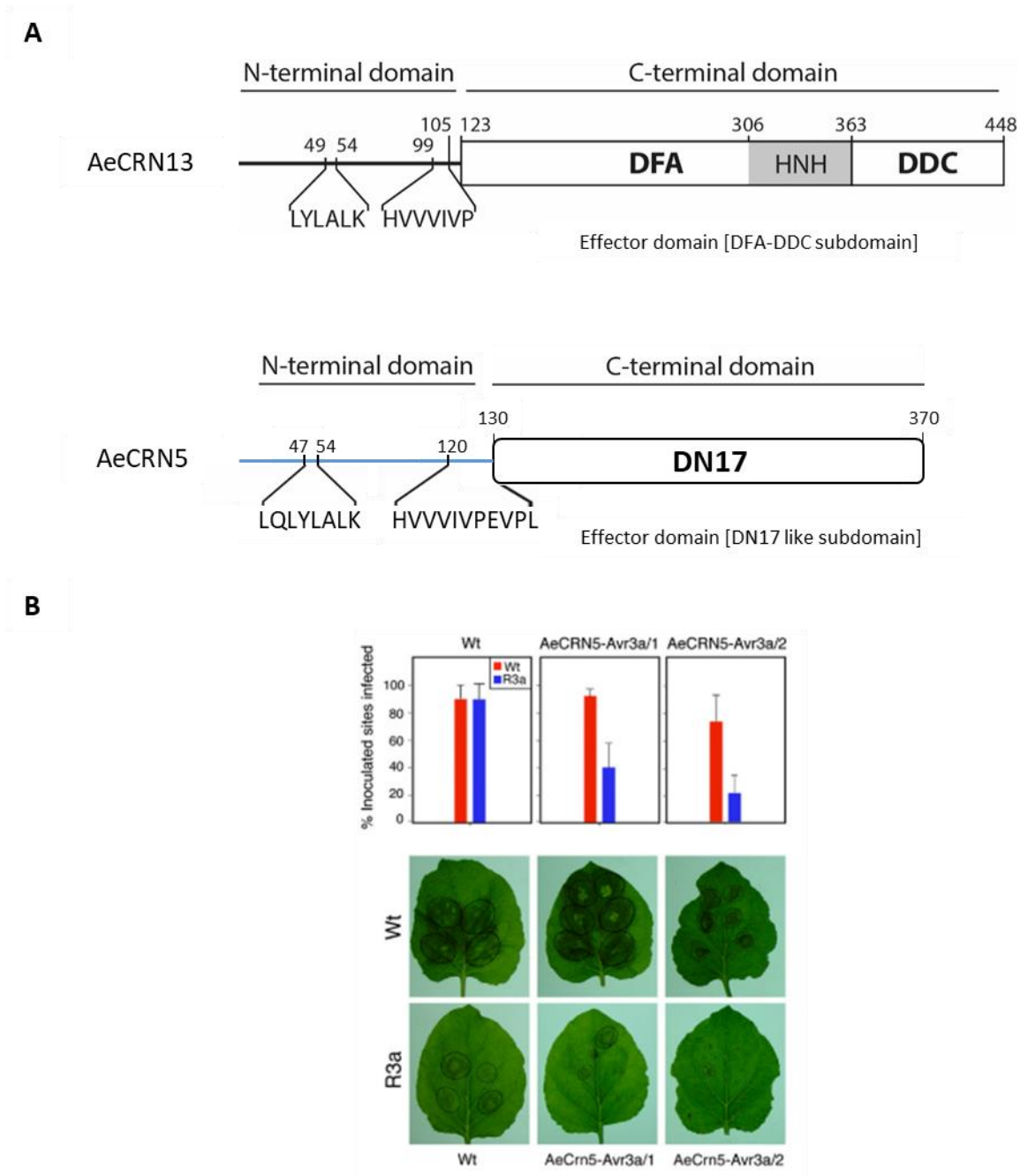


Figure 9: Structure of AeCRN13 / AeCRN5 proteins and translocation assay of AeCRN5.

(A) Diagram depicting the modular architecture of AeCRN13 (upper panel) and AeCRN5 (lower panel) from *A. euteiches* with the conserved N-terminus, which includes the LxLYLALK and HVVVIVP motifs, and the C-terminal region containing the DFA - DDC subdomains for AeCRN13 and the DN17 subdomain for AeCRN5, based on *P. infestans* Crinkler (CRN) domain nomenclature. AeCRN13 DNA binding domain HNH (AA 306-363) is indicated in grey box. Adapted from (Ramirez-Garcés et al., 2016). (B) The AeCRN5 N-terminus fused to C-terminal AVR3a conditions avirulence on R3a but not on wild-type *N. benthamiana* leaves. Top panels: Quantification of infection rates across three independent experiments (4 dpi). Bottom panels: The wild-type and transgenic R3a leaves inoculated with strains analyzed in top panels. Pictures were taken 4 dpi with zoospore suspensions. Lesions are marked by circles. Adapted from (Schornack et al., 2010).

chitrid fungus *B. dendrobatidis* acts similarly. Both Ae and Bd CRN13 proteins contain an HNH motif widespread in metal finger endonucleases present in all life kingdoms. This motif is responsible of the DNA binding ability of AeCRN13 since a mutated version in this domain failed to bind DNA. Hence, AeCRN13 and BdCRN13 trigger DNA double strand breaks. We then reported that the plant senses this insult and activates the DDR pathway to repair its DNA (Ramirez-Garcés et al., 2016).

Sequences analyses of AeCRN5 confirmed the presence of the conserved motifs LxLYLALK and HVVVIVP within the N-terminal domain. Then, DN17-like subdomain was revealed by comparison of the C-terminal domain with *P. infestans* Crinkler domain nomenclature (**Figure 9a**). To assess if the N-terminal domain of CRNs could be responsible of the translocation of the C-terminal domain of the protein in host cells, our research group collaborated with Schornack and colleagues to perform translocation assays on various CRNs from Peronosporales or Saprolegniales members. The principle of these assays is based on the recognition of the C-terminal domain of the avirulence protein Avr3a from *P. infestans* by the resistance protein R3a which takes place in the cytosol of plant cells. This recognition leads to ETI and full depletion of infection. Chimeric constructs containing N-terminal domains of CRNs, notably AeCRN5, fused to C-terminal domain of Avr3a were introduced into *P. capsici*. Inoculation of this *P. capsici* strains on wild-type *N. benthamiana* leaves (lacking R3a) leads to normal infection symptoms, but failed to infect *R3a N. benthamiana* leaves, constitutively expressing R3a resistance proteins, indicating recognition of the AVR3a effector domain by intracellular R3a (**Figure 9b**). These results evidenced that the N-terminal domain of AeCRN5 can mediate the delivery of the effector protein inside host cells (Schornack et al., 2010).

I-5. Scope of the thesis

I joined the LRSV research team in 2011 as CNRS engineer (IE) and I started to work on functional analysis of *Aphanomyces euteiches* effector thanks to my expertise on molecular biology on plant viruses developed in Paris in the team of Isabelle Jupin (Institut Jacques Monod).

When I started my thesis in 2018, the major part of intracellular effectors described in plant pathogenic interactions was reported to target plant nucleus, such as all CRNs and numerous RxLR from phytopathogenic oomycetes, or numerous fungal SSPs. At this time only two microbial effectors were evidenced to target host DNA: AeCRN13 studied in our research group (Ramirez-Garcés et al., 2016) and PsCRN108 from *P. sojae*, a CRN which binds to DNA to deregulate HSP genes expression (Song et al., 2015). In addition, we also discovered by confocal analysis and transient expression in *Nicotiana* cells that AeCRN5 also target plant nucleus, suggesting that this CRN may also play a role at the nuclear level. While there was accumulating evidences that effector from bacteria target host nucleus and act as DNA-damaging compounds in mammalian cells, only AeCRN13 was reported as a eukaryotic DNA-damaging effector.

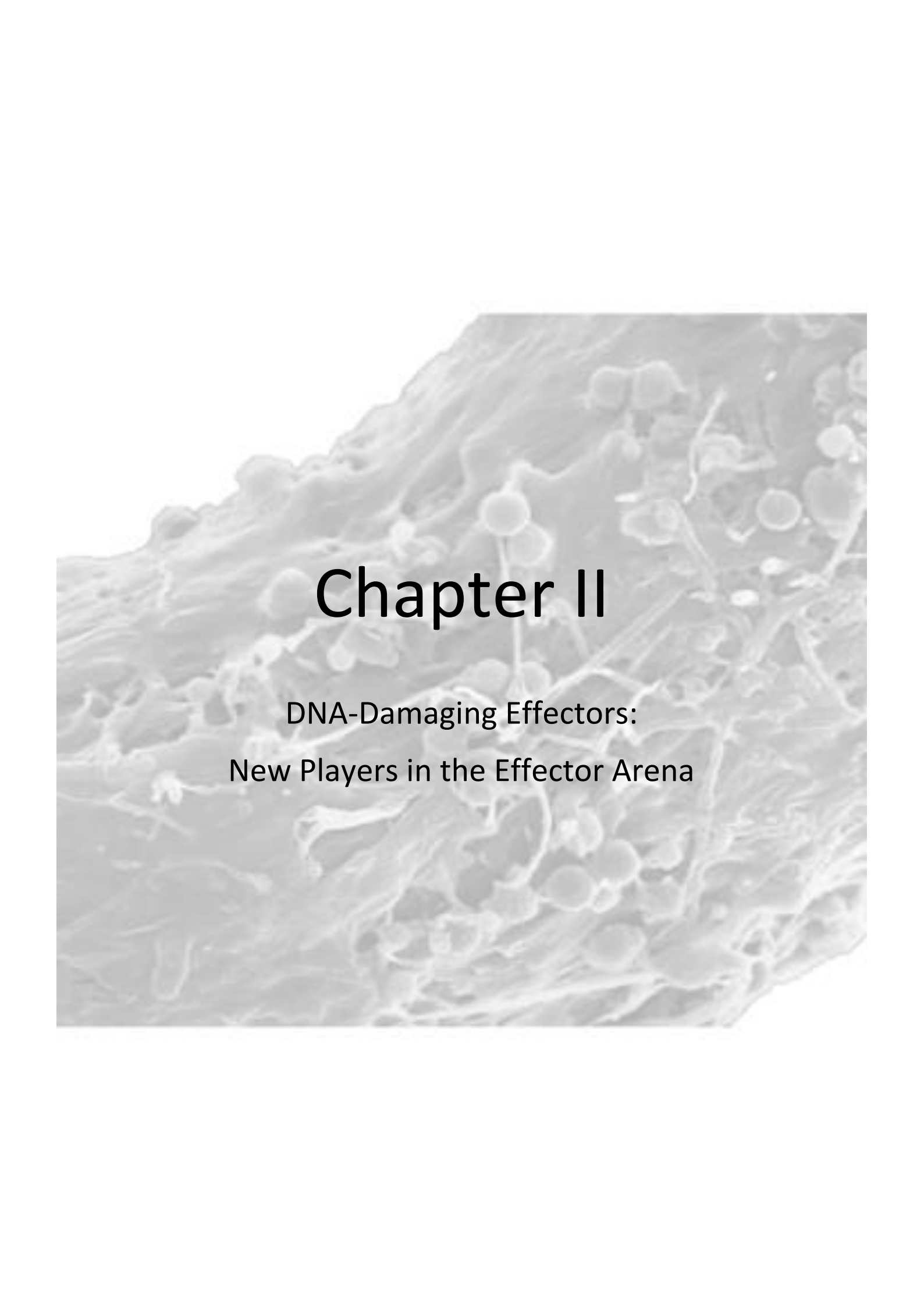
The Chapter II of this manuscript consists to an opinion paper published in Trends in Plant Science in 2019 (doi: 10.1016/j.tplants.2019.09.012.) where I pinpoint DNA-damaging effectors in plant microbe interactions.

The Chapter III reports on functional analyses of AeCRN5. Knowing that its N-terminal domain is an effective host-targeting signal (Schornack et al., 2010) and that AeCRN5 is nuclear localized *in planta*, this CRN gene was selected as candidate to decipher the mode of action of intracellular effector.

In the same time, spectacular advances in sequencing technologies allow us to gain insight into *Aphanomyces ssp.* genomes. We took advantage of the broad host range of *Aphanomyces* genus to make comparative genome analyses between animal and plant *Aphanomyces* strains. The aim of this collaborative work was to confront the different secretomes and to focus on the different classes of effectors. Those analyses lead to the identification of a new class of oomycete effectors related to SSPs. We also undertook

functional characterization of a cluster of SSP genes, and identified AeSSP1256 as a small nuclear localized protein that enhances oomycete colonisation. The results were published in BMC Biology in 2018 (doi: 10.1186/s12915-018-0508-5) and represents the Chapter IV of this manuscript.

We next focused on AeSSP1256 protein to decipher the role and the biological impact of this SSP gene on plant cells and host development. The results are provided in the Chapter V of this manuscript and available in BioRxiv (doi.org/10.1101/2020.06.17.157404) and submitted for evaluation to a peer-journal. Complementary results were obtained during this functional analysis and complete the chapter V of the manuscript.

A grayscale micrograph of a cell culture, likely fibroblasts, showing a dense network of cells with prominent nuclei and cytoplasmic extensions. The image is semi-transparent, allowing text to be overlaid. The text is centered and reads: Chapter II, DNA-Damaging Effectors: New Players in the Effector Arena.

Chapter II

DNA-Damaging Effectors:
New Players in the Effector Arena

II – CHAPTER II: DNA-Damaging Effectors: New Players in the Effector Arena (Camborde et al. TIPS, 2019)

Functional analyses of *A. euteiches* AeCRN13 revealed that this protein targets host DNA to trigger DNA damages. BdCRN13, the closest ortholog in the chytrid fungus *Batrachochytrium dendrobatidis* also induces DNA damages and triggers DNA damage responses (DDR) when expressed in a non-related host, such as plant cell (Ramirez-Garcés et al., 2016).

In this opinion paper, we discuss about DNA damage as a strategy used by pathogens during infection. DSBs and DDR have been evidenced in animal pathogens, especially in pathogenic bacteria, which produce DNA-damaging compounds. These compounds, able to cause directly or indirectly DNA breaks that result in mutations or cell death are named genotoxins. Several examples are described in the paper. We then wonder whether plant pathogens could also produce genotoxins and what could be the role of these compounds during infection. Finally we present the host defence mechanism that consists in a DDR signalling cascade, better characterized in animal than in plant.

Opinion

DNA-Damaging Effectors: New Players in the Effector Arena

Laurent Camborde,¹ Cécile Raynaud,² Bernard Dumas,¹ and Elodie Gaulin^{1,*}

In animal cells, nuclear DNA is the target of genotoxins produced by bacterial pathogens that cause genomic mutations eventually leading to apoptosis, senescence, and carcinogenic development. In response to the insult, the DNA damage response (DDR) is activated to ensure lesion repair. Accumulation of DNA breaks is also detected in plants during microbial infection. In this opinion article we propose that phytopathogens can produce DNA-damaging effectors. The recent identification of a functional genotoxin in devastating eukaryotic plant pathogens, such as oomycetes, supports the concept that DNA-damaging effectors may contribute to pathogenicity. Additionally, this raises the question of how plants can perceive these damages and whether this perception can be connected to the plant immune system.

Bacterial Genotoxins: Virulence Factors Produced by Animal Pathogens

There is accumulating evidence that bacteria produce DNA-damaging compounds in mammalian cells. Cytotoxic distending toxins (CDTs) produced by a number of Gram negative bacteria (i.e., *Escherichia coli*) are among the most characterized genotoxins (see Glossary) [1]. CDTs are heterotrimeric protein toxins that belong to the AB₂ family: the active CdtB (A) subunit and the binding CdtA-CdtC subunits (B₂) form the holotoxin. Cellular exposure to CDT holotoxins is assumed to arrest cell cycle and cause apoptosis [2]. CDT delivery to the host cell requires the binding of bacterial cells to the host cell to allow internalization of the different toxin subunits. Once internalized, the active CdtB unit moves through the Golgi apparatus and the endoplasmic reticulum (ER), using the host retrograde transport system. How CdtB leaves the ER to reach the nucleus is still an open question. The CdtB subunit has a strong homology to DNaseI (both in sequence and structure) and acts as a metal-dependent nuclease that causes host DNA breaks by cleaving phosphodiester bonds [3]. The genotoxic effect of CDTs depends on the DNA repair system that is induced upon DNA damage. Indeed, while high doses of the toxin cause double strand breaks (DSBs) leading to an arrest of cell proliferation and to cell death, low doses induce single strand breaks that are subsequently converted to DSBs after replication [4].

The CDT 'typhoid toxin' was firstly described in *Salmonella enterica typhi*, and recent studies showed that numerous nontyphoidal *Salmonella* serotypes carry genes encoding this toxin [5]. It represents a unique form of CDT with an A₂B₅ architecture with two active subunits (CdtB and PltA) and five binding subunits (PltB) arranged as a pentameric ring [6]. The secretion and export of this AB-toxin is an intricate process. After its secretion into the lumen of 'Salmonella-containing vesicle' (SCV), the typhoid toxin is packaged as cargoes into vesicles budding from the SCV. Then the typhoid toxin is released in the extracellular space via an exocytosis-like process. However *S. enterica* is known to deliver the typhoid toxin into the extracellular environment through outer membrane vesicles secreted from infected cells [7,8]. Upon binding, the toxin acts like other CDTs and requires retrograde transport through the Golgi apparatus to promote DNA damage. However, exit from the ER and translocation to the nucleus is not characterized [8].

Enterobacteriaceae also synthesize colibactin, a hybrid polyketide-nonribosomal peptide compound [1]. Colibactin genotoxins are secondary metabolites synthesized by nonribosomal peptide synthetase (NRPS)-polyketide synthase (PKS) enzymes [1]. Colibactin belongs to a largely uncharacterized family of small molecules. The genotoxic activity of the toxin depends on a direct interaction between the bacteria and the host cells and cannot be detected by using culture supernatant or killed bacteria. These observations suggest that colibactin is an unstable compound and/or that contact with the host cell triggers an unknown 'translocation' process of the toxin within the target cell [1]. In contrast

Highlights

Cells are challenged by numerous DNA-damaging agents, including those produced by pathogens. To maintain the integrity of the genome, animal and plant cells have evolved the DNA damage response (DDR).

In animals, bacterial genotoxins target host DNA and modulate DDR in a way that benefits the pathogen. A link between DDR and immune responses has been identified, suggesting that infected cells can respond to the attack.

In plants, little is known on the role of DNA-damaging effectors during pathogenesis. Plant DNA breaks are observed upon microbial infection and a family of DNA-damaging effectors was recently identified in plant-pathogenic oomycetes.

The DDR can be connected to signaling components of the plant immune responses.

¹Laboratoire de Recherche en Sciences Végétales, Université de Toulouse, CNRS, UPS, France

²Institute of Plant Sciences Paris-Saclay (IPS2), CNRS, INRA, Université Paris-Sud, Université Évry, Université Paris-Saclay, 91405, Orsay, Paris, France

*Correspondence: gaulin@irs.v.ups-tlse.fr



Box 1. Oomycetes and Fungal Effectors

Fungal and oomycete pathogens are known to produce hundreds of extracellular proteins, named effectors, which are potentially able to penetrate inside various compartments of the host cells [53]. In oomycetes, two main families of intracellular effectors were initially characterized, the RxLR and the CRN (Crickler and Necrosis), differing by their N-terminal conserved region thought to play a role in their intracellular localization [54,55]. More recently, a family of small secreted proteins was identified in the legume pathogen *A. euteiches*, some of them being able to localize inside the nuclei of plant cells [56]. In fungi, most of the effectors are usually, but not exclusively, small secreted proteins without any conserved sequences and predicted function [53]. Effectors are able to interact with a large array of intracellular protein targets, to disrupt various signaling or metabolic pathways of the host.

to CDTs, colibactin induces DNA alkylation and interstrand crosslinks that affect DNA replication and transcription, leading to DSBs [9,10].

Taken together, these three examples demonstrate the relevance of genotoxins for pathogen fitness toward animal cells.

Do Plant Pathogens Produce Genotoxins?

Until recently, only indirect evidence suggested plant colonization by pathogens caused DNA damage. For instance, pathogenic stress was reported to increase the frequency of somatic homologous recombination in *Arabidopsis* [11]. Similarly, viral infections of tobacco leaves were shown to increase homologous recombination [12]. However, more direct evidence of DNA damage was obtained during interaction of *Arabidopsis thaliana* with various phytopathogenic microorganisms. Using the phosphorylated form of the histone 2AX (H2AX), γ H2AX, as a probe for the induction of the DNA damage response (DDR) process, in combination with Comet assays, allowed the first observations of plant DNA degradation during plant pathogen interactions [13]. Noteworthy, all the pathogens studied by Song and Bent induce DNA damage in contrast to nonpathogenic bacteria (*E. coli*) [13]. Importantly, this effect was observed in various plant mutants, notably those affected in the production of reactive oxygen species known to induce DNA damage, suggesting that DNA lesions were not induced by the plant in response to the pathogen attack but probably through the production of dedicated effectors produced by pathogens (Box 1).

The first microbial effector causing DNA damage, AeCRN13, was recently identified in the legume pathogenic oomycete *Aphanomyces euteiches* [14,15]. AeCRN13 is a DNA-binding protein triggering γ H2AX accumulation. Expression of AeCRN13 in *Medicago truncatula* roots affected root development and enhanced the presence of enlarged cells, suggesting an effect on cell division. Importantly, phosphorylation of H2AX and expression of several markers of DDR (*BRCAs*, *RAD51*, *SOG1*) were induced in *M. truncatula* roots upon *A. euteiches* infection. These data established for the first time that eukaryotic phytopathogens might produce genotoxins.

Oomycetes are fungal-like eukaryotes, closely related to diatoms and brown algae that include some of the most devastating plant pathogens. Less studied are aquatic oomycetes that cause important diseases in animals [16]. Mining of nucleotide databases revealed that CRN13 genes are almost exclusively distributed in the oomycete lineage, with the notable exception of *Batrachomyces dendrobatidis*, a pathogenic chytrid fungus implicated in worldwide amphibian declines [14,17]. Similarly to AeCRN13, *B. dendrobatidis* CRN13 acts as a DNA-binding protein that causes accumulation of γ H2AX and aberrant development of *Xenopus laevis* embryos [14]. The number of CRN13 sequences ranges from 16 to one in phytopathogenic species such as *Phytophthora sojae* and *Phytophthora megakarya*, respectively (Figure 1A). Albeit the fish-pathogenic oomycete *Saprolegnia parasitica* was reported as a DNA-damaging parasite [18], it does not contain CRN13 related genes. In most cases CRN13 sequences are highly similar in a given genome, whilst they can be divergent such as in *A. euteiches*, suggesting peculiar functional specialization in such species. CRN13s are characterized by the presence of two conserved domains (DFA and DDC [19]). The C terminus of

Glossary

Comet assay: a gel electrophoresis-based method that can be used to measure DNA damage in eukaryotic cells.

DNA damage response (DDR): complex cellular network initiated following DNA breaks that orchestrates different cellular outcomes depending on the severity of DNA lesions (DNA repair, cell cycle arrest, cell death).

Effectors: secreted microbial encoded molecules that target host components to affect host physiology in a way that benefits the microorganism.

Endoreduplication: a process during which cells undergo several rounds of DNA replication without mitosis, leading to an increase in DNA content.

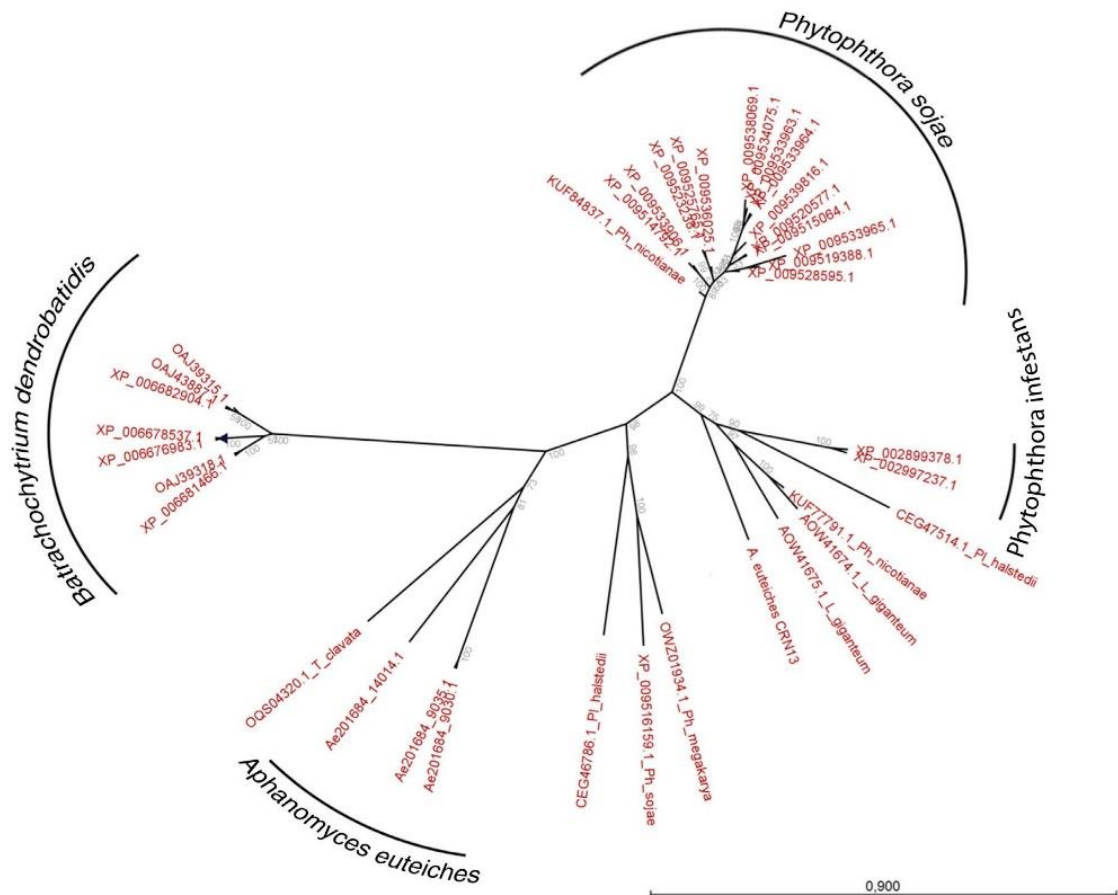
γ H2AX: phosphorylated (Ser139) histone H2AX variant, which serves as a marker for detection of double-strand DNA break (DSB).

Genotoxins: microbial molecules that target host DNA, causing, directly or indirectly, DNA breaks that result in mutations or cell death.

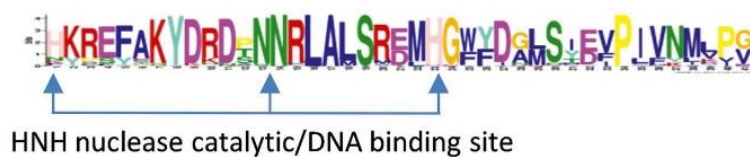
Oomycetes: eukaryotic filamentous microorganisms evolutionary distinct from true fungi, related to diatoms and brown algae, causing major diseases on crops and on some animals.

Virulence factor: microbial encoded molecules that contribute to pathogenicity and/or host colonization.

(A)



(B)



Trends In Plant Science

Figure 1. Phylogenetic Tree of CRN13 Genes and His-Asn-His (HNH) Motif.

(A) Phylogenetic tree of CRN13s. N-terminal sequences corresponding to the putative translocation signal were removed to restrict the analysis on the effector domain. A maximum likelihood phylogenetic tree was created using the neighbor joining method and bootstrap analysis (1000 replicates). (B) A web logo of the HNH nuclease motif of CRN13 sequences using the MEME tool (<http://meme-suite.org/tools/meme>).

the DFA domain contains a sequence showing a weak homology with a family of bacterial endonucleases characterized by a HNH (His-Asn-His) motif [14] (Figure 1B). This motif is found in various bacterial toxins such as colicins, produced by some *E. coli* strains. The core of the colicin DNase active site is the HNH motif, a 34-amino acid sequence at the C terminus of the protein. The HNH motif, first described in 1994 [20,21], has been identified in more than 500 nucleases involved in a wide range of diverse functions, including mobile intron homing, DNA repair, mammalian apoptosis, and DNA restriction [22].

The first identification of a DNA-damaging effector from a phytopathogenic oomycete clearly indicates that host DNA, in addition to RNAs [23], could be a major target of plant pathogens during infection.

DDR in Mammals and Plants

The final outcome of the production of bacterial genotoxins is to provoke DNA damage leading to the induction of DNA repair responses. When the damage is too severe and cannot be repaired, the target cells undergo apoptosis or senescence. Sometimes, the target cells can survive and proliferate but accumulate genomic mutations [24].

The early phase of the DDR signaling cascade is a rapid response after the initial damage and consists of cell cycle arrest to allow time for DNA repair [25]. When the DNA lesions are particularly severe, the DDR can persist and provokes permanent growth arrest or cell death. In case of DNA DSB, the DDR is initiated by the perception of the lesion and recruitment of the MRN complex (MRE11-RAD51-NBS1) to the damaged site (Figure 2, Key Figure). The MRN complex recruits the ATM kinase, a master transducer of DDR since it contributes to the phosphorylation of H2AX (γ H2AX). The ATR kinase appears also to be responsible for a subset of H2AX phosphorylation [26]. Phosphorylation of H2AX facilitates the orderly recruitment of other protein mediators of the DDR signaling to the site of repair. This platform activates downstream components, such as p53 in mammals, that mediate appropriate responses (Figure 2 [27]).

The DDR has been studied in plants, but almost exclusively in *A. thaliana*. Many homologs of animal DDR components have been identified, such as the RAD50 sensors, the ATM and ATR transducers kinases, the BRCA1 mediator checkpoint, or the WEE1 kinase that controls cell-cycle arrest (Figure 2) [27,28]. As for mammals, ATM is the main actor of DSB response linked to the accumulation of γ H2AX in nuclear foci at the damaged sites for proper DNA repair (Figure 2) [26,29]. Downstream of ATM, some signaling elements appear to be missing and plant-specific regulators also exist, suggesting the existence of common and unique DDR mechanisms between animals and plants (for review see [24,27,30]). Notably, the plant-specific transcription factor SOG1 appears to be a key integrator of the DDR, controlling both cell proliferation and DNA repair (Figure 2) [31]. In this respect, it may be a functional homolog of the animal p53 protein, but shares no sequence identity with this factor [30]. Furthermore, **endoreduplication**, which is generally associated with cell enlargement, is frequently observed as a response to DNA damage in plants [32]. The role of such a response is unclear and might contribute to a reduction of the number of damaged cells in developing tissues by stimulating their differentiation [32,33]. Besides SOG1, the E2Fa/RBR pathway also functions in DDR activation in response to DSBs [34,35]. During normal cell cycle progression, E2F transcription factors are positive regulators of the cell cycle that can be inactivated by binding of the RETINOBLASTOMA RELATED (RBR) protein. Reports showed that E2Fa may be involved in the DNA repair transcriptional response [36] and that, at the cellular level, E2F foci colocalize with γ H2AX, suggesting an implication of E2Fs in the DNA repair cellular machinery [29] as well as in the control of programmed cell death linked to unrepaired DNA [37]. These data were corroborated by more recent studies [34,35] and were further linked to the RBR pathway, thereby revealing a new DDR pathway that acts independently of SOG1. Genome-wide identification of RBR target genes further confirmed its involvement in the regulation of DDR genes [38]. Finally, it seems that the plant nuclear envelope might play a role in this new pathway, since *A. thaliana* mutants deficient for actors located at the nuclear envelope and involved in nuclear shaping, such as GIP proteins [39,40], display increased genomic instability at centromeric regions [41]. In addition, CROWDED NUCLEI (CRWN) proteins involved in the control of plant nuclear morphology are also implicated in the protection of genomic DNA against oxidative stress [42]. How nuclear envelope function could interfere with immune responses is not clear, but it may be by affecting the nuclear retention of immunity-related proteins, as suggested by the identification of nuclear pore complex proteins as modifiers of plant immunity [43].

Overall, DNA repair pathways are mostly conserved between plants and mammals but the specificity of plant DDR is becoming clearer.

Key Figure

Induction of DNA Damage Response (DDR) upon Genotoxic Stress Induced by Pathogen Infection

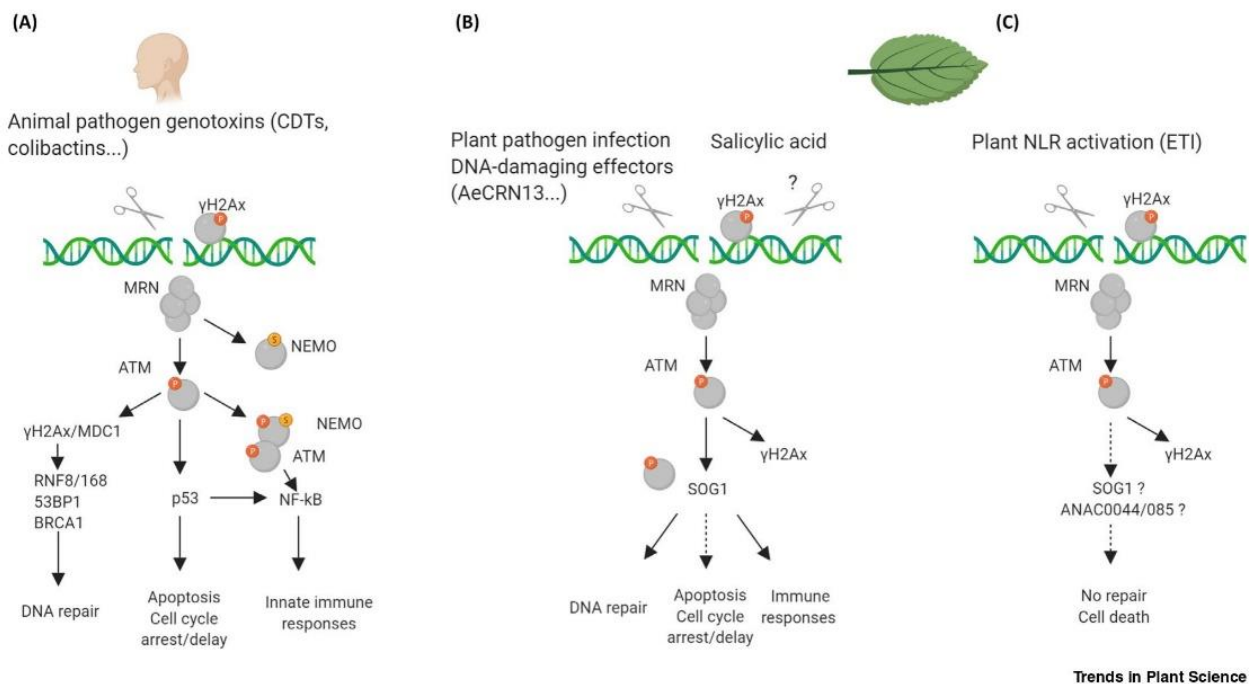


Figure 2. (A) In animal cells, DNA damage produced by bacterial genotoxins are sensed by the MRN complex, leading to the autophosphorylation of the ATM kinase. Activated ATM phosphorylates MRN, MDC1, H2Ax, and p53. DNA damage sensing leads to the SUMOylation of NEMO, which is then phosphorylated by ATM. ATM and NEMO and interaction with other signaling component leads to the activation of NF- κ B. (B) In plant cells, DNA damage sensing also involves the MRN complex and activation of the ATM kinase, which phosphorylates H2AX, SOG1, a transcription factor which transcriptionally induces hundreds of genes controlling the DNA damage response and also genes involved in immune responses, and chromatin remodeling. The pathway leading to apoptosis and cell cycle arrest induced by DNA damaging effectors remains to be elucidated. (C) NLR-mediated DNA damage. Upon direct or indirect perception of specific effectors by NLRs, plant cells engage an effector-triggered immunity (ETI), which results locally in a hypersensitive response characterized by a programmed cell death and which correlates with DNA damage and phosphorylation of H2AX, without induction of genes involved in DDR. This figure was created using BioRender (<https://biorender.com/>). Abbreviations: CDT, Cytolethal distending toxins; MRN, MRE11-RAD51-NBS1; NEMO, NF- κ B essential modulator; NLR, Nucleotide-binding leucine rich receptor.

Role of DNA-Damaging Effectors in Host-Pathogen Interactions

The role of DNA-damaging effectors in plant or animal pathogenesis is still unclear. On one hand, DNA damaging can interfere with the host cell cycle and host responses and can subsequently favor the colonization of the tissues. On the other hand, DNA damage can be sensed as a danger signal leading to the induction of defense responses. In mammals, several studies have identified signaling complexes induced by DNA damage, notably involving ATM, leading to the activation of NF- κ B, a transcriptional regulator which contributes to inflammation and immunity [44]. ATM-dependent activation of NF- κ B involved the NF- κ B essential modulator (NEMO) that is SUMOylated upon DNA damage (Figure 2) [45].

In plants, two layers of immunity have been described [46]. The first layer relies on the perception of microbial components [pathogen-associated molecular pattern (PAMP)] and the induction of basal

responses [PAMP-triggered immunity (PTI)]. Adapted pathogens deliver effectors to suppress these basal responses, leading to plant susceptibility. A second immune layer may detect these effectors inducing a so-called effector-triggered immunity (ETI). ETI involves cytoplasmic nucleotide-binding leucine rich receptors (NLRs) and signaling component such as enhanced disease susceptibility-1 (EDS1). ETI is often accompanied by a programmed cell death at infection sites, designated as the hypersensitive response (HR). HR cell death displays some features of animal apoptosis, such as modification of membrane integrity and DNA fragmentation. This local reaction is generally followed by systemic acquired resistance that enhances immunity in uninfected parts of the plant through the generation of mobile signals and accumulation of the defense hormone salicylic acid (SA).

Recently a model involving SA in the accumulation of DNA damages contributing directly to the activation of plant immune responses emerged [47]. This hypothesis came from the detailed characterization of the *SNI1* (*Suppressor of npr1-1, Inducible*) mutant. The *sni1* mutation was originally isolated as a suppressor of the *npr1* (non-expressor of PR genes) mutant in which activation of defense genes is compromised [48]; *SNI1* is thus considered as a negative regulator of immune responses, its absence leading to SA accumulation and activation of defense genes. Later, tandem-affinity purification experiments identified *SNI1* as a subunit of the structural maintenance of chromosome (SMC) 5/6 complex involved in DDR [47]. The primary defect of the *sni1* mutant thus appears to be the maintenance of genome integrity, and the constitutive accumulation of DNA damage resulting from *SNI1* loss of function was proposed to trigger defense responses. In line with this hypothesis, Wang and colleagues reported that the activation of defense responses in *sni1* mutants depends on *BRCA2* activity and that the repair proteins *RAD51* and *BRCA2* directly bind the promoter of the *PR1* and *PR2* defense genes to activate their expression [49], suggesting that DDR components and repair proteins can also play a role in defense responses. In agreement with this hypothesis, the recent identification of *SOG1*-direct targets revealed significant enrichment of functional categories related to immune responses [50], demonstrating that the DDR integrator *SOG1* directly regulates defense genes. Together, all these reports support a model according to which DNA damage accumulation could be recognized as a signal of pathogen infection and contribute through multiple components of the DDR to the activation of defense genes (Figure 2).

However, this model placing SA as a central modulator of DNA damage during plant pathogen interactions is challenged by contradictory results. Firstly, although Yan and colleagues reported that SA treatment could induce DNA damage accumulation [47], two independent studies failed to reproduce this observation and Song and Bent even proposed that pretreatment with SA before pathogen infection reduced the amount of DNA damage inflicted by biotic stress [13,51]. Secondly, comparative analysis of a number of mutants that display constitutive activation of defense responses with or without concomitant induction of spontaneous cell death, including the *sni1* mutant, revealed that DNA damage accumulation requires the activity of NLR signaling components involved in ETI, such as *EDS1*, and is not a mere consequence of SA accumulation [51]. Indeed, the autoimmune *dnd1* mutant exhibits a strong accumulation of SA and activation of defense responses but no DNA damage, and the *eds1* mutation can suppress defense activation, cell death induction, and DNA damage accumulation of the *sni1* mutants. Interestingly, expression of genes involved in DNA repair is downregulated in autoimmune mutants developing spontaneous HR, suggesting that in these mutants, DNA damage accumulation can be seen as a result of programmed cell death induction [51].

Unifying these apparently contradictory results in a single model is at present difficult but putting together all these data, it is thus likely that DDR activation plays multiple roles during plant-pathogen interactions, depending both on the cell type and the type of interactions. For example, Rodriguez and colleagues showed that DNA repair is suppressed by ETI [51]. This makes sense in the context of programmed cell death (PCD) induction where DNA degradation is a part of the cellular response. However, other components of the DDR that are required for PCD induction may well be activated by ETI. In line with this model, the *SOG1*-targets *ANAC044* and *ANAC085* have recently been shown to control PCD and cell cycle progression in response to DNA damage, but not DNA repair [52]. Likewise, the activation of defense observed in *sni1* may well be a

consequence of defects in DNA repair and cell cycle checkpoint activation, but could require EDS1 for the amplification of the response and massive induction of PCD. In agreement with this hypothesis, the *sn1 eds1* double mutant still shows very severe growth defects, whereas loss of E2Fs fully rescues plant growth. Thus, a balance could exist in plant cells that would involve DDR activation and DNA repair to sustain cell viability in response to biotic stress, and possibly contribute directly to defense gene activation, that could be shifted to promote cell death and extensive DNA damage accumulation. In such a model, the requirement of the plant DDR and the branches of this pathway activated in response to a pathogen could vary: (i) between cell types, for example in infected cells versus neighboring or distant cells; (ii) depending on the type of immune response (i.e., PTI versus ETI); and (iii) depending on the lifestyle of the pathogen. Likewise, response to pathogens with different lifestyles would likely have contrasting requirements for the DDR: cell death induction could help the plant to fight biotrophic pathogens and could be hijacked by pathogen effectors to suppress HR or could, on the contrary, be activated by necrotrophic pathogens to complete their lifecycle. Accordingly, the *sog1* mutation correlates with an increased susceptibility to the fungal pathogen *Colletotrichum higginsianum* (hemibiotrophic), but not to the bacterial pathogen *Pseudomonas syringae* (biotrophic) [50], suggesting that SOG1 is differently required during plant responses to pathogens with different lifestyles. Clearly, further work is needed to extend the role of DDR in plant immunity in other plants and pathosystems.

Concluding Remarks

There is now evidence that genotoxins are not exclusively produced by prokaryotic microbes that infect mammals but also by eukaryotic pathogens of plants (see [Outstanding Questions](#)). Recent studies have begun to characterize the impact of DNA-damaging agents on plant behavior during microbial infection. Since preservation of genomic integrity to limit propagation of aberrant DNA is a common trait in both mammal and plant cells, we suggest that genotoxins may produce similar effects in both types of organisms. Besides their role in pathogenicity, genotoxins can be also perceived as danger signals by the host, leading to induction of defense responses. This model is supported by the existing link between the DDR players involved in DNA repair and signaling components of the immune system.

Acknowledgments

E.G. was supported by Agence Nationale de la Recherche (ANR) Jeunes Chercheuses/Jeunes Chercheurs grant (APHANO-Effect, ANR-12-JSV6-0004-01).

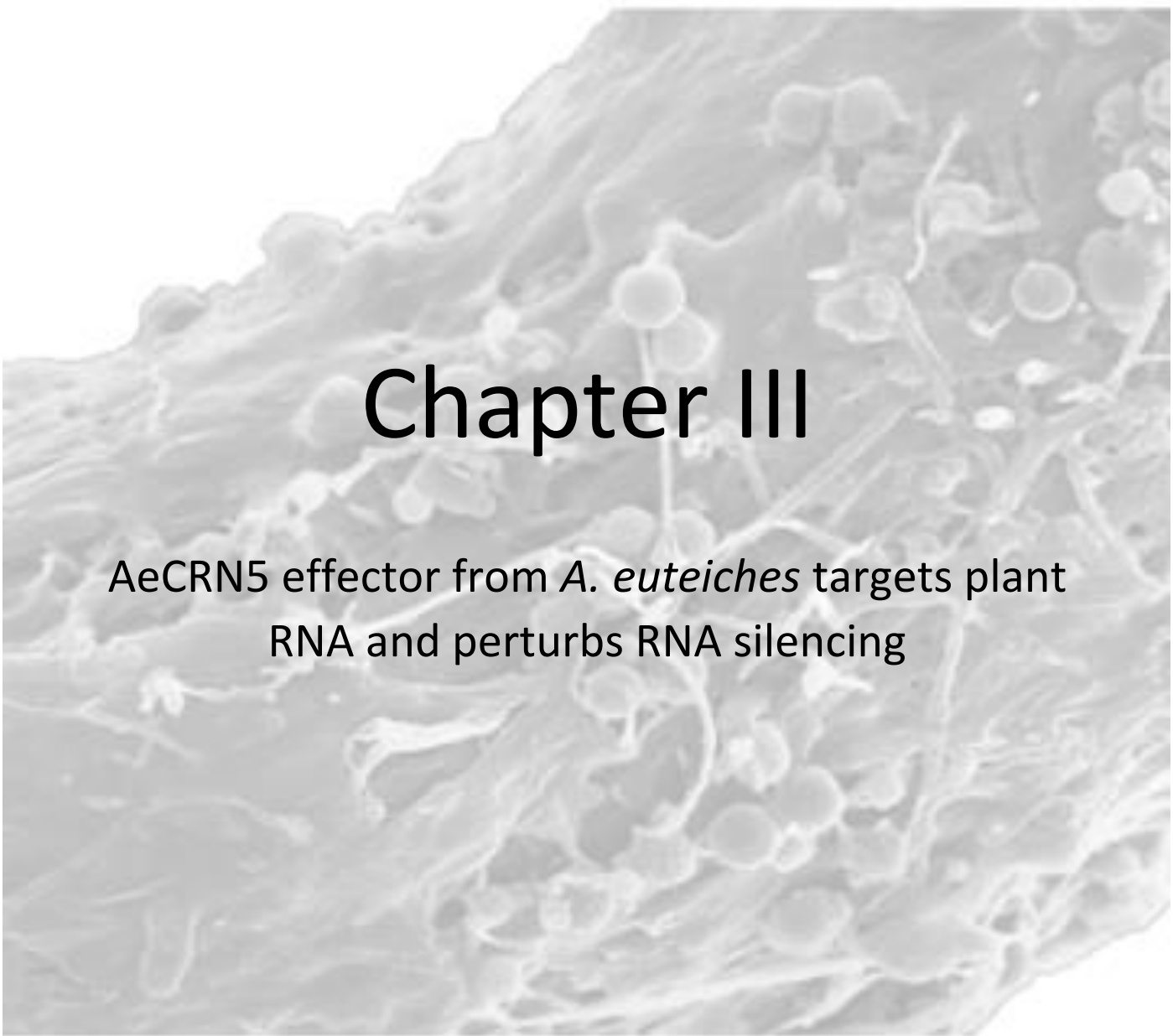
References

1. Taieb, F. et al. (2016) The enterobacterial genotoxins: cytolethal distending toxin and colibactin. *EcoSal. Plus* 7, 1
2. Grasso, F. and Frisan, T. (2015) Bacterial genotoxins: merging the DNA damage response into infection biology. *Biomolecules* 5, 1762–1782
3. Lemerrier, C. (2015) When our genome is targeted by pathogenic bacteria. *Cell Mol. Life Sci.* 72, 2665–2676
4. Fedor, Y. et al. (2013) From single-strand breaks to double-strand breaks during S-phase: a new mode of action of the *Escherichia coli* cytolethal distending toxin. *Cell Microbiol.* 15, 1–15
5. den Bakker, H.C. et al. (2011) Genome sequencing reveals diversification of virulence factor content and possible host adaptation in distinct subpopulations of *Salmonella enterica*. *BMC Genomics* 12, 425
6. Song, J. et al. (2013) Structure and function of the *Salmonella typhi* chimaeric A(2)B(5) typhoid toxin. *Nature* 499, 350–354
7. Guidi, R. et al. (2013) Chronic exposure to the cytolethal distending toxins of Gram-negative bacteria promotes genomic instability and altered DNA damage response. *Cell Microbiol.* 15, 98–113
8. O'Donoghue, E.J. et al. (2017) Lipopolysaccharide structure impacts the entry kinetics of bacterial outer membrane vesicles into host cells. *PLoS Pathog.* 13, e1006760
9. Vizcaino, M.I. and Crawford, J.M. (2015) The colibactin warhead crosslinks DNA. *Nat. Chem.* 7, 411–417
10. Wilson, M.R. et al. (2019) The human gut bacterial genotoxin colibactin alkylates DNA. *Science* 363, eaar7785
11. Lucht, J.M. et al. (2002) Pathogen stress increases somatic recombination frequency in *Arabidopsis*. *Nat. Genet.* 30, 311–314
12. Kovalchuk, I. et al. (2003) Pathogen-induced systemic plant signal triggers DNA rearrangements. *Nature* 423, 760–762
13. Song, J. and Bent, A.F. (2014) Microbial pathogens trigger host DNA double-strand breaks whose abundance is reduced by plant defense responses. *PLoS Pathog.* 10, e1004030
14. Ramirez-Garcés, D. et al. (2016) CRN13 candidate effectors from plant and animal eukaryotic pathogens are DNA-binding proteins which trigger host DNA damage response. *New Phytol.* 210, 602–617

Outstanding Questions

Which pathogenic factors cause DNA damage in infected plant tissues?
 What are the nucleic regions targeted by DNA-damaging effectors?
 What is the benefit for the pathogen to produce DNA damage in plants?
 Do pathogens produce specific effectors that are able to interfere with DDR?
 How do pathogens deal with immune responses induced by DNA damage?
 Which are the signaling proteins that connect DDR and immune responses?
 Are phytopathogens DNA-damaging effectors able to facilitate colonization of the host environment by targeting nucleic acid from other microorganisms?

15. Camborde, L. et al. (2017) Detection of nucleic acid-protein interactions in plant leaves using fluorescence lifetime time imaging microscopy. *Nat. Protoc.* 12, 1933–1950
16. Phillips, A.J. et al. (2008) New insights into animal pathogenic oomycetes. *Trends Microbiol.* 16, 13–19
17. Sun, G. et al. (2011) Evidence for acquisition of virulence effectors in pathogenic chytrids. *BMC Evol. Biol.* 11, 195
18. Trusch, F. et al. (2018) Cell entry of a host-targeting protein of oomycetes requires gp96. *Nat. Commun.* 9, 2347
19. Haas, B. et al. (2009) Genome sequence and analysis of the Irish potato famine pathogen *Phytophthora infestans*. *Nature* 461, 393–398
20. Shub, D.A. et al. (1994) Amino acid sequence motif of group I intron endonucleases is conserved in open reading frames of group II introns. *Trends Biochem. Sci.* 19, 402–404
21. Gorbalenya, A.E. (1994) Self-splicing group I and group II introns encode homologous (putative) DNA endonucleases of a new family. *Protein Sci.* 3, 1117–1120
22. Taylor, G.K. and Stoddard, B.L. (2012) Structural, functional and evolutionary relationships between homing endonucleases and proteins from their host organisms. *Nucleic Acids Res.* 40, 5189–5200
23. Spanu, P.D. (2015) RNA-protein interactions in plant diseases: hackers at the dinner table. *New Phytol.* 207, 991–995
24. Hu, Z. et al. (2016) Mechanisms used by plants to cope with DNA damage. *Annu. Rev. Plant Biol.* 67, 439–462
25. Chatzinikolaou, G. et al. (2014) DNA damage and innate immunity: links and trade-offs. *Trends Immunol.* 35, 429–435
26. Friesner, J.D. et al. (2005) Ionizing radiation-dependent gamma-H2AX focus formation requires ataxia telangiectasia mutated and ataxia telangiectasia mutated and Rad3-related. *Mol. Biol. Cell* 16, 2566–2576
27. Ciccio, A. and Elledge, S.J. (2010) The DNA damage response: making it safe to play with knives. *Mol. Cell* 40, 179–204
28. Nisa, M.-U. et al. (2019) The plant DNA damage response: signaling pathways leading to growth inhibition and putative role in response to stress conditions. *Front. Plant Sci.* 10, 653
29. Lang, J. et al. (2012) Plant γH2AX foci are required for proper DNA DSB repair responses and colocalize with E2F factors. *New Phytol.* 194, 353–363
30. Yoshiyama, K.O. et al. (2014) The role of SOG1, a plant-specific transcriptional regulator, in the DNA damage response. *Plant Signal Behav.* 9, e28889
31. Yoshiyama, K. et al. (2009) Suppressor of gamma response 1 (SOG1) encodes a putative transcription factor governing multiple responses to DNA damage. *Proc. Natl. Acad. Sci. U. S. A.* 106, 12843–12848
32. Cools, T. and De Veylder, L. (2009) DNA stress checkpoint control and plant development. *Curr. Opin. Plant Biol.* 12, 23–28
33. Hudik, E. et al. (2014) Chloroplast dysfunction causes multiple defects in cell cycle progression in the *Arabidopsis* crumpled leaf mutant. *Plant Physiol.* 166, 152–167
34. Horvath, B.M. et al. (2017) *Arabidopsis* RETINOBLASTOMA RELATED directly regulates DNA damage responses through functions beyond cell cycle control. *EMBO J.* 36, 1261–1278
35. Biedermann, S. et al. (2017) The retinoblastoma homolog RBR1 mediates localization of the repair protein RAD51 to DNA lesions in *Arabidopsis*. *EMBO J.* 36, 1279–1297
36. Roa, H. et al. (2009) Ribonucleotide reductase regulation in response to genotoxic stress in *Arabidopsis*. *Plant Physiol.* 151, 461–471
37. Smetana, O. et al. (2012) Non-apoptotic programmed cell death with paraptotic-like features in bleomycin-treated plant cells is suppressed by inhibition of ATM/ATR pathways or NtE2F overexpression. *J. Exp. Bot.* 63, 2631–2644
38. Bouyer, D. et al. (2018) Genome-wide identification of RETINOBLASTOMA RELATED 1 binding sites in *Arabidopsis* reveals novel DNA damage regulators. *PLoS Genet.* 14, e1007797
39. Batzenschlager, M. et al. (2014) GIP/MZT1 proteins orchestrate nuclear shaping. *Front. Plant Sci.* 5, 29
40. Batzenschlager, M. et al. (2013) The GIP gamma-tubulin complex-associated proteins are involved in nuclear architecture in *Arabidopsis thaliana*. *Front. Plant Sci.* 4, 480
41. Batzenschlager, M. et al. (2015) *Arabidopsis* MZT1 homologs GIP1 and GIP2 are essential for centromere architecture. *Proc. Natl. Acad. Sci. U. S. A.* 112, 8656–8660
42. Wang, Q. et al. (2019) Roles of CRWN-family proteins in protecting genomic DNA against oxidative damage. *J. Plant Physiol.* 233, 20–30
43. Cheng, Y.T. et al. (2009) Nuclear pore complex component MOS7/Nup88 is required for innate immunity and nuclear accumulation of defense regulators in *Arabidopsis*. *Plant Cell* 21, 2503–2516
44. Miyamoto, S. (2011) Nuclear initiated NF-κB signaling: NEMO and ATM take center stage. *Cell Res.* 21, 116–130
45. McCool, K.W. and Miyamoto, S. (2012) DNA damage-dependent NF-κB activation: NEMO turns nuclear signaling inside out. *Immunol Rev.* 246, 311–326
46. Jones, J.D. and Dangl, J.L. (2006) The plant immune system. *Nature* 444, 323–329
47. Yan, S. et al. (2013) Salicylic acid activates DNA damage responses to potentiate plant immunity. *Mol. Cell* 52, 602–610
48. Li, X. et al. (1999) Identification and cloning of a negative regulator of systemic acquired resistance, SNI1, through a screen for suppressors of npr1-1. *Cell* 98, 329–339
49. Wang, S. et al. (2010) *Arabidopsis* BRCA2 and RAD51 proteins are specifically involved in defense gene transcription during plant immune responses. *Proc. Natl. Acad. Sci. U. S. A.* 107, 22716–22721
50. Ogita, N. et al. (2018) Identifying the target genes of SUPPRESSOR OF GAMMA RESPONSE 1, a master transcription factor controlling DNA damage response in *Arabidopsis*. *Plant J.* 94, 439–453
51. Rodriguez, E. et al. (2018) DNA damage as a consequence of NLR activation. *PLoS Genet.* 14, e1007235
52. Takahashi, N. et al. (2019) A regulatory module controlling stress-induced cell cycle arrest in *Arabidopsis*. *eLife* 8, e43944
53. Sánchez-Vallet, A. et al. (2018) The genome biology of effector gene evolution in filamentous plant pathogens. *Annu. Rev. Phytopathol.* 56, 21–40
54. Anderson, R.G. et al. (2015) Recent progress in RXLR effector research. *Mol. Plant Microbe Interact.* 28, 1063–1072
55. Amaro, T.M. et al. (2017) A perspective on CRN proteins in the genomics age: evolution, classification, delivery and function revisited. *Front. Plant Sci.* 8, 99
56. Gaulin, E. et al. (2018) Genomics analysis of *Aphanomyces* spp. identifies a new class of oomycete effector associated with host adaptation. *BMC Biol.* 16, 43



Chapter III

AeCRN5 effector from *A. euteiches* targets plant
RNA and perturbs RNA silencing

III – CHAPTER III: AeCRN5 effector from *A. euteiches* targets plant RNA and perturbs RNA silencing

During my PhD I continued the functional analysis of AeCRN5 effector from *A. euteiches*. AeCRN5 was identified in a cDNA library generated from *A. euteiches* grown in close proximity to roots of *M. truncatula* (Gaulin et al., 2008). Its C-terminus was previously shown to trigger necrosis and to localize in nuclei in *N. benthamiana* cells. Furthermore, it was evidenced that its N-terminal domain was able to translocate the C-terminal part of the protein in host cells (Schornack et al., 2010). AeCRN5 harbors a DN17 domain as its C-terminus based on the *Phytophthora* CRNs domains nomenclature, without any predicted functional activity.

Diana Ramirez-Garcés, a previous PhD student in the team, started the functional characterization of AeCRN5 during her PhD in 2014 and evidenced that AeCRN5 triggers necrosis when transiently express in *N. benthamiana* leaves or *M. truncatula* roots. During my PhD I complete the functional analysis to provide new elements to decipher the mode of action of AeCRN5. Briefly, we first identified that AeCRN5 could interfere with RNA silencing but the mechanism is still unclear, and complementary results are required to support this conclusion. Additionally we observed that AeCRN5 could interact with the plant SERRATE protein (SE), known to participate to alternative splicing and microRNA biogenesis pathway in plants like *A. thaliana* (Raczynska et al., 2014). Finally, we found that when expressed in *N. benthamiana* leaves, AeCRN5 seems to interfere with the processing of pre-miRNA, accumulating the longer primary transcripts (pri-miRNAs) which require the activity of different proteins, including the SERRATE protein.

I decided to present the data of the next chapter formatted for submission in peer review journal, keeping in mind that complementary results or repetitions are required to support the main conclusion of this article.

AeCRN5 effector from *A. euteiches* targets plant RNA and interferes with RNA silencing and miRNA processing

Laurent Camborde ^{1,2,+}, Diana Ramirez-Garcés ^{1,2,+}, Alain Jauneau ^{1,2}, Yves Martinez ^{1,2}, Bernard Dumas ^{1,2}, Elodie Gaulin ^{1,2} *.

¹ Université de Toulouse, UPS, Laboratoire de Recherche en Sciences Végétales, 24 chemin de Borde Rouge, Auzeville, F-31326, Castanet-Tolosan, France

² CNRS, Laboratoire de Recherche en Sciences Végétales, 24 chemin de Borde Rouge, Auzeville, F-31326, Castanet-Tolosan, France

***: Corresponding author**

+: participate equally to this work

Address for correspondence: Dr Elodie Gaulin

UMR 5546 CNRS-UPS Pôle de Biotechnologie Végétale

24, chemin de Borde Rouge BP 42617 Auzeville

31320 Castanet-Tolosan, France

Tel.: +33 (0) 5 34 32 38 03 Fax: +33 (0) 5 34 32 38

e-mail: gaulin@lrsv.ups-tlse.fr

Keywords: Effector, Crinkler, *Aphanomyces*, *Medicago*, nuclear bodies, RNA silencing, miRNA biogenesis

Abstract

Oomycete phytopathogens secrete and deliver effector molecules inside host cells to mediate infection. CRN proteins are one major class of host nuclear-localized effectors, able to interfere with various nuclear functions. Here we address the characterization of AeCRN5, from the legume root pathogen *A. euteiches*. AeCRN5 is a modular protein of the CRN effector family containing a functional plant translocation signal at its N-terminus and a cell-death inducing nuclear C-terminus DN17 domain. We report that AeCRN5 is induced during *A. euteiches* infection and displays a dynamic nuclear localization in plant cells, transiently accumulating in nuclear bodies. When expressed in host root cells using *A. rhizogenes*, AeCRN5 triggers strong developmental defects, leading to shorter root system coupled with an increased number of roots. A nucleic acid-protein interaction assay based on FRET-FLIM in *N. benthamiana* leaves revealed the RNA binding ability of AeCRN5 C-ter domain. Furthermore, using a heterologous system, AeCRN5 was shown to interfere with plant RNA silencing mechanism. Additionally, we observed in preliminary experiments that AeCRN5 could associate with the SERRATE protein, a key component of the miRNA biogenesis, leading to a perturbation of the pri-miRNA processing. Altogether, these preliminary data report that AeCRN5 acts through its DN17 C-ter domain as plant RNA silencing suppressor probably to facilitate pathogen infection.

INTRODUCTION

Plant-associated microorganisms rely on the secretion of a particular class of molecules, termed “effectors” to successfully establish infection. These molecules interact with plant targets to suppress plant defence and reprogram host metabolism, contributing in rendering host niche profitable to sustain the growth and the spreading of pathogens (Ökmen et al., 2013). A substantial number of microbial effectors are addressed to plant nuclei and their function, assessed mainly through the identification of their plant target, are best characterized in bacteria (Bhattacharjee et al., 2013; Deslandes and Rivas, 2012). These effectors target different nature of host nuclear factors including proteins, RNA and DNA to perturb plant physiology by, for example, reprogramming host transcription (Bhattacharjee et al., 2013; Deslandes and Rivas, 2012; Canonne and Rivas, 2012).

Oomycetes (Stramenopiles) are eukaryotic filamentous microorganisms comprising several of the most devastating plant pathogens with tremendous impacts on natural and agricultural ecosystems like *P. infestans* and *P. ramorum* (Thines and Kamoun, 2010). In oomycetes, two main classes of effectors able to target plant nucleus have been described: the RxLR effectors and Crinklers (CRN). Crinklers (Crinkling and Necrosis, CRN), firstly reported on the potato late blight agent *Phytophthora infestans* (Torto et al., 2003; Haas et al., 2009), have been reported in all plant pathogenic oomycetes sequenced to date (Amaro et al., 2017), with numbers ranging from 18 genes in *H. arabidopsidis* (Baxter et al., 2010) to more than 400 genes in *P. infestans* (Haas et al., 2009). All CRNs display a conserved LFLAK N-terminal motif, altered as LYLAK in *Albugo sp* (Kemen et al., 2011), LxLYLAR/K in *Pythium sp* (Lévesque et al., 2010) and LYLALK in *A. euteiches* (Gaulin et al., 2008). *Phytophthora* and *Aphanomyces* N-termini motifs have been shown to act as host cytoplasm-delivery signals (Schornack et al., 2010). Not all CRNs harbour a predicted signal peptide, although detected by mass spectrometry in culture medium of *P. infestans* (Meijer et al., 2014). CRN C-termini diversity contrasts to the conservation of N-termini and is thought to be the result of recombination of different subdomains occurring after a HVLVXXP N-terminal motif that occurs prior to the C-terminus. First reported through a genome mining in *P. infestans*, these subdomains associate in

different combinations that define 27 CRN families (Haas et al., 2009) and do not display any significant similarity to known functional domains, except few cases (i.e. serine/threonine kinase D2 domain of PiCRN8 (van Damme et al., 2012)). New CRNs families have been reported upon complete genome analysis of distinct oomycete species (i.e. *Phytophthora capsici*, *Pythium* sp., *A. euteiches*, *Saprolegnia*) suggesting that CRNs belong to an ancient effector family that arose early in oomycete evolution. CRN-like sequences presenting similarities to *Phytophthora* C-termini were recently evidenced in the genome of the amphibian pathogen fungus *Batrachochytrium dendrobatidis* and the arbuscular mycorrhizal fungus *Rhizophagus irregularis* (Sun et al., 2011; Lin et al., 2014; Ramirez-Garcés et al., 2016).

All *Phytophthora* CRNs C-termini localize to the plant nucleus where they display distinct subcellular localisations including nuclei, nucleoli and unidentified nuclear bodies (Stam et al., 2013a) depicting different nuclear activities and targets. Although initially reported as necrosis-inducing proteins when expressed in planta, it has been shown that this is only the case for few CRNs as a large number do not cause cell-death (Haas et al., 2009; Shen et al., 2013). *Phytophthora* CRNs have distinct pattern of expression during various life stages and colonization of host plants (Stam et al., 2013b). Several *Phytophthora* CRNs can suppress cell death triggered by cell-death inducers or other CRNs (Liu et al., 2011; Shen et al., 2013), reduce plant defense gene expression or accumulation of reactive oxygen species (ROS) in *N. benthamiana* (Rajput et al., 2014) sustaining the view that CRNs might act as suppressors of plant immunity, although not all promote infection (Stam et al., 2013b). Biochemical activity identified are kinase activity of CRN8 of *P. infestans* (van Damme et al., 2012), DNA damages capacity of CRN13 from *A. euteiches* (Ramirez-Garcés et al., 2016), affinity for heat shock protein element of PsCRN108 from *P. sojae* (Song et al., 2015), or affinity for transcriptional factor for CRN12_997 of *P. capsici* (Stam et al., 2013b). This work gives first insights into a new mode of action of an eukaryotic effector by deciphering a nuclear activity of *Aphanomyces euteiches* AeCRN5 C-terminal region. The soil born pathogen *A. euteiches* causes root rot disease on various legumes including alfalfa, clover, snap bean, stands as the most notorious disease agent of pea causing 20 to 100% yield losses, and infects the model legume *M. truncatula* (Gaulin et al., 2007). AeCRN5 was firstly identified in a cDNA library from *M. truncatula* roots in contact with *A. euteiches* (Gaulin et al., 2008) and confirm upon the

sequencing of the complete genome (Gaulin et al., 2018). AeCRN5 presents a modular architecture with an N-terminal functional LYLALK ensuring host delivery (Schornack et al., 2010) and a DN17 family domain at its C-terminus.

Here we show that AeCRN5 is induced during infection of *M. truncatula* roots. AeCRN5 C-ter is nuclear localized within the roots and triggers strong developmental defects. When expressed in *N. benthamiana*, the nuclear localisation is required to induce cell death. Furthermore, we observe a dynamic relocalization of AeCRN5 C-ter from nucleoplasm to nuclear bodies that required plant RNA. Additionally, using a FRET-FLIM assay in *N. benthamiana* leaves, we found that AeCRN5 C-ter associates to plant RNA. Finally, AeCRN5 C-ter seems to interfere with plant gene silencing mechanism. Taken together, these results indicate that CRN DN17 family function targets plant RNA and interferes with RNA silencing.

As preliminary results, we identified a putative interaction with the plant SERRATE protein, which seems to modulate miRNA processing.

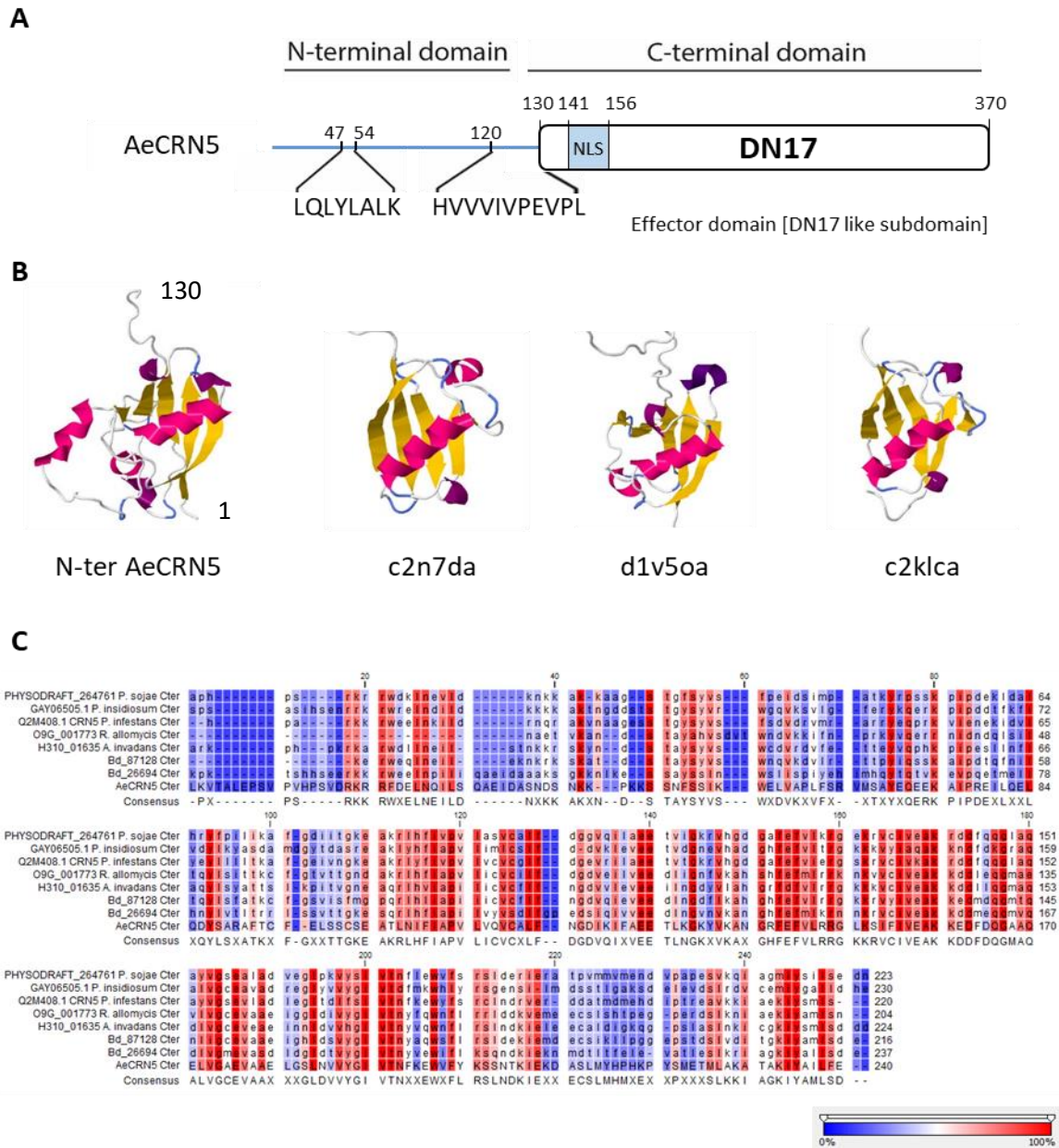


Figure 1: Amino acid sequence analyses of AeCRN5.

(A) Diagram depicting the modular architecture of AeCRN5 from *A. euteiches* with the conserved N-terminus, which includes the LxLYLALK and HVVVIVP motifs, and the C-terminal region containing the DN17 subdomain, based on *P. infestans* Crinkler (CRN) domain nomenclature. NLS sequence is indicated in coloured box. (B) AeCRN5 N-terminus three-dimensional structure predicted by the Phyre2 server. The three most confident (>95%) protein structures used as template by Phyre2 are also represented. Those templates belong to the ubl domain of human ddi2 (c2n7da), to the β -Grasp (Ubiquitin-like) superfamily (d1v5oa) and to human ubiquitin-like domain of ubiquilin 1 (c2klca). (C) Multiple amino acid sequences alignment of the C-termini domains from the closest orthologs of AeCRN5 C-ter domain. Organism names and sequence accession numbers are indicated in front of the sequences, and correspond to Restriction Endonuclease 5 domain in Zhang et al (Zhang et al., 2016) report. Background colours indicate residue conservation according to the legend. Alignment was performed by CLC Workbench (Qiagen).

RESULTS

AeCRN5 is a DN17 family protein with a modular architecture

The AeCRN5 (Ae201684_4018.1, http://www.polebio.lrsv.ups-tlse.fr/cgi-bin/gb2/gbrowse/Ae201684_V3/) N-terminus (1-130aa) is characterized by a LQLYLALK (47-54aa) motif and a HVVVIVPEVPL (120-130aa) motif marking its end (**Figure 1a**). Although it lacks a predicted signal peptide, the AeCRN5 N-terminus is a functional secretion domain mediating translocation of oomycete effectors to plant cell (Schornack et al., 2010). A recent study proposed a new classification of the N-terminal domains of CRNs proteins, based not only on amino acid sequences but also on secondary structure predictions (Zhang et al., 2016). Then we submitted AeCRN5 N-terminal domain to three-dimensional modelling using the structure prediction server Phyre2 (Kelley et al., 2015). The most confident three-dimensional predictions of AeCRN5 N-terminal domain were based on template models from Ubiquitin family, such as the β -Grasp (ubiquitin-like) domain superfamily or the ubl domain of human ddi2 protein (**Figure 1b**). This is in agreement with the analyses conducted by Zhang and colleagues (Zhang et al., 2016) that classify the N-terminal domains of CRNs as header domains containing the ubiquitin-like fold.

The C-terminal region shows a sequence identity of 41% with the CRN DN17 family domain of *P. infestans* (Haas et al., 2009) and harbors a nuclear localisation signal (NLS 141-156aa) consistent with its plant nuclear localization when expressed in *Nicotiana benthamiana* leaves (Schornack et al., 2010). CRN-like sequences including DN17 family have been reported not only in oomycetes, but also in pathogenic or mutualistic fungi, such as in the chytrid fungus *Batrachochytrium dendrobatidis* (Bd), a pathogen of amphibians, and in the arbuscular mycorrhizal fungus *Rhizophagus irregularis* (Ri) (Sun et al., 2011; Lin et al., 2014). Sequence comparison of C-terminal domain of AeCRN5 shows that it is closest to the chytrid *B. dendrobatidis* (45% identity) than to oomycetes CRNs (maximum 41% identity) (**Figure 1c**). Although AeCRN5 C-terminal domain was not included in the analyses of Zhang et al. (2016), the closest orthologs (included in the alignment from **Figure 1C**) were used in this study. Hence, the C-terminal domains of the CRN5-like from the chytrids Bd (Bd_87128 and Bd_26694; 45% identity for both) and *Rozella allomyces* (09G_001773; 44% identity), from oomycetes such as *Aphanomyces invadans* (H310_01635; 43% identity), *P. infestans* (CRN5_Q2M408; 41% identity) or *P. sojae* (Physodraft-264761; 40% identity), were all predicted to contain a Restriction Endonuclease 5 (REase 5) domain (Zhang et al., 2016) at their C-terminus.

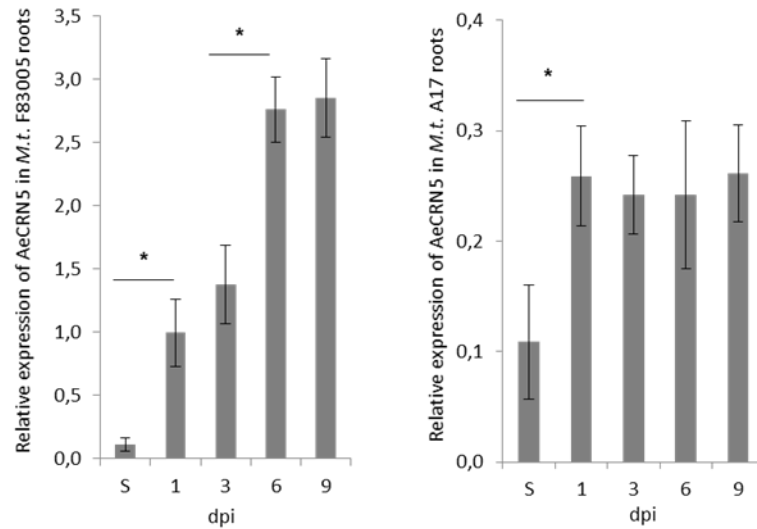
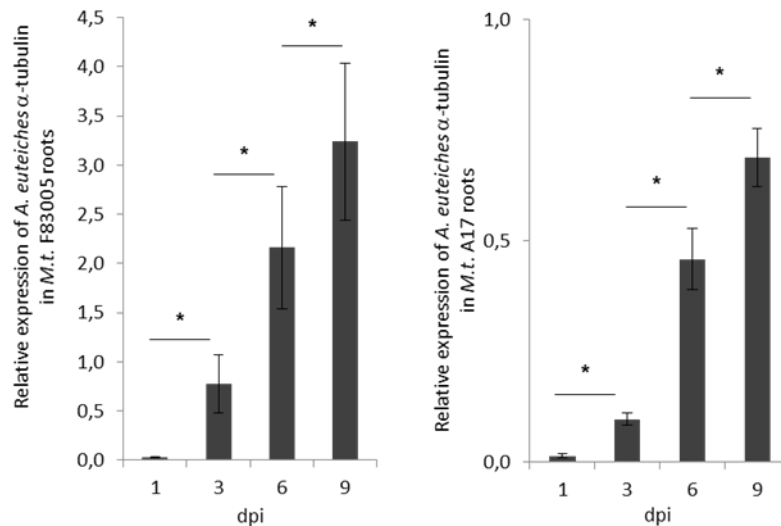
A**B**

Figure 2: AeCRN5 is expressed during *A. euteiches* infection of *M. truncatula*.

(A) Histograms represent the relative expression of AeCRN5 in *M. truncatula* roots infected by *A. euteiches*. AeCRN5 is expressed in saprophytic mycelium (S) but is significantly induced at the early stage of the infection of *M. truncatula* (1 dpi) in both tolerant (A17) and susceptible (F83005) lines. In F83005 infected plants, AeCRN5 is induced again at 6 dpi, whilst its expression is stable in A17 infected plants. (B) *A. euteiches* quantification in infected roots. Histograms represent the relative expression of α -tubulin gene from *A. euteiches* in F83005 or A17 infected plants. For both accessions, the pathogen development is confirmed but is strongly reduced in the tolerant accession A17 compared to the susceptible F83005 plants. Values are the mean of three independent biological replicates. Error bars are standard deviation errors. Asterisks indicate that the values are significantly different (p -value<0.05, Student t-test).

AeCRN5 is induced and expressed during infection of *M. truncatula*

AeCRN5 was firstly identified in a cDNA library from *A. euteiches* mycelium grown in close vicinity of *Medicago truncatula* roots (Gaulin et al., 2007) and the gene latter confirms in the genome of *A. euteiches* (Gaulin et al., 2018). To characterize its expression during infection, we conducted qRT-PCR analyses on saprophytic mycelium (i.e. grown on petri dishes with a standard medium) compared to infected *M. truncatula* roots, using the reference A17 Jemalong accession, considered as a tolerant line, and F83005.5 accession, which is far more susceptible to *A. euteiches* (Badis et al., 2015). AeCRN5 is expressed in saprophytic mycelium but is significantly induced at the early stage of the infection of *M. truncatula* (1 dpi) in both tolerant and susceptible lines (**Figure 2a**). Expression level of AeCRN5 is maintained at 3 dpi, and then induced again at 6 dpi in F83005.5 infected plants, but not in the resistant A17 plants, where expression is stable over the time. In parallel, quantification of *A. euteiches* abundance in roots (**Figure 2b**) confirms its development in host and reveals a sustained development between 3 and 6 dpi. As expected, *A. euteiches* infectious mycelium development is slower in the resistant accession than in the susceptible one (**Figure 2a and b**). These results indicate that although AeCRN5 is expressed during infection, its expression is reduced in the A17 tolerant plants, compare to the susceptible plants.

AeCRN5 is nuclear localized and perturbs root architecture of the host plant *M. truncatula*

AeCRN5 C-terminal (DN17) is nuclear localized and induces cell death symptoms when transiently expresses in *Nicotiana benthamiana* leaves (Schornack et al., 2010). To characterize AeCRN5 activity in host cells, we transformed *M. truncatula* A17 roots with a GFP-tagged AeCRN5 C-terminal (130-370) using *Agrobacterium rhizogenes*-mediated transformation system (Boisson-Dernier et al., 2001). Two weeks after transformation, a large number (around 75%) of the plantlets collapsed without generating new roots, in contrast to control plants (around 30%) suggesting a cytotoxic activity for AeCRN5 in *M. truncatula*.

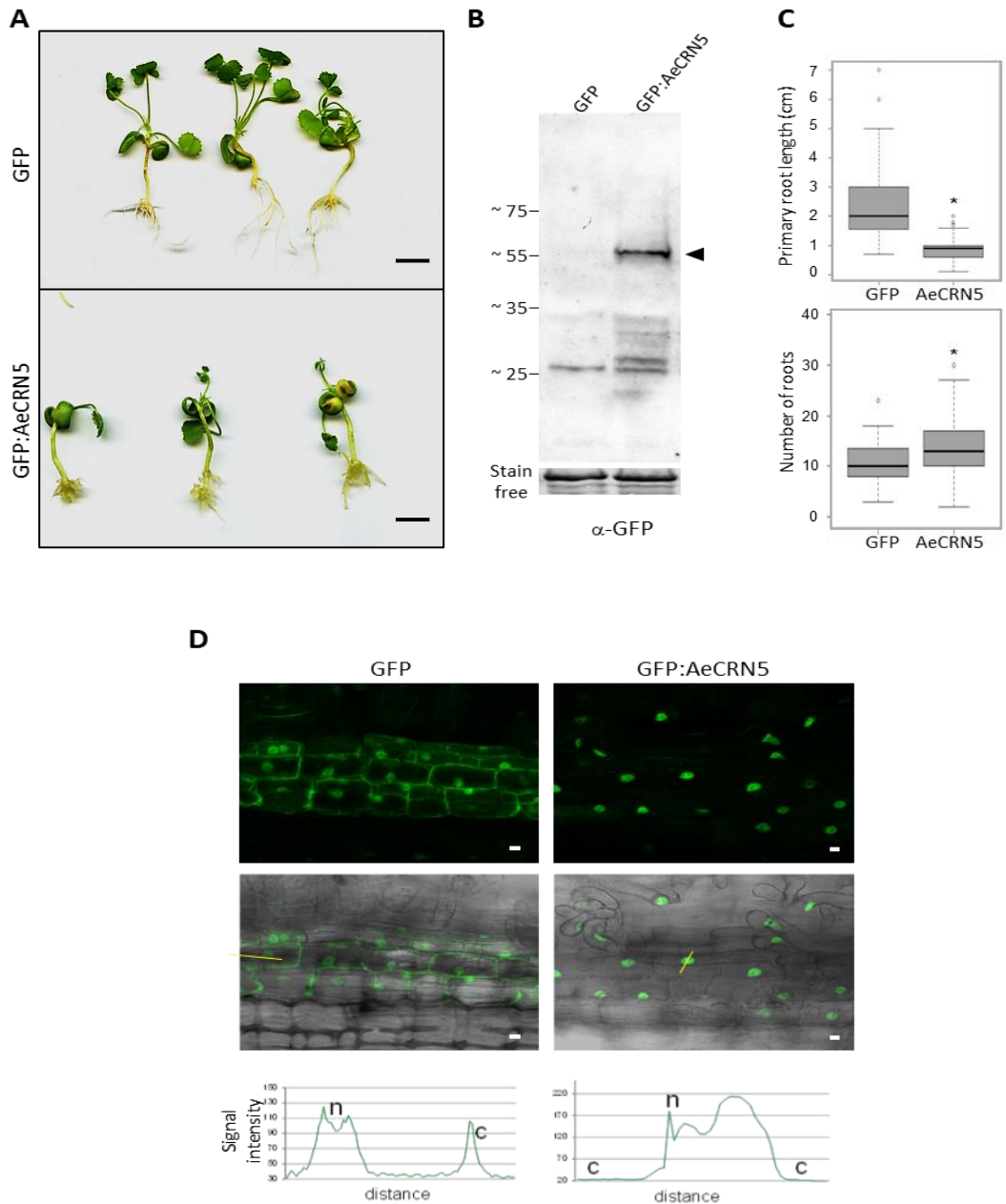


Figure 3: AeCRN5 is nuclear localized and perturbs root architecture in *M. truncatula*.

(A) Representative picture of *M.t.* plants expressing GFP or GFP:AeCRN5 C-ter 3 weeks after transformation. GFP:AeCRN5 plants present reduced aerial and root systems. Scale bars: 1 cm. (B) GFP immunoblot confirms the presence of the proteins. Arrow indicates the GFP:AeCRN5 C-ter band (55.15 kDa). Stain free is equivalent of Ponceau staining. (C) Box plots depicting the decrease in the primary root length and the increase in total root number per plant of the plants showed in (A). Measures and statistical analyses were performed on n=60 (GFP), n=145 (GFP:AeCRN5 C-ter). Asterisks indicate significant differences: *, $P < 0.05$, (Student t-test). (D) Confocal analyses confirming the nuclear localisation of GFP:AeCRN5 C-terminal domain in *M.t.* transformed roots. Scale bars: 10 μ m. Yellow lines indicate sections measured for GFP signal intensity showed in lower panels. n: nucleus; c: cytoplasm.

Within three weeks, plants that developed presented a reduction in development of aerial and root systems (**Figure 3a**). Presence of the protein was confirmed by immunoblot analyses using a GFP antibody and revealed the corresponding band (55.15 kDa) (**Figure 3b**). Quantification of primary root length and total root number (**Figure 3c**) indicated that AeCRN5 transformed roots presented a shorter primary root length, but seems to stimulate root emergence, resulting in a higher number of roots as compare to GFP-control plants. Then, confocal analyses of transformed roots confirmed the nuclear localization of AeCRN5 in host cells (**Figure 3d**). These observations indicate that AeCRN5 is nuclear localized and worries the root architecture in the host plant *M. truncatula*.

AeCRN5 cell-death inducing activity requires nuclear localization

To go further we assessed whether the observed cytotoxic effect of AeCRN5 C-terminus on plant cells is the result of a nuclear-related localization. For this purpose a Nuclear Export Signal (NES) or its mutated (mNES) counterpart was fused in N-ter position to the AeCRN5 C-terminal domain. The corresponding fusion proteins were GFP tagged and the constructs were expressed in *N. benthamiana* leaves by agroinfiltration. Necrotic lesions were observed within 5 days with AeCRN5 construct, whereas no symptoms were detected on leaves treated with NES:AeCRN5, even at longer times (>8 days) (**Figure 4a**). The addition of a mNES restored the cytotoxic activity of AeCRN5 (**Figure 4a**). Confocal microscopy imaging carried 24h after agroinfiltration confirmed that GFP:AeCRN5 fusion proteins were restricted to the nucleus (**Figure 4b**). An enhancement of nuclear export of AeCRN5 protein was detected with NES:AeCRN5 construct, since the GFP signal was recovered also in the cytoplasm. Fluorescence intensity measured in cells, corroborated NES:AeCRN5 partial mislocalization from the nucleus (**Figure 4b, lower panels**). A reestablishment of green fluorescence at the nuclear level was obtained for the mNES:AeCRN5 construct. Immunoblot analysis confirmed the accumulation of the fusion proteins from 1 to 3 days after agroinfiltration (**Figure 4c**). Altogether, these results showed that the cell death phenotype requires AeCRN5 to localize

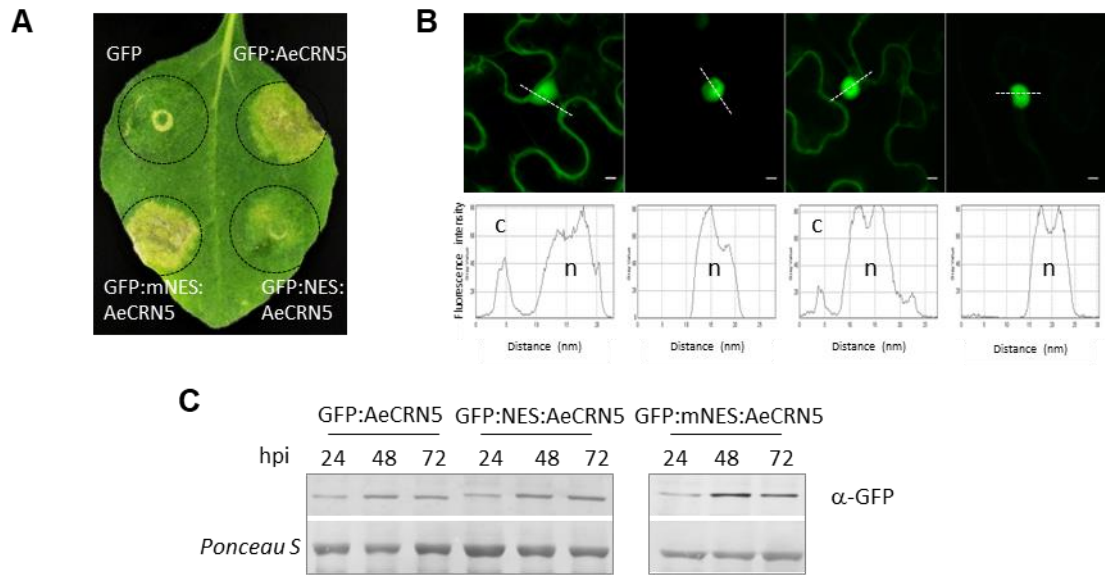


Figure 4: The biological function of AeCRN5 requires nuclear localization.

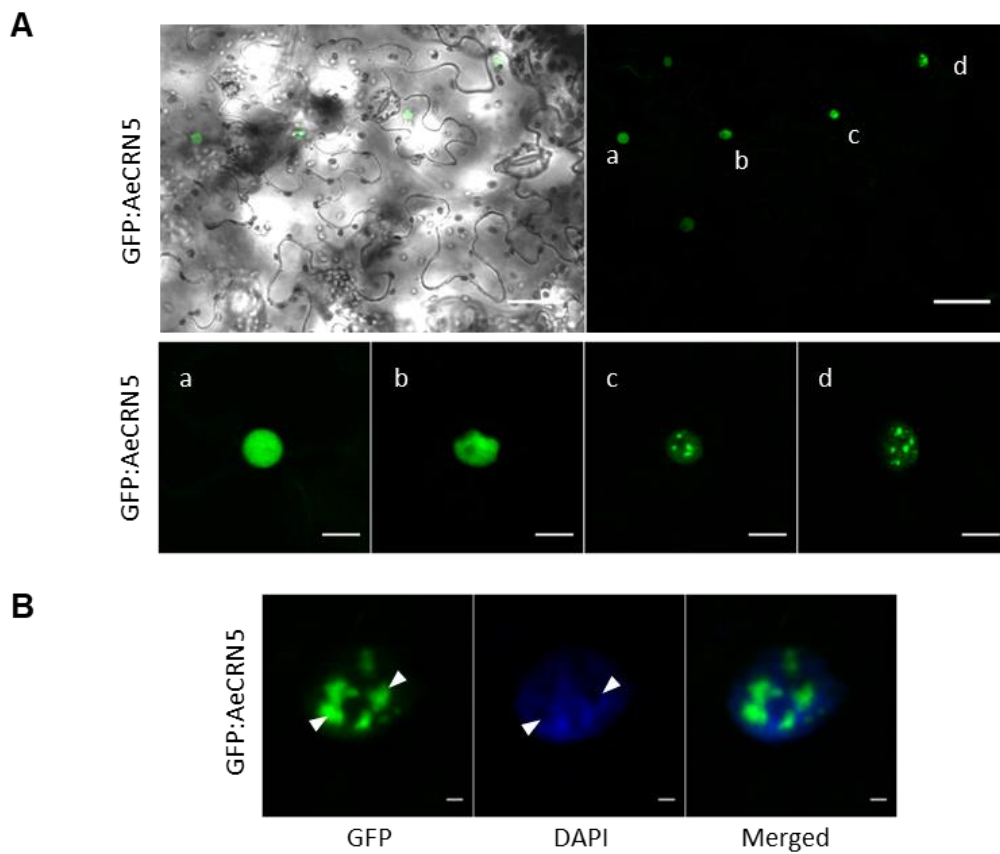


Figure 5: AeCRN5 transiently accumulates in nuclear bodies.

Figure 4: The biological function of AeCRN5 requires nuclear localization.

(A) Representative *N. benthamiana* agroinfiltrated leaf, five days after infiltration. GFP:AeCRN5 triggers necrosis whilst GFP:NES:AeCRN5 failed to induce cell death. In contrast, the construct comprising the mutated version of NES, GFP:mNES:AeCRN5, recovers cell death activity. Black dot circles represent agroinfiltration area. (B) Confocal analyses and fluorescence intensity plots confirmed the nuclear localization of GFP:AeCRN5 and GFP:mNES:AeCRN5. In contrast, GFP:NES:AeCRN5 shows a nucleocytoplasmic localization similar to GFP control. Scale bars: 5 μ m. Fluorescence plots : c : cytoplasm; n: nucleus. (C) GFP Immunoblots analyses confirmed the presence of all proteins (55.15 KDa, 56.92 KDa, 56.79 KDa respectively), 24 to 72h after infiltration.

Figure 5: AeCRN5 transiently accumulates in nuclear compartments.

N. benthamiana agroinfiltrated leaves, 20h after infiltration. (A) Top panel: Confocal pictures revealed distinct GFP:AeCRN5 localizations in nuclei. a,b,c,d: nuclei. Bottom: Enlargement pictures of the different nuclei a to d. (B) DAPI stained nucleus expressing GFP:AeCRN5. White arrows indicates GFP:AeCRN5 aggregates. Scale bars A Top: 50 μ m, Bottom 10 μ m. B: 1 μ m.

and to accumulate in the nucleus. This implies that AeCRN5 perturbs a nuclear-related process probably by interacting with a nuclear compound.

AeCRN5 is transiently localized in nuclear bodies

Upon transient expression experiments in *Nicotiana* cells, we observed different subcellular localizations of AeCRN5 C-ter domain. Indeed, time lapse confocal analyses on GFP:AeCRN5 agroinfiltrated *N. benthamiana* cells revealed that the protein transiently accumulates in nuclear bodies, between 16h and 24h after infiltration (under control of CaMV 35s promotor) (**Figure 5a**). This rearrangement in localization is not synchronized since some nuclei harbor clustered GFP signal accumulation, when others not (**Figure 5a**). DAPI staining performed on infiltrated leaves during this interval of time revealed an absence of complementary fluorescence pattern in these aggregates, where nuclear DNA and GFP fluorescence do not colocalized (**Figure 5b**). Homogeneous nuclear localization of AeCRN5 without any aggregates is observed after 30 hpi. These data suggest a dynamic process for AeCRN5 nuclear localization and therefore activity.

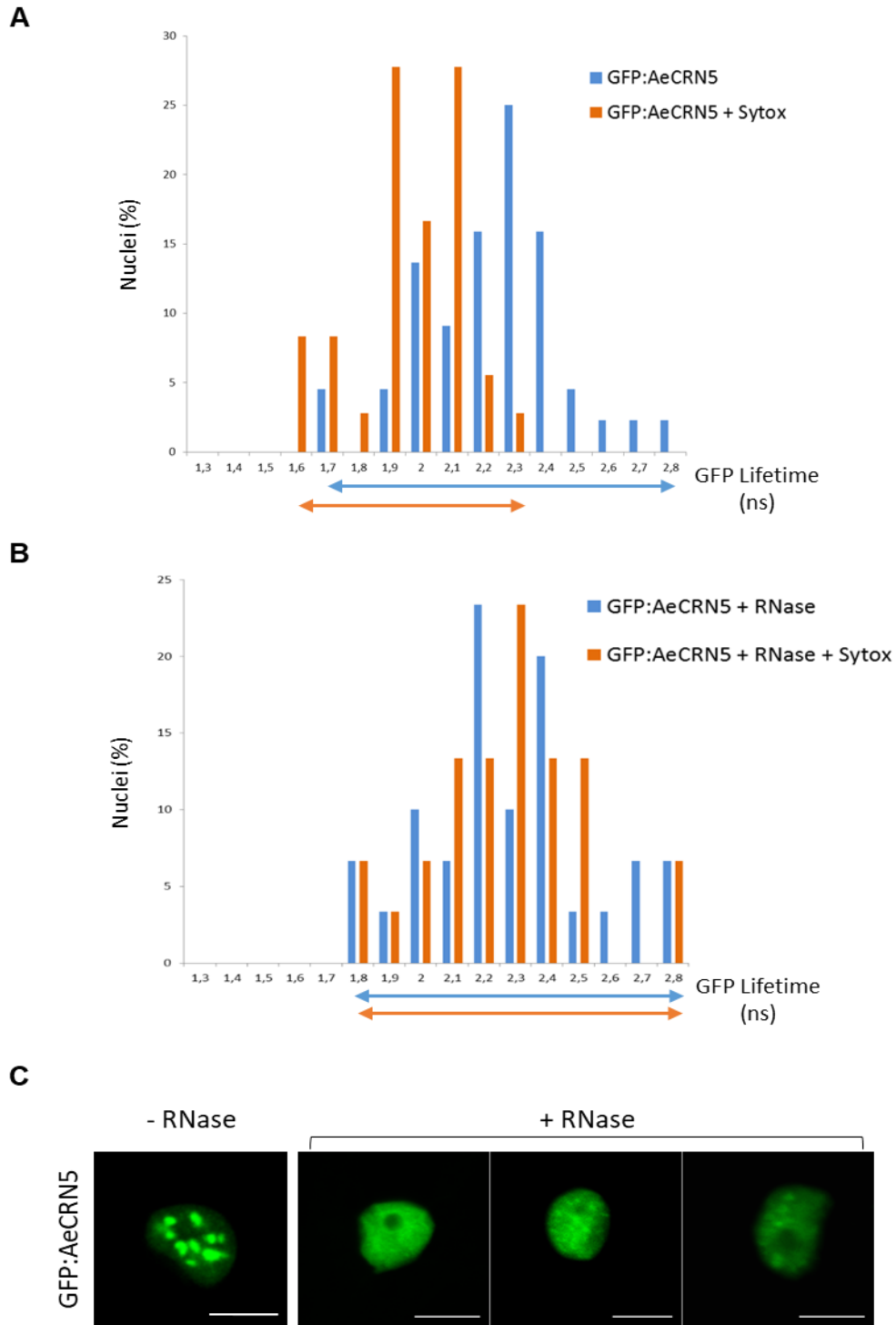


Figure 6: AeCRN5 binds to RNA in planta.

Histograms show the distribution of nuclei (%) according to classes of GFP:AeCRN5 lifetime in the absence (blue bars) or presence (orange bars) of the nucleic acids dye Sytox Orange. Arrows represent GFP lifetime distribution range. (A) In absence of RNase treatment. (B) After RNase treatment. Measurements were performed in *N. benthamiana* agroinfiltrated leaves, 24h after infiltration. (C) Confocal pictures of nuclei expressing GFP:AeCRN5 with or without RNase treatment. The typical clustered GFP signal (left panel) is strongly reduce after RNase treatment (representative nuclei after RNase treatment: right panels). Scale bars: 10 μ m.

AeCRN5 interacts with nuclear plant RNA

Plant nuclear bodies comprise different dynamic structures including for instance the nucleolus, Cajal bodies, nuclear speckles or Dicing bodies (Petrovská et al., 2015). Since RNA is a major component found in those compartments (Petrovská et al., 2015; Bazin et al., 2018), we decided to analyse whether AeCRN5 C-ter may associate with plant RNA. We developed a robust *in planta* system to test protein-nucleic acid interactions based of FRET-FLIM (Fluorescence Resonance Energy Transfer coupled to Fluorescence Lifetime Imaging) to determine whether C-terminal AeCRN5 could interact with nucleic acids, and more specifically to RNAs (Ramirez-Garcés et al., 2016; Camborde et al., 2017). This experiment is based on *N. benthamiana* cells expressing the GFP-fusion proteins in absence or in presence of the nucleic acid dye Sytox Orange. This dye can absorb energy released by GFP-tagged proteins (donor) during fluorescence only if GFP is in close proximity to the dye (acceptor). Such transfer of energy conducts to a decrease of GFP lifetime, inferring its interaction to nucleic acids. Additionally to GFP alone (used as a negative control since GFP proteins do not interact with nucleic acids), we performed measurements on cells expressing the DNA-binding protein H2B in fusion to GFP (GFP:H2B) as a positive control of protein-nucleic acid interactions. Fluorescence lifetime of GFP for all constructs is given in table 1. As expected, no significant decrease in GFP lifetime was observed for the GFP proteins in presence or absence of Sytox Orange (Table 1). In contrast, the GFP lifetime of GFP:H2B proteins decreases from 2.38 ns +/- 0.02 to 1.83 ns +/- 0.04 in presence of Sytox Orange, revealing as expected a close proximity of GFP-tagged H2B proteins with nucleic acids (Table 1). Those results on control proteins are in accordance with our previous study (Ramirez-Garcés et al., 2016). In the case of GFP:AeCRN5, GFP lifetime was measured in nuclei harbouring a GFP clustered fluorescence, corresponding to nuclear bodies. In that case, GFP lifetime significantly decreases from 2.20 ns +/- 0.04 in absence of acceptor to 1.90 ns +/- 0.03 in presence of Sytox Orange, indicating that the C-terminal domain of AeCRN5 is in close association with nucleic acids (Table 1 and **Figure 6a**). Since Sytox Orange labels DNA and RNA, in order to discriminate the nature of nucleic acids targeted by AeCRN5, foliar discs were treated with RNase and GFP lifetime was measured with or without Sytox Orange staining. Efficiency of this treatment was already confirmed on an RNA-binding protein called NSR-b, which lost the interaction with RNA in those conditions (Camborde et al., 2017). After RNase treatment, in absence of Sytox, the

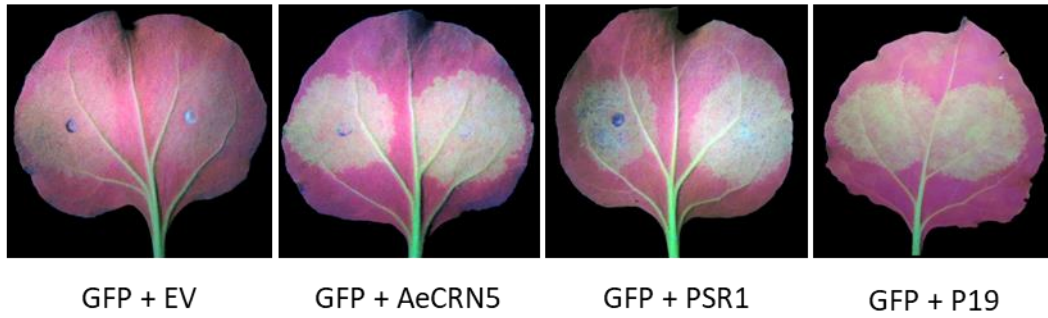
mean GFP lifetime of GFP:AeCRN5 proteins was 2.25 ns +/- 0.06 and remains at 2.24 ns +/- 0.06 in presence of Sytox Orange, indicating an absence of FRET (Table 1 and **Figure 6b**). Interestingly, the clustered GFP signal was strongly reduced or abolished after RNase treatment, suggesting that accumulation of GFP:AeCRN5 in nuclear bodies requires interaction with host RNAs (**Figure 6c**). Taken together, those results reveal that the C-ter domain of AeCRN5 binds plant RNAs.

Table 1: FRET-FLIM measurements for GFP, GFP:H2B and GFP:AeCRN5 in absence or presence of Sytox Orange dye.

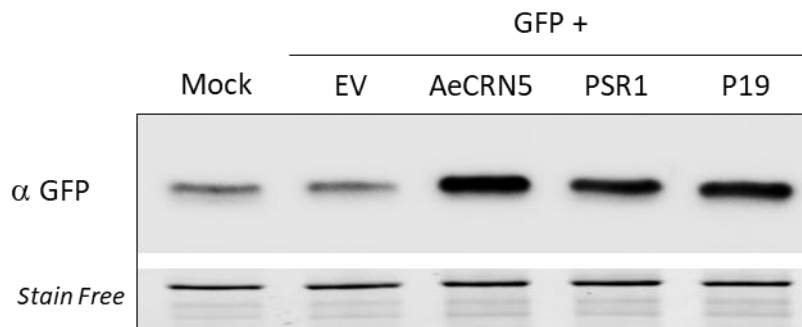
Donor	Acceptor	τ ^(a)	sem ^(b)	N ^(c)	E ^(d)	^(e) p-value
GFP	-	2.266	0.025	25	-	-
GFP	Sytox Orange	2.254	0.028	25	0.5	0.67
GFP:H2B	-	2.391	0.020	25	-	-
GFP:H2B	Sytox Orange	1.831	0.038	25	24	1.89E-19
GFP:AeCRN5	-	2.201	0.042	44	-	-
GFP:AeCRN5	Sytox Orange	1.902	0.030	36	14	5,57E-07
GFP:AeCRN5	- (RNase treatment)	2.249	0.056	32	-	-
GFP:AeCRN5	Sytox Orange (RNase treatment)	2.243	0.061	30	0.3	0.55

^{a)} τ : mean lifetime in nanoseconds (ns). For each nucleus, average fluorescence decay profiles were plotted and lifetimes were estimated by fitting data with exponential function using a non-linear least-squares estimation procedure. ^(b) sem.: standard error of the mean. ^(c) N: total number of measured nuclei. ^(d) E: FRET efficiency in % : $E=1-(\tau_{DA}/\tau_D)$. ^(e) p-value (Student's *t* test) of the difference between the donor lifetimes in the presence or absence of acceptor.

A



B



C

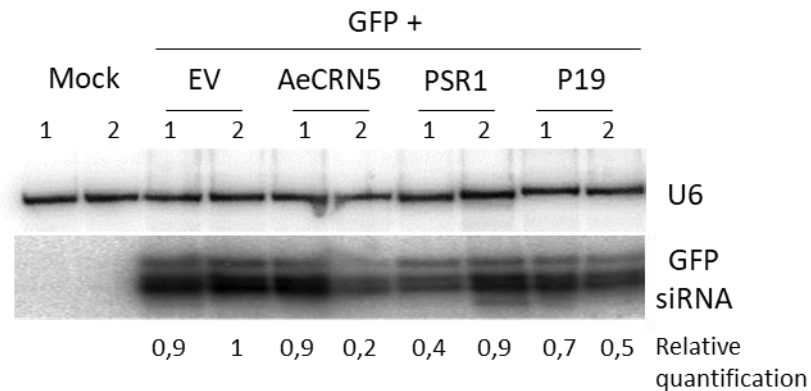


Figure 7: AeCRN5 interferes with post transcriptional gene silencing.

(A) *N. benthamiana* 16c agroinfiltrated leaves. Strong fluorescence is visible in leaves expressing AeCRN5, PSR1 or P19 proteins but not in leaves infiltrated with empty vector (EV). Pictures were taken at 3 d.p.i. (B) Representative GFP immunoblot on protein extracts from 3 d.p.i. leaves. Strong GFP bands confirm the accumulation of the GFP protein in the samples AeCRN5, PSR1 and P19. In contrast, weak bands in controls indicate lower accumulation. (C) GFP siRNA Northern blot. RNA were extracted from 3 d.p.i. leaves. Number 1 and 2 under the construct names indicate independent experiments. U6 was used as loading control. Numbers below represent the relative abundance of GFP siRNA, with the level in the leaves expressing only GFP and empty vector set to 1.

AeCRN5 interferes with post-transcriptional gene silencing mechanism

Since AeCRN5 is localized in nuclear bodies and interacts with RNA, we test whether it may acts on silencing mechanisms as previously reported for others intracellular effectors from oomycetes (Qiao et al., 2013, 2015). To test whether AeCRN5 could disturb siRNA silencing defense pathway, we performed a post-transcriptional gene silencing (PTGS) assay, described by Qiao et al. (Qiao et al., 2013). In this system, leaves of *N. benthamiana* 16c which constitutively express GFP under the control of the cauliflower mosaic virus 35S promoter are dually infiltrated with a GFP vector, in combination with an 'empty vector' (which not produce any proteins in plant). In this context, both endogenous and exogenous GFP genes are silenced by siRNAs induced by the infiltrated GFP construct, resulting in very low green fluorescence in the infiltrated zone (**Figure 7a**). When the empty vector is replaced by a plasmid p35S:AeCRN5C-ter, which expresses AeCRN5 C-terminal domain, a strong GFP fluorescence is observed in the treated area, suggesting an inhibition of silencing mechanism. Same distinct GFP fluorescence was observed when coexpressing GFP and PSR1, the *Phytophthora sojae* effector suppressor of RNA Silencing (Qiao et al., 2013, 2015). To support this finding we used another positive control by coinfiltrating GFP and P19 from tombusviruses, a protein known to suppress siRNA-silencing pathway. A strong fluorescence in the infiltrated leaves was observed, similar to the one obtained in presence of AeCRN5 C-ter or PSR1 (**Figure 7a**). Fluorescence levels were confirmed by GFP immunoblotting experiments, showing a strong accumulation of GFP proteins in the samples obtained in presence of AeCRN5, PSR1 and P19, compared to empty vector (**Figure 7b**). P19 binds to siRNA and decreases the level of free siRNA which prevent their association in RISC complexes and then block the silencing process (Lakatos et al., 2004). In contrast, PSR1 was shown to affect small RNA biogenesis directly, not their activity (Qiao et al., 2013). We then examined the abundance of GFP siRNA in those *N. benthamiana* 16c leaves. Northern blot performed on two independent experiments revealed a decrease in the accumulation of GFP siRNA in P19 samples (**Figure 7c**), but lower than expected compared to other study (Ying et al., 2010). AeCRN5 activity leads to a strong decrease in GFP siRNA levels compared to the control (GFP + empty vector EV) only in one experiment but not in the other (**Figure 7c**). Similarly, PSR1 expression strongly reduced the abundance of GFP siRNA as previously shown (Qiao et al., 2013) but only in one experiment,

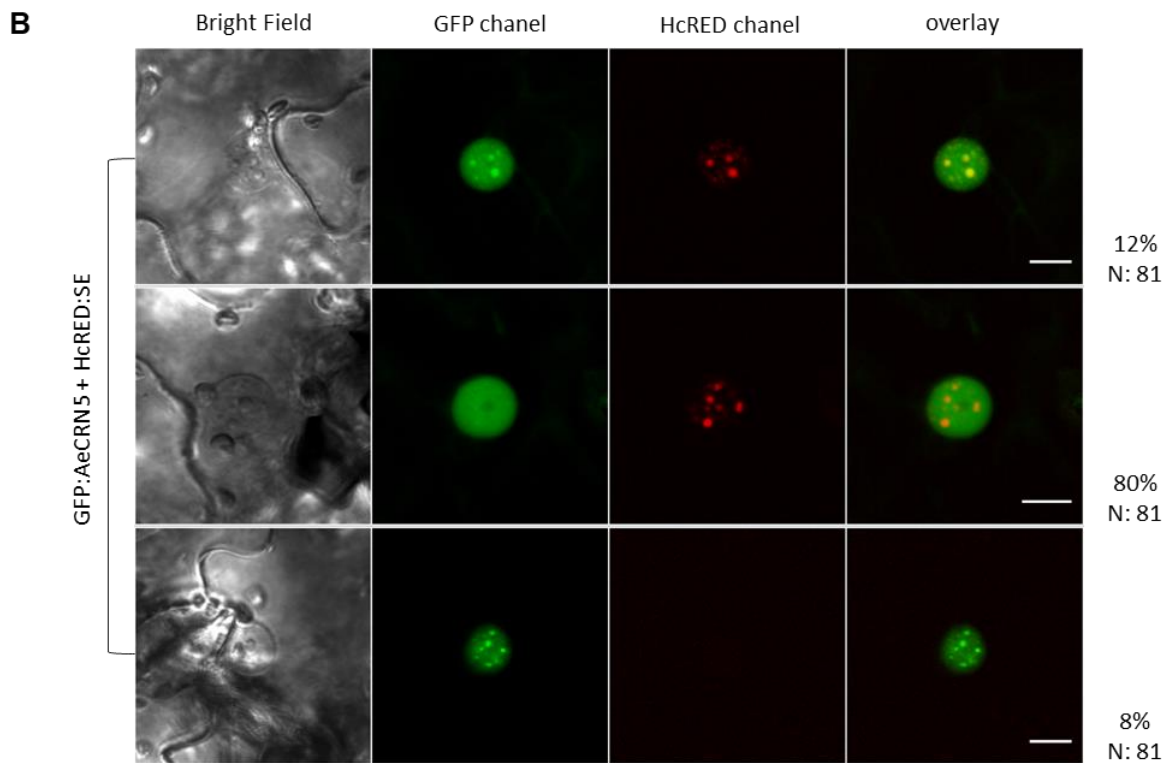
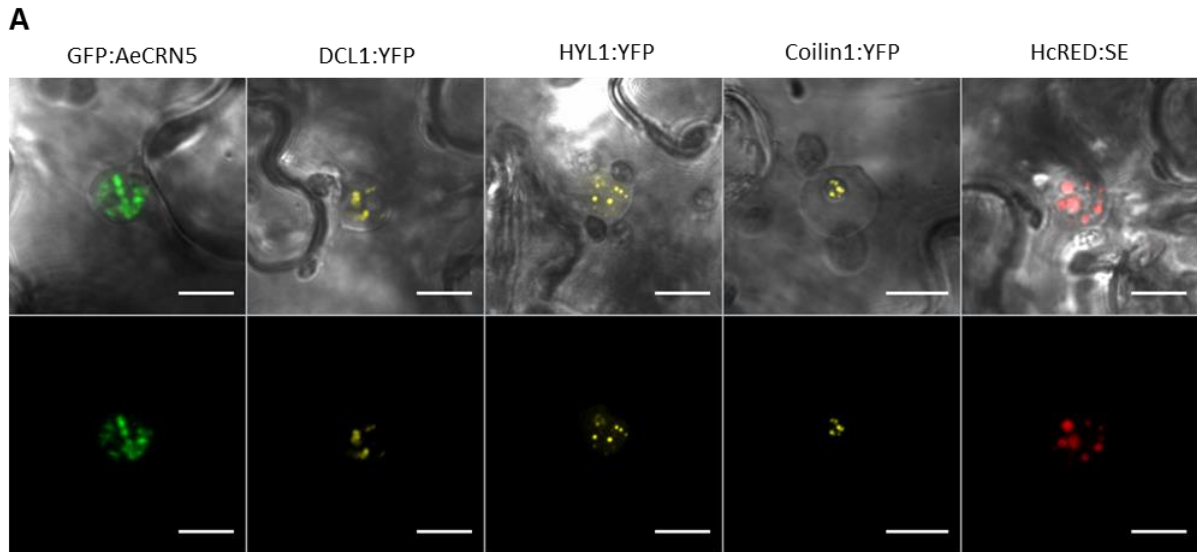


Figure 8: AeCRN5 partially colocalizes with SERRATE proteins in D-bodies.

(A) Confocal pictures of GFP:AeCRN5, DCL1:YFP, HYL1:YFP, Coilin1:YFP and HcRED:SE proteins 24h after infiltration in *N. benthamiana* leaves. GFP:AeCRN5 has a distinct localization from Coilin1, a Cajal body marker and has a closer localization to D-bodies markers. Scale bars: 10 μ m. (B) Confocal analyses of co-infiltrated *N. benthamiana* leaves with GFP:AeCRN5 and HcRED:SE constructs. While in 12% of the observed nuclei, AeCRN5 partially colocalizes with SERRATE protein, 80% harboured a homogenous GFP fluorescence, without aggregates, in presence of HcRED:SE proteins. In nuclei expressing GFP:AeCRN5 but not HcRED:SE (around 8% of observed nuclei), the typical localization of GFP:AeCRN5 in dots/aggregates was confirmed. Scale bars: 10 μ m.

not in the other (**Figure 7c**). Altogether, these results suggest that AeCRN5 can interfere with PTGS mechanism but supplementary experiments are needed to support this conclusion.

PRELIMINARY RESULTS

AeCRN5 is transiently localized in nuclear Dicing-bodies

To precise the nuclear localisation of AeCRN5 we infiltrated in *N. benthamiana* leaves with several nuclear markers to visualize Cajal bodies (such as Coilin-1) and D-bodies (such as Dicer-like 1 DCL1, HYPONASTIC LEAVES1 HYL1 and SERRATE SE). Coilin-1, DCL1 and HYL1 are cloned with a YFP tag in C-ter, whereas SE was fused with HcRED in N-ter. Cloning with other fluorescent tags is in progress. We compared the localization of GFP:AeCRN5 with each marker in *N. benthamiana* cells 20-24h after agroinfiltration. Confocal analyses revealed a distinct localization for Coilin-1:YFP, with fluorescent dots close or inside nucleolus. DCL1, HYL1 and SE localize in D-bodies and this profile could be partially similar to AeCRN5 (**Figure 8a**). To go further we next co-infiltrated GFP:AeCRN5 and HcRED:SE and observed their localization one day after treatment. In 92% of the observed nuclei, both proteins were detected in same nuclei with two types of labelling pattern. The preferential pattern observed in 80% of the nuclei correspond to a homogenous GFP fluorescence, without any aggregates (**Figure 8b**). In 12% of the nuclei, both proteins seems to colocalize in nuclear bodies probably D-bodies (**Figure 8b**). In nuclei expressing only GFP:AeCRN5 but not HcRED:SE (around 8% of observed nuclei), GFP:AeCRN5 is detected as typical clustered accumulation (**Figure 8b**). Although nuclear bodies markers and experimental repetitions are required, these suggest that AeCRN5 could localize in D-bodies, where it could interact with the SERRATE proteins.

AeCRN5 interferes with miRNA biogenesis

SERRATE (SE) is a major actor involved in the biogenesis of micro-RNA (miRNAs) (Lobbès et al., 2006; Wang et al., 2019). Since AeCRN5 transiently colocalizes with SE and interacts with RNA, we also hypothesize that AeCRN5 could perturb SE proteins during the maturation of miRNA. SE is involved in maturation of the primary transcripts (pri and pre-miRNA) into mature miRNA.

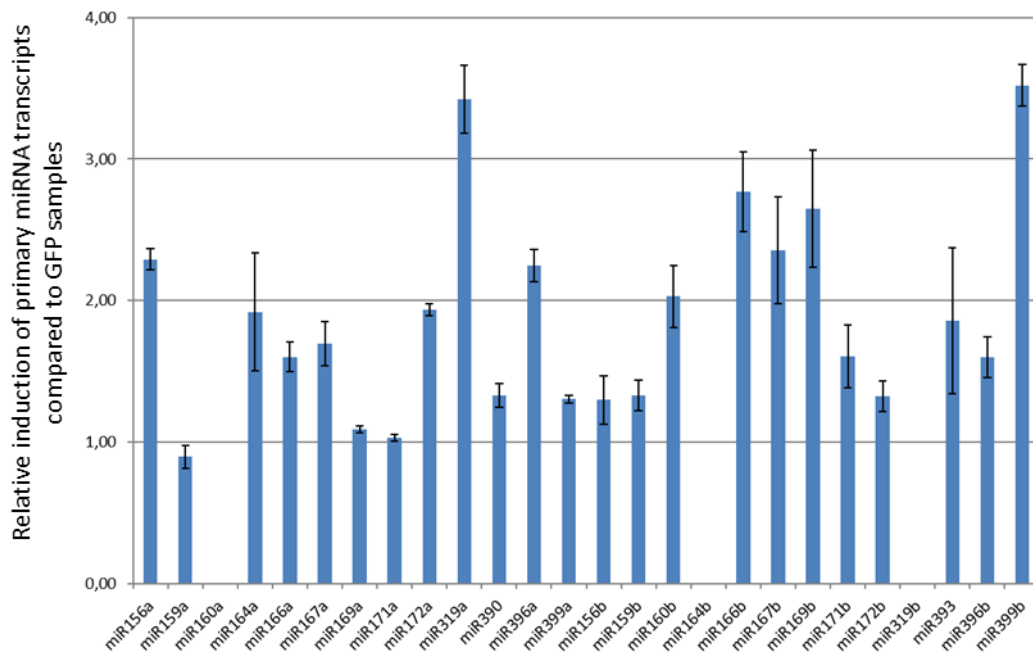


Figure 9: AeCRN5 interferes with the maturation of primary miRNA transcripts.

qPCR results showing the relative induction of 26 primary miRNA transcripts (pri+pre miRNA), 24h after infiltration of *N. benthamiana* leaves with GFP:AeCRN5 compared to GFP control leaves. No bars indicate that the amplification failed, probably due to wrong primer sequences. N: 10 leaves for GFP:AeCRN5, 10 leaves for GFP.

Therefore, interference in the maturation process will trigger an accumulation of primary miRNA transcripts. We decided to analyse several primary miRNA transcript levels, described in the literature as key regulators of root architecture and biotic interactions, on *N. benthamiana* leaves agroinfiltrated with GFP:AeCRN5 or GFP (as a negative control). The presence of the GFP:AeCRN5 localization in D-bodies from 20h to 24h after agroinfiltration was confirmed by confocal observations and before sampling the corresponding leaves. We next selected 26 miR, already sequenced and analysed in various reports (for review see (Couzigou and Combier, 2016)). Primers for qPCR amplification were designed according to miRBase (Kozomara et al., 2019) (<http://www.mirbase.org/>) based on *Nicotiana tabacum* sequences (*N. benthamiana* is not available). QPCR analyses were performed on ten GFP:AeCRN5 and ten GFP agroinfiltrated leaves. Results revealed that most of the primary transcripts analysed accumulates in the AeCRN5 samples compared to the GFP controls (**Figure 9**), suggesting that AeCRN5 perturbs the miRNA biogenesis.

DISCUSSION

To favor the establishment of disease, microorganisms have gained the ability to deliver effector molecules inside host cells. The important number of effectors targeting host nuclei places this organelle, and functions related to it, as important hubs whose perturbations might be of crucial importance for the outcome of infection (Bhattacharjee et al., 2013; Khan et al., 2018). A recent study reported that in average, 38% of phytopathogenic oomycete intracellular effectors target nucleus, close to the number reported for plant bacterial pathogens (35%) (Khan et al., 2018). CRN proteins are a family of nuclear-localized effectors widespread in oomycete lineage, with related sequences found in fungal species *B. dendrobatidis* and *R. irregularis*. In this work, we undertook the characterization of AeCRN5 of the root pathogen *A. euteiches*. We show that AeCRN5 is express during *M. truncatula* infection and perturbs host root development. We reveal that AeCRN5 is mainly localized in Nuclear bodies (D-bodies) and targets plant RNA at the nuclear level as well as SERRATE protein, to interfere with RNA processes.

AeCRN5 is a modular CRN DN17 protein family with orthologous sequences in *Phytophthora* sp. and true fungal species including the chytrid *B. dendrobatidis* and the endomycorrhiza *R. irregularis*. The functional translocation signal of AeCRN5 is characterized by LYLALK and HVVVIP motifs and the absence of an obvious signal peptide (Schornack et al., 2010; Gaulin et al., 2007). Since a study from Zhang et al. proposed to reconsider the N-terminal CRNs classification (Zhang et al., 2016), we submitted to a structure prediction server the N-terminal sequence of AeCRN5. This *in silico* analysis confirms the classification of AeCRN5 N-ter as a header domain containing ubiquitin-like fold.

The C-terminus corresponds to a CRN DN17 domain family with a NLS, according to the classification established from *Phytophthora* CRNs (Haas et al., 2009; Schornack et al., 2010), which have no significant similarity to functional domain. Although AeCRN5 was not included in the analysis of Zhang and colleagues, the closest orthologs of AeCRN5 found in *Bd* fungus, other *Aphanomyces* species or *Phytophthora* species, were included and were predicted to contain a Restriction Endonuclease 5 domain (Zhang et al., 2016). Here we confirm this prediction for AeCRN5. *Phytophthora* CRNs were originally identified as activators of plant cell death upon their *in planta* expression (Torto et al., 2003), although not all CRNs promote infection including the AeCRN5 ortholog from *P. capsici* (Stam et al., 2013a). CRN5 sequences from *A. euteiches* were firstly reported in a cDNA library from mycelium grown in close vicinity of *M. truncatula* roots (Gaulin et al., 2008). Here we showed by qRT-PCR analysis, that AeCRN5 is expressed during vegetative growth and expression goes up during root infection, but is differentially induced depending on the susceptibility of the plants. In susceptible line, an increase in expression is observed firstly at 1 dpi, then between 3 and 6 dpi, a stage where browning of roots is observed in combination to an entire colonization of the root cortex of *M. truncatula*, and the initiation of propagation to vascular tissues (Djébali et al., 2009). In contrast, in tolerant line, AeCRN5 expression is stable after a rapid induction at 1 dpi. This could be related to differential plant responses, involving for instance cross-kingdom RNAi, where plant transports small RNAs into pathogens to suppress the expression of virulence related genes. This defense response was recently reported in fungal plant association, where it was evidenced that *Arabidopsis* sRNAs are delivered into *Botrytis cinerea* cells to induce silencing of pathogenicity-related genes (Cai et al., 2018). In a same way, an alpha/beta hydrolase gene from *Fusarium graminearum*, required for fungal infection, is targeted and

silenced by a miRNA produced by wheat (Jiao and Peng, 2018). Interestingly, this defense mechanism has been recently reported in plant-oomycete interaction. *Arabidopsis* infection by *Phytophthora capsici* leads to an increased production of plant small interfering RNAs (siRNAs) which are delivered into *Phytophthora* to silence target genes during natural infection (Hou et al., 2019). However, this cross-kingdom silencing has not yet been mentioned for *Medicago truncatula* or other legume in plant-pathogen interactions. Furthermore, transcriptomic analyses conducted on infected F83005 susceptible accession compared to *A. euteiches* mycelium or zoospores samples indicate that only 2% of CRNs genes were induced at 3 and 9 dpi (1 dpi was not possible to analyse) (Gaulin et al., 2018), consistent with AeCRN5 expression in F83005 roots. Given that 13% of CRN genes are upregulated in zoospores as compared to *in vitro* grown mycelium, a subset of AeCRNs is potentially involved at the early stage of *Medicago* infection (Gaulin et al., 2018). Finally, in *P. capsici*, CRNs genes were divided in two groups according to their expression patterns. *P. capsici* DN17 ortholog fell in Class 2 where gene expression gradually increases to peak in the late infection stages (Stam et al., 2013b), as observed for AeCRN5 gene expression in susceptible *Medicago* line, suggesting a role in the later stage of colonization.

We further explored the function of AeCRN5 by using a GFP-tagged version of the C-terminal domain. As observed in *N. benthamiana* leaves (Schornack et al., 2010), AeCRN5 is nuclear localized also in host *Medicago* cells. Overexpression of AeCRN5 in *M. truncatula* roots displayed a cytotoxic effect leading in few days to death of transformed plants. The surviving dwarfed plants harbored reduced root systems with a higher number of roots. These results corroborate observations made during *M. truncatula* roots infection, where susceptible accessions present, within few days after *A. euteiches* infection, a decrease of secondary root development and necrosis of roots (Djébali et al., 2009).

Confocal studies on transiently transformed *N. benthamiana* leaves showed that DN17 cytotoxic effect of AeCRN5 required a plant nuclear accumulation. It is in accordance with the observed reduction of cell death on *N. benthamiana* leaves, upon nuclear exclusion of CRN8 (D2 domain) from *P. infestans* (Schornack et al., 2010). Similar results were reported for *P. sojae* and *P. capsici* CRNs (PsCRN63 and PcCRN4) (Liu et al., 2011; Mafurah et al., 2015) and AeCRN13 from *A. euteiches* (Ramirez-Garcés et al., 2016). Our results confirm that nuclear

localization is an important requirement for the cell-death inducing activity of necrotic CRN effectors.

We observed that AeCRN5 DN17 shuttles between nucleoplasm and plant nuclear bodies where DNA is excluded. Previous study on *P. capsici* DN17 CRN domain revealed a clustered distribution pattern confined to the nucleoplasm upon overexpression in *N. benthamiana* leaves (Stam et al., 2013a). Furthermore, FRET-FLIM measurements revealed the close vicinity of AeCRN5 C-ter domain with plant nucleic acids. This FRET-FLIM assay has been successfully used to demonstrate protein-RNA specific interaction in plant cells (Camborde et al., 2017). Here this assay confirms the RNA binding ability of AeCRN5 C-terminal domain.

Recently, Khan and colleagues reviewed some properties of effector targets across diverse phytopathogens, including bacteria, fungi and oomycetes. They reported that only 1 to 3% of effector targets had a molecular function related to RNA processing (Khan et al., 2018). Candidate effectors of the fungus *Blumeria graminis* display similarities to microbial RNases and, although not carrying hydrolytic site, are speculated to interact with host RNA; among these, BEC1054 has been described as a ribonuclease-like effector (Pedersen et al., 2012; Pliego et al., 2013). Host RNA perturbation has also been proposed for some effectors of the nematode *M. incognita* as they harbor putative RNA binding domains (Bellafiore et al., 2008).

The dynamics and clustered localization of AeCRN5 DN17 domain in combination with its proximity to plant RNA, strongly suggest a 'nuclear bodies pattern'. Even if further experiments are on going to precise the subnuclear localization of AeCRN5, we decided to test the activity of the C-ter DN17 domain on silencing mechanisms as previously reported for others intracellular effectors from oomycetes (Qiao et al., 2013, 2015). Using transient expression assay in *N. benthamiana* 16c, we found that AeCRN5 DN17 domain interferes with post-transcriptional gene silencing, even if the effect on siRNA biogenesis is still unclear. Hence, the biological function of AeCRN5 could be similar to the one reported for RxLR PSR1 from *P. sojae*. However, PSR1 do not interact with RNA, but with a host DEAD-box RNA helicase (named PINP1) required for the accumulation of endogenous small RNAs and considered as a positive regulator of plant immunity. Other studies describe the role of intracellular effectors on RNA-binding proteins (RBPs), such as Pi04089, an RxLR effector from *P. infestans* that targets a host RBP to promote infection (Wang et al., 2015), but without interacting with RNA. Further experiments are required to decipher the role of AeCRN5 on

RNAs, for instance using mutated version of AeCRN5 C-ter domain, unable to bind RNA, or by testing the nuclease activity of the C-terminal domain, classified as a REase5 domain by Zhang et al. (Zhang et al., 2016). Hence, it seems that manipulation of host RNA and related processes may be a common infection strategy.

We also present some preliminary results where we detected a putative interaction of AeCRN5 with the SERRATE (SE) protein, localized in nuclear Dicing-bodies. Co-immunoprecipitation experiments coupled with FRET-FLIM analyses for instance are necessary to confirm a physical interaction between the two partners. miRNA biogenesis is a highly controlled and complex process, in which SE is a core component in interaction with multiple protein partners. For instance, a very recent study reported the role of the *Arabidopsis* RNA-binding protein MAC5 that interacts with SE to protect pri-miRNAs from SERRATE-dependent exoribonuclease activities (Li et al., 2020). Due to the central role of SE in the miRNA biogenesis, we further tested the impact of AeCRN5 expression on miRNA primary transcripts accumulation in *N. benthamiana* leaves. Interestingly, in most of the selected sequences, we found a significant induction of primary transcripts in presence of AeCRN5 C-ter proteins. Despite we can not exclude that expression of AeCRN5 triggers an increase in miRNA primary transcripts production, we hypothesise that AeCRN5 interferes with the dicing complex where SE is a major component, perturbs its activity, resulting in an accumulation of pri-pre miRNA. Interestingly, the *P. sojae* RxLR effector PSR1 that acts on siRNA accumulation was also proposed to interfere with miRNA biogenesis. Indeed, even if qPCR measurements didn't reveal a significant effect on pri-miRNA, RNA blotting experiments on 2 selected genes revealed a reduce accumulation of pre-miRNA. Then authors suggest that PSR1 could inhibit DCL1-mediated processing of pri-miRNAs (Qiao et al., 2013).

To go further on the biological function of AeCRN5, we need to perform quantitative PCR on mature miR sequences to confirm our hypothesis. A mutated version of AeCRN5 C-ter domain, unable to bind RNA and to localize in D-bodies should not interfere with miRNA biogenesis. Additionally, resistance to *A. euteiches* in *M. truncatula* plants overexpressing SE or in opposite silenced SE gene could be measured to analyse the impact of SE activity on infection process. Finally, pri-miRNA or mature miRNA analyses (using RT-qPCR) in *M. truncatula* plants

infected by *A. euteiches*, or in AeCRN5 overexpressing *M.t* plants could strengthen the role of AeCRN5 on miRNA biogenesis.

In conclusion, AeCRN5 is an effector with a functional Ubi N-ter domain and a C-ter domain that targets RNA to interfere with RNA processes such as post-transcriptional gene silencing or miRNA biogenesis.

MATERIAL AND METHODS

Plant material, microbial strains, and growth conditions

M. truncatula F83005.5 or Jemalong A17 seeds were scarified, sterilized, and cultured *in vitro* for root transformation and infection as previously described (Djébali et al., 2009; Boisson-Dernier et al., 2001). Infection of roots with zoospores of *A. euteiches* (strain ATCC 201684) was performed as Djébali et al., 2009. *N. benthamiana* plants were grown from seeds in growth chambers at 70% of humidity with a 16h/8h dark at 24/20°C temperature regime. *A. euteiches* (ATCC 201684) was grown on saprophytic conditions as previously reported (Badreddine et al., 2008). All *E.coli* strains (DH5 α , DB3.5, BL21AI), *A. tumefaciens* (GV3101::pMP90RK) and *A. rhizogenes* (Arqual) used were grown in LB medium with the appropriate antibiotics.

Sequence analyses

AeCRN5 N-terminal domain was submitted to structure prediction Phyre2 server (Kelley et al., 2015). Oomycetal and fungal orthologs of AeCRN5 (Ae201684_4018.1, http://www.polebio.lrsv.ups-tlse.fr/cgi-bin/gb2/gbrowse/Ae201684_V3/) was retrieved by BlastP searches on the National Center for Biotechnology Information (NCBI) website using AeCRN5 C-terminal domain as query. From this result, sequences from the closest orthologs (*B. dendrobatidis* Bd_26694 and Bd_87128; *A. invadans* H310_01635; *R. allomycis* O9G_001773; *P. infestans* CRN5_Q2M408.1; *P. insidiosum* GAY06505.1 and *P. sojae* Physodraft_264761) were extracted and C-termini domains were aligned using CLC Workbench software (Qiagen).

RNA extraction and qRT-PCR

For AeCRN5 quantification: Samples were ground on liquid nitrogen and total RNA extracted using the RNAeasy kit (Qiagen). Reverse transcription was performed on 1 µg of total RNA using the AppliedBiosystems kit (Life Technologies-Invitrogen). cDNAs were diluted 50-fold for qPCR reaction. Each qPCR reaction was performed on a final volume of 10 µl corresponding to 8 µl of PCR mix (0.5 µM of each primer and 5 µl SYBRGreen, Applied Biosystems) and 2 µl of the diluted cDNA and was conducted on a QuantStudio 6 (Applied Biosystems, Foster City, CA, USA) device using the following conditions: 5 min at 95°C, followed by 45 cycles of 15 s at 95°C and 1 min at 60°C. Each reaction was conducted on triplicates for cDNAs of four biological replicates. Primers F: 5'-GAAATTCTGCAAGAACTCCA-3' and R: 5'-CAATAAAGATGTTGAGAGTGGC-3' were used for the detection of AeCRN5 (Ae201684_4018.1). Primers F: 5'-TGTCGACCCACTCCTTGTTG-3' and R: 5'-TCGTGAGGGACGAGATGACT-3' were used to assess the expression of *A. euteiches*'s α -tubulin gene (Ae_22AL7226) and normalized AeCRN5 expression. Histone 3-like of *M. truncatula*, previously described (Rey et al., 2013) was used to normalize *A. euteiches* abundance during infection. Relative expression of AeCRN5 and α -tubulin genes were calculated using the $2^{-\Delta\Delta Cq}$ method described by (Livak and Schmittgen, 2001).

For Pri-miRNA measurements: Ten *N. benthamiana* leaves were agroinfiltrated with GFP or GFP:AeCRN5. 20h to 24h after agroinfiltration, confocal observations confirm the clustered localisation for GFP:AeCRN5 and the corresponding leaves were sampled and frozen in liquid nitrogen. Total RNA was extracted using the RNAeasy kit (Qiagen) and reverse transcription was performed on 1 µg of total RNA using the AppliedBiosystems kit (Life Technologies-Invitrogen) using random primers. Primers of the 26 pri-miRNA selected were designed according to miRBase (Kozomara et al., 2019) (<http://www.mirbase.org/>) based on *Nicotiana tabacum* sequences (*N. benthamiana* is not available) and are listed in Supplementary Table 1. For each gene, expression levels were standardized using *N. benthamiana* L23 gene (TC19271-At2g39460 ortholog) and F-box gene (Niben.v0.3.Ctg24993647-At5g15710 ortholog) validated for qPCR (Liu et al., 2012). Relative abundance was calculated using the $2^{-\Delta\Delta Cq}$ method.

Construction of plasmid vectors

Sequence and names of primers used are listed in the Supplementary Table 1. AeCRN5 C-terminal version carrying Gateway adaptors were generated by PCR on a template corresponding to the Ae201684_4018.1 (named Ae_1AL4462 in previous aphanoDB version). Full length C-terminus AeCRN5 (130aa-370aa) was generated using primer AttB1AeCRN5-F and AttB2AeCRN5-R. Amplicons were BP recombined in pDONR-Zeo vector (Invitrogen) and subsequently inserts were introduced in vector pK7WGF2 by means of LR recombination (Invitrogen). GFP:NES:AeCRN5 and GFP:mNES:AeCRN5 constructs were generated by adding NES sequence (LQLPPLERLTL) and non-functional mutated NES sequence (mNES: LQAPPAERATL) to the N-terminal moiety of AeCRN5. Amplicons NES:AeCRN5 and mNES:AeCRN5 were obtained using primers NES:AeCRN5-F and AeCRN5_end-R and mNES_AeCRN5-F and AeCRN5_end-R respectively and introduced in pENTR/D-TOPO vector by means of TOPO cloning (Invitrogen) before insertion on vector pK7WGF2. Amplification of the histone 2B of *A. thaliana* was performed on vector pBI121:H2B:YFP (Boisnard-Lorig et al., 2001) with primers cacch2B-F and H2B-R. Amplicons were cloned in pENTR/D-TOPO and subsequently introduced in vector pK7WGF2 to obtain GFP:H2B fusion construct. The obtained pK7WGF2 recombined vectors were introduced in *Agrobacterium* strains for agroinfiltration and root transformation.

Coilin1:YFP, DCL1:YFP, HYL1:YFP and HcRED:SE corresponds to *A. thaliana* genes cloned in pCambia1300 and were kindly provided by S. Whitham (Liu and Whitham, 2013).

Supplemental Table 1: List of primers used in this study.

gene	primer F	primer R
AeCRN5	TTCCGCGTGAAATTCTGCAA	GCACATACTTGGACCAGCAC
Ae α -tubulin	TGTCGACCCACTCCTTGTTG	TCGTGAGGGACGAGATGACT
attB1_AeCRN5-F	GGGGACAAGTTTGTACAAAAAAGCAGGCTTCTTGAA GGTGACCGCTCTAGAACCC	
attB2_AeCRN5-R		GGGGACCACTTTGTACAAGAAAGCTGGGTGTT GTTATTCAAAAAGTATGGCG
AeCRN5_end-R		TTGTTATTCAAAAAGTATGGCGTAAATTTGGC

NESAeCR N5-F	CACCCTTCAACTTCCTCCTCTTGAAAGACTTACTCTTTT GAAGGTTGACCGCTCTAGAACCC	
mNESAe CRN5-F	CACCCTTCAAGCTCCTCCTGCTGAAAGAGCTACTCTTT TGAAGGTGACCGCTCTAGAACCC	
cacCH2B- F	CACCATGGCGAAGGCAGATAAGAAACCAGC	
H2B-R		TTAAGAACTCGTAAACTTCGTAACCGCC
mGFP5-F	GATCATATGAAGCGGCACGACTTCT	
mGFP5- R_T7pro m		ATCGAGTAATACGACTCACTATAGGGTTCCAA CTTGTGGCCGAGGATG
Nb_L23	AAGGATGCCGTGAAGAAGATGT	GCATCGTAGTCAGGAGTCAACC
Nb_F- BOX	GGCACTCACAAACGTCTATTTTC	ACCTGGGAGGCATCCTGTTAT
miR156a	CGGAGGTGAAATTTTTGAA	AAAAGGGACAGTGCAACTCAA
miR156b	TCCTGCACCCATATTGAACA	GAGGAAGCGGATTGAAAGTG
miR159a	TAAGCTGCCGACCTATGGAT	GGCAATGAAGCTCCTGACAT
miR159b	CCAGCTAGGCTACCTCGTGA	TATTGAGCGGGAGCTGTCTT
miR160a	TGGATGACTTTGAGCCCTTT	GATCACGGATACGCTCCAAT
miR160b	TATTTCCGGGATATGCTTGG	TTGCAGAGCTCATCGGAATA
miR164a	AACCATTGATCGGAGCTGAG	GAAGAAGGGCACATGGAAAA
miR164b	GCAGGGCATGTGCACTACTA	TTTGACGGAAAATCACGACA
miR166a	ATGTTGTCTGGCTCGAGGTC	CCGACGACACTAAACCATGA
miR166b	GCTGGCTCGACACAATTACTC	TGAGAGGAATGAAGCCTGGT
miR167a	CCAGCATGATCTGGTACGAA	GGAAAAGCCAGACCTCAAGA
miR167b	TTTTCTGTTTTGGTTGGA	TATTGGTGGCGAGTGATTGA
miR169a	GAAGGTTCAATGCCCTTTTG	CTGCGCAAATATGAGAGGT
miR169b	GATGACTTGCCTGGTCCATT	AAGATGACTTGCCTGCAACC
miR171a	GAGAATTGTCCGGCCAGTAA	CTAAGCTTGAGGCAGCTGGT
miR171b	GGTGAGGTTCAATCCGAAGA	CGGCTCAATCTGAGATCGTT
miR172a	TGTCAACAGTTTTTGCAGATG	GGATCCATAGGGAGCAAAAA
miR172b	GGCCAAAACAGATCTCCAC	ATTTTCCTGCTCCCTCCTTC
miR319a	GCCGACTCATTATCCAAT	CTACGGAGGTGCGTTTGACT
miR319b	CCCTAGTGGGTGCAGATGAT	CGAGGAACAAGGGTAATCCA
miR390	GGAGGGATAGCACCATGAAA	GCGCCAAAATGATTGAAAGT
miR393	GATCGCATTGATCCCATTTC	AGTCCGAAGGGATAGCATGA
miR396a	GCTTTATTGAACCGCAACAA	TGGCTCTCTTTGTATTTTTCCA
miR396b	TTCAGTGGGGAAGAAGTTCAA	CAAGTCCTATCATGCTTTTCCA
miR399a	ATTGATCCCTGCTGACGATG	TACATCGGTCGTTGTTGGAA
miR399b	AGAGAAATGCGAGCGAAGAT	TTCTCCTTTGGCAAATCCAG

Immunoblot analyses

Samples corresponding to agroinfiltrated *N. benthamiana* leaves were frozen in liquid nitrogen. Protein extraction was performed as Schornack et al., 2010. Proteins were separated by SDS-PAGE and electroblotted on nitrocellulose membranes (BioRad). GFP-tagged proteins were revealed using anti-GFP monoclonal antibodies 1:1000 (Merck #11814460001) followed by Goat Anti-Mouse IgG-HRP Conjugate (BioRad #1706516). Clarity ECL (BioRad #1705060) was used for the revelation step.

Agrobacterium-mediated transformation

Generation of *M. truncatula* composite plants was performed as described by Boisson-dernier et al, 2001 using ARQUA-1 (*A. rhizogenes*) strain. Leaf infiltration were performed with *A. tumefaciens* (GV3101::pMP90RK) as described by Schornack et al., 2010.

Confocal microscopy

Foliar discs (5-8 mm of diameter) of infiltrated leaves of *N. benthamiana* were sampled at different time points after agroinfiltration and mounted on microscope slides for live cell imaging. For DAPI staining, discs were fixed in a PBS, 4% (v/v) paraformaldehyde solution and then stained with DAPI (3 µg/µL). Scans were performed on a Leica TCS SP8 device using wavelengths 488nm (GFP) and 350 nm (DAPI) and with a 40x water immersion lens. Acquisitions were performed in a sequential mode to avoid overlapping fluorescence signals. Images were treated with Image J software and correspond to Z projections of scanned tissues.

Preparation of *N. benthamiana* epidermal leaves for FRET / FLIM experiments

Samples were prepared as described in (Camborde et al., 2017; Ramirez-Garcés et al., 2016; Le Roux et al., 2015). Briefly, discs of *N. benthamiana* agroinfiltrated leaves were fixed 20-24 hours after treatment by vacuum infiltrating a TBS (TRIS 25 mM, NaCl 140 mM, KCl 3 mM) 4 % (w/v) paraformaldehyde solution before incubation 20 min at 4°C. Samples were

permeabilized 10 min at 37°C using a digestion buffer supplemented with 20 µg/ml of proteinase K (Invitrogen) as described in (Camborde et al., 2017; Escouboué et al., 2019). Nucleic acid staining was performed by vacuum-infiltration of a 5 µM of Sytox Orange (Invitrogen) solution, before incubation of the samples 30 min at room temperature. When RNase treatment was performed, foliar discs were incubated 15 min at room temperature with 0.5 µg/ml of RNase A (Roche) before acid nucleic staining. Foliar discs were washed with and mounted on TBS before observations on an inverted microscope (Eclipse TE2000E, Nikon, Japan).

FRET / FLIM measurements

Fluorescence lifetime measurements were performed in time domain using a streak camera (Camborde et al., 2017). The light source is a mode-locked Ti:sapphire laser (Tsunami, model 3941, Spectra-Physics, USA) pumped by a 10W diode laser (Millennia Pro, Spectra-Physics) and delivering ultrafast femtosecond pulses of light with a fundamental frequency of 80MHz. A pulse picker (model 3980, Spectra-Physics) is used to reduce the repetition rate to 2MHz to satisfy the requirements of the triggering unit (working at 2MHz). The experiments were carried out at $\lambda = 820$ nm (multiphoton excitation mode). All images were acquired with a 60x oil immersion lens (plan APO 1.4 N.A., IR) mounted on an inverted microscope (Eclipse TE2000E, Nikon, Japan). The fluorescence emission is directed back into the detection unit through a short pass filter ($\lambda < 750$ nm) and a band pass filter (515/30 nm). The detector is a streak camera (Streakscope C4334, Hamamatsu Photonics, Japan) coupled to a fast and high-sensitivity CCD camera (model C8800-53C, Hamamatsu). For each nucleus, average fluorescence decay profiles were plotted and lifetimes were estimated by fitting data with exponential function using a non-linear least-squares estimation procedure. Fluorescence lifetime of the donor (GFP) was experimentally measured in the presence and absence of the acceptor (Sytox Orange). FRET efficiency (E) was calculated by comparing the lifetime of the donor in the presence (τ_{DA}) or absence (τ_D) of the acceptor: $E = 1 - (\tau_{DA} / \tau_D)$. Statistical comparisons between control (donor) and assay (donor + acceptor) lifetime values were performed by Student t-test. For each experiment, a minimum of four leaf discs removed from two agroinfiltrated leaves were used to collect data.

Post-Transcriptional Gene Silencing assay

PTGS assays were performed as described by (Qiao et al., 2013, 2015). Briefly, *N. benthamiana* 16c at the six-leaf stage (with a constitutive GFP expression) were agroinfiltrated with p35S::GFP vector combined with pEG100 as empty vector, or pK2GW7::AeCRN5-Cter, pEG101::PSR1 (Qiao et al., 2013) or pK2GW7::P19. pEG100, p35S::GFP and pEG101::PSR1 were kindly provided by Dr W. Ma, and pK2GW7::P19 by Dr N. Pauly from LIPM lab.

Green fluorescence was visualized using a handheld long-wavelength UV lamp (Black-Ray B-100AP, Ultraviolet Products). *Agrobacterium* carrying the empty vector pEG100 was used as negative control whilst PSR1 and P19 constructs were used as positive controls.

Leaves were examined 3 days after *Agrobacterium* infiltration in the infiltrated leaf areas and sampled in liquid nitrogen. GFP Immunoblots were performed after total protein extraction as described in this paper. To produce siRNA probe, we first amplified approx. 200bp of the mGFP5 using cDNA from 16c leaves (RNA extraction and RT were performed as described in this paper), with mGFP5-F and mGFP5-R_T7prom primers (Supplemental Table 1). The GFP siRNA probe was generated using the MEGAScript high-yield T7 kit (Ambion) in the presence of [α -³²P] UTP. U6 served as a loading control.

References

- Amaro, T.M.M.M., Thilliez, G.J.A., Motion, G.B., and Huitema, E.** (2017). A Perspective on CRN Proteins in the Genomics Age: Evolution, Classification, Delivery and Function Revisited. *Front. Plant Sci.* **8**: 99.
- Badis, Y., Bonhomme, M., Lafitte, C., Huguet, S., Balzergue, S., Dumas, B., and Jacquet, C.** (2015). Transcriptome analysis highlights preformed defences and signalling pathways controlled by the *prAe1* quantitative trait locus (QTL), conferring partial resistance to *Aphanomyces euteiches* in *Medicago truncatula*. *Mol. Plant Pathol.* **16**: 973–986.
- Badreddine, I., Lafitte, C., Heux, L., Skandalis, N., Spanou, Z., Martinez, Y., Esquerré-Tugayé, M.T., Bulone, V., Dumas, B., and Bottin, A.** (2008). Cell wall chitosaccharides are

essential components and exposed patterns of the phytopathogenic oomycete *Aphanomyces euteiches*. Eukaryot. Cell **7**: 1980–1993.

Baxter, L. et al. (2010). Signatures of adaptation to obligate biotrophy in the *Hyaloperonospora arabidopsidis* genome. Science (80-.). **330**: 1549–1551.

Bazin, J., Romero, N., Rigo, R., Charon, C., Blein, T., Ariel, F., and Crespi, M. (2018). Nuclear Speckle RNA Binding Proteins Remodel Alternative Splicing and the Non-coding *Arabidopsis* Transcriptome to Regulate a Cross-Talk Between Auxin and Immune Responses. Front. Plant Sci. **9**: 1209.

Bellafiore, S., Shen, Z., Rosso, M.N., Abad, P., Shih, P., and Briggs, S.P. (2008). Direct identification of the *Meloidogyne incognita* secretome reveals proteins with host cell reprogramming potential. PLoS Pathog. **4**.

Bhattacharjee, S., Garner, C.M., and Gassmann, W. (2013). New clues in the nucleus: transcriptional reprogramming in effector-triggered immunity. Front. Plant Sci. **4**: 364.

Boisnard-Lorig, C., Colon-Carmona, a, Bauch, M., Hodge, S., Doerner, P., Bancharel, E., Dumas, C., Haseloff, J., and Berger, F. (2001). Dynamic analyses of the expression of the HISTONE::YFP fusion protein in arabidopsis show that syncytial endosperm is divided in mitotic domains. Plant Cell **13**: 495–509.

Boisson-Dernier, A., Chabaud, M., Garcia, F., Bécard, G., Rosenberg, C., and Barker, D.G. (2001). *Agrobacterium rhizogenes*-transformed roots of *Medicago truncatula* for the study of nitrogen-fixing and endomycorrhizal symbiotic associations. Mol. Plant-Microbe Interact. **14**: 695–700.

Cai, Q., Cai, Q., Qiao, L., Wang, M., He, B., Lin, F., Palmquist, J., Huang, H., and Jin, H. (2018). Plants send small RNAs in extracellular vesicles to fungal pathogen to silence virulence genes. **4142**: 1–9.

Camborde, L., Jauneau, A., Brière, C., Deslandes, L., Dumas, B., and Gaulin, E. (2017). Detection of nucleic acid–protein interactions in plant leaves using fluorescence lifetime imaging microscopy. Nat. Protoc. **12**: 1933–1950.

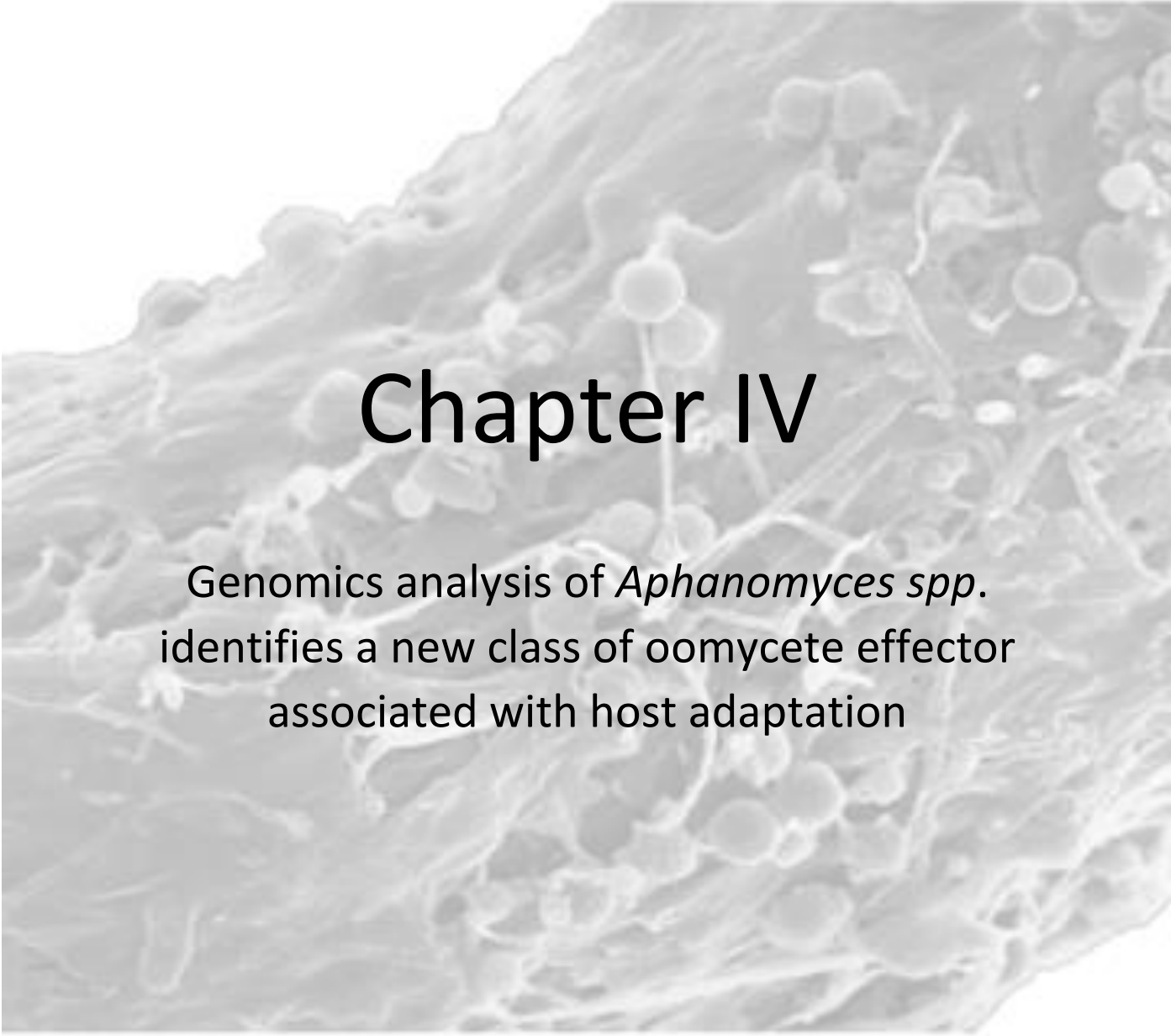
- Canonne, J. and Rivas, S.** (2012). Bacterial effectors target the plant cell nucleus to subvert host transcription. *Plant Signal. Behav.* **7**.
- Couzigou, J.M. and Combier, J.P.** (2016). Plant microRNAs: key regulators of root architecture and biotic interactions. *New Phytol.* **212**.
- van Damme, M., Bozkurt, T.O., Cakir, C., Schornack, S., Sklenar, J., Jones, A.M.E., and Kamoun, S.** (2012). The Irish Potato Famine Pathogen *Phytophthora infestans* Translocates the CRN8 Kinase into Host Plant Cells. *PLoS Pathog.* **8**.
- Deslandes, L. and Rivas, S.** (2012). Catch me if you can: Bacterial effectors and plant targets. *Trends Plant Sci.* **17**.
- Djébali, N. et al.** (2009). Partial Resistance of *Medicago truncatula* to *Aphanomyces euteiches* is associated with protection of the root stele and is controlled by a major QTL rich in proteasome-related genes. *Mol. Plant-Microbe Interact.* **22**: 1043–1055.
- Escouboué, M., Camborde, L., Jauneau, A., Gaulin, E., and Deslandes, L.** (2019). Preparation of plant material for analysis of protein–Nucleic acid interactions by FRET-FLIM. In *Methods in Molecular Biology* (Humana Press Inc.), pp. 69–77.
- Gaulin, E. et al.** (2018). Genomics analysis of *Aphanomyces spp.* identifies a new class of oomycete effector associated with host adaptation. *BMC Biol.* **16**.
- Gaulin, E., Haget, N., Khatib, M., Herbert, C., Rickauer, M., and Bottin, A.** (2007). Transgenic sequences are frequently lost in *Phytophthora parasitica* transformants without reversion of the transgene-induced silenced state. *Can. J. Microbiol.* **53**: 152–157.
- Gaulin, E., Madoui, M.-A., Bottin, A., Jacquet, C., Mathé, C., Couloux, A., Wincker, P., and Dumas, B.** (2008). Transcriptome of *Aphanomyces euteiches*: new oomycete putative pathogenicity factors and metabolic pathways. *PLoS One* **3**: e1723.
- Haas, B.J. et al.** (2009). Genome sequence and analysis of the Irish potato famine pathogen *Phytophthora infestans*. *Nature* **461**: 393–398.
- Hou, Y. et al.** (2019). A *Phytophthora* Effector Suppresses Trans-Kingdom RNAi to Promote Disease Susceptibility. *Cell Host Microbe* **25**: 153-165.e5.
- Jiao, J. and Peng, D.** (2018). Wheat microRNA1023 suppresses invasion of *Fusarium*

- graminearum* via targeting and silencing fgsg_03101. J. Plant Interact. **13**.
- Kelley, L.A., Mezulis, S., Yates, C.M., Wass, M.N., and Sternberg, M.J.E.** (2015). The Phyre2 web portal for protein modeling, prediction and analysis. Nat. Protoc. **10**.
- Kemen, E., Gardiner, A., Schultz-Larsen, T., Kemen, A.C., Balmuth, A.L., Robert-Seilaniantz, A., Bailey, K., Holub, E., Studholme, D.J., MacLean, D., and Jones, J.D.G.** (2011). Gene gain and loss during evolution of obligate parasitism in the white rust pathogen of *Arabidopsis thaliana*. PLoS Biol. **9**.
- Khan, M., Seto, D., Subramaniam, R., and Desveaux, D.** (2018). Oh, the places they'll go! A survey of phytopathogen effectors and their host targets. Plant J. **93**: 651–663.
- Kozomara, A., Birgaoanu, M., and Griffiths-Jones, S.** (2019). MiRBase: From microRNA sequences to function. Nucleic Acids Res. **47**.
- Lakatos, L., Szittyá, G., Silhavy, D., and Burgyán, J.** (2004). Molecular mechanism of RNA silencing suppression mediated by p19 protein of tombusviruses. EMBO J. **23**: 876–84.
- Le Roux, C. et al.** (2015). A Receptor Pair with an Integrated Decoy Converts Pathogen Disabling of Transcription Factors to Immunity. Cell **161**: 1074–1088.
- Lévesque, C.A. et al.** (2010). Genome sequence of the necrotrophic plant pathogen *Pythium ultimum* reveals original pathogenicity mechanisms and effector repertoire. Genome Biol. **11**.
- Li, S., Li, M., Liu, K., Zhang, H., Zhang, S., Zhang, C., and Yu, B.** (2020). MAC5, an RNA-binding protein, protects pri-miRNAs from SERRATE-dependent exoribonuclease activities. Proc. Natl. Acad. Sci.: 202008283.
- Lin, K. et al.** (2014). Single Nucleus Genome Sequencing Reveals High Similarity among Nuclei of an Endomycorrhizal Fungus. PLoS Genet. **10**.
- Liu, D., Shi, L., Han, C., Yu, J., Li, D., and Zhang, Y.** (2012). Validation of Reference Genes for Gene Expression Studies in Virus-Infected *Nicotiana benthamiana* Using Quantitative Real-Time PCR. PLoS One **7**.
- Liu, J.-Z. and Whitham, S. a** (2013). Overexpression of a soybean nuclear localized type-III DnaJ domain-containing HSP40 reveals its roles in cell death and disease resistance. Plant J. **74**: 110–21.

- Liu, T., Ye, W., Ru, Y., Yang, X., Gu, B., Tao, K., Lu, S., Dong, S., Zheng, X., Shan, W., Wang, Y., and Dou, D.** (2011). Two host cytoplasmic effectors are required for pathogenesis of *Phytophthora sojae* by suppression of host defenses. *Plant Physiol.* **155**: 490–501.
- Livak, K.J. and Schmittgen, T.D.** (2001). Analysis of relative gene expression data using real-time quantitative PCR and the 2- $\Delta\Delta$ CT method. *Methods* **25**: 402–408.
- Lobbes, D., Rallapalli, G., Schmidt, D.D., Martin, C., and Clarke, J.** (2006). SERRATE: a new player on the plant microRNA scene. *EMBO Rep.* **7**: 1052–1058.
- Mafurah, J.J., Ma, H., Zhang, M., Xu, J., He, F., Ye, T., Shen, D., Chen, Y., Rajput, N.A., and Dou, D.** (2015). A Virulence Essential CRN Effector of *Phytophthora capsici* Suppresses Host Defense and Induces Cell Death in Plant Nucleus. *PLoS One* **10**: e0127965.
- Meijer, H.J.G., Mancuso, F.M., Espadas, G., Seidl, M.F., Chiva, C., Govers, F., and Sabidó, E.** (2014). Profiling the secretome and extracellular proteome of the potato late blight pathogen *Phytophthora infestans*. *Mol. Cell. Proteomics* **13**.
- Ökmen, B., Etalo, D.W., Joosten, M.H.A.J., Bouwmeester, H.J., de Vos, R.C.H., Collemare, J., and de Wit, P.J.G.M.** (2013). Detoxification of α -tomatine by *Cladosporium fulvum* is required for full virulence on tomato. *New Phytol.* **198**: 1203–1214.
- Pedersen, C. et al.** (2012). Structure and evolution of barley powdery mildew effector candidates. *BMC Genomics* **13**: 694.
- Petrovská, B., Šebela, M., and Doležel, J.** (2015). Inside a plant nucleus: Discovering the proteins. *J. Exp. Bot.* **66**: 1627–1640.
- Pliego, C. et al.** (2013). Host-induced gene silencing in barley powdery mildew reveals a class of ribonuclease-like effectors. *Mol. Plant-Microbe Interact.* **26**.
- Qiao, Y. et al.** (2013). Oomycete pathogens encode RNA silencing suppressors. *Nat. Genet.*: 1–6.
- Qiao, Y., Shi, J., Zhai, Y., Hou, Y., and Ma, W.** (2015). *Phytophthora* effector targets a novel component of small RNA pathway in plants to promote infection. *Proc. Natl. Acad. Sci. U. S. A.* **112**: 5850–5855.

- Raczynska, K.D., Stepien, A., Kierzkowski, D., Kalak, M., Bajczyk, M., McNicol, J., Simpson, C.G., Szweykowska-Kulinska, Z., Brown, J.W.S., and Jarmolowski, A. (2014).** The SERRATE protein is involved in alternative splicing in *Arabidopsis thaliana*. *Nucleic Acids Res.* **42**: 1224–1244.
- Rajput, N.A., Zhang, M., Ru, Y., Liu, T., Xu, J., Liu, L., Mafurah, J.J., and Dou, D. (2014).** *Phytophthora sojae* Effector PsCRN70 Suppresses Plant Defenses in *Nicotiana benthamiana*. *PLoS One* **9**: e98114.
- Ramirez-Garcés, D., Camborde, L., Pel, M.J.C., Jauneau, A., Martinez, Y., Néant, I., Leclerc, C., Moreau, M., Dumas, B., and Gaulin, E. (2016).** CRN13 candidate effectors from plant and animal eukaryotic pathogens are DNA-binding proteins which trigger host DNA damage response. *New Phytol.* **210**.
- Rey, T., Nars, A., Bonhomme, M., Bottin, A., Huguet, S., Balzergue, S., Jardinaud, M.-F., Bono, J.-J., Cullimore, J., Dumas, B., Gough, C., and Jacquet, C. (2013).** NFP, a LysM protein controlling Nod factor perception, also intervenes in *Medicago truncatula* resistance to pathogens. *New Phytol.* **198**: 875–886.
- Schornack, S., van Damme, M., Bozkurt, T.O., Cano, L.M., Smoker, M., Thines, M., Gaulin, E., Kamoun, S., and Huitema, E. (2010).** Ancient class of translocated oomycete effectors targets the host nucleus. *Proc. Natl. Acad. Sci. U. S. A.* **107**: 17421–6.
- Shen, D., Liu, T., Ye, W., Liu, L., Liu, P., Wu, Y., Wang, Y., and Dou, D. (2013).** Gene Duplication and Fragment Recombination Drive Functional Diversification of a Superfamily of Cytoplasmic Effectors in *Phytophthora sojae*. *PLoS One* **8**.
- Song, T., Ma, Z., Shen, D., Li, Q., Li, W., Su, L., Ye, T., Zhang, M., Wang, Y., and Dou, D. (2015).** An Oomycete CRN Effector Reprograms Expression of Plant HSP Genes by Targeting their Promoters. *PLoS Pathog.* **11**: 1–30.
- Stam, R., Howden, A.J.M., Delgado-Cerezo, M., Amaro, T.M.M.M., Motion, G.B., Pham, J., and Huitema, E. (2013a).** Characterization of cell death inducing *Phytophthora capsici* CRN effectors suggests diverse activities in the host nucleus. *Front. Plant Sci.* **4**.

- Stam, R., Jupe, J., Howden, A.J.M., Morris, J. a., Boevink, P.C., Hedley, P.E., and Huitema, E.** (2013b). Identification and Characterisation CRN Effectors in *Phytophthora capsici* Shows Modularity and Functional Diversity. *PLoS One* **8**: e59517.
- Sun, G., Yang, Z., Kosch, T., Summers, K., and Huang, J.** (2011a). Evidence for acquisition of virulence effectors in pathogenic chytrids. *BMC Evol. Biol.* **11**: 195.
- Thines, M. and Kamoun, S.** (2010). Oomycete-plant coevolution: recent advances and future prospects. *Curr. Opin. Plant Biol.* **13**: 427–33.
- Torto, T.A., Li, S., Styer, A., Huitema, E., Testa, A., Gow, N.A.R., van West, P., and Kamoun, S.** (2003). EST mining and functional expression assays identify extracellular effector proteins from the plant pathogen *Phytophthora*. *Genome Res.* **13**: 1675–1685.
- Wang, J., Mei, J., and Ren, G.** (2019). Plant microRNAs: Biogenesis, homeostasis, and degradation. *Front. Plant Sci.* **10**: 360.
- Wang, X., Boevink, P., McLellan, H., Armstrong, M., Bukharova, T., Qin, Z., and Birch, P.R.J.** (2015). A host KH RNA binding protein is a susceptibility factor targeted by an RXLR effector to promote late blight disease. *Mol. Plant.*
- Ying, X.B., Dong, L., Zhu, H., Duan, C.G., Du, Q.S., Lv, D.Q., Fang, Y.Y., Garcia, J.A., Fang, R.X., and Guo, H.S.** (2010). RNA-dependent RNA polymerase 1 from *Nicotiana tabacum* suppresses RNA silencing and enhances viral infection in *Nicotiana benthamiana*. *Plant Cell* **22**: 1358–1372.
- Zhang, D., Burroughs, A.M., Vidal, N.D., Iyer, L.M., and Aravind, L.** (2016). Transposons to toxins: the provenance, architecture and diversification of a widespread class of eukaryotic effectors. *Nucleic Acids Res.:* gkw221.

A grayscale scanning electron micrograph (SEM) showing a dense network of filamentous hyphae and numerous spherical spores. The hyphae are thin and interconnected, forming a complex web-like structure. The spores are larger, roughly spherical, and some appear to be attached to the hyphae. The overall appearance is that of a highly branched, multicellular organism.

Chapter IV

Genomics analysis of *Aphanomyces spp.*
identifies a new class of oomycete effector
associated with host adaptation

IV – CHAPTER IV: Genomics analysis of *Aphanomyces spp.* identifies a new class of oomycete effector associated with host adaptation (Gaulin et al. BMC Biol, 2018)

The first aim of this study was to provide a genome reference for *Aphanomyces* genus, by working on *A. euteiches* ATCC201684 pea strain. A combination of 454 and Illumina reads were generated to provide a 57 Mb assembly. In order to identify components that could explain adaptation to various hosts (plant vs animals), Illumina reads were assembled to provide a draft genome of the crayfish pathogen *A. astaci* and the saprotroph *A. stellatus*. All the data are publicly available in AphanoDB repository (<http://www.polebio.lrsv.ups-tlse.fr/aphanoDB/>).

Comparative analyses of *A. astaci* and *A. euteiches* proteomes lead us to identify ~300 genes encoding small-secreted proteins specific to *Aphanomyces euteiches* (AeSSP) devoid of any functional annotations. Transcriptomic data (RNASeq) obtained on *M. truncatula* roots (infected or not with *Ae*) revealed that around half of these SSPs were highly induced during interaction with *M. truncatula*. We noticed that some of these SSPs were organized in clusters.

To evaluate the biological activity of AeSSP genes, a SSP cluster comprising six AeSSPs genes was selected for starting functional studies (**Figure 10a**). This cluster is unique because it is the only one that contains three AeSSPs (Ae1251, Ae1254, and Ae1256) with a predicted Nuclear-Localisation-Signal (NLS). This genomic architecture suggests that these proteins could be addressed to the host cells to target nuclear components. Sequence alignments revealed that AeSSP1250 and AeSSP1253 differ only by two amino acids, but the other genes have no sequence similarities (**Figure 10b**). Expression of GFP tagged versions of each gene of this cluster in *N. benthamiana* leaves confirms the nuclear localization for the three genes harbouring NLS (Ae1251, Ae1254, and Ae1256), whilst AeSSP1250 and AeSSP1253 display a nucleocytoplasmic localization when AeSSP1255 seems excluded from nucleus (**Figure 10c**). While AeSSP1251 and AeSSP1254 accumulated in the nucleolus, AeSSP1256 displays a subnuclear localization, spotted in dots and accumulating in a perinucleolar ring (**Figure 10c** and see paper from this chapter). Intriguingly, for each construct, same localisation was

Figure 10: Complementary results on the SSP cluster containing AeSSP1256.

(A) Scheme of the SSP cluster organization. Six genes on the same orientation, among 8 kB, compose this cluster. Each gene contains a signal peptide and three genes harbour a NLS (AeSSP1251, 1254 and 1256). (B) Amino acid sequence alignment of the six genes, performed on CLC Workbench. AeSSP1250 and AeSSP1253 differ by only 2AA. Except these two genes, no sequence similarities are observed among the cluster. (C) Localization of AeSSP1256 cluster proteins expressed in *N. benthamiana* leaves. For each gene, GFP was fused in C-ter and transform in *Agrobacterium tumefaciens*. Confocal analyses were conducted 24h after agroinoculation in *N. benthamiana* leaves. AeSSP1250 and AeSSP1253 have a similar nucleocytoplasmic localization (pictures correspond to AeSSP1250, similar pictures were obtained from AeSSP1253), when AeSSP1255 is excluded from nucleus. Similar nuclear localization was observed for AeSSP1251 and AeSSP1254 (pictures correspond to AeSSP1254), with an accumulation in nucleolus, indicating that the NLS was functional. In the same way, AeSSP1256 is nuclear localized but spotted in dots and accumulates in a perinucleolar ring. Same localisation was observed in presence (upper panels) or absence (lower panels) of their own signal peptide (SP). White dotted lines indicate nuclei. n: nucleus. Scale bars: 10µm.

observed in presence or absence of their own signal peptide (SP) (**Figure 10c**). We then evidenced that the AeSSP1256 entered the plant secretory pathway thanks to its native signal peptide, using endoplasmic reticulum (ER) retention motif and drug assay (see Fig. 8 - BMC biology paper from this chapter).

Due to the fact that *A. euteiches* transformation is not yet available, we used *Phytophthora capsici* infection assay to investigate whether those SSPs could act as effectors. After expression of each member of the AeSSP cluster on tobacco leaves, followed by *P. capsici* inoculation, it appeared that only AeSSP1256 enhances *N. benthamiana* susceptibility to *P. capsici*. These data suggest that AeSSP1256 and therefore SSPs are a new class of oomycete effectors.

RESEARCH ARTICLE

Open Access



Genomics analysis of *Aphanomyces* spp. identifies a new class of oomycete effector associated with host adaptation

Elodie Gaulin^{1*}, Michiel J. C. Pel¹, Laurent Camborde¹, H el ene San-Clemente¹, Sarah Courbier^{1,10}, Marie-Alexane Dupouy¹, Juliette Lengell e¹, Marine Veyssiere¹, Aur elie Le Ru², Fr ed eric Grandjean³, Richard Cordaux³, Bouziane Moumen³, Cl ement Gilbert⁴, Lilliana M. Cano⁵, Jean-Marc Aury⁶, Julie Guy⁶, Patrick Wincker⁷, Olivier Bouchez⁸, Christophe Klopp⁹ and Bernard Dumas¹

Abstract

Background: Oomycetes are a group of filamentous eukaryotic microorganisms that have colonized all terrestrial and oceanic ecosystems, and they include prominent plant pathogens. The *Aphanomyces* genus is unique in its ability to infect both plant and animal species, and as such exemplifies oomycete versatility in adapting to different hosts and environments. Dissecting the underpinnings of oomycete diversity provides insights into their specificity and pathogenic mechanisms.

Results: By carrying out genomic analyses of the plant pathogen *A. euteiches* and the crustacean pathogen *A. astaci*, we show that host specialization is correlated with specialized secretomes that are adapted to the deconstruction of the plant cell wall in *A. euteiches* and protein degradation in *A. astaci*. The *A. euteiches* genome is characterized by a large repertoire of small secreted protein (SSP)-encoding genes that are highly induced during plant infection, and are not detected in other oomycetes. Functional analysis revealed an SSP from *A. euteiches* containing a predicted nuclear-localization signal which shuttles to the plant nucleus and increases plant susceptibility to infection.

Conclusion: Collectively, our results show that *Aphanomyces* host adaptation is associated with evolution of specialized secretomes and identify SSPs as a new class of putative oomycete effectors.

Keywords: *Aphanomyces*, Oomycete, Effector, Secretome, Host adaptation, SSP

Background

Oomycetes are filamentous eukaryotes that have colonized all terrestrial and oceanic ecosystems [1]. Oomycete evolution started from marine habitats, and their closest cousins are probably free-living phagotrophic protists [1]. The great diversity of lifestyles displayed by oomycetes raised questions about genetic and molecular mechanisms involved in their evolution and rapid adaptation to environmental changes [2, 3]. Oomycete pathogenicity mainly relies on large repertoires of secreted proteins, known as effectors. They show rapid evolution

within a given genome as a result of co-evolution with their hosts and are often associated with transfers to unrelated hosts [4, 5]. For instance, protease inhibitors produced by two sister *Phytophthora* species evolved to target plant proteases of their respective unrelated hosts, linking effector specialization and host diversification [6]. *Phytophthora* spp. whole genome studies revealed a bipartite genome architecture that evolved at different rates [5] and where effector genes are associated with transposable elements (TEs) in gene-sparse regions [4]. RxLR and Crinklers (CRNs) are the two main effector families found in these fast-evolving genomic regions of *Phytophthora* spp. [4, 7]. These two large families of effectors consist of modular proteins with a conserved N-terminus host-addressing signal (i.e., a trafficking sequence), while the variable Cter region harbors the

* Correspondence: gaulin@rsv.ups-tse.fr

¹Laboratoire de Recherche en Sciences V eg etales, CNRS UMR5546 Universit e de Toulouse, Paul Sabatier, 24, chemin de Borde Rouge BP 42617 Auzeville, 31326 Castanet-Tolosan, France

Full list of author information is available at the end of the article



  Gaulin et al. 2018 **Open Access** This article is distributed under the terms of the Creative Commons Attribution 4.0 International License (<http://creativecommons.org/licenses/by/4.0/>), which permits unrestricted use, distribution, and reproduction in any medium, provided you give appropriate credit to the original author(s) and the source, provide a link to the Creative Commons license, and indicate if changes were made. The Creative Commons Public Domain Dedication waiver (<http://creativecommons.org/publicdomain/zero/1.0/>) applies to the data made available in this article, unless otherwise stated.

effector function [8, 9]. Besides their role in pathogenicity, numerous RxLR proteins are specifically detected by host plants able to produce cognate resistance proteins to trigger resistance [10, 11]. Specific interactions between RxLR effectors and resistance proteins are on the basis of the gene-for-gene concept, a fundamental process of the plant immune system, also known as effector-triggered immunity (ETI) [12]. In that case, rapid evolution of RxLR effectors allows the pathogen to counteract this surveillance system.

Phylogenetic analyses placed the *Aphanomyces* genus in the Saprolegnial lineage, which includes several species pathogenic in plants and aquatic animals such as the salmon pathogen *Saprolegnia parasitica* [13]. In contrast, most of the species in the Peronosporalean lineage are mainly pathogenic on plants, one of the best-studied species being *Phytophthora infestans*, which causes late blight on solanaceous crops such as potato or tomato [8]. The *Aphanomyces* genus has been shown to contain three major lineages, including plant pathogens, aquatic animal pathogens, and saprophytic species [13], making this genus a unique model to understand evolutionary mechanisms involved in adaptation of oomycetes to distantly related hosts and environmental niches. Among the most damaging *Aphanomyces* species is the legume pathogen *Aphanomyces euteiches*, which causes significant damage to various legume crops (peas, alfalfas, faba beans, lentils, etc.) [14]. First reported by Drechsler in 1925 as the causal agent pathogen of root rot in peas in Wisconsin (USA) [15], the pathogen is now recorded in Europe, Australia, New Zealand, and throughout the USA. *Aphanomyces euteiches* is a major problem affecting the field pea in most pea-growing regions [16].

Aphanomyces euteiches is composed of distinct subspecific groups based on genotype and host preference (i.e., pea, alfalfa, etc.) [17, 18]. The infection is initiated by oospore germination in close vicinity to a root plant host. The oospores form a germ tube and a long terminal zoosporangium that can release more than 300 primary motile zoospores [19]. The zoospores locate and encyst on the host root within minutes, and the cysts are able to germinate and penetrate the cortical cells within hours. The mycelium then grows intercellularly through the root tissue and forms oospores within a few days of infection [14]. Although the symptoms caused by *A. euteiches* can be difficult to distinguish from symptoms caused by other root-infecting plant pathogens (such as *Pythium* or *Fusarium*), a characteristic colored soft rot of the roots is generally observed [14]. Under optimal field conditions, legume infection by *A. euteiches* can result in symptoms within 10 days, and oospores can be detected between 7 and 14 days [14]. The oospores of *A. euteiches* are long-lived and can remain dormant in soil and organic debris for many years [14], making legume cultivation inefficient. Effective chemical controls for *Aphanomyces* root rot of

legumes are not available, and the development of tolerant cultivars appears to be the more effective management technique available to farmers. Partial resistance in pea or the legume model *Medicago truncatula* to *A. euteiches* is mediated by several quantitative trait loci (QTLs). Recent whole genome sequencing data in conjunction with genome-wide association studies (GWASs) on *M. truncatula* have allowed the identification of promising candidate genes [20, 21] to manage the parasite.

Aphanomyces astaci is an obligate parasite of freshwater decapods, particularly crayfish (but crabs could act as potential vectors as well [22, 23]). It presumably originates from North America, where infected native crayfish do not show disease symptoms. Five distinct *A. astaci* genotype groups (from A to E) are known in Europe and were isolated from infected European crayfish specimens. *A. astaci* reproduces asexually through the formation of short-lived bi-flagellated zoospores that spread in aquatic ecosystems [23]. After the encystment of the zoospore on the host cuticle and its germination, the growing hypha penetrates into the cuticle. In resistant crayfish, the hyphal growth is stopped by encapsulation and melanization, resulting from the host immune response. In susceptible crayfish, hyphae penetrate deeper into tissues and organs, generally killing the host [24]. The time required for development varies depending on the *A. astaci* strain and water temperature [25]. Like plant pathogens, *A. astaci* presumably secretes a battery of virulence proteins to promote infection and facilitate host adaptation. Indeed, infection experiments have shown that *A. astaci* strains from group E had a high level of virulence, comparable to that of group B [26]. *A. astaci* has been nominated among the "100 of the World's Worst Invasive Alien Species" in the Global Invasive Species Database [27].

In contrast to species from the Peronosporalean lineage, little is known regarding the molecular mechanisms that govern host adaptation and environmental niche colonization for *Aphanomyces* species. A previous analysis of a collection of expressed sequence tags (ESTs) from the legume pathogen *A. euteiches* revealed the uniqueness of its effector repertoire, which is composed of numerous CRN effector genes without any RxLR effectors [28–30]. This observation led to the suggestion that CRNs are ancestral in the oomycete lineage and specific to phytopathogenic species [7, 9]. Indeed, CRN coding genes have been detected in all plant pathogenic oomycetes sequenced to date, but never in animal pathogenic species such as *S. parasitica* [31]. This has also raised the possibility that, besides the RxLR family, CRNs and maybe other oomycete effectors may have important roles in triggering host susceptibility.

Here we report on the whole genome sequencing and annotation of a pea-infecting strain of *A. euteiches*. To characterize genetic factors involved in plant adaptation by comparative genomics, we generated a first genomic draft of the crustacean pathogen *A. astaci*. In combination with RNA-seq data, we showed that *Aphanomyces* adaptation to plant or animal hosts is correlated with the expression of highly specialized secretomes. Moreover, our study led to the identification of a set of small secreted proteins (SSPs) which can be considered as a new class of oomycete effectors.

Results

Aphanomyces spp. genome sequencing and phylogeny relationship

The genome of the *A. euteiches* ATCC201684 strain was sequenced by combining 454 and Illumina sequencing technologies providing a high-quality reference assembly of 57 Mb (Table 1). The estimated genome size of *A. euteiches* is consistent with the size range of most previously sequenced oomycete genomes except *P. infestans* (240 Mb) [32] and close to the assembled *S. parasitica* fish pathogen genome (63 Mb) [31]. The GC content (~47%) is one of the lowest detected in oomycetes and in close agreement with the *Albugo laibachii* [33] and *Plasmopara viticola* genomes [34]. The benchmarking universal single-copy orthologs (BUSCO) method [35] was used to estimate the degree of completeness of the assembled gene space. Most of the gene space was covered as 83.1% complete, and a 3.8% partial model of conserved fungal genes was identified within the genome of *A. euteiches*. The number of genes (19,548) is more important in *A. euteiches* than in other sequenced oomycetes, while the gene length mean (~1.5 kb) is similar to that of various oomycetes [33, 34, 36]. The *A. euteiches* genome is thus highly compact with the second-highest gene density (one gene per 2.9 kb) reported so far for oomycetes and similar to the *S. parasitica* genome (one

gene per 2.6 kb). The completeness of the *A. euteiches* sequenced genome and prediction of open reading frames were validated by the analyses of expressed sequences. In total, 87% of ESTs previously generated from *A. euteiches* mycelium (MYC) and mycelium grown in contact with *M. truncatula* roots (INT) [28] mapped to the assembly. In addition, ~90% of assembled Illumina reads generated during this study by using MYC and INT samples, mapped to the *A. euteiches* genome assembly. The completeness of the assembly was further evaluated with the BUSCO method [35] using the Alveolata-Stramenopiles dataset. The same analysis was performed with eight sequenced oomycetes (Additional file 1: ST1a, b). The *A. euteiches* assembly contained >94% of the Stramenopiles dataset and appears as the better one among the sequenced oomycetes. All the data were included in an updated version of the AphanoDB database dedicated to "omics" studies on the *Aphanomyces* genus [37]. AphanoDB v2.0 provides new tools as a genome browser, gene annotation facilities, and Basic Local Alignment Search Tool (BLAST) tools.

Genome sequences and assemblies of the crayfish pathogen *A. astaci* and the opportunistic pathogen *A. stellatus* were generated, giving an estimated size of 45 Mb and 62 Mb (Table 1) with 16,479 and 25,573 predicted genes, respectively. As expected, genome assemblies of *A. astaci* and *A. stellatus* compiled only from short reads generated by Illumina are more fragmented and must be considered as drafts.

These data were used to perform a phylogenetic analysis with a gene set recently used to estimate timescale evolution of oomycetes [38] (see Methods for further details). *Aphanomyces* species form a group which diverged from other Saprolegniales (*Saprolegnia parasitica*, *Achlya hypogena*, *Thraustotheca clavata*) more than 100 Mya (Fig. 1). This analysis also shows that divergence times are very deep within the *Aphanomyces* genus, with the three *Aphanomyces* species diverging from each other more than 50 Mya.

Table 1 Main features of *A. euteiches*, *A. astaci*, and *A. stellatus* genomes

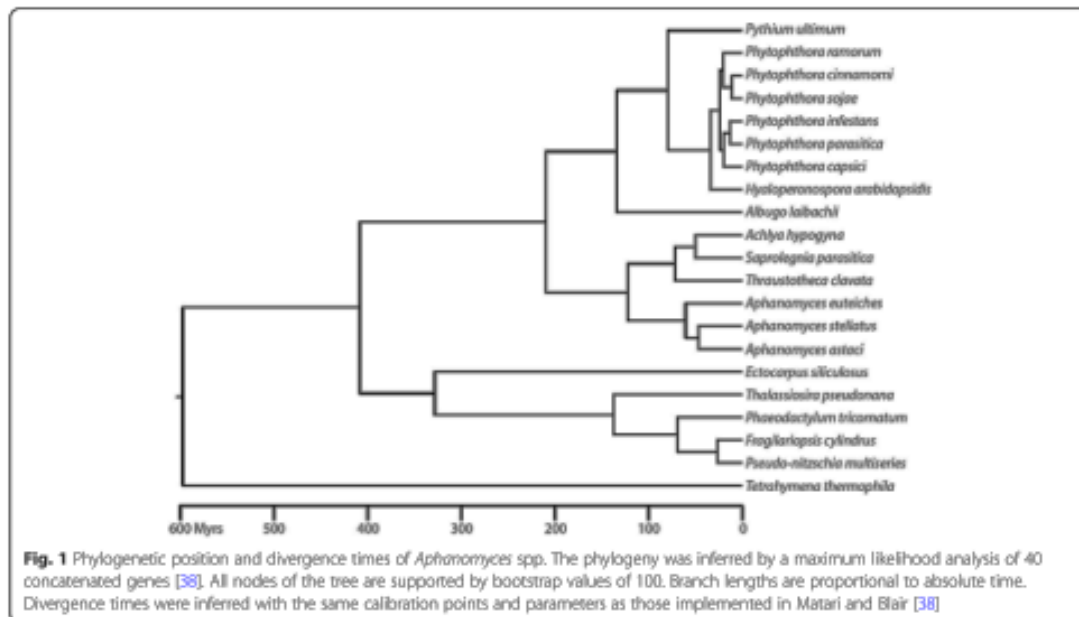
	<i>A. euteiches</i> ^a	<i>A. astaci</i> ^b	<i>A. stellatus</i> ^b
Estimated genome size (Mb)	61	94	71.6
Total contig length (Mb)	56.9	45.3	62.1
GC content (%)	47.69	48.51	52.55
Protein-coding genes	19,548	16,479	25,573
Average exons per gene	3.7	2.7	3.2
Mean gene size (kb)	1.503	1.132	1.467
N50 (bp)	275,164	3659	34,018
Gene density (number of genes per Mb)	343	364	412

^aCombination of 454 and Illumina sequencing technologies

^bIllumina sequencing technology

Transposable Elements (TE)

TEs are known to play a prevalent role in the evolution of eukaryotic pathogens [2, 3]. A de novo characterization of TEs was thus performed on all *Aphanomyces* genomes. The aim of the TE analysis was to uncover and annotate all TE copies in all three *Aphanomyces* genomes to facilitate future studies that will investigate the origin, evolution, and genomic impact of these elements in more detail. The fraction of *Aphanomyces* genomes occupied by TEs (5–13%; Additional file 1: ST1d) is lower than that for all other sequenced oomycetes (17–74%) in which TEs have been mined, such as *Phytophthora* species [32, 39], the downy mildew *Plasmopara viticola* [35], and the white rust *Albugo laibachii* [34], with the exception of *Pythium*

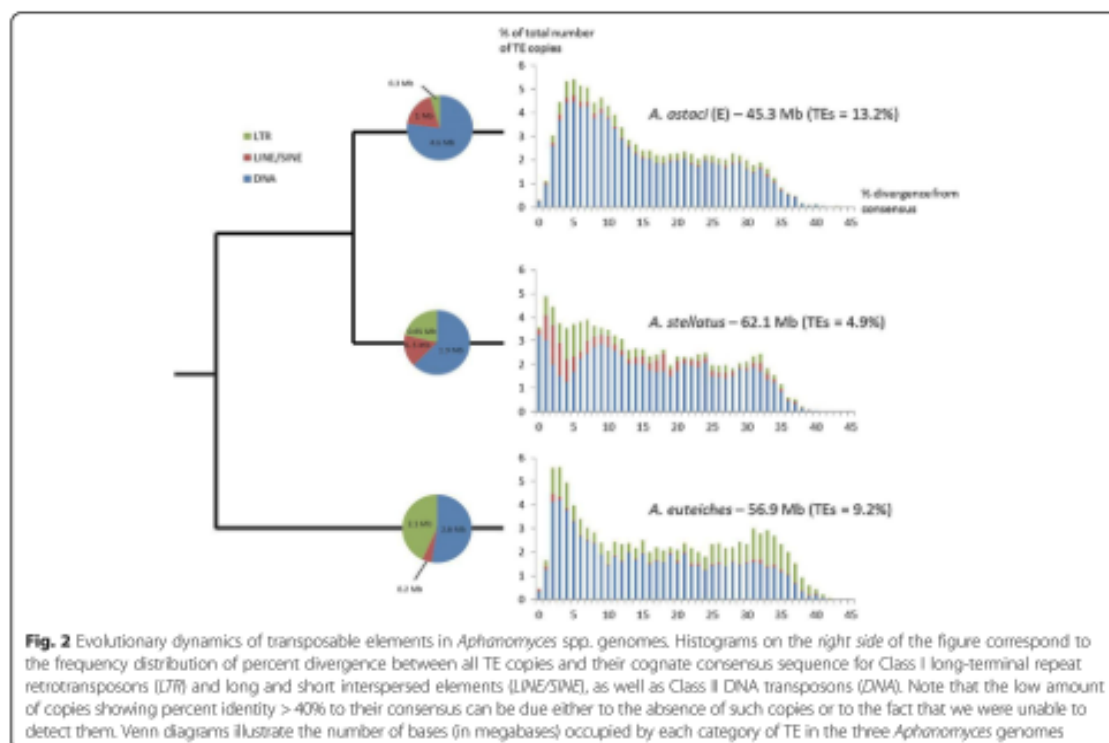


ultimum (5%) [40]. It is noteworthy that in oomycetes genome size is strongly correlated with TE content ($R^2 = 0.85$), supporting the hypothesis that TEs are a major determinant of genome size in these taxa [32]. In all three *Aphanomyces* species, the most abundant TEs are DNA transposons of the Tc1-mariner superfamily (up to 2.5% of the genome in *A. astaci*). Interestingly, none of the TEs that we identified are shared between all three *Aphanomyces* species, and very few TEs are shared between two species: two are shared between *A. astaci* and *A. euteiches* (74 and 83% identity over 741 and 170 bp respectively), two are shared between *A. stellatus* and *A. euteiches* (84 and 86% identity over 334 and 1262 bp respectively), and four are shared between *A. astaci* and *A. stellatus* (between 78% identity over 1820 bp and 84% identity over 195 bp) (Fig. 2). Furthermore, BLASTN searches using all TEs identified in *Aphanomyces* spp. as queries against all Repbase TEs did not reveal any significant hit. Together, these results suggest that *Aphanomyces* species TE families are characterized by a high rate of turnover.

Comparative analysis of *A. euteiches* and *A. astaci* proteomes

To identify conserved and specific features of *Aphanomyces* proteomes, an OrthoMCL analysis [41] was performed using *A. euteiches* and *A. astaci* proteomes and nine deep-sequenced oomycete proteomes (*S. parasitica*, *P. infestans*, *P. sojae*, *P. parasitica*, *P. ramorum*, *Hyaloperonospora arabidopsidis*, *A. laibachii*, *Py. ultimum*, and *Py. irregulare*) (Additional file 1: ST1e). A total of

2296 orthologous groups (34,404 genes) were detected in the 11 genomes defining a "core proteome" set (Additional file 1: ST1f). In this set 104 groups corresponding to 1528 genes defined the "core secretome" (Additional file 1: ST1f). A focus on the *A. euteiches* secretome (1240 genes, ~6% of the proteome, Additional file 1: ST1g) shows that 70% of the sequences harboring a Gene Ontology (GO) term are related to the "hydrolase activity" category (GO: 0016787) (Additional file 1: ST1h and Fig. 3a). This category is enriched in enzymes with glycosyl hydrolase or peptidase functions and other typical oomycete secreted proteins, such as protease inhibitors. The secretome of *A. astaci* is predicted to contain 744 genes (< 5% of the proteome). While this set is probably not complete, 323 sequences harbor a GO annotation and more than 65% (217 sequences) fall into the "hydrolase activity" category with a predominance of "peptidase GO:0008233" function (160 sequences, 73%). A closer examination of both secretomes showed that numerous genes detected in *A. euteiches* are not reported in *A. astaci* (Fig. 3a). In addition, about 72% of the *A. euteiches*-specific secretome (i.e., sequences not present in other oomycetes including *A. astaci*, 506 genes) did not display a putative functional domain (368 genes), and 80% encoded proteins below 300 amino residues in size (296/368, Additional file 1: ST1i, Fig. 3b). The same observation was made for the *A. astaci*-specific secretome, where 160 specific genes did not harbor a functional annotation and 86% (138/160, Additional file 1: ST1i) coded for small proteins (Fig. 3b). Interestingly, 59% of these small proteins were predicted to be putative effectors from



A. euteiches or *A. astaci* using EffectorP (Additional file 1: ST1i), a software based on properties shared by fungal effectors [42]. This suggests that *Aphanomyces* species presented a set of SSPs similar to fungal effectors.

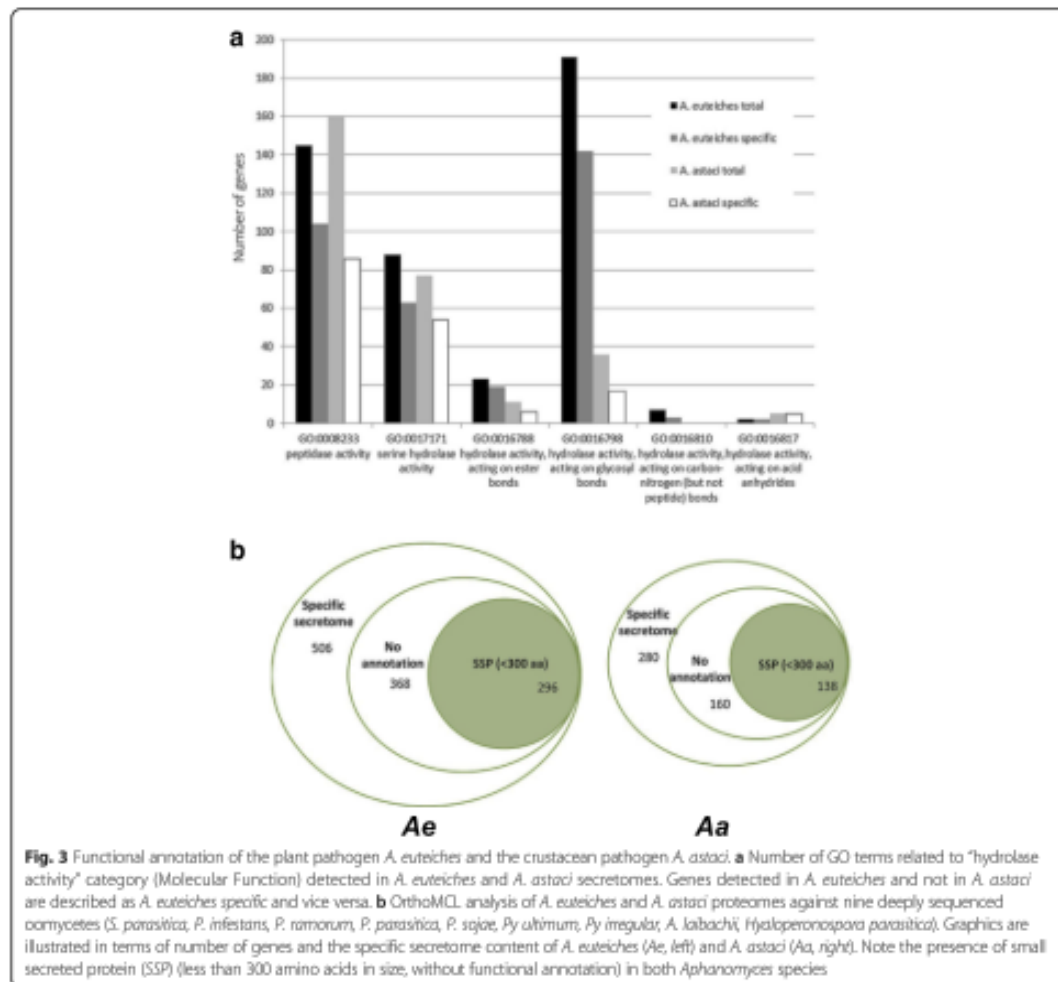
Carbohydrate-Active enZymes (CAZy) and carbohydrate-binding modules (CBMs)

Since comparative analyses suggested that the repertoires of glycosyl hydrolases are divergent between *A. euteiches* and *A. astaci*, a global prediction of CAZy domains (glycosyl hydrolases (GH), carbohydrate esterases (CE), polysaccharide lyases (PL), and carbohydrate-binding modules (CBM)) was performed. This analysis revealed that the *A. euteiches* genome is enriched in gene coding for proteins with CAZy domains compared to the *A. astaci* genome (Fig. 4, Additional file 1: ST1j). For example, more than 300 genes coding for proteins with at least one predicted GH domain were detected in the *A. euteiches* genome, a repertoire size similar to those predicted in oomycete genomes such as *Phytophthora* species [43], whereas only 109 genes were found in the *A. astaci* genome.

A closer examination of this repertoire revealed that several enzyme families targeting plant-specific polysaccharides (pectins, hemicellulases) are expanded in *A.*

euteiches and absent in *A. astaci*. Clearly, the *A. astaci* genome lacks genes coding for hemicellulases (e.g., GH, 10, 11, CE4 families) and pectinases (e.g., GH28, PL1, PL3, and PL4), which are largely represented in the *A. euteiches* genome (Fig. 4, Additional file 1: ST1j). Based on the CAZy database, eight GH families correspond to eukaryotic cellulases. The GH5, GH6, and GH7 families, which encode endocellulases and cellobiohydrolases, are highly represented in *A. euteiches* as compared to other oomycetes. Since oomycete cell walls contain cellulose, these enzymes can play a role in oomycete cell wall remodeling. Interestingly, while GH5 and GH6 cellulases are present in *A. astaci* and *A. euteiches*, a large family of GH7 was found only in *A. euteiches* (39 GH7-encoding gene), suggesting that this class of enzymes could play a role in plant pathogenesis (Fig. 4).

In phytopathogenic fungi it is suggested that α -L-arabinofuranosidases such as GH62 and GH54 are involved in plant penetration and pathogenesis [44, 45]. While GH62 are absent in oomycetes belonging to the Peronosporalean lineage analyzed so far, 12 putative GH62-coding sequences are detected in *A. euteiches*, while GH54 are missing (Fig. 4, Additional file 1: ST1j). Among GH62, seven are predicted to be secreted. It has also been suggested that α -L-arabinofuranosidases, by

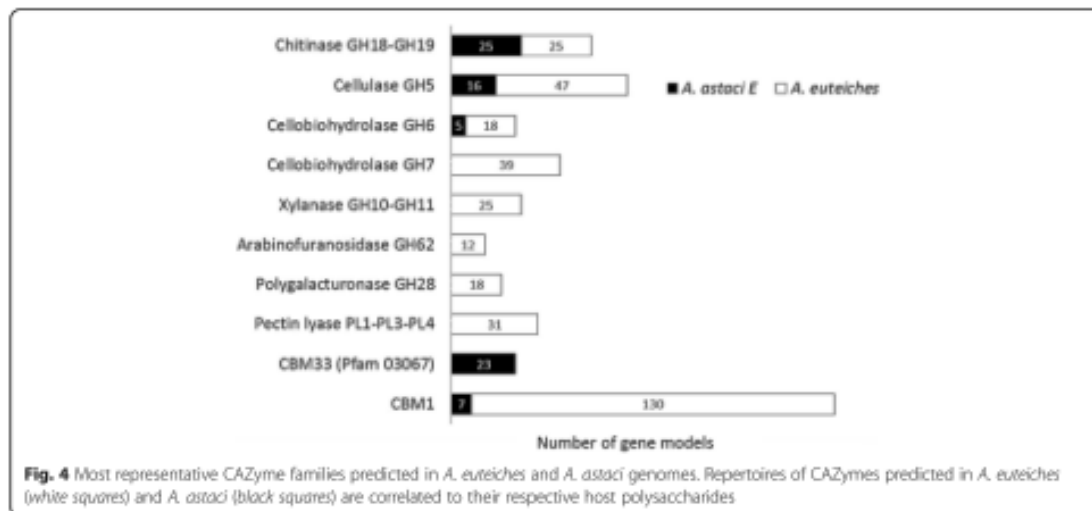


degrading arabinofuranose side chains, improve the accessibility of the xylan backbone of hemicellulose to xylanases as GH10 and GH11 [46], which are present in *A. euteiches* (22 and 3 sequences respectively). Thus, the presence of genes coding for these enzymes suggests that *A. euteiches* can express a complete repertoire of hemicellulose-degrading enzymes, distinct from those produced by other oomycetes.

The availability of CAZyme repertoires from distantly related oomycetes offers the opportunity to investigate their origin. Since most of these genes are closely related to fungal genes, it has been suggested that some of them were acquired by oomycetes by horizontal gene transfer (HGT) events from true fungi [47]. In certain cases, this hypothesis was sustained by phylogenetic analyses. This is the case for a pectate lyase gene from *P. infestans*

(EEY64154) [48] for which seven orthologous genes, corresponding to the PL1 family, were detected in the *A. euteiches* genome but not in *A. astaci* (Additional file 1: ST1j). Phylogenetic analysis using these sequences (Additional file 1: ST1k, Additional file 2: Figure S1) supports the hypothesis that these genes were acquired early in the evolution of oomycetes, before the Saprolegniale-Peronosporale divergence, and probably lost during the specialization of *Aphanomyces* species to animal hosts.

Numerous CAZymes are associated with CBMs to facilitate enzyme activity [49]. In *A. euteiches*, many CAZymes are associated with CBMs, and 130 CBM1 (cellulose-binding modules) predicted proteins are detected in this species, but only 7 genes in *A. astaci* (Additional file 1: ST1j, Fig. 4). In contrast, *A. astaci* harbors a set of genes encoding proteins with a putative chitin-



binding domain (PF03067, IPR004302, CBM33, now reclassified as the AA10 domain in CAZy) that are not detected in *A. euteiches* (Additional file 1: ST1j, Fig. 4). Interestingly, > 80% (19/23) of these domains are associated with a predicted signal peptide. These data suggested that CBM33 from *A. astaci* might play a role in the interaction with the crustacean shell, as reported for the PICBP49 CBM33-containing virulence factor of the honey bee pathogen *Paenibacillus larvae* that degrades chitin [50].

Aphanomyces spp. cytoplasmic effectors (RxLR and CRN oomycete effectors)

An important discovery regarding oomycete genome sequencing projects resides in the identification of predicted secreted proteins that could be delivered into host cells to aid pathogenicity. Two types of cytoplasmic effectors dominate the oomycete secretome: the RxLR effectors and the Crinklers (CRNs). These effector proteins are characterized by an amino acid signature located at the N-terminus of the sequence. We thus investigated the presence of these host-targeting signals in *A. euteiches* and *A. astaci* species. The genomes of both *Aphanomyces* were searched for RxLRs and CRNs as previously reported [17, 40]. This approach did not allow the identification of RxLR effectors on both *Aphanomyces* genomes, as previously suggested upon analysis of EST libraries from the same strain of *A. euteiches* [17]. This analysis sustains the view that RxLR effectors seem to be absent in the Saprolegnia lineage [20]. For predicting CRNs, a combination of automatic searches (hidden Markov model (HMM), regular expression) and manual curation methods was used, and 160 and 31

CRNs and CRN-like genes were detected in the *A. euteiches* and *A. astaci* genomes respectively (Additional file 1: ST1k). For *A. euteiches*, this number is similar to the one reported in phytopathogenic *Phytophthora* species (> 80 *P. capsici*; > 200 *P. sojae*; > 400 *P. infestans* [32, 51]).

Consistent with previous data on oomycete genomes [7, 52, 53], fewer than 25% of *A. euteiches* CRNs and none in *A. astaci* were predicted to be secreted by means of SignalP analysis. By contrast, around 60% of AeCRNs and AeCRN-like genes harbor a predicted nuclear-localization signal (NLS). Among them 16 have both a predicted signal peptide and an NLS. A majority of AeCRNs (> 60%) harbor a LYLAK motif at the N-terminal rather than the canonical *Phytophthora* LxLFLAK motif, as previously reported upon complementary DNA (cDNA) annotation of *A. euteiches* [28, 29, 54]. We noticed that the N-terminal trafficking signal is less conserved in *A. astaci* as compared to CRNs from *A. euteiches*, and only five sequences harbor a putative header signal in combination with a C-terminal domain (Additional file 1: ST1k). The headers of CRNs are followed by a more diverse C-terminal domain that confers effector activity [32]. Based on sequence similarity, 36 domains were initially defined for the CRN repertoire of *P. infestans*, and new C-terminal domains have been characterized upon the CRN repertoire annotation of various oomycete species [53, 55]. HMM searches and manual assignment on AeCRNs and AeCRN-like sets showed that the necrotic DXZ, D5, and D2 kinase domains are among the most widespread C-terminal domains in *A. euteiches* (Additional file 1: ST1k). The DC domain, reported as a putative DNA-binding helix-hairpin-helix (HhH) motif in PsCRN108 from *P. sojae* [56], is also

largely represented in *A. euteiches* but not in *A. astaci*. The DXZ and DN17 domains frequently detected in phytopathogenic oomycetes and the chytrid *Batrachomyces dendrobatidis* [32, 55, 57] are well represented in *A. astaci*.

Dynamic changes of *A. euteiches* transcriptome during infection of *M. truncatula* roots

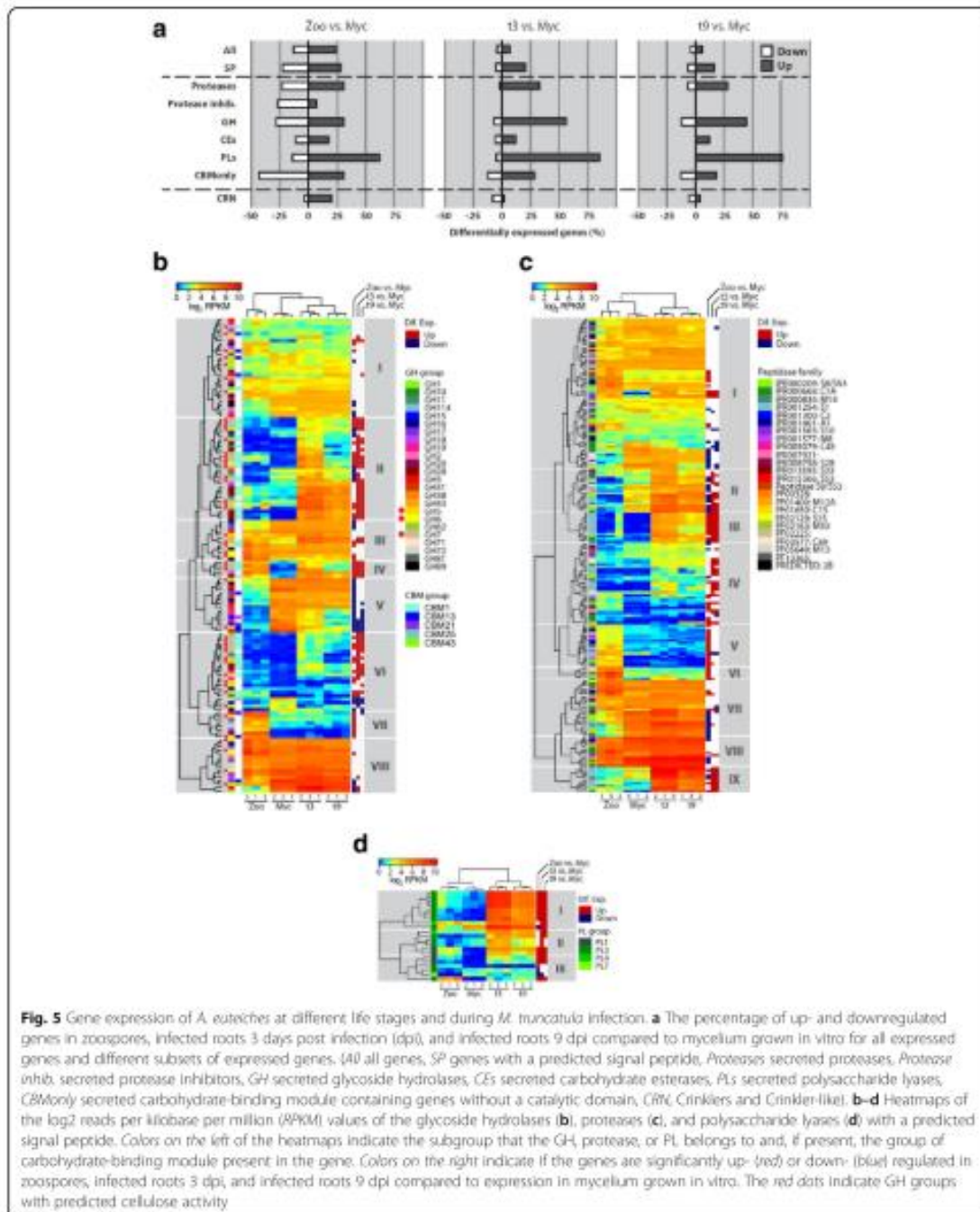
To get an insight into the expression and regulation of *A. euteiches* genes during different life stages, RNA-seq analyses were performed on RNAs isolated from *A. euteiches* zoospores and mycelium grown in liquid culture as well as in infected *M. truncatula* roots harvested 1, 3, and 9 days post inoculation (dpi). For the zoospores and the in vitro mycelium libraries, around 50 M reads were obtained, of which 70–77% were mapped in pairs to gene-coding regions (Additional file 3: ST2a). For *M. truncatula*-infected roots, 46–71 M reads were obtained, of which most could not be mapped to the *A. euteiches* genome, since a high amount of *M. truncatula* material was present in the samples. In addition, since less than 1% of the reads of 1 dpi could be mapped to the *A. euteiches* genome, this time point was excluded from the analysis (data not shown). For time points 3 and 9 dpi, 6–13% of the reads could be mapped in pairs to gene-coding regions (Additional file 3: ST2a). After filtering for lowly expressed genes and data normalization, a multi-dimensional scaling plot revealed a clear separation between expression patterns of the different life stages of *A. euteiches*, while the biological repeats of each life stage (mycelium, zoospore, 3 dpi, and 9 dpi) clustered together (Additional file 4: Figure S2). This plot suggested that different gene subsets are expressed during *M. truncatula* infection.

For the 16,786 (85.8%) genes that were expressed, differential expression between the different life stages was determined. Around 36–37% of the genes were differentially expressed between zoospores and the other life stages, while only 10–11% of the genes showed differential expression between the in vitro grown *A. euteiches* mycelium and the infected root material (Additional file 3: ST2b). This could reflect a transcriptome remodeling during host infection. To further investigate in what processes the differentially expressed genes are involved, a Gene Ontology (GO) enrichment analysis was performed. During infection, genes that are upregulated between 3 and 9 dpi are mainly involved in “carbohydrate metabolic (GO:0005975)” and “proteolysis (GO:0006508)” processes, while downregulated genes belonged mainly to transport processes (GO:0055085, GO:0030001). The opposite situation is detected when comparing zoospores with in vitro grown mycelium

(Additional file 3: ST2c–e), suggesting important physiological differences between zoospores and mycelium life stages of *A. euteiches* as reported for *Phytophthora infestans* [58].

We then investigated the expression pattern of the *A. euteiches* secretome with a focus on CAZymes, proteases and protease inhibitors, CBMs, and CRNs/CRN-like effectors (Fig. 5a). When zoospores and mycelium stages are compared, most groups of genes encoding secreted proteins show a similar percentage of differential expression with the exception of the “polysaccharide lyase (PL)” category, which displays the highest percentage of differentially expressed genes. In contrast, during infection (3 and 9 dpi) around three times as much of the genes coding for secreted proteins are upregulated, with proteases, glycoside hydrolases (GH), and PL (86% and 76%) showing the highest percentages of upregulated genes (Fig. 5a). Less than 2% of CRN genes are upregulated at 3 and 9 dpi, while 13% are upregulated in zoospores as compared to in vitro grown mycelium, suggesting that a subset of AeCRN is present at the early stage of *Medicago* infection (Fig. 5a).

Heatmaps to visualize expression level of genes rather than differential expression show that, for GH, several groups can be identified (Fig. 5b, Additional file 3: ST2f) with groups II, IV, and VI containing genes that are upregulated during infection compared to mycelium. These groups contain a large number of genes coding for proteins with predicted cellulase (GH5, GH6, and GH7) and polygalacturonase (GH28) activity. They also include numerous hemicellulase genes (GH10, GH11) and one secreted arabinofuranosidase (GH62). Most of the polysaccharide lyases (PL) are also strongly induced during infection (Fig. 5d, Additional file 3: ST2g). Secreted PL1 are detected in group II or III, where gene expression is less abundant in mycelium as compared to zoospore and infection stages. This pattern is similar to the one observed in *Phytophthora capsici*, where the PL1 family in combination with PL16 and PL20 (absent in the *Ae* genome) account for nearly all of the contribution of the 22 PL genes to *Phytophthora* virulence [59]. Most of the carbohydrate esterases (CE) showed a consistent low to medium expression in the different life stages (Additional file 5: Figure S3A, Additional file 3: ST2i). For the CBM-containing proteins without a predicted catalytic site mostly composed of CBM1 domains (cellulose-binding), several groups of genes can be identified with group II being strongly induced and expressed during infection while groups III and V are specifically upregulated or downregulated respectively in the zoospore stage (Additional file 5: Figure S3B, Additional file 3: ST2j). This expression pattern suggested that *A. euteiches*-



secreted CBM1 domains may contribute either to *A. euteiches* virulence or microorganism development, as reported for the CBM1-containing protein CBEL from

P. parastica that mediates adhesion to cellulosic substrates and contributes to *Phytophthora* cell wall architecture [60, 61].

For the secreted peptidases, several groups can also be identified (Fig. 5b, Additional file 3: ST2h). Many peptidases show constitutive expression during all life stages (groups I, VII, and VIII), while some are induced in zoospores (groups V and VI) or during *M. truncatula* root infection (groups II, III, IV, and IX). These last groups contain a high number of serine proteases (S1 family) that could be considered as candidates for pathogenicity factors. Indeed, serine proteases have been characterized as the major extracellular proteolytic enzymes secreted by *Phytophthora* spp. and indispensable for necrosis [62]. Notably, none of the secreted protease inhibitors is differentially expressed during infection. However, most of the secreted protease inhibitors are highly expressed during all life stages of *Ae* (Additional file 5: Fig. 3C, Additional file 3: ST2k).

Together, these analyses indicate that expression of several families of genes coding secreted proteins are induced in zoospores and during infection of *M. truncatula* roots compared to saprophytically grown mycelium. This supports an important role in the pathogenesis of cell wall-degrading enzymes specifically found in *A. euteiches* and not in *A. astaci* targeting plant cell wall polysaccharides (pectins, hemicellulose).

Identification and functional characterization of small secreted proteins in *A. euteiches* (AeSSPs)

As reported above, 40% of *A. euteiches*-specific genes that encoded putative secreted proteins did not display a functional annotation and are below 300 amino acid residues in size (< 300 genes, Fig. 3b, Additional file 1: ST1i). Consequently, putative AeSSPs represented 24% of the secretome. Around 5% are organized in clusters (≥ 3 adjacent SSP genes, Additional file 6: ST3a). The clusters are distributed all over the genome and comprise 3 to 9 genes each. The clusters mainly contain AeSSP genes from the same OrthoMCL group, indicating that they might have arisen by duplication.

To ascertain the expression of AeSSPs during host infection, we checked the expression data presented above (e.g., mycelium, zoospore, interaction 3 dpi (T3), interaction 9 dpi (T9)). Since we could not exploit RNA-seq data generated at 1 day post infection, we included data from our previous set of cDNA generated from mycelium (MYC library) and *A. euteiches* grown in contact with roots during 1 or 2 days (INT T1 + T2, [28] (Additional file 6: ST3a). As shown in Fig. 6a, a large set of AeSSPs are upregulated in zoospores, in mycelium in contact with plant roots, or during infection. In total, 120 AeSSPs have been found to be induced in at least one condition.

We selected in AphanoDB v2.0, the AeSSP cluster from scaffold2_1449549_1653277 (Fig. 6b) and scaffold2_134062_1449527 to evaluate the effector function

of AeSSP genes. These clusters are unique, since in addition to their expression at the beginning of the interaction, they contain AeSSPs with a predicted NLS (AeSSP1251 and AeSSP1254, AeSSP1256), suggesting that these proteins could be translocated to the host cell to target nuclear components. To investigate if the AeSSPs can play a role in virulence, *Nicotiana benthamiana* leaves transiently expressing the AeSSPs were infected with *P. capsici* (Fig. 7a). In the assay, one side of the leaf was infiltrated with *Agrobacterium tumefaciens* containing an AeSSP:green fluorescent protein (GFP) fusion construct (AeSSP1250, AeSSP1254, AeSSP1255, and AeSSP1256), while on the other side of the leaf GFP was delivered alone. Quantification of the lesion surfaces at 3 dpi showed that AeSSP1256 significantly enhanced the susceptibility of *Nicotiana* compared to GFP alone, while no differences were observed for AeSSP1250, AeSSP1254, and AeSSP1255 (Fig. 7b). This indicates that AeSSP1256 may efficiently contribute to oomycete pathogenicity.

To investigate the subcellular localization of AeSSPs, chimeric genes encoding AeSSPs independently with (full-length version) or without (matured form) their own signal peptide under the control of the *CaMV35S* promoter were generated in fusion with a GFP marker. As shown in Fig. 7c, both versions of AeSSP1250 are detected either in the nucleus or the cytoplasm of *Nicotiana* cells, while AeSSP1255 versions are mainly cytoplasmic. The NLS-containing AeSSP1254 and AeSSP1256 are nuclear localized without any labeling of the nucleolus. The pattern of fluorescence is similar with the full version or the matured form of AeSSP1254 and AeSSP1256. We noticed that the expression of both versions of AeSSP1256 led to the detection of fluorescence as a ring surrounding the nucleolus in addition to filament-like structures. A closer view of AeSSP1256 in fusion with its own signal peptide confirmed the accumulation around the nucleolus and also as filament-like structures (Fig. 7d). This unexpected nuclear localization is reminiscent of the one observed with the cytoplasmic effector CRN79_188 from *Phytophthora capsici* upon its transient expression in *Nicotiana* leaf [63].

Since in all cases the presence of the native signal peptide did not alter the localization of the corresponding AeSSP, we tested whether the AeSSP entered the plant secretory pathway. A functional endoplasmic reticulum (ER) retention signal (KDEL motif) was added at the C-terminal of the full-length form of AeSSP1256 to trap the protein in the ER. In *Nicotiana* leaves expressing a +SP:AeSSP1256:GFP:KDEL construct, an extensive network throughout the cytoplasm was labeled as observed with an ER-marker [64] (Fig. 8a). In contrast, expression of the matured form -SP:AeSSP1256:GFP:KDEL produced fluorescence in the nucleus. This indicates that

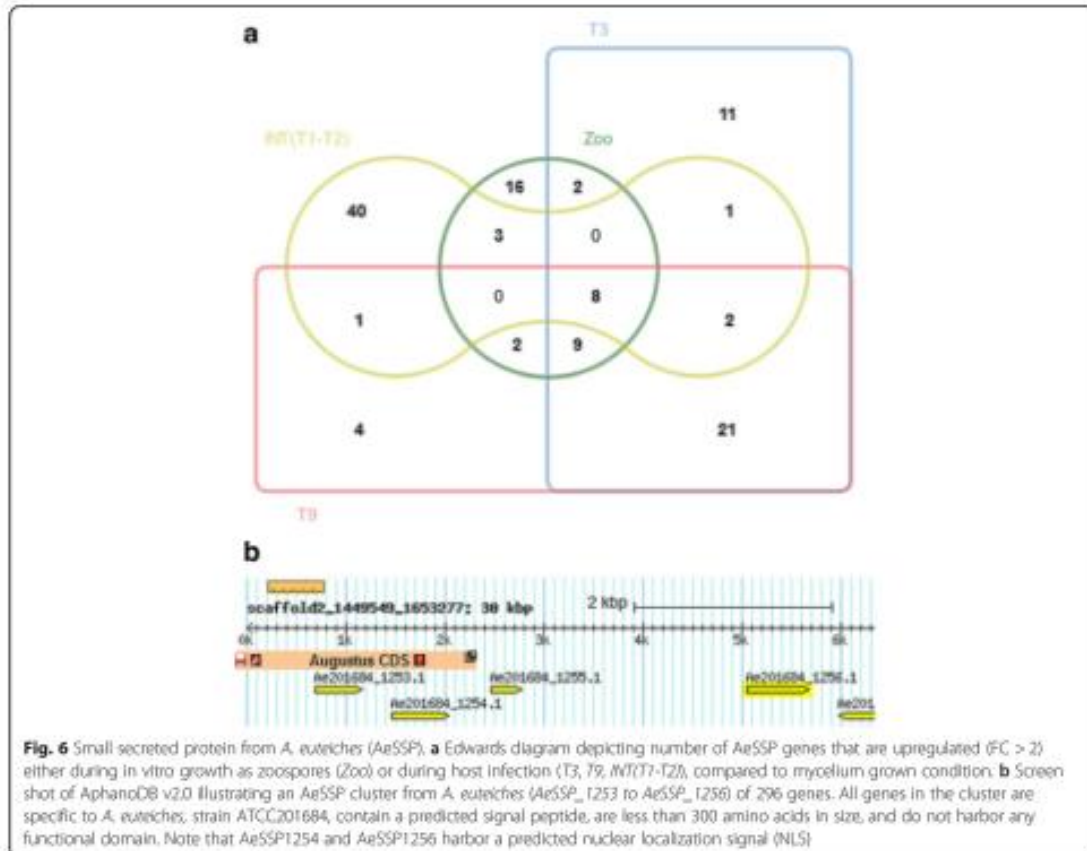
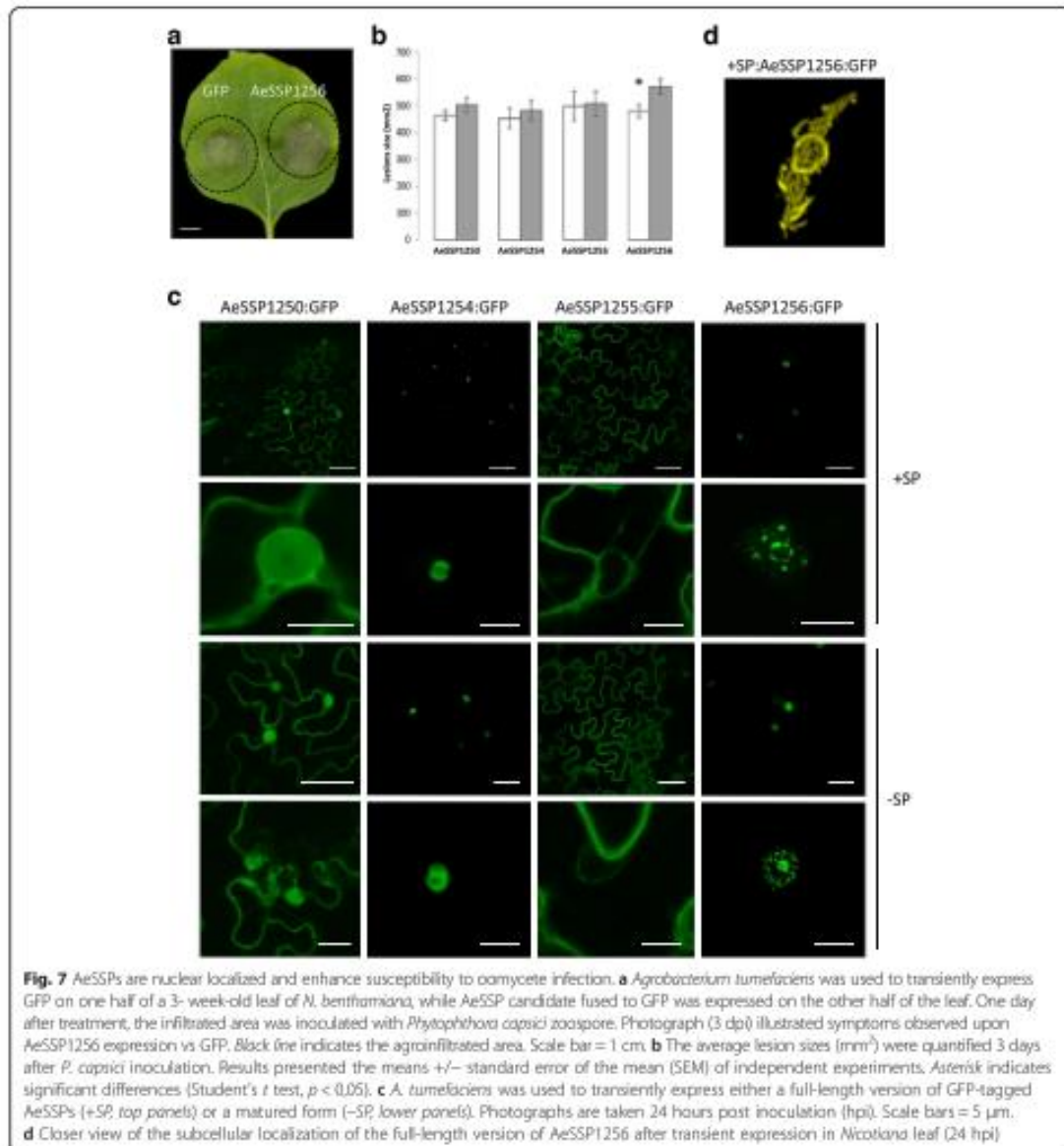


Fig. 6 Small secreted protein from *A. euteiches* (AeSSP). **a** Edwards diagram depicting number of AeSSP genes that are upregulated ($FC > 2$) either during in vitro growth as zoospores (Zoo) or during host infection (T3, T8, *inT*(T7-T2)), compared to mycelium grown condition. **b** Screenshot of AphanosDB v2.0 illustrating an AeSSP cluster from *A. euteiches* (AeSSP_1253 to AeSSP_1256) of 296 genes. All genes in the cluster are specific to *A. euteiches*, strain ATCC201684, contain a predicted signal peptide, are less than 300 amino acids in size, and do not harbor any functional domain. Note that AeSSP1254 and AeSSP1256 harbor a predicted nuclear localization signal (NLS)

+SP:AeSSP1256 is delivered to the ER secretion pathway and that the predicted signal peptide of AeSSP1256 is active in *N. benthamiana*. To confirm AeSSP1256 trafficking in *Nicotiana* cells, we used the Brefeldin A (BFA) drug. BFA inhibits transport from the ER to the Golgi and causes the formation of membranous islands throughout the cell [65]. As expected, the localization of the full-length version of AeSSP1256 is disrupted by BFA, while the treatment did not affect the localization of the matured form. Thus, only +SP:AeSSP1256 transits through the Golgi in *Nicotiana* (Fig. 8b). Finally, we checked the effect and subcellular localization of AeSSP1256 in *Medicago* composite plants expressing the +SP:AeSSP1256-GFP construct. The expression of AeSSP1256 did not provoke any necrosis or alteration of root system development (data not shown). As illustrated in Fig. 8c, AeSSP1256 in fusion with its own signal peptide is nuclear localized 15 days after root transformation by *A. rhizogenes*, as observed previously in *Nicotiana* leaf.

Discussion

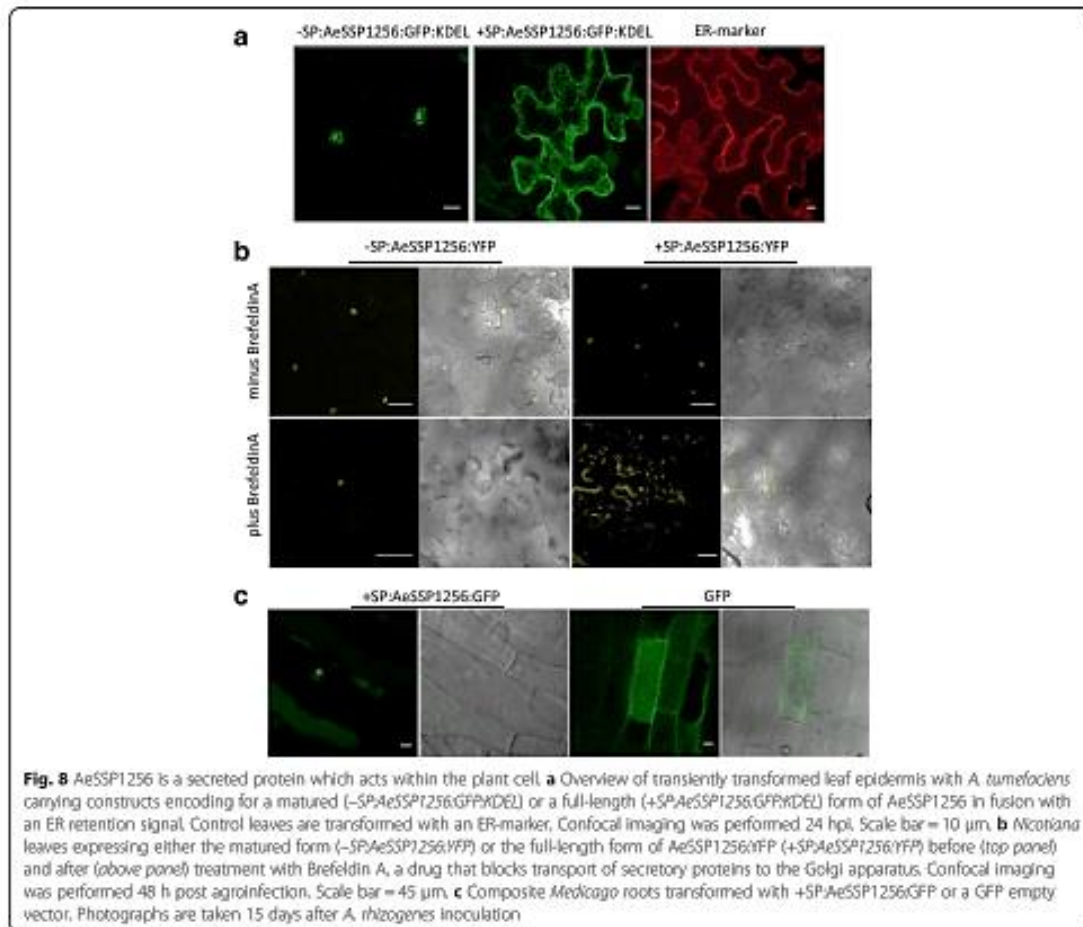
In this study, we used a combination of genomics and transcriptomics approaches to identify gene repertoires involved in the adaptation of *Aphanomyces* pathogens to plant or animal hosts. This work provides the first genomics insight into the *Aphanomyces* genus, allowing one to precisely locate the phylogenetic position of *Aphanomyces* spp. within the oomycete lineage and providing clues for understanding animal and plant pathogenic evolution among oomycetes. Phylogenetic analysis suggested that specialization of *Aphanomyces* species to plant or animal hosts is an ancient event (more than 50 Mya), and analysis of gene contents revealed that phytopathogenic *A. euteiches* possesses a large and diverse repertoire of genes coding cell wall-degrading enzymes (CWDEs) which target plant cell wall polysaccharides, absent in *A. astaci*. In turn, *A. astaci* shows an expansion of protease genes, and during evolution it acquired genes coding proteins predicted to target chitin, the main component of the crayfish shell. These results



indicate that host specialization is correlated with the presence of secretomes, which has been shaped by various evolutionary events including gene acquisition, gene losses, and gene amplification. Interestingly, transcriptome analyses showed that most of the genes coding enzymes able to degrade plant cell wall polysaccharides such as pectins and hemicellulases are strongly expressed during pathogenesis, strengthening their role

in pathogenesis. Analyses performed on distantly related oomycete species, notably *Phytophthora* and *Saprolegnia*, gave similar results [31, 43, 66, 67], pointing out the key roles of degrading enzymes for pathogenesis and adaptation to specific ecological niches.

These results also raised the question of the origin of CWDE sequences in the *Aphanomyces* genus. Most of the secreted *A. euteiches* CWDEs acting against plant



wall polysaccharides, such as pectinases and hemicellulases, show strong similarities to *Phytophthora* enzymes. Some of these genes have been suggested to be acquired by lateral gene transfer from a fungal donor, notably in *Phytophthora* [47, 48]. A striking example is a pectate lyase gene [48]. Interestingly, several paralogs of this gene were found in *A. euteiches* but not in *A. astaci*, suggesting that this gene was acquired before the divergence between the Saprolegnian and Peronosporalean lineages and was lost by *A. astaci* during adaptation to animal hosts. Availability of more oomycete genomes is needed to further define the origin of oomycete CWDEs involved in interactions with plants; however, our results indicate that acquisitions of plant CWDEs in oomycetes occur early during oomycete evolution.

By combining comparative genomics and transcriptomics, we identified a large set of SSPs which may

represent new oomycete putative effectors. Among the 296 AeSSP genes, 120 are induced during at least one infection condition analyzed. Functional studies on four of these candidates revealed that these proteins are localized in various subcellular compartments, and one of them enhanced plant susceptibility to oomycete infection. Large repertoires of SSPs have been evidenced upon genome annotation of fungi interacting with plants [68, 69], animals [70], and insects [71]. Also unexpected was the large repertoire of SSPs predicted in mycorrhizal fungi [72, 73]. SSPs were also recently reported in bacteria such as the plant pathogen *Pseudomonas syringae* [74], but up to now no SSPs were described in oomycete genomes. Comparative fungal genomics studies showed evidences of rapid evolution of SSPs in related pathogens with different host ranges [70, 75]. A survey on 136 fungal secretomes archived in the Fungal Secretome

Database (FSD) established that microorganisms living in close interaction with their hosts (symbiotic organisms, biotrophs) have commonly higher proportions of species-specific SSPs than necrotrophs or hemibiotrophs [76]. SSPs are frequently lineage specific and associated with host adaptation/specialization and are considered as putative effectors. Therefore, our work makes SSPs new candidates to be crucial players in oomycete adaptation to new hosts, particularly in species lacking the large family of RxLR effectors found in the Peronosporalean lineage.

Conclusion

In this paper, we have analyzed the genomes of two close *Aphanomyces* species with the aim of identifying genetic determinants involved in host adaptation. However, the divergence between *A. euteiches* and *A. astaci* is still substantial, and these two species occupy two distinct ecological niches (soil vs aquatic environments). Thus, it is expected that many of the differences observed do not apply exclusively to pathogenesis but also to adaptation to these ecological niches. Importantly, it has been suggested that effectors can also play a role in competition or co-operation with other microorganisms occupying the same ecological niche. Sequencing of more *Aphanomyces* species is underway and will certainly help to refine the set of genes involved in host pathogenesis.

Methods

Aphanomyces spp. isolates and DNA preparation

The mycelia of *A. euteiches* isolate ATCC201684, *A. astaci* (Genotype E, strain Li07, provided by A. Petrussek, Czech Republic), and *A. stellatus* isolate CBS 578.67 were grown for 4 days in liquid YG medium (2.5% yeast extract, 5% glucose) at 23 °C in the dark. Biological samples were frozen in liquid nitrogen and the DNA extracted as reported in [31].

Aphanomyces euteiches genome sequencing and assembly

CNS-Genoscope, Evry, France performed the sequencing and assemblies of the *A. euteiches* ATCC201684 genome, using a combination of Sanger and Illumina technologies. For 454 libraries of *A. euteiches*, DNA was extracted and fragmented to a range of 5–10 kb or around 20 kb using a HydroShear instrument. Fragments were end-repaired, and the extremities were ligated to 454 circularization adapters. Fragments were size selected respectively to 8 kb or 20 kb through regular gel electrophoresis and circularized using Cre-Lox recombination. Circular DNA was fragmented again by nebulization or using the Covaris E210 instrument (Covaris, Inc., Woburn, MA, USA). Fragments were end-repaired and

ligated with library adapters. Mate-pair libraries were amplified and purified. Single-stranded libraries were isolated, then bound to capture beads and amplified in an oil emulsion (emPCR). The libraries were then loaded on a picotiter plate and sequenced using a GS FLX sequencer according to the manufacturer's protocol. We also prepared 454 single-end read libraries according to the Roche standard procedure using RL (GS FLX Titanium Rapid Library Preparation Kit, Roche Diagnostics, Indianapolis, IN, USA). The libraries were sequenced using a 1/4 Pico Titer Plate on a 454 GS FLX instrument with Titanium chemistry (Roche Diagnostics). For the Illumina library, 2 µg of genomic DNA (gDNA) of *A. euteiches* was sheared to a 150–700-bp range using the Covaris E210 instrument (Covaris, Inc.). Sheared DNA was used for Illumina library preparation according to a semiautomated protocol. Briefly, end repair, A tailing, and Illumina-compatible adapter (BioScientific) ligation were performed using the SPRIworks Library Preparation System and SPRI TE instrument (Beckman Coulter, Simsbury, CT, USA) according to the manufacturer's protocol. A 300–600-bp size selection was applied in order to recover most of the fragments. The DNA fragments were amplified by 10 cycles of PCR using Kapa HiFi HotStart DNA Polymerase (Life Technologies) and Illumina adapter-specific primers. The libraries were purified with 0.8× AMPure XP beads (Beckman Coulter). After library profile analysis with an Agilent 2100 Bioanalyzer (Agilent Technologies, Santa Clara, CA, USA) and qPCR quantification, the library was sequenced using 100 base-length read chemistry in paired-end mode on the Illumina HiSeq2000 (Illumina, Canton, MA, USA). All reads were assembled with Newbler version vMapAsmResearch-04/19/2010-patch-08/17/2010. The 6319 contigs were linked into 349 scaffolds. The sequence quality of scaffolds from the Newbler assembly was improved as described previously [77] by automatic error corrections with Solexa/Illumina reads (146-fold genome coverage), which have a different bias in error type compared with 454 reads. Finally, the assembly was gap closed using Illumina data and GapCloser [78]. Putative misassemblies were identified and corrected using default parameters of REAPR (version 1.0.17) [79]. Assembly completeness was estimated using BUSCO v3 [35] based on a set of common fungal genes (F) or Alveolata/Stramenopiles genes (AS), aka benchmarking universal single-copy orthologs (BUSCOs). We found 83.1% (F)/78.6% (AS) complete BUSCOs, 3.8% (F)/0% (AS) duplicated BUSCOs, and 3.1% (F)/1.7% (AS) fragmented BUSCOs, leading to 13.8% (F)/19.7% (AS) missing BUSCOs in *A. euteiches*. Statistics for different sequencing technologies performed in this study for the *A. euteiches* ATCC201684 genome are presented below.

	Sequencing technology	Library preparation	Number of reads	Number of bp	Coverage
<i>Aphanomyces euteiches</i> (AFCC2016F4)	Roche/454 Titanium	Single end reads	3,448,970	1,312,184,108	21.9X
	Roche/454 Titanium	Meta-pair reads	1,436,086	479,402,183	8X
	Illumina HiSeq2500	Paired-end reads (2x101bp)	43,311,587	8,748,940,574	145.9X

Aphanomyces astaci and *Aphanomyces stellatus* genome sequencing and assemblies

The GeT-PlaGe core facility, Toulouse, France realized Illumina sequencing of the *A. astaci* and *A. stellatus* genomes, and the assemblies were performed by the Genotoul Bioinformatic Platform, Toulouse, France. DNA-seq libraries were prepared using an Illumina TruSeq DNA v2 Library Prep Kit following the manufacturer's instructions. DNA was fragmented by sonication, size selection was performed using E-Gel 0.8% (Thermo Fisher Scientific, Waltham, MA, USA), and the adapters were ligated. Ten PCR cycles were applied to amplify the library before final purification with Agencourt AMPure XP beads (Beckman Coulter). Library quality was assessed using an Agilent Bioanalyzer, and the libraries were quantified by qPCR using the Kapa Library Quantification Kit. DNA-seq experiments were performed on an Illumina HiSeq2000 Sequencer using a paired-end read length of 2 × 100 pb with the HiSeq v3 Reagent Kit. The raw reads have been quality checked and stored in NG6 [80]. FastQC (version 0.10.0) (<http://www.bioinformatics.babraham.ac.uk/projects/fastqc/>) was used to produce quality metrics and bwa aln (version 0.6.1-r104) to search *Escherichia coli*-, yeast-, and phage-contaminated reads. The reads of *A. astaci* and *A. stellatus* were assembled using MaSuRCA, version 2.0 [81], and the assembly metrics were calculated using the `assemblathon_stats.pl` script [82].

Structural and functional annotation of *Aphanomyces* genomes

The assembled data of *Aphanomyces* were annotated with Augustus v2.757 [83] trained with the assembled RNA-seq transcript generated in this study and the publicly available ESTs previously obtained from *A. euteiches* [28] using `autoAug.pl` [84] and PASA [85]. RNA-seq reads were first assembled with `trinityrna-seq_r2012-10-05` [86]. The accuracy of the prediction was evaluated by mapping the RNA-seq reads to the genomes using `bwa` [87]. Genes were annotated using BLASTP against the RefSeq database [88]. For protein family classification, InterProScan [89] and the Pfam protein domain database [90] were used. Gene

ontologies were classified based on InterProScan annotation IDs. Kyoto Encyclopedia of Genes and Genomes (KEGG) and Enzyme Commission (EC number) data were obtained with KEGG Automatic Annotation Server (KAAS) predicted protein sequences [91] and were also mapped to the Clusters of Orthologous Groups (COG) classification system [92]. Predictions of signal peptides were performed using SignalP 4.1 [93]. Carbohydrate-Active enZymes (CAZymes) in the protein models were predicted using the `dbCAN` pipeline [94]. Orthology comparisons between the predicted *Aphanomyces* genomes and protein datasets from nine deeply sequenced oomycete genomes were performed via OrthoMCLcompanion [95] using standard parameters. Interspersed repeat sequences were *de novo* identified in the genomes of *A. euteiches*, *A. stellatus*, and *A. astaci* using the RepeatModeler 1.0.8 pipeline [96]. Short (< 1000 bp) Class II transposons that were devoid of recognizable open reading frames were classified as miniature inverted-repeat transposable elements (MITEs). When possible, we assigned them to a superfamily based on the nature of their target site duplication (TSD): piggybac (TTAA motif), Tc1-mariner (TA motif), and PIF-Harbinger (TTA or TAA motif) [97]. The remaining RepeatModeler unclassified consensus sequences (producing no BLASTX hits and having no distinct boundaries) were classified as "unclear". A library of repeated sequences was then constructed for each species and used to mask each genome with RepeatMasker 4.0.5 [96]. To characterize the global evolutionary dynamics of *Aphanomyces* TEs, we plotted the frequency distribution of the percent divergence between each consensus and all their cognate copies. To assess the extent to which the TEs are related to each other and to other known TEs, we used each library as a query to perform BLASTN searches on the other libraries and on the Repbase [98] library of TEs (e-value cut-off = 10⁻²⁰). Gene annotations were visualized in Apollo [99]. All the data generated in this work were incorporated in an updated version (version 2.0) of AphanoDB [37, 100].

Preparation of RNA material

Seeds of *M. truncatula* Gaertn. F83005.5 were scarified, sterilized, and *in vitro* cultured as previously

described [101, 102]. Roots of 10-day-old plants were inoculated with *A. euteiches* ATCC201684 zoospores as described in [103]. Infected roots were harvested 1 dpi, 3 dpi, and 9 dpi. In parallel, flasks with 50 mL PG medium (20.0 g/L animal peptone; 5.0 g/L glucose) were inoculated with 1000 zoospores of *A. euteiches*. Mycelium samples were collected from the PG medium 1 dpi, 3 dpi, and 9 dpi. Zoospores were collected by centrifugation at 14,000× g at 4 °C for 45 min. For all samples three biological replicates were collected. RNA was isolated using the RNA Plant Mini Kit (QIAGEN, Hilden, Germany) according to the manufacturer's protocol, except for the DNase treatment (RNase-free DNase, QIAGEN), which was done on the column for 20 min. The RNA concentration was determined, and the quality of the RNA was verified using a Fragment Analyzer (Advanced Analytical, Ankeny, IA, USA).

RNA sequencing

Illumina sequencing of RNA samples generated from *A. euteiches* mycelium (MY) and mycelium grown in contact with *M. truncatula* roots (INT) [28], was performed by CNS-Genoscope, Evry, France. Starting with 2 µg of total RNA, double-stranded cDNA was first generated using the TruSeq RNA sample prep kit (Illumina, Canton, MA, USA), and then paired-end libraries were prepared using NEBNext Sample Reagent Set (New England Biolabs, Ipswich, MA, USA). Briefly, the messenger RNAs (mRNAs) were polyA-selected, chemically fragmented, and converted into single-stranded cDNA using random hexamer priming. The second strand was generated to create double-stranded cDNA. The cDNA was then end-repaired and 3'-adenylated, and Illumina adapters were added. The ligation products were purified and the DNA fragments (> 200 pb) were PCR-amplified using Platinum Pfx DNA Polymerase (Life Technologies) and Illumina adapter-specific primers. After library profile analysis by the Agilent 2100 Bioanalyzer (Agilent Technologies) and qPCR quantification (MxPro, Agilent Technologies), the libraries were sequenced on an Illumina HiSeq2000 instrument using 101 base-length read chemistry in a paired-end mode. Statistics for INT and MY libraries are reported below.

In this study new RNA samples were generated from *A. euteiches* mycelium, zoospores, or infected *M. truncatula* roots (1 dpi, 3 dpi, and 9 dpi) according to [103, 104]. RNA-seq libraries were prepared according to Illumina's protocols using the Illumina TruSeq Stranded mRNA Sample Prep Kit to analyze mRNA, at the GeT-PlaGe core facility, Toulouse. Briefly, mRNA was selected using poly-T beads, and cDNA was generated using random hexamer priming, and adapters were then added. Ten cycles of PCR were applied to amplify the libraries. Library quality was assessed using an Agilent Bioanalyzer, and the libraries were quantified by qPCR using the Kapa Library Quantification Kit. RNA-seq experiments have been performed on an Illumina HiSeq2500 using a paired-end read length of 2 × 100 pb with the Illumina TruSeq SBS Sequencing Kits v3. Statistics are presented in the manuscript.

RNA-sequencing data analysis

Reads obtained from the different life stages of *A. euteiches* (zoospore, mycelium) or infected roots (1 dpi, 3 dpi, and 9 dpi), were mapped to the *A. euteiches* genome with CLC Genomics Workbench 10.1.1 (QIAGEN). Predefined settings were used except for the similarity fraction, which was set at 0.98, and the read counts per gene (paired reads count as one) were exported. Using the R package edgeR [105], the data were filtered for genes with low counts across all libraries (counts per million (cpm) > 2 in at least three libraries) and then trimmed mean of M (TMM) normalized [106], the tagwise dispersion was estimated, and the differential expression was calculated. Using the generalized linear model likelihood ratio test, *p* values were obtained, and multiplicity correction was performed by applying the Benjamini-Hochberg method [107, 108]. The multi-dimensional scaling plot was created using the 500 genes with the highest dispersion over all libraries. The enrichment of GO terms in up- or down-regulated genes was tested using a Fisher's exact test with the classical algorithm in the topGO R package [109]. Heatmaps were created using the gplots R package [110], and clustering was performed according to the complete linkage method with Euclidean distance measure.

	Sequencing technology	Library	Number of reads	Number of bp
<i>Aphanosyceae euteiches</i> (ATCC201684)	Illumina HiSeq2000	MY	60,035,046	12,127,083,332
	Paired-end reads (2x101bp)	INT	62,472,895	12,619,524,790

Phylogenetic and divergence time analysis of *Aphanomyces* species

To assess the phylogenetic position and divergence times of *A. astaci*, *A. euteiches*, and *A. stellatus* within oomycetes, we followed the methodology of Matari and Blair [38], who produced a robust timetree of oomycetes. We used the amino acid alignments of 40 genes that were assembled for 17 oomycetes and one outgroup species (*Tetrahymena thermophila*), to which we added the sequences of the three *Aphanomyces* species. These 40 datasets were selected among 70 initial alignments of genes involved in regulation of gene expression, because there was strong evidence supporting their orthology relationships and they contained minimal missing data [38]. Amino acid sequences were retrieved from the proteomes of the three *Aphanomyces* species using sequences of the three Saprolegniales (*Thraustotheca clavata*, *Saprolegnia parasitica*, and *Achlya hypogyna*) as queries in BLASTP searches. Most genes could be identified for the three *Aphanomyces* species, except six in *A. astaci* (*HMG-CBF-BFY*, *MnmA*, *p15*, *Ssl1*, *TAF6*, *TAF12*) and one in *A. stellatus* (*TFIIB*). The 40 alignments were then concatenated and subjected to a maximum likelihood phylogenetic analysis in PhyML v3.0 [111] using the WAG model of amino acid substitutions as in [38]. The robustness of the tree was evaluated by performing 1000 bootstrap replicates. Divergence times were conducted in BEAST v1.8.2 [112] using the same parameters as in [38]. Briefly, we performed 50 million generations run using the PhyML-generated tree as a guide tree and treating each of the 40 datasets as a separate partition with the WAG substitution model, a Yule speciation process (uniform distribution; 0–100; initial value 0.01), and the random local clock model, which was shown to best fit the data by [38]. The calibration strategy follows that of [38] and consists of three calibration points modeled with a gamma prior distribution: (1) diatom node: 5–95% quantiles = 74–100 Myrs, (2) diatom + *Ectocarpus* node: 5–95% quantiles = 176–202 Myrs, and (3) oomycetes + ochrophytes node: (5–95% quantiles = 418–550 Myrs). The root age was modeled using a uniform prior distribution (408–1750 Myrs; initial value 635). We used Tracer v1.6 [113] to visualize convergence and determine the burn-in and FigTree v1.4 [113] to generate the dated tree of oomycetes.

Construction of plasmid vectors and *Agrobacterium*-mediated transformations

The AeSSPs sequences were amplified by PCR from *A. euteiches* gDNA with specific primers (Additional file 6: ST3b). The CACC cloning site was added to each forward primer. PCR products were purified using the PCR Clean-Up Kit (Promega, Madison, WI, USA) and introduced in the pENTRY-D-TOPO vector (pENTR/D-

TOPO Cloning Kit, Invitrogen). Positive clones were introduced in a pK7FWG2 vector (Invitrogen) or pAM-pAT/YFP vector. After sequencing, positive clones were introduced in *A. tumefaciens* GV3101 and *A. rhizogenes* ARqual. For the KDEL fusion, the GFP construct was amplified from the obtained pK7FWG2 vector by PCR using primers that introduced a C-terminal SEKDEL sequence (Additional file 6: ST3b). Cloning was performed as previously reported using a pK2GW7 vector (Invitrogen). For leaf infiltration, *A. tumefaciens* GV3101-transformed strains were syringe-infiltrated as described in [61]. For *M. truncatula* roots transformation, *A. rhizogenes* ARqual strains were used and confocal imaging was performed at 28 dpi, as described in [29].

Brefeldin A treatment and *P. capsici* infection assay

Brefeldin A (BFA, Sigma-Aldrich, St. Louis, MO, USA) treatment was performed 24 h after agroinfiltration of *N. benthamiana*. Leaf discs were vacuum infiltrated with TBS1X (50 mM Tris-HCl; 150 mM NaCl pH 7.6) and 15 µg/mL BFA for 30 min, and incubated for 24 h at room temperature. Leaf discs were washed in TBS1X before confocal imaging. For the infection assay, *Phytophthora capsici* LT3112 was grown on V8 agar plates for 7 days at 22 °C. Zoospore preparation and inoculation on agroinfiltrated *N. benthamiana* leaf and symptom measurement were performed as reported in [29].

Confocal microscopy

Imaging was performed on Leica DM6B-Z-CS or Leica AOB5 TCS SP2 SE laser scanning confocal microscopes. Excitation wavelengths and emission filters were 488 (GFP) or 514 nm (YFP) long-pass. Images were acquired with a 40× water immersion lens or a 25× Fluotar Visir water objective, and corresponded to Z projections of scanned tissues. Image processing was performed using ImageJ software including three-dimensional reconstruction to compute projections of serial confocal sections.

Additional files

Additional file 1: ST1. Genome features and annotations. 1a. Genome resources and nomenclature used in this study. 1b. BUSCO analysis. 1c. TE analysis. 1d. Orthology analysis (OrthoMCL) summary (nine oomycetes and *Ae*, *Az*). 1e. OrthoMCL, group ID (11 oomycete proteomes). 1f. *Ae*, *Az* predicted secreted genes ID. 1g. *Ae*, *Az* GO analysis (secretome). 1h. *Ae*, *Az* specific secretomes analysis. 1i. CAZyme analysis. 1j. Fungal and oomycete pectate lyase sequences. 1k. CRN effectors predicted in *Ae* and *Az* genomes. (XLSX 2962 kb)

Additional file 2: Figure S1. Phylogenetic analysis of the *A. euteiches* PL1 gene family. A maximum likelihood phylogeny analysis was performed on an oomycete and fungal PL1 sequence alignment using the neighbor joining construction methods and the WAG protein substitution model. Bootstrap analysis was performed with 1000 replicates. (PPTX 89 kb)

Additional file 3: ST2. *A. euteiches* expression analysis. 2a. Statistics of RNA-seq experiments. 2b. Percentage of up- and downregulated *A.*

eutiches genes. 2c. Overrepresented GO terms in zoospores vs mycelium. 2d. Overrepresented GO terms at 3 dpi vs mycelium. 2e. Overrepresented GO terms at 9 dpi vs mycelium. 2f. Expression data for heatmap construction (GH). 2g. Expression data for heatmap construction (PL). 2h. Expression data for heatmap construction (proteases). 2i. Expression data for heatmap construction (CE). 2j. Expression data for heatmap construction (CBM). 2k. Expression data for heatmap construction (protease inhibitor). (XLSX 131 kb)

Additional file 4: Figure S2. RNA-seq samples relationship. Multi-dimensional scaling plot (Euclidean distance; top = 500 genes) showing the leading log₂-fold change (leading log₂FC) between the normalized samples of *A. eutiches*. Three biological replicates per condition. (PPTX 85 kb)

Additional file 5: Figure S3. Gene expression of *A. eutiches*. Heatmaps of the Log₂ RPM values of carbohydrate esterases (A), carbohydrate-binding module (B) and proteases inhibitors (C). Colors on the left of the heatmaps indicate the subgroup the CE, the CBM or the Plnh belongs to and if present the group of the corresponding class, and colors on the right indicate if the genes are significantly up- (red) or down- (blue) regulated in zoospores, infected roots 3 dpi and infected roots 9 dpi compared to expression in mycelium grown *in vitro*. (PPTX 99 kb)

Additional file 6: ST3. *A. eutiches* small secreted proteins (AeSSPs). 3a. AeSSP classification and expression. 3b. Primers used in this study. (XLSX 37 kb)

Abbreviations

BFA: Brefeldin A; CBM: Carbohydrate-binding module; CRN: Crinkler; CWDE: Cell wall-degrading enzyme; GH: Glycosyl hydrolase; GO: Gene Ontology; PL: Polysaccharide lyase; SSP: Small Secreted Protein; TE: Transposable Element

Acknowledgements

We would like to thank Adam Petrušek (Charles University in Prague, Czech Republic) for the gift of the *Aphanomyces astaci* strain.

Funding

EG was supported by an IBISA-Genoscope project (APHANO-GP: AP09/10-No.19) and an Agence Nationale pour la Recherche JCJC grant (APHANO-Effect, ANR-12-JSV6-0004-01). This work was performed in collaboration with the GeT core facility, Toulouse, France (<http://get.genotoul.fr>), and was supported by France Génomique National Infrastructure, funded as part of the "Investissement d'avenir" program (ANR-10-INBS-09).

Availability of data and materials

Assemblies, sequencing, annotation, and expression data are available in AphanoDB v2.0 (<http://www.polebio.irv.ups-tlse.fr/aphanoDB/>). Genome assemblies and raw data are also available at the EMBL | European Nucleotide Archive (ENA) (<https://www.ebi.ac.uk/ena/browse>) under study numbers PRJEB24016, PRJEB24021, and PRJEB24018. Transcriptomic data are available at the National Center for Biotechnology Information (NCBI) | Gene Expression Omnibus (GEO) (<https://www.ncbi.nlm.nih.gov/geo/>) under accession number GSE109500. *Aphanomyces* spp. strains are available on request.

Authors' contributions

EG conceived, designed, annotated, and analyzed the experiments, contributed to the AphanoDB v2.0 update, managed the collaborative work, and wrote the manuscript. CP prepared and analyzed the RNA-seq experiments, designed and performed molecular studies on AeSSPs, and wrote the manuscript. LC designed and performed molecular approaches on AeSSPs. HSC performed Ae, Aa, and As genome annotations, developed and maintained AphanoDB v2.0, and wrote the manuscript. MV performed BUSCO and RNA-seq analyses. LIC participated in the *Aphanomyces* spp. genome annotation. SC and MAD contributed to AeSSP confocal imaging and cloning. ALR performed microscopical studies and three-dimensional reconstruction. JL performed manual curation of Crinkler genes. CG, RC, BM, and FG performed TE analysis and phylogeny studies and wrote the manuscript. CK assembled the Ae and As genomes. PW, JMA, and JG sequenced and assembled the Ae genome, performed RNA-seq of the INT and MY libraries, and wrote the manuscript. OB performed Ae and As genome sequencing and RNA-seq of *M. musculus*-infected roots, Ae zoospores, and mycelium. BD analyzed the data and wrote the manuscript. All authors read and approved the final manuscript.

Ethics approval and consent to participate

Does not apply for this study.

Competing interests

The authors declare that they have no competing interests.

Publisher's Note

Springer Nature remains neutral with regard to jurisdictional claims in published maps and institutional affiliations.

Author details

¹Laboratoire de Recherche en Sciences Végétales, CNRS UMR5546 Université de Toulouse, Paul Sabatier, 24, chemin de Borde Rouge BP 42617 Auzeville, 31326 Castanet-Tolosan, France. ²Fédération de Recherche 3450, Plateforme Imagerie, Pôles de Biotechnologie Végétale, 31326 Castanet-Tolosan, France. ³Laboratoire Ecologie et Biologie des Interactions, UMR CNRS 7267, Université de Poitiers, Poitiers, France. ⁴Laboratoire Evolution, Génomes, Comportement, Ecologie CNRS Université Paris-Sud UMR 9191, RD 247, Gif sur Yvette, France. ⁵University of Florida, UF/IFAS, Indian River Research and Education Center IRREC, 2199 South Rock Road, Fort Pierce, FL 34945, USA. ⁶Commissariat à l'Energie Atomique (CEA), Institut de Biologie François-Jacob, Genoscope, CNRS UMR 8030, Université d'Evry, Evry, France. ⁷INRA, US 1426, GeT-PlaGe, Genotoul, Castanet-Tolosan, France. ⁸INRA, UR875, Plateforme Bioinformatique Genotoul, Castanet-Tolosan, France. ⁹Present Address: Plant Ecophysiology, Institute of Environmental Biology, Utrecht University, Utrecht, The Netherlands.

Received: 24 January 2018 Accepted: 20 March 2018

Published online: 18 April 2018

References

- Beakes GW, Gockling SL, Sekimoto S. The evolutionary phylogeny of the oomycete "fungi". *Protospasma*. 2011;249(1):3–19.
- Raffaële S, Kamoun S. Genome evolution in filamentous plant pathogens: why bigger can be better. *Nat Rev Microbiol*. 2012;10(6):417–30.
- Judelson HS. Dynamics and innovations within oomycete genomes: insights into biology, pathology, and evolution. *Eukaryot Cell*. 2012;11(11):1304–12.
- Dong S, Raffaële S, Kamoun S. The two-speed genomes of filamentous pathogens: waltz with plants. *Curr Opin Genet Dev*. 2015;35:57–65.
- Raffaële S, Farrer RA, Cano LM, Studholme DJ, MacLean D, Thines M, Jiang RH, Zody MC, Kunjeti SG, Donofrio NM, et al. Genome evolution following host jumps in the Irish potato famine pathogen lineage. *Science*. 2010;330:1540–3.
- Dong S, Stam R, Cano LM, Song J, Sklenar J, Yoshida K, Bodkuir TO, Olive R, Liu Z, Tian M, et al. Effector specialization in a lineage of the Irish potato famine pathogen. *Science*. 2014;343(6170):552–5.
- Amaro TM, Thilliez GJ, Moton GB, Huitema E. A perspective on CRN proteins in the genomics age: evolution, classification, delivery and function revisited. *Front Plant Sci*. 2017;8:99.
- Whisson SC, Boevink PC, Wang S, Birch PR. The cell biology of late blight disease. *Curr Opin Microbiol*. 2016;34:127–35.
- Schomack S, van Damme M, Bodkuir TO, Cano LM, Smoker M, Thines M, Gaulin E, Kamoun S, Huitema E. Ancient class of translocated oomycete effectors targets the host nucleus. *Proc Natl Acad Sci U S A*. 2010;107(40):17421–6.
- Engelhardt S, Boevink PC, Armstrong MR, Ramos MB, Hein I, Birch PR. Relocalization of late blight resistance protein R3a to endosomal compartments is associated with effector recognition and required for the immune response. *Plant Cell*. 2012;24(11):25142–58.
- Du Y, Berg J, Govers F, Bouwmeester K. Immune activation mediated by the late blight resistance protein R1 requires nuclear localization of R1 and the effector AVR1. *New Phytol*. 2015;207(3):735–47.
- Hein I, Gilroy EM, Armstrong MR, Birch PR. The zig-zag-zig in oomycete-plant interactions. *Mol Plant Pathol*. 2009;10(4):547–62.
- Dieguez-Urbeondo J, Garcia MA, Cerenius L, Kozubikova E, Ballesteros I, Windels C, Welland J, Kator H, Soderhall K, Martin MP. Phylogenetic relationships among plant and animal parasites, and saprotrophs in *Aphanomyces* (Oomycetes). *Fungal Genet Biol*. 2009;46(5):365–76.

14. Gaulin E, Jacquet C, Bottin A, Dumas B. Root rot disease of legumes caused by *Aphanomyces euteiches*. Mol Plant Pathol. 2007;8(5):539–48.
15. Jones FR, Drechsler C. Root rot of peas in the United States caused by *Aphanomyces euteiches*. J Agric Res. 1925;30:293–325.
16. Gaulin E, Bottin A, Jacquet C, Dumas B. *Aphanomyces euteiches* and legumes. In: Lamour K, Kamoun S, e, editors. Oomycetes genetics and genomics: diversity, interactions, and research tools. Hoboken: Wiley; 2009.
17. McKick D, Grau C. Characteristics and frequency of *Aphanomyces euteiches* races 1 and 2 associated with alfalfa in the Midwestern United States. Plant Dis. 2001;85:740–4.
18. Wicker E, Rouel F, Hulle M. Pathogenic characteristics and frequency of *Aphanomyces euteiches* from pea in France. Plant Pathol. 2001;50:433–42.
19. Scott W. A monograph of the genus *Aphanomyces*. Virginia Agr Exp Sta Tech Bull. 1961;151:1–95.
20. Bonhomme M, André D, Badis Y, Ronfort J, Burgarella C, Chantret N, Prosper JM, Brisikine R, Mudge J, Debélle F, et al. High-density genome-wide association mapping implicates an F-box encoding gene in *Medicago truncatula* resistance to *Aphanomyces euteiches*. New Phytol. 2014;201(4):1328–42.
21. Pilet-Nayel ML, Muehlbauer FJ, McGee RJ, Kraft JM, Balanger A, Coyne CJ. Quantitative trait loci for partial resistance to *Aphanomyces* root rot in pea. Theor Appl Genet. 2002;106:28–39.
22. Svoboda J, Mrugala A, Kozubikova-Balcarova E, Kouba A, Dieguez-Urbeondo J, Petrussek A. Resistance to the crayfish plague pathogen, *Aphanomyces astaci*, in two freshwater shrimps. J Invertebr Pathol. 2014;121:97–104.
23. Svoboda J, Mrugala A, Kozubikova-Balcarova E, Petrussek A. Hosts and transmission of the crayfish plague pathogen *Aphanomyces astaci* – a review. J Fish Dis. 2017;40:127–40.
24. Souty-Grosset C, Holdich DM, Noel PY, Reynolds JD, Halfner P. (eds) Atlas of crayfish in Europe. Muséum National d'Histoire Naturelle, Paris. 2006.
25. Dieguez-Urbeondo J, Huang TS, Cerenius L, Soderhall K. Physiological adaptation of an *Aphanomyces astaci* strain isolated from the freshwater crayfish *Procambarus clarkii*. Mycol Res. 1995;99:574–8.
26. Becking T, Mrugala A, Delauray C, Svoboda J, Raimond M, Wijama-Dirks S, Petrussek A, Grandjean F, Braquant-Vamier C. Effect of experimental exposure to differently virulent *Aphanomyces astaci* strains on the immune response of the noble crayfish *Astacus astacus*. J Invertebr Pathol. 2015;132:115–24.
27. Global Invasive Species Database. http://www.iucn.org/dg/000_worst.php.
28. Gaulin E, Madoui MA, Bottin A, Jacquet C, Mathé C, Couloux A, Winkler P, Dumas B. Transcriptome of *Aphanomyces euteiches*: new oomycete putative pathogenicity factors and metabolic pathways. PLoS One. 2008;3(3):e1723.
29. Ramirez-Garcos D, Camboire L, Pel MJ, Jaunesou A, Martinez Y, Neant I, Leclerc C, Moreau M, Dumas B, Gaulin E. CRN13 candidate effectors from plant and animal eukaryotic pathogens are DNA-binding proteins which trigger host DNA damage response. New Phytol. 2016;210(2):602–17.
30. Camboire L, Jaunesou A, Brière C, Deslandes L, Dumas B, Gaulin E. Detection of nucleic acid-protein interactions in plant leaves using fluorescence lifetime time imaging microscopy. Nature Protocol. 2017;12(9):1993–50.
31. Jiang RH, de Bruijn I, Haas BJ, Belmonte R, Lobach L, Christie J, van den Ackerveken G, Bottin A, Bulone V, Diaz-Moreno SM, et al. Distinctive expansion of potential virulence genes in the genome of the oomycete fish pathogen *Saprolegnia parasitica*. PLoS Genet. 2013;9(5):e1003272.
32. Haas B, Kamoun S, Zody MC, Jiang RH, Handsaker RE, Cano LM, Grabherr M, Kodira CD, Raffaele S, Torto-Alalibo T, et al. Genome sequence and analysis of the Irish potato famine pathogen *Phytophthora infestans*. Nature. 2009; 461(7262):393–8.
33. Kemen E, Gardiner A, Schultz-Larsen T, Kemen AC, Balmuth AL, Robert-Seilaniantz A, Bailey K, Holub E, Studholme DJ, Madean D, et al. Gene gain and loss during evolution of obligate parasitism in the white rust pathogen of *Arabidopsis thaliana*. PLoS Biol. 2011;9:e1001094.
34. Sharma R, Xia X, Cano LM, Evangelisti E, Kemen E, Judelson H, Corne S, Sambles C, van den Hoogen DJ, Witter M, et al. Genome analyses of the sunflower pathogen *Plasmopara halstedii* provide insights into effector evolution in downy mildews and *Phytophthora*. BMC Genomics. 2015;16(1):741.
35. Waterhouse RM, Seppely M, Simao FA, Manni M, Ioannidis P, Kloutchnikov G, Kriventseva EV, Zdobnov EM. BUSCO applications from quality assessments to gene prediction and phylogenomics. Mol Biol Evol. 2017; 35(3):543–8.
36. Yin L, An Y, Qu J, Li X, Zhang Y, Dry I, Wu H, Lu J. Genome sequence of *Plasmopara viticola* and insight into the pathogenic mechanism. Sci Rep. 2017;7:46553.
37. Madoui M, Gaulin E, Mathe C, Clemente H, Couloux A, Winkler P, Dumas B. AphanoDB: a genomic resource for *Aphanomyces* pathogens. BMC Genomics. 2007;8:471.
38. Matarl NH, Blair JE. A multilocus timescale for oomycete evolution estimated under three distinct molecular clock models. BMC Evol Biol. 2014; 14:101.
39. Tyler B, Tripathy S, Zhang X, Dehal P, Jiang R, Aerts A, Arredondo F, Baxter L, Bensasson D, Beynon J, et al. *Phytophthora* genome sequences uncover evolutionary origins and mechanisms of pathogenesis. Science. 2008; 313(5791):1261–6.
40. Lévesque CA, Brouwer H, Cano L, Hamilton JP, Holt C, Hultema E, Raffaele S, Robideau GP, Thines M, Win J, et al. Genome sequence of the necrotrophic plant pathogen *Pythium ultimum* reveals original pathogenicity mechanisms and effector repertoire. Genome Biol. 2010; 11(7):R73.
41. Li L, Stoeckert CJ Jr, Roos DS. OrthoMCL: identification of ortholog groups for eukaryotic genomes. Genome Res. 2003;13(9):2178–89.
42. Sperschneider J, Gardiner DM, Dodds PN, Tini F, Covarelli L, Singh KB, Manners JM, Taylor JM. EffectorP: predicting fungal effector proteins from secretomes using machine learning. New Phytol. 2016; 210(2):743–61.
43. Brouwer H, Coutinho PM, Henrissat B, de Vries RP. Carbohydrate-related enzymes of important *Phytophthora* plant pathogens. Fungal Genet Biol. 2014;72:192–200.
44. Lanver D, Berndt P, Tollot M, Naik V, Vanes M, Warmann T, Munch K, Rosell N, Kahmann R. Plant surface cues prime *Ustilago maydis* for biotrophic development. PLoS Pathog. 2014;10(7):e1004272.
45. Yajima W, Liang Y, Kav NN. Gene disruption of an arabinofuranosidase/beta-xylosidase precursor decreases *Sclerotinia sclerotiorum* virulence on canola tissue. Mol Plant-Microbe Interact. 2009;22(7):783–9.
46. de Vries RP, Kester HC, Poulsen CH, Benen JA, Visser J. Synergy between enzymes from *Aspergillus* involved in the degradation of plant cell wall polysaccharides. Carbohydr Res. 2000;327(4):401–10.
47. Sawoy F, Leonard G, Richards TA. The role of horizontal gene transfer in the evolution of the oomycetes. PLoS Pathog. 2015;11(5):e1004805.
48. Richards TA, Soanes DM, Jones MD, Vasileva O, Leonard G, Paszkiewicz K, Foster PG, Hall M, Talbot NJ. Horizontal gene transfer facilitated the evolution of plant parasitic mechanisms in the oomycetes. Proc Natl Acad Sci U S A. 2011;108(37):15258–63.
49. Lamoque M, Barriot R, Bottin A, Barre A, Rougé P, Dumas B, Gaulin E. The unique architecture and function of cellulose-interacting proteins in oomycetes revealed by genomic and structural analyses. BMC Genomics. 2012;13:605.
50. Garcia-Gonzalez E, Poppinga L, Furrhous A, Hertlein G, Hechtke K, Jakubowska A, Genersch E. *Fonsecaea* larvae chitin-degrading protein PICBP49 is a key virulence factor in American foulbrood of honey bees. PLoS Pathog. 2014;10(7):e1004284.
51. Shen D, Liu T, Ye W, Liu L, Liu P, Wu Y, Wang Y, Dou D. Gene duplication and fragment recombination drive functional diversification of a superfamily of cytoplasmic effectors in *Phytophthora sojae*. PLoS One. 2013;8(7):e70036.
52. Adhikari BN, Hamilton JP, Zerillo MM, Tisserat N, Lévesque CA, Buell CR. Comparative genomics reveals insight into virulence strategies of plant pathogenic oomycetes. PLoS One. 2013;8(10):e75072.
53. As-sadi F, Carrese S, Gasquel Q, Hourlier T, Rengel D, Le Paslier MC, Bardat A, Boniface MC, Brunel D, Gouzy J, et al. Transcriptomic analysis of the interaction between *Helianthus annuus* and its obligate parasite *Plasmopara halstedii* shows single nucleotide polymorphisms in CRN sequences. BMC Genomics. 2011;12:498.
54. Gaulin E. Effector mediated communication of filamentous plant pathogens with their hosts. Advances Botanical Research. 2017;82:161–85.
55. Stam R, Jube J, Howden AJ, Morris JA, Boevink PC, Hedley PE, Hultema E. Identification and characterisation CRN effectors in *Phytophthora capsici* shows modularity and functional diversity. PLoS One. 2013;8(3):e59517.
56. Song T, Ma Z, Shen D, Li Q, Li W, Su L, Ye T, Zhang M, Wang Y, Dou D. An oomycete CRN effector reprograms expression of plant HSP genes by targeting their promoters. PLoS Pathog. 2015;11(12):e1005348.
57. Sun G, Yang Z, Kosch T, Summers K, Huang J. Evidence for acquisition of virulence effectors in pathogenic chytrids. BMC Evol Biol. 2011;11:195.
58. Ah-Fong AM, Kim KS, Judelson HS. RNA-seq of life stages of the oomycete *Phytophthora infestans* reveals dynamic changes in metabolic, signal transduction, and pathogenesis genes and a major role for calcium signaling in development. BMC Genomics. 2017;18(1):198.

59. Fu L, Zhu C, Ding X, Yang X, Morris DP, Tyler BM, Zhang XG. Characterization of cell death-inducing members of the pectate lyase gene family in *Phytophthora capsici* and their contributions to infection of pepper. *Mol Plant-Microbe Interact.* 2015;28(7):766–75.
60. Gaulin E, Drame N, Lafitte C, Torto-Alalibo T, Martinez Y, Ameline-Torregrosa C, Khatib M, Mazarqui H, Vilalba-Mateos F, Kamoun S, et al. Cellulose binding domains of a *Phytophthora* cell wall protein are novel pathogen-associated molecular patterns. *Plant Cell.* 2005;18(7):1766–77.
61. Gaulin E, Jauneau A, Vilalba F, Rickauer M, Esquiere-Tugayre M, Bottin A. The CBEL glycoprotein of *Phytophthora parasitica* var. *nicotianae* is involved in cell wall deposition and adhesion to cellulosic substrates. *J Cell Sci.* 2002; 115(23):4565–75.
62. Hosseini S, Elfstrand M, Heyman F, Funck Jensen D, Karlsson M. Deciphering common and specific transcriptional immune responses in pea towards the oomycete pathogens *Aphanomyces euteiches* and *Phytophthora pisii*. *BMC Genomics.* 2015;16:627.
63. Stam R, Howden AJ, Delgado-Cerezo M, Amaro TM MM, Motion GB, Pham J, Huitema E. Characterization of cell death inducing *Phytophthora capsici* CRN effectors suggests diverse activities in the host nucleus. *Front Plant Sci.* 2013;4:387.
64. Nelson BK, Cai X, Nebenfuhr A. A multicolored set of in vivo organelle markers for co-localization studies in *Arabidopsis* and other plants. *Plant J.* 2007;51(5):1126–36.
65. Lam SK, Cai Y, Tse YC, Wang J, Law AH, Pimpl P, Chan HY, Xia J, Jiang L. BFA-induced compartments from the Golgi apparatus and trans-Golgi network/early endosome are distinct in plant cells. *Plant J.* 2009;60(5):865–81.
66. Ospina-Gialdo MD, Griffith JG, Laird EW, Mingosa C. The CAZyme of *Phytophthora* spp: a comprehensive analysis of the gene complement coding for carbohydrate-active enzymes in species of the genus *Phytophthora*. *BMC Genomics.* 2010;11:525.
67. Zerillo MM, Adhikari BN, Hamilton JP, Buehl CR, Lévesque CA, Tisserat N. Carbohydrate-active enzymes in *Pythium* and their role in plant cell wall and storage polysaccharide degradation. *PLoS One.* 2013;8(9):e72572.
68. Duplessis S, Cuomo CA, Lin YC, Aerts A, Tisserat E, Veneault-Fourmy C, Joly DL, Haquard S, Amsalem J, Cantarel BL, et al. Obligate biotrophy features unraveled by the genomic analysis of rust fungi. *Proc Natl Acad Sci U S A.* 2011;108(22):9166–71.
69. O'Connell RJ, Thon MR, Haquard S, Amyotte SG, Kleemann J, Torres MF, Damm U, Bulzeez EA, Epstein L, Allan N, et al. Lifestyle transitions in plant pathogenic *Colletotrichum* fungi deciphered by genome and transcriptome analyses. *Nat Genet.* 2012;44(9):1060–5.
70. Meerupati T, Andersson KM, Firman E, Kumar D, Tunlid A, Ahren D. Genomic mechanisms accounting for the adaptation to parasitism in nematode-trapping fungi. *PLoS Genet.* 2013;9(11):e1003909.
71. Hu X, Xiao G, Zheng P, Shang Y, Su Y, Zhang X, Liu X, Zhan S, St Leger RJ, Wang C. Trajectory and genomic determinants of fungal-pathogen speciation and host adaptation. *Proc Natl Acad Sci U S A.* 2014;111(47):16796–801.
72. Martin F, Selosse MA. The *Laccaria* genome: a symbiont blueprint decoded. *New Phytol.* 2008;180(2):296–310.
73. Kamel L, Tang N, Malbreil M, San Clemente H, Le Marquer M, Roux C, Friei Dik Frey N. The comparison of expressed candidate secreted proteins from two arbuscular mycorrhizal fungi unravels common and specific molecular tools to invade different host plants. *Front Plant Sci.* 2017;8:124.
74. Shindo T, Kaschani F, Yang F, Kovacs J, Tian F, Kourelis J, Hong TN, Colby T, Shabab M, Chawla R, et al. Screen of non-annotated small secreted proteins of *Pseudomonas syringae* reveals a virulence factor that inhibits tomato immune proteases. *PLoS Pathog.* 2016;12(9):e1005874.
75. Condon BJ, Leng Y, Wu D, Bushley KE, Ohm RA, Ollilar R, Martin J, Schackwitz W, Gilmwood J, MohdZainudin M, et al. Comparative genome structure, secondary metabolite, and effector coding capacity across *Cochliobolus* pathogens. *PLoS Genet.* 2013;9(1):e1003233.
76. Kim KT, Jeon J, Choi J, Cheong K, Song H, Choi G, Kang S, Lee YH. Kingdom-wide analysis of fungal small secreted proteins (SSPs) reveals their potential role in host association. *Front Plant Sci.* 2016;7:186.
77. Aury JM, Cruaud C, Berbe V, Rogier O, Mangenot S, Samson G, Paulain J, Anthouard V, Scarpelli C, Artiguenave F, et al. High quality draft sequences for prokaryotic genomes using a mix of new sequencing technologies. *BMC Genomics.* 2008;9:603.
78. Luo R, Liu B, Xie Y, Li Z, Huang W, Yuan J, He G, Chen Y, Pan Q, Liu Y, et al. SOAPdenovo2: an empirically improved memory-efficient short-read de novo assembler. *Gigascience.* 2012;1(1):18.
79. Hunt M, Kikuchi T, Sanders M, Newbold C, Beniman M, Otto TD. REAPR: a universal tool for genome assembly evaluation. *Genome Biol.* 2013;14(5):R47.
80. Mariette J, Escudie F, Allias N, Salin G, Noirat C, Thomas S, Klopp C. NGC: integrated next generation sequencing storage and processing environment. *BMC Genomics.* 2012;13:462.
81. Zimin AV, Marais G, Puiu D, Roberts M, Salzberg SL, Yorke JA. The MaSuRCA genome assembler. *Bioinformatics.* 2013;29(21):2669–77.
82. Script to calculate basic set of metrics from a genome assembly. http://korfbal.ucdavis.edu/datasets/Assemblathon/Assemblathon2/Basic_metrics/assemblathon_stats.pl
83. Stanke M, Waack S. Gene prediction with a hidden Markov model and a new intron submodel. *Bioinformatics.* 2003;19(Suppl 2):i215–25.
84. Pipeline for training and running the gene finder AUGUSTUS automatically. <https://fossies.org/linux/augustus/scripts/README.autoAug>.
85. Haas BJ, Delcher AL, Mount SM, Wortman JR, Smith RK Jr, Hannick LI, Mall R, Ronning CM, Rusch DB, Town CD, et al. Improving the *Arabidopsis* genome annotation using maximal transcript alignment assemblies. *Nucleic Acids Res.* 2003;31(19):5654–66.
86. Grabherr MG, Haas BJ, Yassour M, Levin JZ, Thompson DA, Amit I, Adiconis X, Fan L, Raychowdhury R, Zeng Q, et al. Full-length transcriptome assembly from RNA-Seq data without a reference genome. *Nat Biotechnol.* 2011;29(7):644–52.
87. Li H, Durbin R. Fast and accurate long-read alignment with Burrows-Wheeler transform. *Bioinformatics.* 2010;26(5):589–95.
88. Altschul S, Madden T, Schaffer A, Zhang J, Zhang Z, Miller W, Lipman D. Gapped BLAST and PSI-BLAST: a new generation of protein database search programs. *Nucleic Acids Res.* 1990;18(9):3398–402.
89. Jones P, Binns D, Chang HY, Fraser M, Li W, McAnulla C, McWilliam H, Madden J, Mitchell A, Nuka G, et al. InterProScan 5: genome-scale protein function classification. *Bioinformatics.* 2014;30(9):1236–40.
90. Finn RD, Coghill P, Eberhardt RY, Eddy SR, Mistry J, Mitchell AL, Potter SC, Punta M, Qureshi M, Sangrador-Vegas A, et al. The Pfam protein families database: towards a more sustainable future. *Nucleic Acids Res.* 2016;44(D1):D279–85.
91. Moriya Y, Itoh M, Okuda S, Yoshizawa A, Kanehisa M. KEGG: an automatic genome annotation and pathway reconstruction server. *Nucleic Acids Res.* 2007;35(9):182–5.
92. Tatusov RL, Fedorova ND, Jackson JD, Jacobs AR, Knapin B, Koonin EV, Krylov DM, Mazumder R, Melfredov SL, Nikolskaya AN, et al. The COG database: an updated version includes eukaryotes. *BMC Bioinformatics.* 2003;4:41.
93. A server to predict the presence and location of signal peptide cleavage sites in amino acid sequences from different organisms. <http://www.cbs.dtu.dk/services/SignalP/>.
94. Yin Y, Mao X, Yang J, Chen X, Mao F, Xu Y. dbCAN: a web resource for automated carbohydrate-active enzyme annotation. *Nucleic Acids Res.* 2012; 40(Web Server issue):W445–51.
95. A pipeline to analyse genomics data. <https://bbicr.coulbuse.inra.fr/hub/cgi/hub.cgi>.
96. A de-novo repeat family identification and modeling package. <http://www.repeatmasker.org/>.
97. Wicker T, Sabot F, Hua-Van A, Bennetzen JL, Capi P, Chalouh B, Flavell A, Leroy P, Morgante M, Panaud C, et al. A unified classification system for eukaryotic transposable elements. *Nat Rev Genet.* 2007;8(12):973–82.
98. Jurka J, Kapitonov VV, Pavlicek A, Bionowski P, Kohany O, Walichewicz J. Repbase Update, a database of eukaryotic repetitive elements. *Cyrogenet Genome Res.* 2005;11(1):1–4162–7.
99. Lewis SE, Searle SM, Harris N, Gibson M, Lyer V, Richter J, Wief C, Bayraktaroglu L, Bimsey E, Crosby MA, et al. Apollo: a sequence annotation editor. *Genome Biol.* 2002;3(12):Research0082.
100. A genomic database dedicated to *Aphanomyces* genus. <http://www.polebio.lsv.ups-the.fr/aphanoDB/>.
101. Boisson-Demeris A, Chabaud M, Garcia F, Becard G, Rosenberg C, Barker DG. *Agrobacterium rhizogenes*-transformed roots of *Medicago truncatula* for the study of nitrogen-fixing and endomycorrhizal symbiotic associations. *Mol Plant-Microbe Interact.* 2001;14(8):695–700.
102. Djebaili M, Jauneau A, Ameline-Torregrosa C, Chardon F, Jauneau V, Mathe C, Bottin A, Cazaux M, Flet-Nayel ML, Basinger A, et al. Partial resistance of *Medicago truncatula* to *Aphanomyces euteiches* is associated with protection of the root stele and is controlled by a major QTL rich in proteasome-related genes. *Mol Plant-Microbe Interact.* 2009;22(9):1043–55.

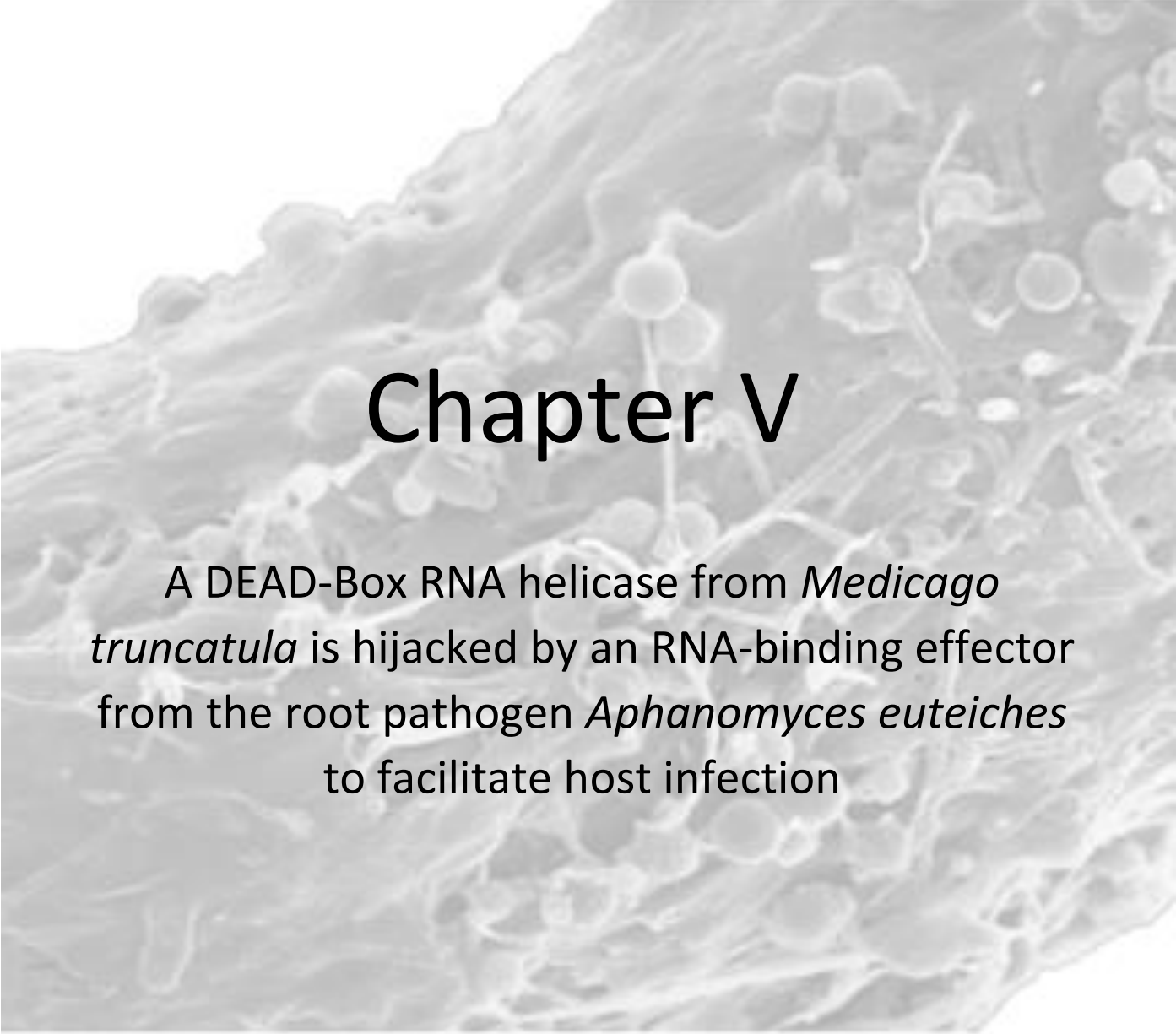
103. Badreddine I, Lafitte C, Heux L, Skandalis N, Spanou Z, Martínez Y, Esquerre-Tugayé M, Bulone V, Dumas B, Bottin A. Cell wall chitosaccharides are essential components and exposed patterns of the phytopathogenic oomycete *Aphanomyces euteiches*. *Eukaryot Cell*. 2008;7(11):1980–93.
104. Badis Y, Bonhomme M, Lafitte C, Huguet S, Balbergue S, Dumas B, Jacquet C. Transcriptome analysis highlights preformed defences and signalling pathways controlled by the *prAel* quantitative trait locus *KITL*, conferring partial resistance to *Aphanomyces euteiches* in *Medicago truncatula*. *Mol Plant Pathol*. 2015;16(9):973–86.
105. Robinson MD, McCarthy DJ, Smyth GK. edgeR: a Bioconductor package for differential expression analysis of digital gene expression data. *Bioinformatics*. 2010;26(1):139–40.
106. Robinson MD, Oshlack A. A scaling normalization method for differential expression analysis of RNA-seq data. *Genome Biol*. 2010;11(3):R25.
107. Benjamini Y, Hochberg Y. Controlling the false discovery rate: a practical and powerful approach to multiple testing. *J R Statist Soc*. 1995;57(1):289–300.
108. McCarthy DJ, Chen Y, Smyth GK. Differential expression analysis of multifactor RNA-Seq experiments with respect to biological variation. *Nucleic Acids Res*. 2012;40(10):4288–97.
109. Alexa A, Rahnenfuhrer J. topGO: Enrichment analysis for Gene Ontology. R package version 2.20.0. 2010.
110. Warnes G, Bolker B, Bonebakker L, Gendelman R, Liaw W, Lumley T, Maechler M, Magnusson A, Moeller S, Schwartz M, et al. gplots: various R programming tools for plotting data. R package version 2.17.0. 2015. <https://cran.r-project.org/web/packages/gplots/index.html>.
111. Guindon S, Dufayard JF, Lefort V, Anisimova M, Hordijk W, Gascuel O. New algorithms and methods to estimate maximum-likelihood phylogenies: assessing the performance of PhyML 3.0. *Syst Biol*. 2010;59(3):307–21.
112. Drummond AJ, Suchard MA, Xie D, Rambaut A. Bayesian phylogenetics with BEAUti and the BEAST 1.7. *Mol Biol Evol*. 2012;29(8):1969–73.
113. A cross-platform program for Bayesian analysis of molecular sequences. <http://beast.bio.ed.ac.uk>.

Submit your next manuscript to BioMed Central and we will help you at every step:

- We accept pre-submission inquiries
- Our selector tool helps you to find the most relevant journal
- We provide round the clock customer support
- Convenient online submission
- Thorough peer review
- Inclusion in PubMed and all major indexing services
- Maximum visibility for your research

Submit your manuscript at
www.biomedcentral.com/submit



A grayscale scanning electron micrograph (SEM) showing a cross-section of plant tissue. The surface is covered with a dense network of fine, branching hyphae, characteristic of a fungal infection. The underlying plant cells are visible as larger, more rounded structures. The overall appearance is that of a root being colonized by a pathogen.

Chapter V

A DEAD-Box RNA helicase from *Medicago truncatula* is hijacked by an RNA-binding effector from the root pathogen *Aphanomyces euteiches* to facilitate host infection

V – CHAPTER V: A DEAD-Box RNA helicase from *Medicago truncatula* is hijacked by an RNA-binding effector from the root pathogen *Aphanomyces euteiches* to facilitate host infection

(Camborde et al., submitted and available at BioXiv: doi: <https://doi.org/10.1101/2020.06.17.157404>)

In a previous study we identified among a cluster composed of six SSP that AeSSP1256 enhances oomycete infection and harbour a nuclear-localisation when transiently express in *Nicotiana benthamiana* cells (Gaulin et al., 2018). We then undertake a functional characterization of AeSSP1256 to decipher its activity by using *M. truncatula*. Sequence analyses predict that AeSSP1256 sequence contains RNA binding motifs (Figure 1 from this Chapter). By using FRET-FLIM analyses based on a method that I developed in collaboration with the Imagery Platform Tri-IBIsa Genotoul (Camborde et al., 2017; Escouboué et al., 2019), we showed that AeSSP1256 binds plant RNA (Figure 1 from this Chapter).

When expressed in *M. truncatula* roots, AeSSP1256 is localized around the nucleolus of the host cells and induces a strong delay in root development (Figure 2 from this Chapter). Furthermore, the presence of AeSSP1256 enhances the susceptibility to *A. euteiches* infection (Figure 2 from this Chapter).

Transcriptomic analyses revealed that expression of AeSSP1256 in *M. truncatula* roots leads to a downregulation of genes implicated in ribosome biogenesis pathway (Figure 3 from this Chapter), suggesting that the effector provokes ribosomal stress when present in the host. A yeast-two hybrid approach using cDNA library obtained from *A. euteiches*-infected *Medicago* roots allows the identification of host targets (Supplemental Table 2 from this Chapter) and *A. euteiches* targets (complementary results of this Chapter).

Among *Medicago* targets, we confirmed that AeSSP1256 associates with a nucleolar L7 ribosomal protein and a *M. truncatula* RNA helicase (MtRH10) orthologous to the *Arabidopsis* RNA helicase RH10 (Figure 4 from this Chapter).

Whereas MtRH10 is able to interact with nucleic acids, this association is abolished in the presence of AeSSP1256 (Figure 5 from this Chapter).

Promoter:GUS composite plants revealed that MtRH10 is expressed preferentially in the meristematic root cells (Figure 6 from this Chapter).

Missense MtRH10 plants displayed similar phenotype than overexpressing AeSSP1256 plants, leading to shorter roots with developmental delay and are more susceptible to *A. euteiches* infection (Figure 7 from this Chapter).

These results show that the effector AeSSP1256 facilitates pathogen infection by causing stress on plant ribosome biogenesis and by hijacking a host RNA helicase involved in root development and resistance to root pathogens.

A DEAD BOX RNA helicase from *Medicago truncatula* is hijacked by an RNA-binding effector from the root pathogen *Aphanomyces euteiches* to facilitate host infection

L. Camborde¹, A. Kiselev¹, M.J.C. Pel^{1, *}, A. Leru², A. Jauneau², C. Pouzet², B. Dumas¹, E. Gaulin¹

Affiliations

¹Laboratoire de Recherche en Sciences Végétales (LRSV), Université de Toulouse, CNRS, UPS, France

²Plateforme d'Imagerie FRAIB-TRI, Université de Toulouse, CNRS, France

*Present address: Bacteriology Group, National Reference Centre (NRC), Dutch National Plant Protection Organization (NPPO-NL), P.O. Box. 9102, 6700 HC Wageningen, the Netherlands

Corresponding author: Elodie Gaulin

LRSV, UMR CNRS 5546 Université de Toulouse,

24, Chemin de Borde-Rouge

31320 Auzeville, France

Mail : gaulin@lrsv.ups-tlse.fr

Keywords: effectors, RNA-helicase, plant development, ribosome biogenesis pathway, oomycete, *Medicago*, nucleolar stress

Abstract

Microbial effectors from plant pathogens are molecules that target host components to facilitate colonization. While eukaryotic pathogens are virtually able to produce hundreds of effectors, the underlying molecular mechanisms allowing effectors to promote infection are still largely unexplored. In this study, we show that the effector AeSSP1256 from the soilborne oomycete pathogen *Aphanomyces euteiches* is a RGG/RG protein able to interact with nuclear RNA *in vivo*. Heterologous expression of AeSSP1256 delays *Medicago truncatula* root development and facilitates pathogen colonization. We found by transcriptomic analyses of AeSSP1256 expressing roots that AeSSP1256 downregulated genes implicated in ribosome biogenesis pathway. Transcriptomic analyses of AeSSP1256-expressing roots show a downregulation of genes implicated in ribosome biogenesis pathway. A yeast-two hybrid approach reveals that AeSSP1256 associates with a nucleolar L7 ribosomal protein and a *M. truncatula* RNA helicase (MtRH10) orthologous to the *Arabidopsis* RNA helicase RH10. Association of AeSSP1256 with MtRH10 impaired the capacity of MtRH10 to bind nucleic acids. Promoter:GUS composite plants revealed that MtRH10 is expressed preferentially in the meristematic root cells. Missense MtRH10 plants displayed shorter roots with developmental delay and are more susceptible to *A. euteiches* infection. These results show that the effector AeSSP1256 facilitates pathogen infection by causing stress on plant ribosome biogenesis and by hijacking a host RNA helicase involved in root development and resistance to root pathogens.

Introduction

Plant pathogens divert host cellular physiology to promote their own proliferation by producing effector proteins that interact with molecular targets (Gaulin et al., 2018). Numerous studies indicate large variation in the effector repertoire of plant pathogens suggesting that a large number of molecular mechanisms are targeted.

Oomycetes constitute a large phylum that includes important eukaryotic pathogens, and many of which are destructive plant or animal pathogens (Kamoun et al., 2015; van West and Beakes, 2014). They share common morphological characteristics with true fungi as filamentous growth, osmotrophic feeding or the presence of a cell wall, but they evolved independently (Judelson, 2017). Oomycetes are included in the Stramenopile lineage and have diatoms and brown algae as closest cousins. These filamentous microorganisms have the capacity to adapt to different environment as illustrated by their capacity to develop resistance to anti-oomycete chemicals or quickly overcome plant resistance (Rodenburg et al., 2020).

Comprehensive identification of oomycete proteins that act as effectors is challenging. Up to now, computational predictions of effector proteins have provide a fast approach to identify putative candidate effectors in oomycetes (Haas et al., 2009; Tabima and Grünwald, 2019). Based on their predictive subcellular localization within the host cells they are classified as extracellular (apoplasmic) or intracellular (cytoplasmic) effectors. As example, RxLR and Crinklers (CRNs) constitute the two largest family of oomycetes intracellular effectors that contain hundreds of members per family (McGowan and Fitzpatrick, 2017). While oomycete effector proteins have probably different mechanism of action, what they have in common might be the ability to facilitate pathogen development. Nonetheless, computational predictions do not give any clues regarding the putative role of theses effectors since numerous effectors are devoid of any functional domains. Therefore, biochemical and molecular studies are used to discover and confirm the functional activity of these proteins. To promote infection oomycete intracellular effectors interfere with many host routes which include for example signaling such as MAPKinase cascades (King et al., 2014), phytohormone-mediated immunity (Boevink et al. 2016; Liu et al. 2014), trafficking vesicles secretion (Du et al., 2015) or autophagosome formation (Dagdas et al., 2016). Growing evidences point to plant nucleus as an important compartment within these interactions thanks to the large portfolio

of putative nucleus-targeted effectors predicted in oomycete genomes. The study of subcellular localization of fifty-two *Phytophthora infestans* RxLR effectors upregulated during the early stage of host infection show that nucleocytoplasmic distribution is the most common pattern, with 25% effectors that display a strong nuclear association (Wang et al. 2019). The CRN family was firstly reported as a class of nuclear effector from *P. infestans* (Schornack et al., 2010), around 50% of predicted NLS-containing CRN effectors from *P. capsici* showed nuclear localization (Stam et al., 2013b) and numerous CRNs effectors from *P. sojae* such as PsCRN108, PsCRN63 or PsCRN115 harbor a nuclear localization (Song et al., 2015; Zhang et al., 2015). In agreement with this, different mechanisms of action at the nuclear level have been reported for oomycete effectors such as the alteration of genes transcription (Wirthmueller et al., 2018; Song et al., 2015; He et al., 2019), the mislocalisation of transcription factor (McLellan et al., 2013), the suppression of RNA silencing by inhibition of siRNA accumulation (Qiao et al., 2015; Xiong et al., 2014) or the induction of plant DNA-damage (Camborde et al. 2019; Ramirez-Garcés et al. 2016). However specific function has been assigned to very few effectors.

We previously use comparative genomics and predictive approaches on the *Aphanomyces* genus to identify putative effectors and characterized a large family of small secreted proteins (SSPs) (Gaulin et al., 2018). SSPs harbor a predicted N secretion signal, are less than 300 residues in size and devoid of any functional annotation. More than 290 SSPs are predicted in the legume pathogen *A. euteiches* (AeSSP) while 138 members with no obvious similarity to AeSSP members are reported in the crustacean parasite *A. astaci* (Gaulin et al., 2018). This specific SSP repertoire suggests its role in adaption of *Aphanomyces* species to divergent hosts. We have previously identified one AeSSP (AeSSP1256) based on a screen aiming to identify SSP able to promote infection of *Nicotiana benthamiana* plants by the leaf pathogen *Phytophthora capsici*. AeSSP1256 harbors a nuclear localization signal indicating its putative translocation to host nucleus. However, the function of this protein remained to be identified.

Here we report on the functional analysis of AeSSP1256 and the characterization of its plant molecular target. We show that AeSSP1256 binds RNA *in planta*, induces developmental defects when expressed in *M. truncatula* roots and promotes *A. euteiches* infection. This phenotype is correlated with a downregulation of a set of ribosomal protein genes. A yeast

two hybrid approach identified a host RNA helicase (MtRH10) and a L7 ribosomal protein as interactors of AeSSP1256. By FRET-FLIM analyses we reveal that AeSSP1256 co-opts MtRH10 to abolish its nucleic acid binding capacity. We provide a mechanistic explanation of this observation by demonstrating the implication of MtRH10 in roots development by generating missense and overexpressing *Medicago* lines. Finally we observed that silenced-MtRH10 roots are highly susceptible to *A. euteiches* infection like AeSSP1256-expressing roots, showing that MtRH10 as AeSSP1256 activities modify the outcome of the infection. We now present results supporting effector-mediated manipulation of a nuclear RNA helicase as a virulence mechanism during plant-eukaryotic pathogens interactions.

A

MKTMMAALFALLALALAQAGESSPPAETQLELVDPNPVWVQEVIALPLDSQTEVR
 VAGGARAGGAVRVAGGRKGRGGVRVGGVKIGGDLNGGGGGGVKIG
 GGVRVGGNVNIGGRRGGGGIKVGGKIGGRIGGGVRVGGGIRAGGGARVGGSS
 VRVGGVRVGGGIKVGGRVVRGRGRIGVAVRAGESDDIGQSATGESKEDH

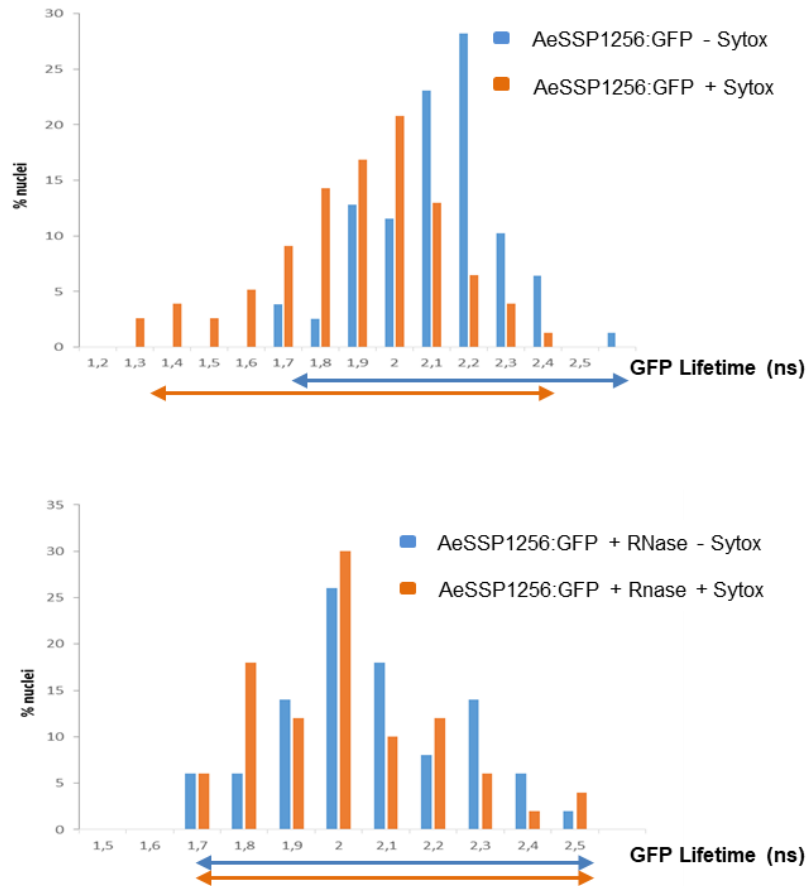
B

Figure 1: AeSSP1256 is a RNA-binding protein

(A) AeSSP1256 protein sequence that shows the signal peptide (underlined), GGRGG boxes (red), RGG domains (bolt, underlined and linked), RG motifs (bolts with asterisks) predicted with Eukaryotic Linear Motif Prediction (Gouw *et al.*, 2018). **(B)** One day after agroinfection of *N. benthamiana* leaves with a AeSSP1256:GFP construct, infiltrated area are collected for FRET-FLIM analysis to detect protein/nucleic acid interactions as described by Camborde *et al.*, 2018. Without RNase treatment and in presence of nucleic acids dye Sytox Orange, the AeSSP1256:GFP lifetime decreases to shorter values, indicating that the proteins bounded to nucleic acids (top panel). After RNase treatment, no significant decrease in the GFP lifetime was observed in presence of Sytox Orange, indicating that AeSSP1256:GFP proteins were bounded specifically to RNA (bottom panel). Histograms show the distribution of nuclei (%) according to classes of AeSSP1256:GFP lifetime in the absence (blue bars) or presence (orange bars) of the nucleic acids dye Sytox Orange. Arrows represent GFP lifetime distribution range.

Results

AeSSP1256 contains RGG/RG domains and binds RNA *in planta*

AeSSP1256 is a member of a large family of *A. euteiches* effectors devoid of any predicted functional domain, except the presence a peptide signal at the Nterminus (Gaulin et al., 2018). As showed in **Figure 1A**, AeSSP1256 protein is enriched in glycine (30% of the amino acid sequence), residues. Analysis using the Eukaryotic Linear Motif database (Gouw et al., 2018) revealed 3 GGRGG motifs (positions 81-85; 95-99 and 99-103). These motifs are variant arginine methylation site from arginine-glycine(-glycine) (RGG/RG) domains, presents in many ribonucleoproteins and involved in RNA binding (Thandapani et al., 2013; Bourgeois et al., 2020).. We then noticed the presence of two di-RGG domains (RGG(X₀₋₅)RGG) (position 75-85 and 97-103) and one di-RG domains (RG(X₀₋₅)RG) (position 123-126) corresponding to RGG or RG motifs that are spaced less than 5 residues (Chong et al., 2018). According to RGG/RG definition, those repeats occur in low-complexity region of the protein (position 60-180) (Chong et al., 2018) and are associated with di-glycine motifs and GR or GGR sequences (**Figure 1A**), which are also common in RGG/RG-containing proteins (Chong et al., 2018). Considering that RGG/RG domains are conserved from yeast to humans (Rajyaguru and Parker, 2012) and represent the second most common RNA binding domain in the human genome (Ozdilek et al., 2017), we thereby investigated the RNA binding ability of AeSSP1256.

To test this, we performed a FRET-FLIM assay on *N. benthamiana* agroinfiltrated leaves with AeSSP1256:GFP fusion protein in presence or absence of Sytox Orange to check its capacity to bind nucleic acids (Camborde et al. 2017). Briefly AeSSP1256:GFP construct is transiently express in *N. benthamiana* leaves where it accumulates in the nucleus (Gaulin et al., 2018). Samples are collected 24h after treatment and nucleic acids labeled with the Sytox Orange dye. In presence of Sytox, if the GFP fusion protein is in close proximity (<10nm) with nucleic acids, the GFP lifetime of the GFP tagged protein will significantly decrease, due to energy transfer between the donor (GFP) and the acceptor (Sytox). To distinguish RNA interactions from DNA interactions, an RNase treatment can be performed. In the case of a specific RNA-protein interaction, no FRET acceptor will be available due to RNA degradation and the lifetime of the GFP tagged protein will then return at basal values. It appeared that GFP

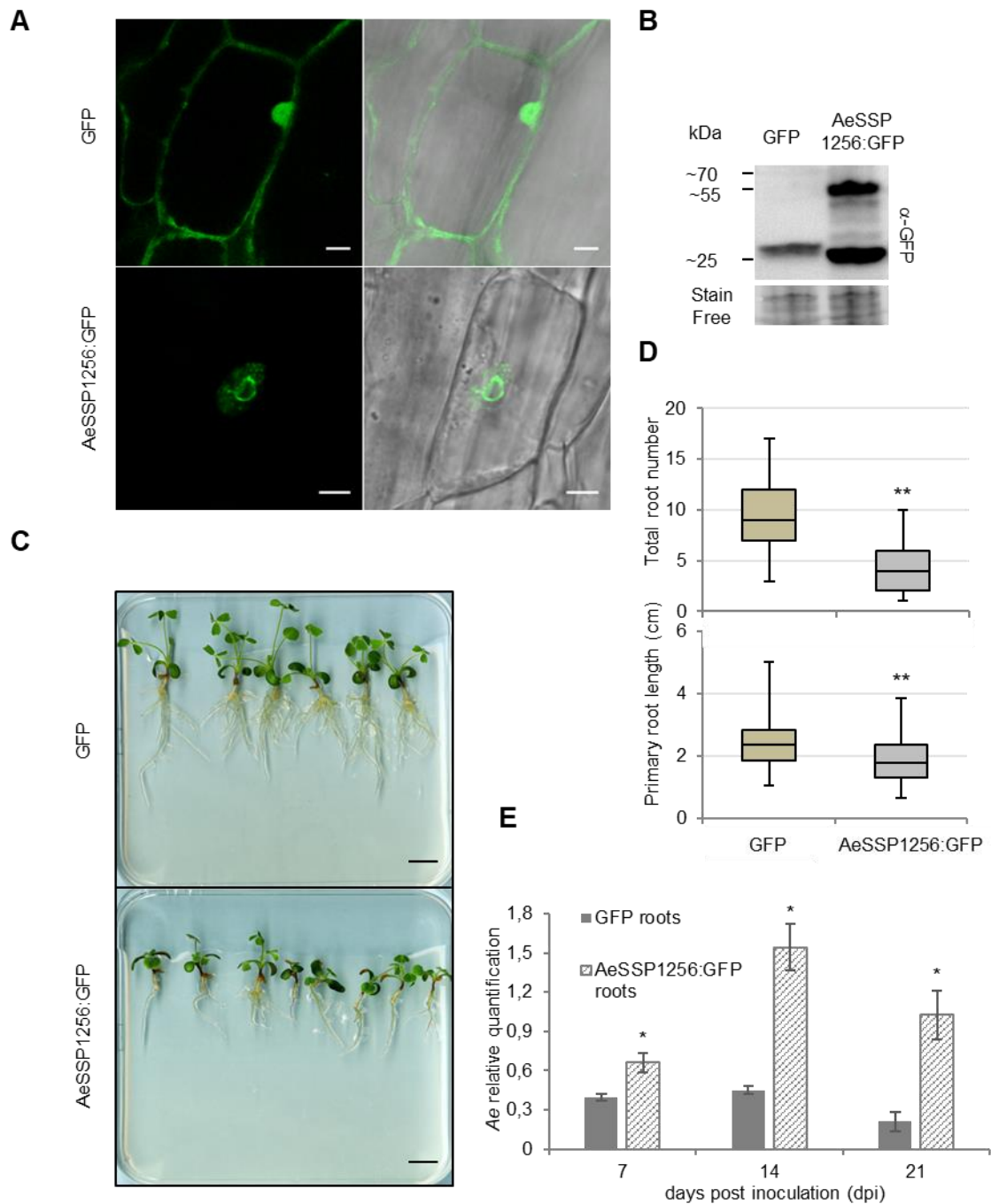


Figure 2: AeSSP1256 pertubs *M. truncatula* root development and enhances *A. euteiches* susceptibility

M. truncatula A17 plants were transformed using *Agrobacterium rhizogenes*-mediated transformation system to produce GFP or AeSSP1256:GFP composite plants. **(A)** Confocal analysis of *M. truncatula* transformed roots 21 days after transformation (d.a.t). The GFP control protein presents a nucleocytoplasmic localisation (upper panel), while AeSSP1256 effector is localized as a ring around the nucleolus (bottom panel). Scale bars: 10 μ m. **(B)** Total proteins were extracted from transformed *M. truncatula* roots at 21 d.a.t and subjected to western-blot analysis using anti-GFP antibodies. A representative blot shows a band around 28 kDa that represents the

GFP protein and a band corresponding to the AeSSP1256:GFP protein (expected size 46.5 kDa). **(C)** Representative photographs of AeSSP1256:GFP plants and GFP control plants at 21 d.a.t. Note the reduction in the growth of roots expressing the AeSSP1256 effector as compared to GFP control plants. Scale bar: 1cm. **(D)** Diagram depicting the total root number per plant (upper panel) and primary root length (in cm) per plant (bottom panel) of transformed *M. truncatula* plants at 21 d.a.t. n= 126 plants for GFP and n=79 plants for AeSSP1256:GFP. **(E)** qPCR results showing relative quantification of the *A. euteiches* tubulin gene in *M. truncatula* GFP or AeSSP1256:GFP infected roots at 7, 14 and 21 days post inoculation (d.p.i). For each time point, 45 to 75 plants per construct were used. Asterisks indicate significant differences (Student's t-test; *: P < 0.05; **: P<0.001).

lifetime of AeSSP1256:GFP decreased significantly in presence of Sytox Orange as reported in **table 1** and in **Figure 1B**, decreasing from 2.06 +/- 0.02 ns to 1.84 +/- 0.03 ns. This indicates that AeSSP1256 is able to bind nucleic acids. After an RNase treatment, no significant difference on GFP lifetime was observed in absence (2.01 ns +/- 0.02) or in presence (1.96 ns +/- 0.02) of Sytox Orange, meaning that the FRET was not due to DNA interaction but was specific to RNA (**table 1** and **Figure 1B**). These results indicate that AeSSP1256 is able to bind nuclear RNA in plant cells.

Table 1: FRET-FLIM measurements for AeSSP1256:GFP with or without Sytox Orange

Donor	Acceptor	τ ^(a)	sem ^(b)	N ^(c)	E ^(d)	^(e) p-value
AeSSP1256:GFP	-	2.06	0.020	78	-	-
AeSSP1256:GFP	Sytox	1.84	0.026	77	11	1.34E ⁻⁰⁹
AeSSP1256:GFP	- (+ RNase)	2.01	0.026	50	-	-
AeSSP1256:GFP	Sytox (+ RNase)	1.96	0.027	50	2.6	0.17

τ : mean life-time in nanoseconds (ns). ^(b) s.e.m.: standard error of the mean. ^(c) N: total number of measured nuclei. ^(d) E: FRET efficiency in %: $E=1-(\tau_{DA}/\tau_D)$. ^(e) p-value (Student's t test) of the difference between the donor lifetimes in the presence or absence of acceptor.

AeSSP1256 impairs *M. truncatula* root development and susceptibility to *A. euteiches*

To check whether expression of AeSSP1256 may have an effect on the host plant, we transformed *M. truncatula* (*Mt*) roots, with a native version of GFP tagged AeSSP1256. As previously observed (Gaulin et al., 2018), confocal analyses confirmed the nuclear localization of the protein in root cells, with accumulation around the nucleolus as a perinucleolar ring (**Figure 2A**) despite the presence of signal peptide (Gaulin et al., 2018). Anti-GFP western blot analysis on total proteins extracted from transformed roots confirmed the presence of GFP-tagged AeSSP1256 (46.7 kDa expected size) (**Figure 2B**). We noticed the presence of a second band around 28 kDa, which is probably free GFP due to the cleavage of the tagged protein. AeSSP1256:GFP transformed plants showed delayed development (**Figure 2C**), with total number of roots and primary root length per plant being significantly lower than values obtained with GFP control plants (**Figure 2D**). As previously observed in *N. benthamiana*, when a KDEL-endoplasmic reticulum (ER) retention signal is added to the native AeSSP1256 construct (Gaulin et al., 2018), AeSSP1256:KDEL:GFP proteins mainly accumulates in the ER (**Supplemental Figure 1A-C**) and roots showed no significant differences in development as compared to GFP control roots (**Supplemental Figure 1D and E**). In contrast a construct devoid of native signal peptide (SP) shows that the proteins accumulated in root cell nuclei (**Supplemental Figure 1B**), leading to abnormal root development, with symptoms similar to those observed in presence of the AeSSP1256:GFP construct, including shorter primary root and lower number of roots (**Supplemental Figure 1D and E**). Altogether these data show that within the host, AeSSP1256 triggers roots developmental defects thanks to its nuclear localization.

To investigate whether AeSSP1256 modifies the outcome of the infection, AeSSP1256-transformed roots were inoculated with *A. euteiches* zoospores. RT-qPCR analyses at 7, 14 and 21 days post inoculation were performed to follow pathogen development. At each time of the kinetic, *A. euteiches* is more abundant in *M. truncatula* roots expressing the effector than in GFP control roots (respectively 1.5, 3 and 5 times more) (**Figure 2E**). This indicates that roots are more susceptible to *A. euteiches* in presence of AeSSP1256. Transversal sections of A17-transformed roots followed by Wheat-Germ-Agglutinin (WGA) staining to detect the presence of *A. euteiches*, showed that the pathogen is still restricted to the root cortex either in the

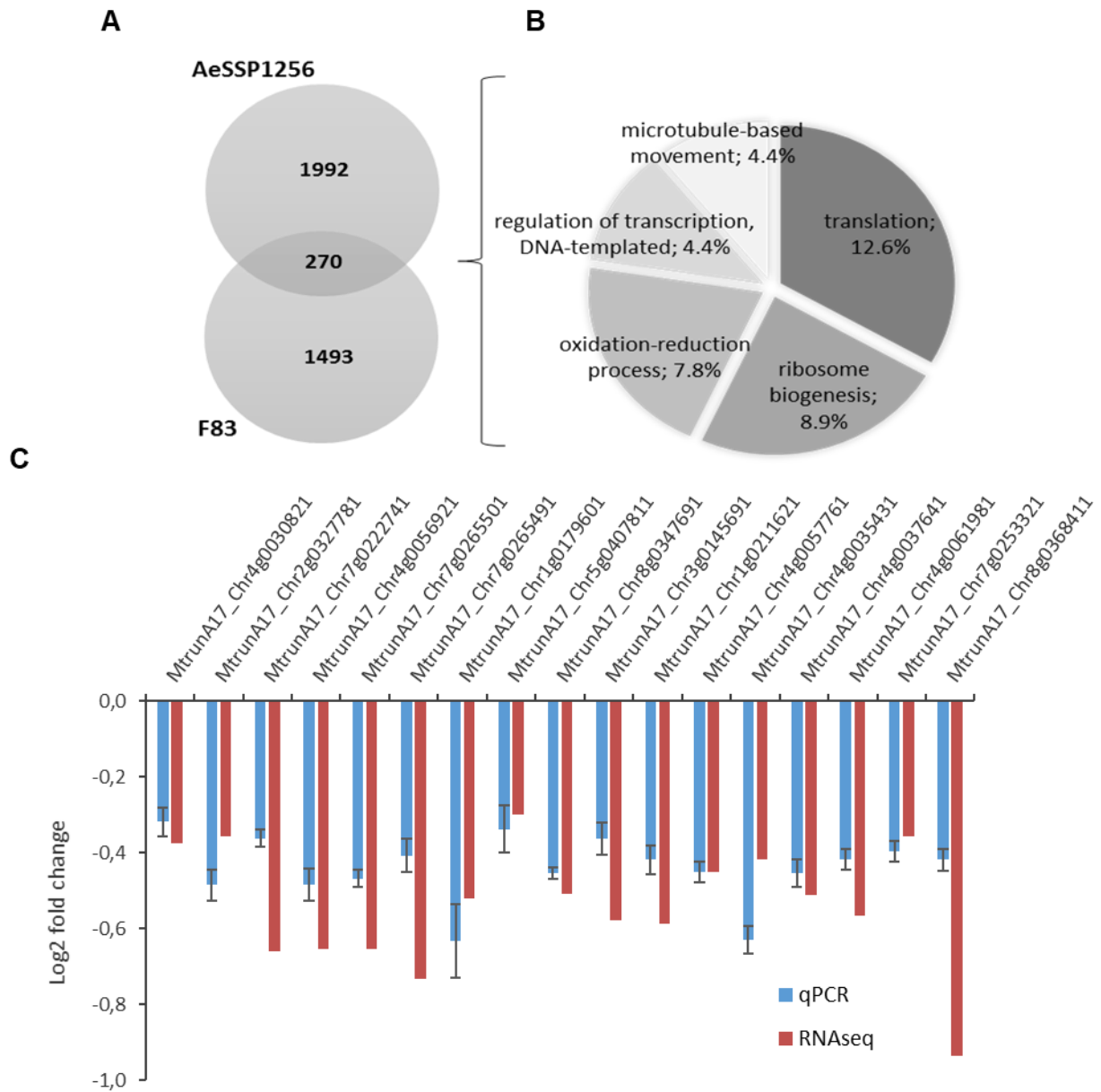


Figure 3: Transcriptomic analyses reveal downregulation of genes related to ribosome biogenesis in both AeSSP1256 roots or *A. euteiches*-infected root

(A) Venn diagram on downregulated genes (number of genes) of two RNASeq experiments: F83 (*M. truncatula* F83005.5 susceptible roots infected by *A. euteiches* at 9 dpi), AeSSP1256 (*M. truncatula* Jemalong A17 transiently expressing AeSSP1256:GFP). **(B)** The most represented GO-terms common between F83-infected line and AeSSP1256-expressing roots of downregulated genes are related to ‘translation and ribosome-biogenesis’. Only GO terms containing more than 10 genes are represented on the pie chart. Numbers on the graph indicate percent of genes with a GO term. **(C)** Comparison of RNASeq (n=4) and qRT-PCR (n=5) on selected ribosome biogenesis-related genes.

presence or absence of AeSSP1256 (**Supplemental Figure 2**). This phenotype is similar to the one observed in the natural A17 *M. truncatula* tolerant line infected by *A. euteiches* (Djébali et al., 2009). This data suggests that defence mechanisms like protection of the central cylinder (Djébali et al., 2009) are still active in AeSSP1256-expressing roots.

AeSSP1256 affects the expression of genes related to ribosome biogenesis

To understand how AeSSP1256 affects *M. truncatula* roots development and facilitates *A. euteiches* infection, we performed expression analyses by RNASeq using AeSSP1256-expressing roots and GFP controls roots. 4391 genes were differentially expressed (DE) between the two conditions (p adjusted-value $<10^{-5}$) (**Supplemental Table 1a**). Enrichment analysis of 'Biological process' GO-terms showed the presence of 'ribosome biogenesis' and 'organonitrogen compound biosynthetic, cellular amide metabolic' processes terms among the most enriched in AeSSP1256 roots as compared to GFP-expressing roots (**Supplemental Table 1b**). We noticed that over 90% of DE-genes from 'ribosome biogenesis' and 'translation' categories are downregulated in AeSSP1256-expressing roots, suggesting that expression of the effector within the roots affects ribosome biogenesis pathway (**Supplemental Table 1a**). To evaluate whether expression of AeSSP1256 mimics infection of *M. truncatula* by *A. euteiches* infection through downregulation of genes related to ribosome biogenesis, we analyzed RNASeq data previously generated on the susceptible F83005.5 *M. truncatula* line nine days after root infection (Gaulin et al., 2018). As shown on the Venn diagram depicting the *M. truncatula* downregulated genes in the different conditions (**Figure 3A, Supplemental Table 1c**), among the 270 common downregulated genes between AeSSP1256-expressing roots and susceptible F83-infected lines, 58 genes (>20%) are categorized in the 'ribosome biogenesis' and 'translation' GO term (Figure 3B). We next selected seventeen *M. truncatula* genes to confirm the effect via qRT-PCR. First, we selected ten *A. thaliana* genes related to plant developmental control (i.e mutants with shorter roots phenotype) (**Supplemental Table 1d**) by Blast searches (>80% identity) in A17 line r5.0 genome portal (Pecrix et al., 2018). In addition, seven nucleolar genes coding for ribosomal and ribonucleotides proteins and related to the 'ribosome biogenesis' in *M. truncatula* were selected for expression analysis based on KEGG pathway map (https://www.genome.jp/kegg-bin/show_pathway?ko03008) (**Supplemental Table 1d**). As shown on Figure 3C, all of the selected genes from *M. truncatula*

are downregulated in presence of AeSSP1256, supporting the RNAseq data. Altogether, these expression data show that the effector by itself mimics some effects induced by pathogen infection of the susceptible F83 line. At this stage of the study, results point to a perturbation of the ribosome biogenesis pathway of the host plant by the AeSSP1256 effector.

AeSSP1256 targets a DEAD-box RNA helicase and a L7 ribosomal protein

To decipher how AeSSP1256 can affect ribosome biogenesis pathway of the host plant and knowing that numerous RNA-binding proteins interact with protein partners, we searched for AeSSP1256 host protein targets. For this, a Yeast two hybrid (Y2H) library composed of cDNA from *M. truncatula* roots infected with *A. euteiches* was screened with the mature form of the effector. Eight *M. truncatula* coding genes were identified as potential protein targets (**Supplemental Table 2a**), all these genes but one (a lecithin retinol acyltransferase gene) correspond to putative nuclear proteins in accordance with the observed subcellular localization of AeSSP1256.

To confirm the Y2H results, we first expressed AeSSP1256 and candidates in *N. benthamiana* cells to observe their subcellular localization and performed FRET-FLIM experiments to validate protein-protein interactions. Only two candidates showed co-localization with AeSSP1256, a L7 ribosomal protein (RPL7, MtrunA17_Chr4g0002321) and a predicted RNA helicase (MtrunA17_Chr5g0429221). CFP-tagged version of RPL7 displays a nucleolar localization, with partial co-localization areas in presence of AeSSP1256 (**Supplemental Figure 3, Table 2b**). FRET-FLIM measurements confirmed the interaction of RPL7:CFP protein with AeSSP1256:YFP effector (**Supplemental Figure 3, Table 2b**), with a mean CFP lifetime of 2.83 ns +/- 0.03 in absence of the SSP protein, leading to 2.46 ns +/- 0.03 in presence of AeSSP1256:YFP (**Supplemental Table 2b**).

The second candidate is a predicted DEAD-box ATP-dependent RNA helicase (MtrunA17_Chr5g0429221), related to the human DDX47 RNA helicase and the RRP3 RH in yeast. Blast analysis revealed that the closest plant orthologs were AtRH10 in *Arabidopsis thaliana* and OsRH10 in *Oryza sativa*. Consequently the *M. truncatula* protein target of AeSSP1256 was named MtrRH10. The conserved domains of DEAD-box RNA helicase are depicted in the alignment of MtrRH10 with DDX47, RRP3, AtRH10, OsRH10 proteins

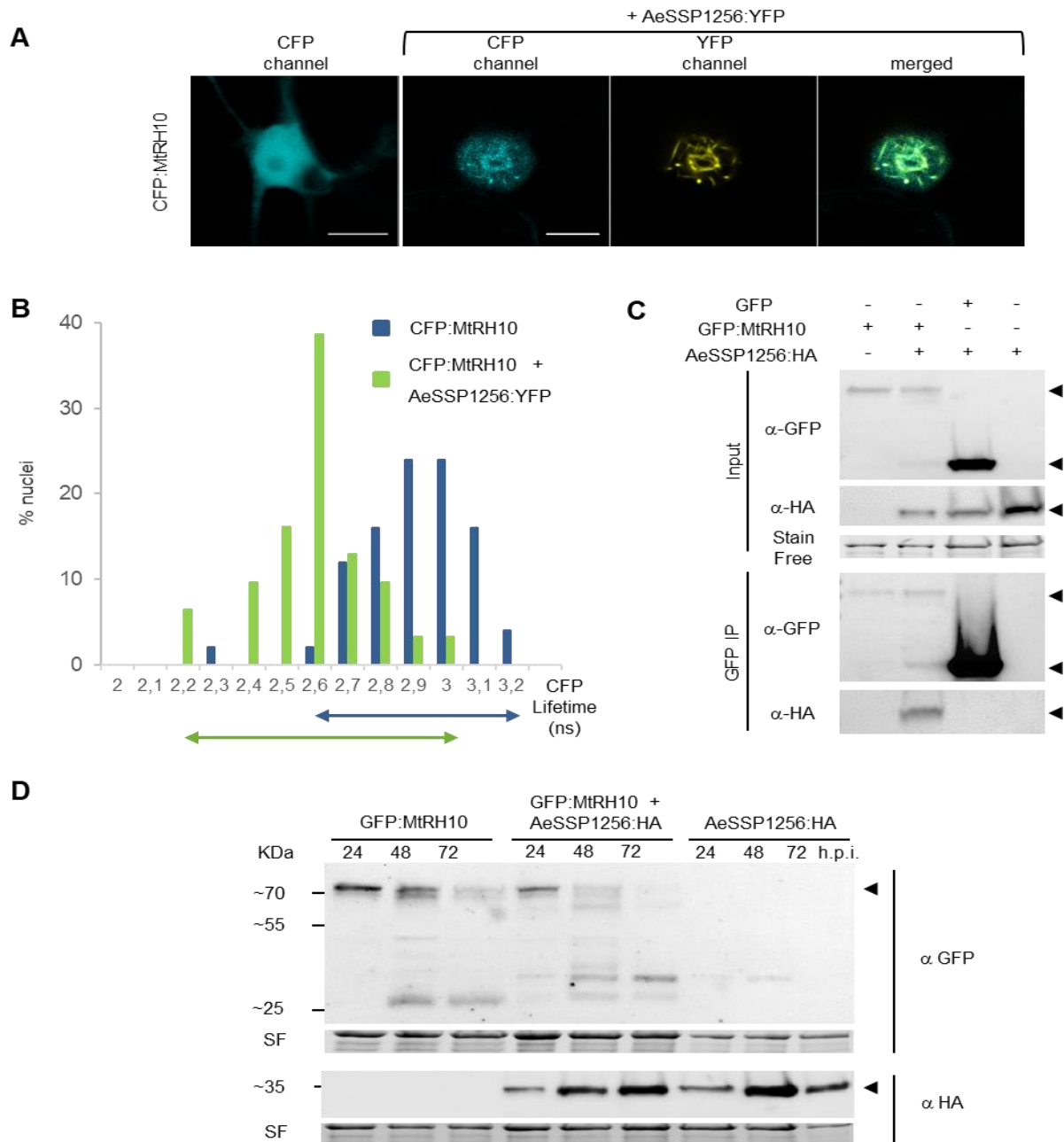


Figure 4: AeSSP1256 interacts and re-localizes the nuclear MtrRH10 RNA Helicase around the nucleolus

(A) Confocal analyses on *N. benthamiana* agroinfiltrated leaves. The CFP:MtRH10 candidate presents a nucleocytoplasmic localization when expressed alone (Left panel), and is re-localized in the nucleus, mostly around nucleolus, in the presence of AeSSP1256:YFP proteins (Right panels). Pictures were taken at 24h post agroinfection. Scale bars: 10 μ m. **(B)** FRET-FLIM experiments indicate that CFP:MtRH10 and AeSSP1256:YFP proteins are in close association when co-expressed in *N. benthamiana* cells. Histograms show the distribution of nuclei (%) according to classes of CFP:MtRH10 lifetime in the absence (blue bars) or presence (green bars) of AeSSP1256:YFP. Arrows represent CFP lifetime distribution range. **(C)** Co-immunoprecipitation experiments

confirm the direct association of the two proteins. Upper panel: anti-GFP and anti-HA blots confirm the presence of recombinant proteins in the input fractions. Lower panel: anti-GFP and anti-HA blots on output fractions after GFP immunoprecipitation. Arrows indicate the corresponding proteins. **(D)** anti-GFP and anti-HA blots on *N. benthamiana* leaf extracts expressing the GFP:MtRH10 alone or in combination with AeSSP1256:HA protein after 24, 48 or 72h post agroinfection. Arrows indicate the corresponding proteins. GFP:MtRH10 is degraded faster in presence of AeSSP1256:HA.

(Supplemental Figure 4A) (Schütz et al., 2010; Gilman et al., 2017). MtRH10 CFP-tagged fusion protein harbors nucleocytoplasmic localization when transiently express in *N. benthamiana* cells **(Figure 4A)**, in accordance with the presence of both putative nuclear export signals (NESs) (position 7-37; 87-103; 261-271) and nuclear localization signal (NLS) sequences (position 384-416). When MtRH10 is co-expressed with YFP-tagged version of AeSSP1256, the fluorescence is mainly detected as a ring around the nucleolus, indicating a partial relocation of MtRH10 to the AeSSP1256 sites **(Figure 4A)**. FRET-FLIM measurements on these nuclei confirm the interaction between AeSSP1256 and the *Medicago* RNA helicase **(Figure 4B)**, with a mean CFP lifetime of 2.86 ns +/- 0.02 in absence of the effector protein, to 2.53 ns +/- 0.03 in presence of AeSSP1256:YFP **(Table 2)**.

Table 2: FRET-FLIM measurements of CFP:MtRH10 in presence or absence of AeSSP1256:YFP

Donor	Acceptor	τ ^(a)	sem ^(b)	N ^(c)	E ^(d)	^(e) p-value
CFP:MtRH10	-	2.86	0.023	50	-	-
CFP:MtRH10	AeSSP1256:YFP	2.53	0.031	31	11.1	2.56E ⁻¹²

τ : mean life-time in nanoseconds (ns). ^(b) s.e.m.: standard error of the mean. ^(c) N: total number of measured nuclei. ^(d) E: FRET efficiency in % : $E=1-(\tau_{DA}/\tau_D)$. ^(e) p-value (Student's *t* test) of the difference between the donor lifetimes in the presence or absence of acceptor.

To confirm this result, co-immunoprecipitation assays were carried out. A GFP:MtRH10 construct was co-transformed with AeSSP1256:HA construct in *N. benthamiana* leaves. As expected, the localization of GFP:MtRH10 protein in absence of AeSSP1256 was nucleocytoplasmic while it located around the nucleolus in the presence of the effector

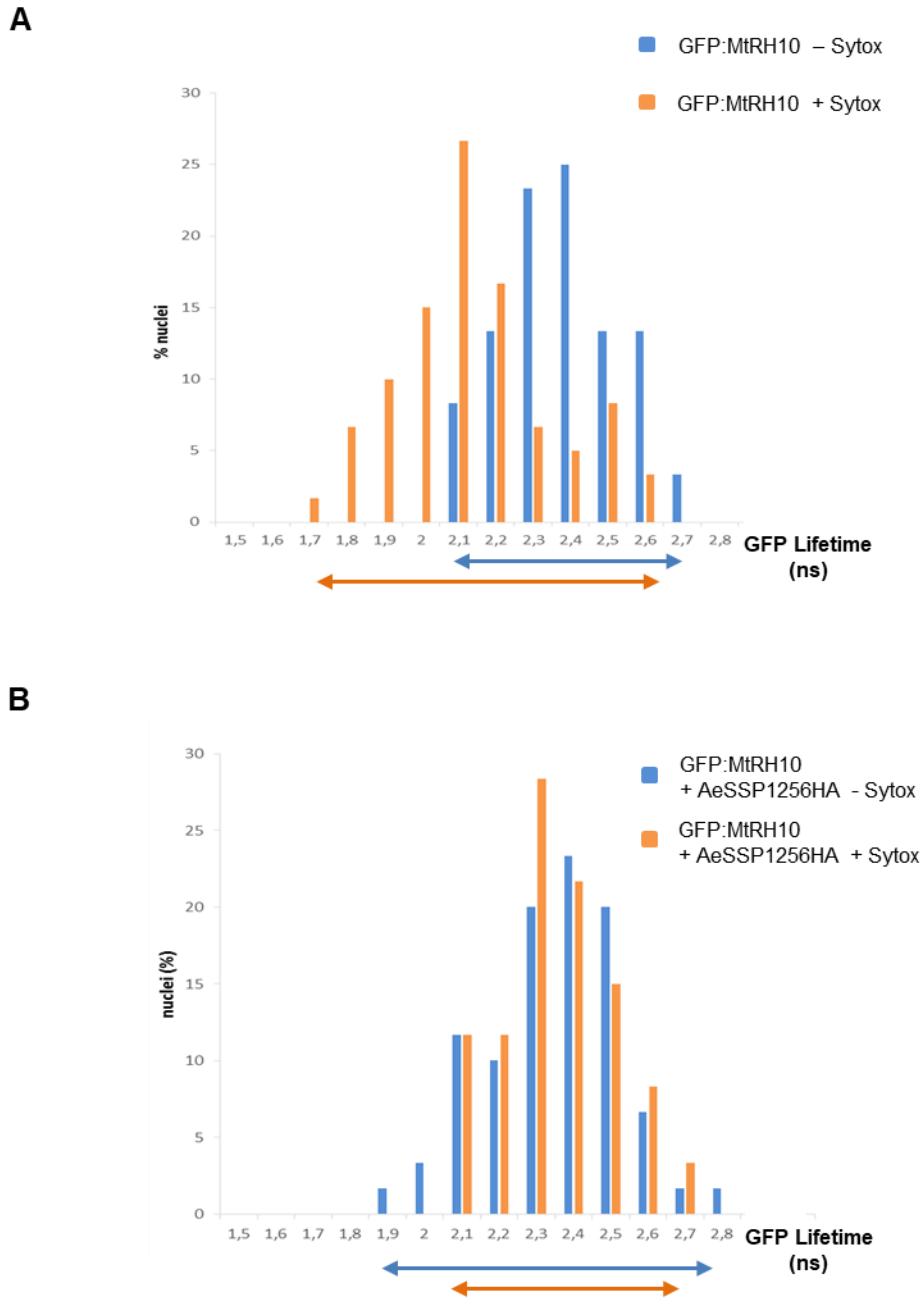


Figure 5: AeSSP1256 inhibits RNA binding activity of MtrRH10

(A) FRET-FLIM experiments on *N. benthamiana* cells expressing GFP:MtrRH10 in presence or absence of nucleic acids dye Sytox Orange. In presence of Sytox Orange, the GFP:MtrRH10 lifetime decreases to shorter values, indicating that the proteins bounded to nucleic acids. **(B)** In presence of AeSSP1256:HA, when GFP:MtrRH10 is re-localized around the nucleolus and interacts with AeSSP1256, no significant decrease in the GFP lifetime was observed in presence of Sytox Orange, meaning that the re-localized GFP:MtrRH10 proteins were not able to interact with nucleic acids. Histograms show the distribution of nuclei (%) according to classes of GFP:MtrRH10 lifetime in the absence (blue bars) or presence (orange bars) of the nucleic acids dye Sytox Orange. Arrows represent GFP lifetime distribution range.

(**Supplemental Figure 4B**). Immunoblotting experiments using total proteins extracted from infiltrated leaves (24 hpi) showed that AeSSP1256:HA proteins were co-immunoprecipitated with GFP:MtRH10, but not with the GFP alone (**Figure 4C**). These data indicate that AeSSP1256 associates with MtRH10 in the nucleus. To go further we checked the stability of the two proteins when expressed alone or in combination in *N. benthamiana* cells during 72 hours. While GFP:MtRH10 was still detected at 72h after agroinfiltration, it started to be degraded 48hpi (**Figure 4D**). Expression of the effector alone is stable along the time. In contrast, when the two proteins are co-expressed, GFP:MtRH10 is almost entirely processed at 48h, and no more detectable at 72h (**Figure 4D**), suggesting that the effector enhance instability of its host target. Taken together, these results strongly suggest an interaction between AeSSP1256 and two type of components, a ribosomal protein and a nuclear RNA helicase from *M. truncatula*.

AeSSP1256 alters the RNA binding activity of MtRH10

DEAD-box RNA helicases are RNA binding proteins involved in various RNA-related processes including pre-rRNA maturation, translation, splicing, and ribosome assembly (Jarmoskaite and Russell, 2011). These processes are dependent to the RNA binding ability of the proteins. Therefore we checked whether MtRH10 is able to bind nucleic acids *in planta* using FRET-FLIM assays as described previously. As reported in **Table 3** and in **Figure 5A**, GFP lifetime of GFP:MtRH10 decreased in presence of the acceptor, from 2.32 ns +/- 0.02 to 2.08 ns +/- 0.03 due to FRET between GFP and Sytox, confirming as expected that MtRH10 protein is bounded to nucleic acids.

Table 3: FRET-FLIM measurements for GFP:MtRH10 with or without Sytox Orange, in presence or in absence of AeSSP1256:HA

Donor	Acceptor	τ ^(a)	sem ^(b)	N ^(c)	E ^(d)	^(e) p-value
GFP:MtRH10	-	2.32	0.020	60	-	-
GFP:MtRH10	Sytox Orange	2.08	0.027	60	10.3	1.30E ⁻¹⁰

GFP:MtRH10 (relocalized)	- (+ AeSSP1256:HA)	2.30	0.023	60	24	-
GFP:MtRH10 (relocalized)	Sytox Orange (+ AeSSP1256:HA)	2.30	0.020	60	0	0.789

τ : mean life-time in nanoseconds (ns). ^(b) s.e.m.: standard error of the mean. ^(c) N: total number of measured nuclei. ^(d) E: FRET efficiency in % : $E=1-(\tau_{DA}/\tau_D)$. ^(e) p-value (Student's *t* test) of the difference between the donor lifetimes in the presence or absence of acceptor.

To evaluate the role of AeSSP1256 on the function of MtRH10 we reasoned that the effector may perturb its binding capacity since it is required for the activity of numerous RH protein family (Jankowsky, 2011). We then co-expressed the GFP:MtRH10 construct with AeSSP1256:HA in *N. benthamiana* leaves and performed FRET-FLIM assays. Measurements made in nuclei where both proteins are detected due to the re-localization of MtRH10 indicated that GFP lifetime of GFP:MtRH10 remained unchanged with or without Sytox (2.3 ns in both conditions) showing that MtRH10 was not able to bind nucleic acids in the presence of the effector (**Table 3 and Figure 5B**). These data reveal that AeSSP1256 hijacks MtRH10 binding to RNA, probably by interacting with MtRH10.

MtRH10 is expressed in meristematic root cells and its deregulation in *M. truncatula* impacts root architecture and susceptibility to *A. euteiches* infection

To characterize the function of MtRH10, we firstly consider the expression of the gene by mining public transcriptomic databases including Legoo (<https://lipm-browsers.toulouse.inra.fr/k/legoo/>), Phytozome (<https://phytozome.jgi.doe.gov/pz/portal.html>) and MedicagoEFP browser on Bar Toronto (<http://bar.utoronto.ca/efpmedicago/cgi-bin/efpWeb.cgi>). No variability was detected among the conditions tested in the databases and we do not detect modification of MtRH10 expression upon *A. euteiches* inoculation in our RNAseq data. To go further in the expression of the MtRH10 gene, transgenic roots expressing an MtRH10 promoter-driven GUS (β -glucuronidase) chimeric gene were generated. GUS activity was mainly detectable in meristematic cells, at the root tip or in lateral emerging roots (**Figure 6A**) suggesting a role in meristematic cell division. To assess the effect of MtRH10 on root physiology and resistance

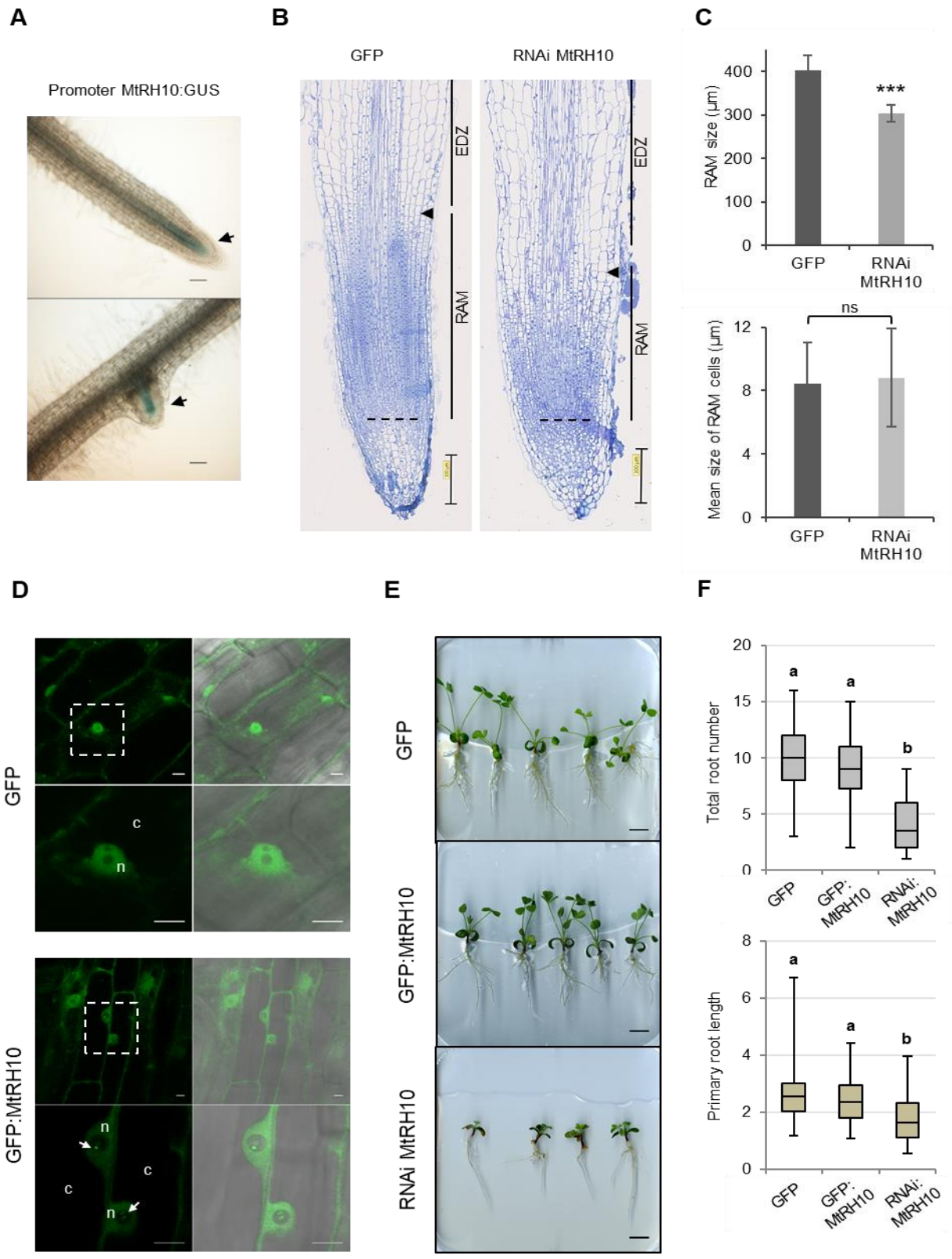


Figure 6: M_tRH10 is expressed in meristematic cells of *Medicago truncatula* and its deregulation impacts root architecture

Figure 6: MtrRH10 is expressed in meristematic cells of *Medicago truncatula* and its deregulation impacts root architecture

(A) GUS staining of MtrRH10 promoter:GUS plants 21 d.a.t. Top panel: Root tip, bottom panel: emerging lateral root. Arrows indicate blue cells. Scale bars: 100 μ m. **(B)** Representative longitudinal section of *M. truncatula* root tips expressing GFP or RNAi MtrRH10 construct. Root apical meristem (RAM) size is determined from quiescent center (dot line) till the elongation/differentiation zone (EDZ), defined by the first elongated cortex cell of second cortical layer (arrowhead). Scale bars: 100 μ m. **(C)** Histograms of total RAM size and mean RAM cortical cell size. RAM of RNAi MtrRH10 roots are smaller than in GFP control, but average cell size of cortical cells in RAM is not significantly different. Bars represent mean values and error bars are standard deviation. Asterisks indicate a significant p-value (t-test $P < 0,0001$, ns: not significant). **(D)** Confocal pictures of *M. truncatula* roots transformed with GFP (top) or GFP:MtrRH10 construct (bottom). GFP:MtrRH10 proteins harbor a nucleocytoplasmic localization with some fluorescence dots in the nucleolus (arrows). Bottom panels represent nucleus enlargements. n: nucleus, c: cytoplasm. Scale bars: 10 μ m. Left panel : 488nm, right panel: overlay (488nm + bright field) **(E)** Representative pictures of *M. truncatula* plants expressing either a GFP, a GFP:MtrRH10 or RNAi MtrRH10 construct 21 d.a.t. No particular phenotype was observed in the overexpressing MtrRH10 plants. At the opposite, developmental delay appeared in missense MtrRH10 plants. Scale bar: 1cm. **(F)** Total root number per plant (left panel) and primary root length per plant (right panel) in cm. Letters a and b indicate Student's t-test classes (different classes if $P < 0,01$).

to *A. euteiches*, a pK7GWiWG2:RNAi MtrRH10 vector was design to specifically silence the gene in *Medicago* roots. RNA helicase gene expression was evaluated by qPCR 21 days after transformation. Analyses confirmed a reduced expression (from 3 to 5 times) compared to roots transformed with a GFP control vector (**Supplemental Figure 5**). The silenced roots displayed a delay in development, which starts with a shorter root apical meristem (RAM) (**Figure 6B and C**). This reduction is not due to smaller RAM cortical cell size (**Figure 6C**) suggesting a decrease in cell number. We also observed a reduced number of roots coupled with shorter primary roots (**Figure 6E and F**). In contrast, no developmental defects were detected in roots overexpressing MtrRH10 (**Figure 6E and F**). Longitudinal sections of roots expressing either RNAi MtrRH10 or AeSSP1256 performed in elongation/differentiation zone (EDZ) revealed comparative defects in cortical cell shape or cell size (**Supplemental Figure 6A**). Cell area in missense MtrRH10 or in AeSSP1256 roots is approximately reduced 2 times compared to GFP control roots (**Supplemental Figure 6B**) but proportionally the perimeter of those cells is longer than GFP cells, indicating a difference in cell shape (**Supplemental Figure**

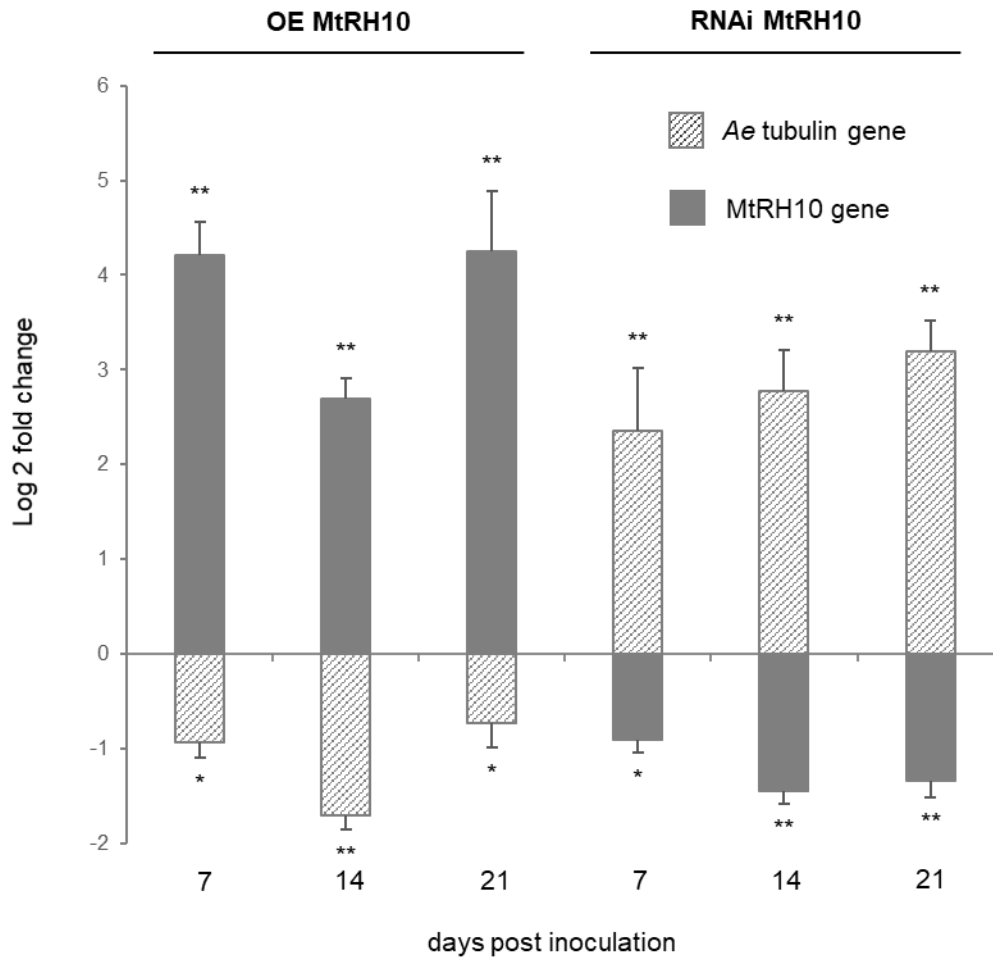


Figure 7: Deregulation of MtrRH10 helicase gene expression in *Medicago truncatula* impacts *Aphanomyces euteiches* susceptibility

Expression values (Log₂ fold change) for *A. euteiches* tubulin or MtrRH10 genes in *M. truncatula* infected plants at 7, 14 and 21 d.p.i. in overexpressing GFP:MtrRH10 plants (OE MtrRH10) or in RNAi MtrRH10 expressing plants compared to GFP control plants. Plants overexpressing MtrRH10 gene are less susceptible to *A. euteiches* infection. In contrast, reduced expression of MtrRH10 by RNAi enhances plant susceptibility to *A. euteiches*. Asterisks indicate significant differences (Student's t-test; *: P < 0,05, **: p < 0,01). Bars and error bars represent respectively means and standard errors from three independent experiments. In total, N: 91 plants for GFP, 50 plants for GFP:MtrRH10 and 50 plants for RNAi MtrRH10 construct.

6C). We noticed that most of EDZ cells in GFP roots present a rectangular shape, which seem impaired in missense MtrRH10 and AeSSP1256 expressing roots. Thus we measured the perimeter-bounding rectangle (PBR) which calculates the smallest rectangle possible to draw with a given cell. A perimeter/PBR ratio of 1 indicates that the cell is rectangular. As presented in **Supplemental Figure 6D**, the perimeter/PBR ratio in GFP roots is close to 1 and significantly different than those observed in RNAi MtrRH10 and AeSSP1256 roots. This analysis reveals that the reduction of MtrRH10 expression or the expression of the effector AeSSP1256 in *Medicago* roots, impairs the cortical cell shape. The similar phenotypic changes observed on MtrRH10-silenced roots and AeSSP1256-expressing roots, suggest that the effector may affect MtrRH10 activity in cell division regions.

Having shown that MtrRH10 is implicated in *M. truncatula* roots development, we test whether this biological function is related to pathogen colonisation. We therefore investigate by qPCR the presence of *A. euteiches* in silenced and overexpressed MtrRH10 roots infected by the pathogen. As shown on **Figure 7**, overexpression of MtrRH10 reduce the amount of mycelium in roots after 7, 14 and 21 dpi (1.8, 3.3 and 1.6 times less, respectively). We note by western-blot analyses a slight decrease in MtrRH10 amount upon the time probably due to the accumulation of the AeSSP1256 effector (**Supplemental Figure 7**). As expected in roots where MtrRH10 is silenced to 2 to 3 times as compared to GFP control roots, qPCR analyses revealed approximately 5 to 10 times more of the pathogen at 7, 14 and 21 dpi (**Figure 7**). Taken together these infection assays show that MtrRH10 is involved in conferring basal resistance to *A. euteiches* at the root level.

Discussion

Protein effectors from filamentous plant pathogens such as fungi and oomycetes facilitate host colonization by targeting host components. However, the molecular mechanisms that enhance plant susceptibility to the pathogen are still poorly understood. Here we report that the *A. euteiches* AeSSP1256 RNA-binding effector facilitate host infection by downregulating expression of plant ribosome-related genes and by hijacking from its nucleic target MtRH10, a *Medicago* nuclear RNA-helicase (RH). Thus, the current study unravels a new strategy in which pathogenic oomycete triggers plant nucleolar stress to promote infection.

AeSSP1256 is an effector from the oomycete root pathogen *A. euteiches* previously shown to enhance oomycete infection (Gaulin et al., 2018). Despite the absence of any functional domain, *in silico* RGG/RG RNA-binding motif prediction (see for review (Thandapani et al., 2013)) prompt us to show by FRET/FLIM analysis that the secreted AeSSP1256 effector is an RNA-binding protein (RBP). RNAs play essential role in cell physiology and it is not surprising that filamentous plant pathogens may rely on RNA-dependent process to control host infection (for review see (Göhre et al., 2013; Pedersen et al., 2012). Moreover RBPs are key players in the regulation of the post-transcriptional processing and transport of RNA molecules (Yang et al., 2018b). However, to our knowledge only three examples of RBPs acting as virulence factor of plant pathogens are known. This includes the glycine-rich protein MoGrp1 from the rice pathogen *Magnaporthe oryzae* (Gao et al., 2019), the UmRrm75 of *Ustilago maydis* (Rodríguez-Kessler et al., 2012) and the secreted ribonuclease effector CSEP0064/BEC1054 of the fungal pathogen *Blumeria graminis* which probably interferes with degradation of host ribosomal RNA (Pennington et al., 2019). This situation is probably due to the absence of conventional RNA-binding domain which render this type of RBP undetectable by prediction algorithms. The future studies that will aim to unravel the atlas of RNA-binding effectors in phytopathogens should not only rely on computational analysis but will have to use functional approaches such as crystallization of the protein to validate function as performed with CSEP0064/BEC1054 effector (Pennington et al., 2019) or screening method like the RNA interactome capture (RIC) assay develops in mammals (Castello et al., 2012).

We observed that when expressed inside roots of the partially resistant Jemalong A17 *M. truncatula* line, AeSSP1256 triggers developmental defects such as shorter primary roots and delay in roots development. In addition, those composite plants promote infection of *A. euteiches*. This modification in the output of the infection is highly relevant since we previously observed that *M. truncatula* quantitative resistance to *A. euteiches* is correlated to the development of secondary roots (Rey et al., 2016). Defects in roots development and retarded growth are typical characteristics of auxin-related and ribosomal proteins mutants reported in *Arabidopsis* (Ohbayashi et al., 2017; Wieckowski and Schiefelbein, 2012).

This activity is dependent on the nucleolar rim localization of AeSSP1256, closed to the nucleolus. The nucleolus is a membrane-free subnuclear compartment essential for the highly complex process of ribosome biogenesis (reviewed in (Shaw and Brown, 2012)). Ribosome biogenesis is linked to cell growth and required coordinated production of processed ribosomal RNA (rRNA), ribosomal biogenesis factors and ribosomal proteins (RP). In the nucleolus, ribosome biogenesis starts with the transcription of pre-rRNAs from rRNA genes, followed by their processing and assembly with RPs into two ribosome subunits (ie small and large subunit). In animals, perturbation of any steps of ribosome biogenesis in the nucleolus can cause a nucleolar stress or ribosomal stress which stimulates specific signaling pathway leading for example to arrest of cell growth (Pfister, 2019). The nucleolar rim localization of AeSSP1256 within the host cells suggested that this effector could interfere with ribosome biogenesis pathway to facilitate infection. This speculation was further strengthened by RNAseq experiments, which showed that within A17-roots, AeSSP1256 downregulated numerous genes implicated in ribosome biogenesis pathway, notably ribosomal protein genes. This effect was also detected in susceptible F83 *M. truncatula* lines infected by *A. euteiches* indicating that AeSSP1256, mimics some *A. euteiches* effects during roots invasion.

Y2H approach led to the identification of putative AeSSP1256 plant targets and all but one correspond to predicted nuclear *M. truncatula* proteins. By a combination of multiple experiments as FRET-FLIM to detect protein/protein interactions, a L7 ribosomal protein (MtrunA17_Chr4g0002321) and a DExD/H box RNA helicase ATP-dependent (MtrunA17_Chr5g0429221) were confirmed as AeSSP1256-interacting proteins. The DExD/H (where x can be any amino acid) box protein family include the largest family of RNA-helicase (RH). Rather than being processive RH, several DExD/H box proteins may act as 'RNA

chaperone' promoting the formation of optimal RNA structures by unwinding locally the RNA (for review see (Fuller-Pace, 2006)). These proteins are of major interest due to their participation to all the aspects of RNA processes such as RNA export and translation, splicing but the most common function of these proteins is in ribosome biogenesis including assembly (Jarmoskaite and Russell, 2011). Specific function of RH is probably due to the presence of a variable C-terminal 'DEAD' domain in contrast to the well conserved N-terminal 'helicase core' domain (for review see (Fuller-Pace, 2006)). This structural organization was detected in the MtRH10. This *M. truncatula* protein corresponds to the ortholog of the nucleolar human DDX47 (Sekiguchi et al., 2006), the nuclear yeast RRP3 (O'Day, 1996) and the nucleolar *Arabidopsis* AtRH10 RNA-helicases, all involved in ribosome biogenesis (Liu and Imai 2018; Matsumura et al. 2016), and the nucleolar rice OsRH10 (TOGR1) involved in rRNA homeostasis (Wang et al. 2016).

Like its human ortholog DDX47 (Sekiguchi et al., 2006), MtRH10 possesses a bipartite nuclear transport domain which can function as a nuclear localization signal (NLS) and two nuclear export signal (NES), and thereby it probably shuttles between the cytoplasm and the nucleus as reported for many others RNA helicases involved in rRNA biogenesis and splicing function (Sekiguchi et al. 2006; Wang et al. 2009). Fluorescence analysis showed a relocalization of the nucleocytoplasmic MtRH10 in the nucleoli periphery, when it is transiently co-express with AeSSP1256 in *N. benthamiana* cells. The change in MtRH10 distribution suggests that the interaction between the two proteins caused a mislocation of MtRH10 that can probably affect its activity. We thereby check the nucleic acid binding capacity of MtRH10 by FRET-FLIM approach. The decrease in the lifetime of GFP revealed the ability of MtRH10 to bind nucleic acids. Knowing that both proteins display the same properties, we further evidenced that the presence of AeSSP1256 effector inhibits the nucleic binding capacity of MtRH10. This mechanism was also reported for the RNA-binding HopU1 effector from the plant bacterial pathogen *Pseudomonas syringae* which associate to the glycin-rich RNA binding 7 protein (GRP7) of *Arabidopsis* to abolish GRP7 binding to immune gene transcripts (ie FLS2 receptor, (Nicaise et al., 2013)). Here we cannot exclude that AeSSP1256 also blocks the putative helicase activity of MtRH10, but we favored an inhibitory mechanism of AeSSP1256 on MtRH10 activity as complex and at least in part due to both protein-protein interaction and nucleic acid interaction with the two proteins. Interestingly, we also noticed that co-

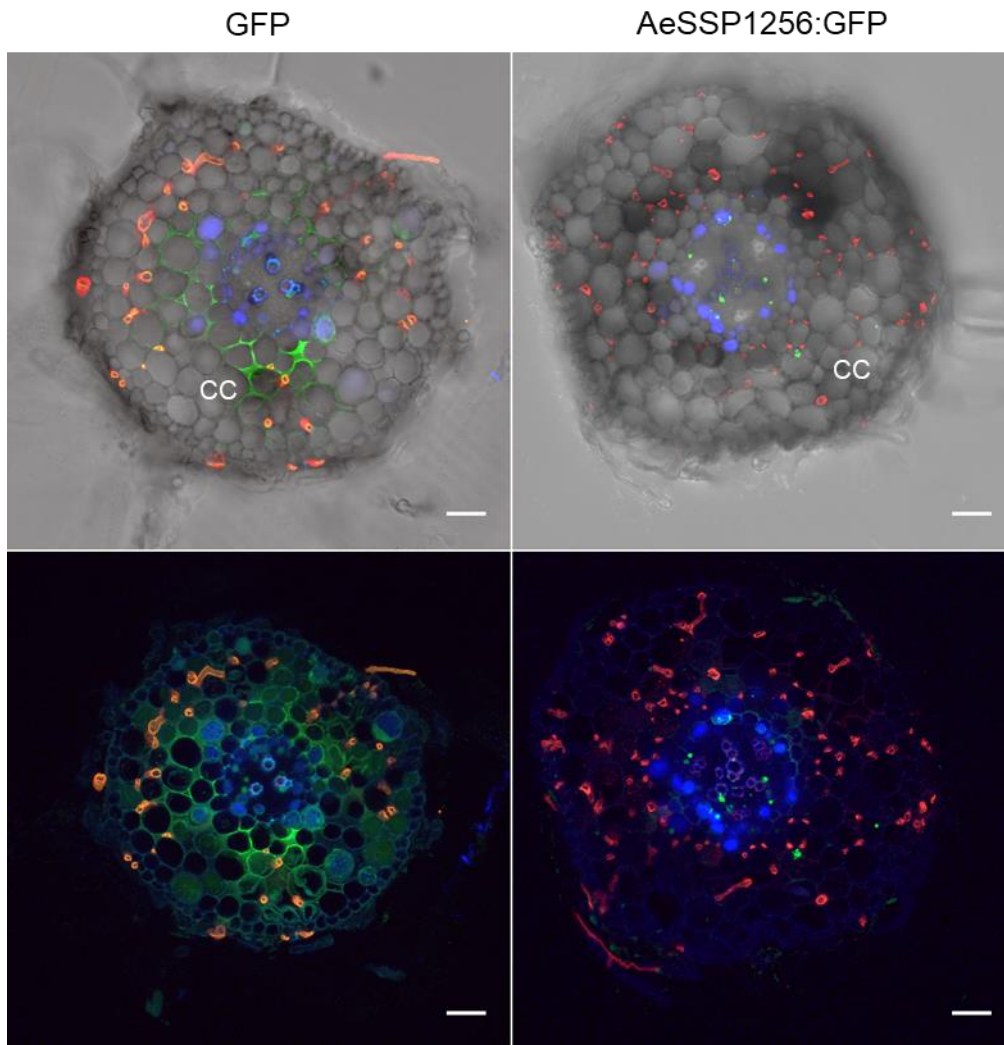
expression of both proteins led to decrease in MtRH10 probably due to degradation of the protein. While this observation warrants further analyses, this effect is reminiscent of other effector activities which destabilize their targets (for review see (Langin et al., 2020)).

Plant genomes encode a large variety of DExD/H RH family in comparison to other organisms and numerous studies have shown that several are associated through their activity with plant development, hormone signaling or responses to abiotic stresses (for review see (Liu and Imai 2018)). Very few studies reported that DExD/H RH could also be involved in biotic stresses, like responses to pathogens. One example is the DExD/H RH OsBIRH1 from rice that enhanced disease resistance against *Alternaria brassicicola* and *Pseudomonas syringae* through activation of defense-related genes (Li et al. 2008). A recent study on oomycete reports the binding of the *Phytophthora sojae* RxLR PSR1 effector to a putative nuclear DExD/H RH. Although the affinity for nucleic acids was not evaluated for the RH, association of both partners promote pathogen infection by suppressing small RNA biogenesis of the plant (Qiao et al., 2015). Here we showed that MtRH10 knockdown tolerant A17 lines supported higher-level accumulation of *A. euteiches* in contrast to overexpressed MtRH10 lines, indicating the importance of MtRH10 for *M. truncatula* roots defense against soil-borne pathogens.

This work reveals that MtRH10 expression is restricted at the root apical meristematic zone (RAM) where cells divide (ie, primary and lateral roots). Missense MtRH10 roots harbor defects in the primary root growth and reduced number of roots. Longitudinal sections in elongation zone (EDZ) of these composite roots show a significant reduction in the size and shape modification of cortical cells indicating that MtRH10 is required for normal cell division. Defect in primary roots elongation is also detected in silenced AtRH10 and OsRH10 mutant (Matsumura et al. 2016; Wang et al. 2016). Thus MtRH10 plays a role on *Medicago* root development as its orthologs OsRH10 and AtRH10. At the cellular level we also observed in AeSSP1256-expressing roots, reduction in cell size in elongation zone, with defects in cell shape and in adhesion between cells of the cortex, maybe due to a modification of the middle lamella (Zamil and Geitmann, 2017). Thus AeSSP1256 triggers similar or enhanced effect on host roots development as the one detected in defective MtRH10 composite plants, supporting the concept that the activity of the effector on MtRH10 consequently leads to developmental roots defects. Several reports have indicated that *Arabidopsis* knockout of genes involved in rRNA biogenesis or in ribosome assembly cause abnormal plant

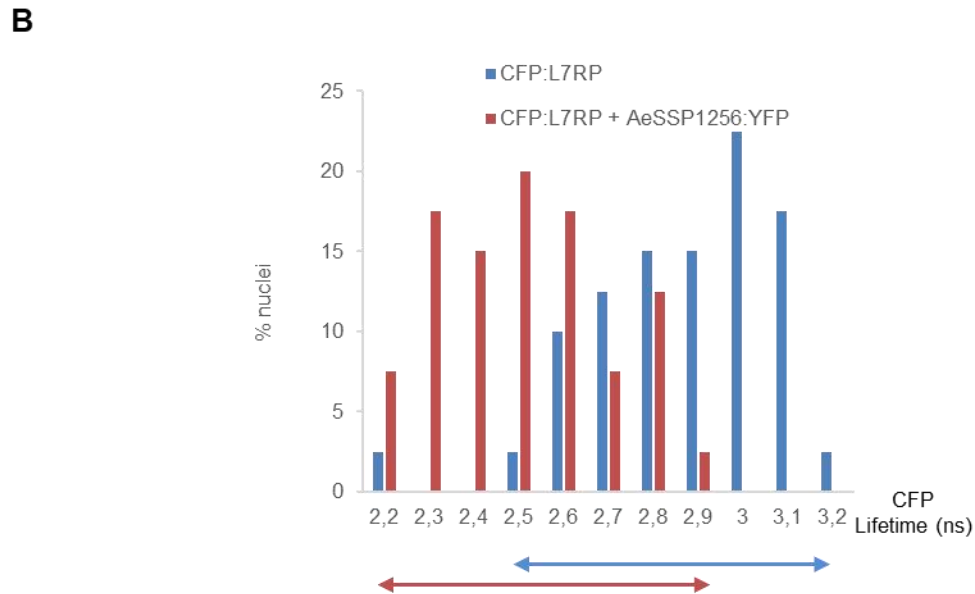
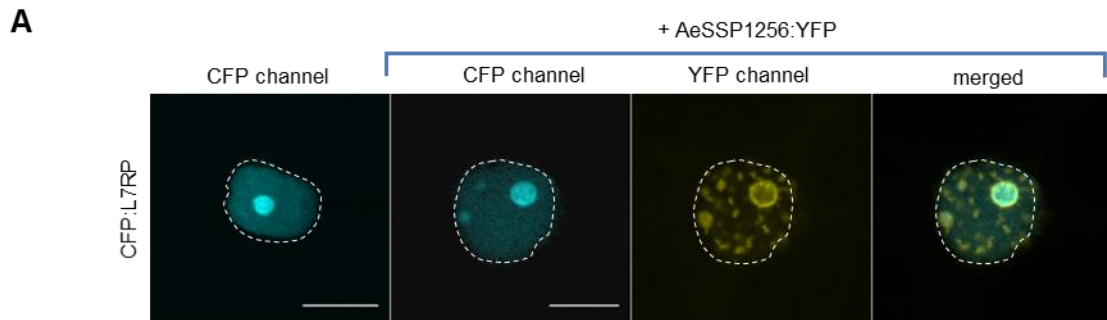
development including restriction and retardation in roots growth (Ohtani et al., 2013; Huang et al., 2016, 2010). These common features suggest the existence of a common mechanism that regulate growth in response to insults of the ribosome biogenesis pathway, known as nucleolar stress response (for review see (Ohbayashi and Sugiyama, 2018)). How plant cells sense perturbed ribosome biogenesis and nucleolar problems is still an opening question (Sáez-Vásquez and Delseny, 2019), but the ANAC082 transcription factor from *Arabidopsis* can be a ribosomal stress response mediator (Ohbayashi et al., 2017). In addition the recent report on the activity of the nucleolar OsRH10 (TOGR1, MtrRH10 ortholog) implicated in plant primary metabolism through its activity on rRNA biogenesis, suggests that metabolites may play a role in this process. Finally our current study indicates that nuclear RNA-binding effector like AeSSP1256, by interacting with MtrRH10, can act as a stimulus of the ribosomal stress response.

This work established a connection between the ribosome biogenesis pathway, a nuclear DExD/H RH, root development and resistance against oomycetes. Our data document that the RNA binding AeSSP1256 oomycete effector that the parasite expresses during infection downregulated expression of ribosome-related genes and hijacked MtrRH10, a nuclear DExD/H RH involved in root development, to promote host infection. This work not only provides insights into plant-root oomycete interactions but also reveals the requirement of fine-tuning of plant ribosome biogenesis pathways for infection success.



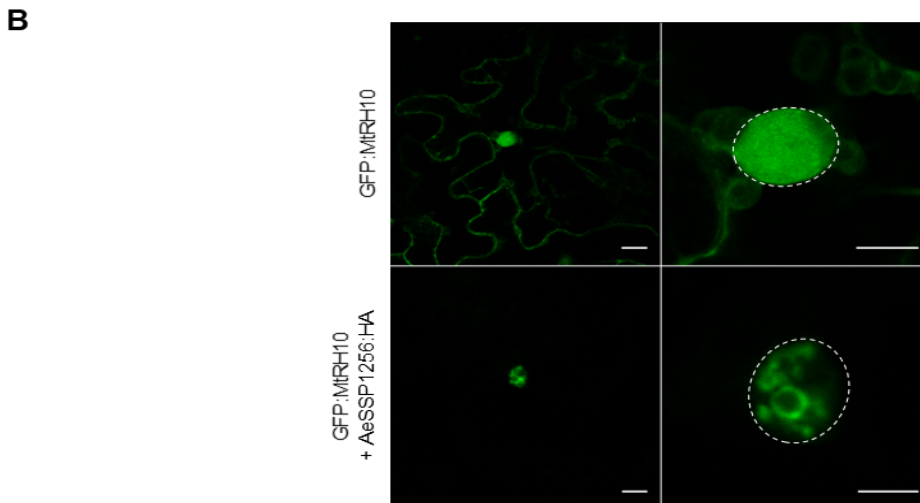
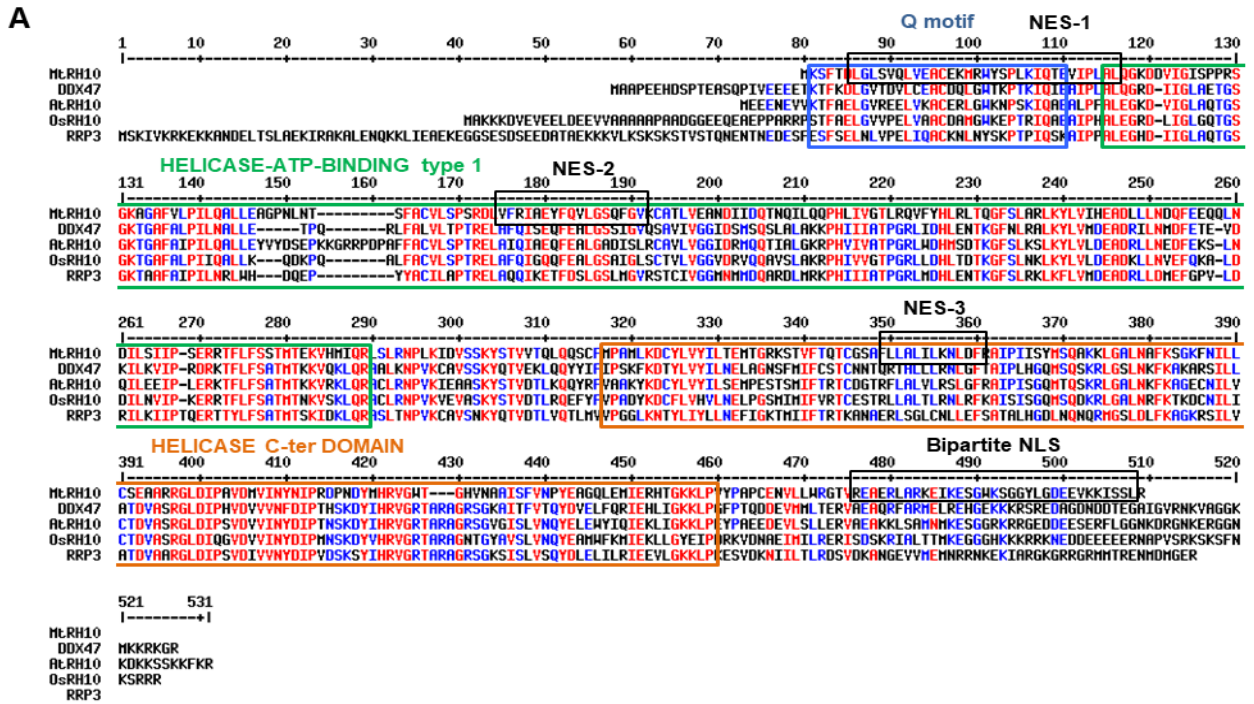
Supplemental Figure 2: Invasion of *M. truncatula* roots by the pathogen is unchanged in AeSSP1256 effector-expressing roots.

Cross-section of tolerant A17 *M. truncatula* lines expressing either the GFP control vector (left) or the effector AeSSP1256:GFP (right) construct and infected by *A. euteiches*, 21 days after infection. Mycelium was stained by Wheat Germ Agglutinin (Red) assay. Green fluorescence indicate GFP alone or the GFP-tagged effector. Accumulation of phenolic compounds due to the presence of the pathogen is visualized in blue (Djebali et al., 2009). No notable modification in the infection process is detected and the pathogen is still restricted to the root cortex in the effector-transformed roots as in wild type tolerant A17 line. CC: cortical cells. Scale bars: 100 μ m



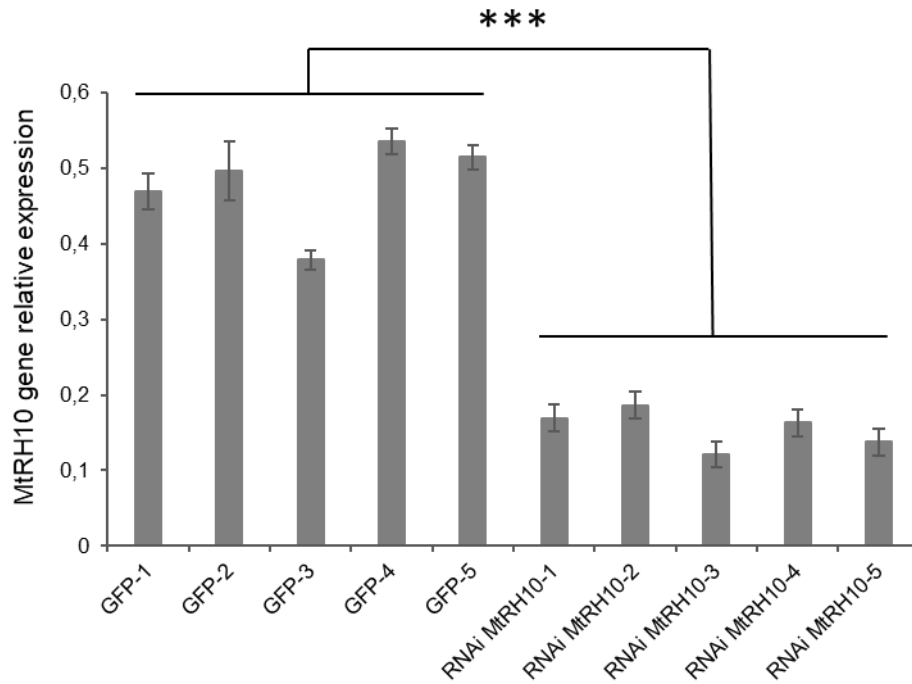
Supplemental Figure 3: CFP:L7RP candidate and AeSSP1256:YFP are in close association.

Confocal and FRET-FLIM experiments indicate that CFP:L7RP and AeSSP1256:YFP proteins are in close association when co-expressed in *N. benthamiana* cells. **(A)** Confocal analysis revealed partial colocalization of CFP:L7RP and AeSSP1256:YFP. White dashes represent nucleus membrane. Pictures were taken at 24h. Scale bars: 10 μ m. **(B)** FRET-FLIM measurements. Histograms show the distribution of nuclei (%) according to classes of CFP:L7RP lifetime in the absence (blue bars) or presence (red bars) of AeSSP1256:YFP. Arrows represent CFP lifetime distribution range.



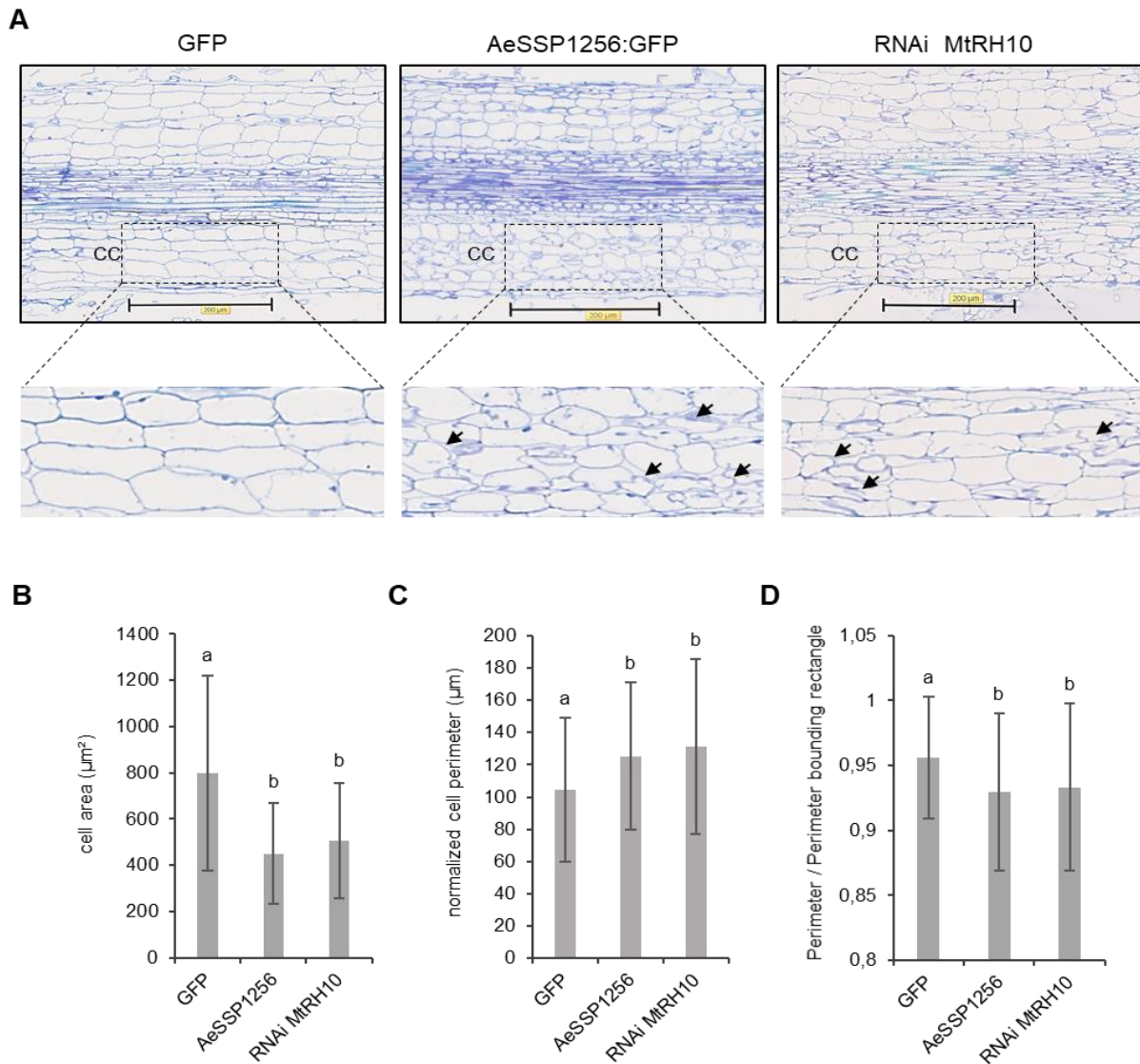
Supplemental Figure 4: AeSSP1256 drives the re-localisation of the nuclear *MtrRH10* RNA helicase, around the nucleolus in *N. benthamiana* cells.

(A) Multiple sequence alignment of DEAD-box RNA Helicases (RH) from *Medicago truncatula* (MtrRH10, MtrunA17_Ch5g0429221), *Homo sapiens* (DDX47, UniprotKb: Q9H0S4), *Saccharomyces cerevisiae* (RRP3, UniprotKB: P38712), *Arabidopsis thaliana* (AtRH10, UniprotKB: Q8GY84) and *Oryza sativa* (OsRH10, UniprotKb: A2XKG2) which display >50% similarity. Colored boxes indicate conserved DEAD-box RH domains. Black boxes indicate putative NES and NLS sequences for MtrRH10 protein. Alignment was performed with Multalin (<http://multalin.toulouse.inra.fr/multalin/>). Red: identical aligned residues, Blue: similar aligned residues (B) Transient expression in *N. benthamiana* leaves of GFP:MtrRH10 alone or in combination with AeSSP1256:HA. White dashes represent nucleus membrane. Pictures were taken by confocal 24h after infiltration. Note the re-localisation of MtrRH10 in presence of the effector, as a ring around the nucleolus. Right pictures are zooms of nucleus of the left panel. Scale bars: 10 μ m.



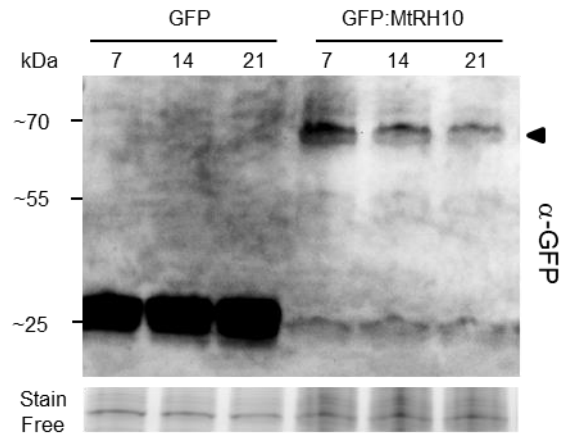
Supplemental Figure 5: Expression of MtrRH10 is reduced in *M. truncatula* silenced-roots.

qPCR analyses of MtrRH10 gene expression level in *M. truncatula* RNAi MtrRH10 transformed plants. Each sample represents a mix of five RNAi MtrRH10 plants or GFP control plants. Bars and error bars represent mean and standard deviation. Asterisks indicate t-test significant difference (***: $p < 0,0001$). Samples were harvested 21 days post transformation.



Supplemental Figure 6: *M. truncatula* cell morphology is affected in RNAi MtrRH10 and AeSSP1256:GFP expressing roots.

Host cell shape and size are affected by the expression of AeSSP1256:GFP construct or by the downregulation of MtrRH10 **(A)** Representative longitudinal sections of GFP, AeSSP1256:GFP or RNAi MtrRH10 roots. Rectangles show enlarged areas. CC: cortical cells. Arrow shows example of cells with shape or size perturbations. Samples were harvested 21 days post transformation. Scale bars: 200 µm. **(B)** Histograms of cortical cells area. RNAi MtrRH10 or AeSSP1256 cells are smaller than GFP control cells. **(C)** Histograms of normalized cell perimeter of cortical cells. Each cell perimeter is proportionally recalculated for a of 500 µm² area standard cell. Normalized cell perimeter is longer in missense MtrRH10 and AeSSP1256 samples due to proportionally longer perimeters, indicating a different shape compare to GFP control cells. **(D)** Histograms showing perimeter / perimeter bounding rectangle ratio. The perimeter bounding rectangle (PBR) calculates the smallest rectangle possible to draw with a given cell. A ratio perimeter / PBR of 1 indicates that the cell is rectangular. This graph shows that missense MtrRH10 and AeSSP1256 cells are less rectangular than GFP cells (perimeter / PBR ratio closer to 1 in GFP cells). Letters a and b represent statistical different classes (t-test, different letters if p<0,001). Bars represent mean values and error bars are standard deviation. Three roots from three independent experiments were used and measurements were performed in the elongation/differentiation zone (EDZ) of the roots, using approx. 300x600 µm selection.



Supplemental Figure 7: Western blot on MtrRH10-overexpressed roots infected by *A. euteiches*.

Representative anti-GFP blot on transformed plants infected by *A. euteiches* after 7, 14 or 21 days post inoculation. Note a slight decrease of MtrRH10 protein accumulation during *A. euteiches* infection. Each sample represents a mix of five GFP:MtrRH10 overexpressing plants or GFP control plants. Roots were inoculated 21 days post transformation. Arrowhead indicates GFP:MtrRH10 fusion proteins (68 kDa).

Material and Methods

Plant material, microbial strains, and growth conditions

M. truncatula A17 seeds were *in vitro*-cultured and transformed as previously described (Boisson-Dernier et al., 2001; Djébali et al., 2009). *A. euteiches* (ATCC 201684) zoospore inoculum were prepared as in (Badreddine et al., 2008). For root infections, each plant was inoculated with a total of 10 μ l of zoospores suspension at 10^5 cells.ml⁻¹. Plates were placed in growth chambers with a 16h/8h light/dark and 22/20°C temperature regime. *N. benthamiana* plants were grown from seeds in growth chambers at 70% of humidity with a 16h/8h light/dark and 24/20°C temperature regime. *E.coli* strains (DH5 α , DB3.5), *A. tumefaciens* (GV3101::pMP90) and *A. rhizogenes* (ARQUA-1) strains were grown on LB medium with the appropriate antibiotics.

Construction of plasmid vectors and *Agrobacterium*-mediated transformation

GFP control plasmid (pK7WGF2), +SPAeSSP1256:GFP and +SPAeSSP1256:YFP (named AeSSP1256:GFP and AeSSP1256:YFP in this study for convenience) and minus or plus signal peptide AeSSP1256:GFP:KDEL constructs were described in (Gaulin et al., 2018). Primers used in this study are listed in **Supplemental Table 3**. *M. truncatula* candidates sorted by Y2H assay (MtrunA17_Chr7g0275931, MtrunA17_Chr2g0330141, MtrunA17_Chr5g0407561, MtrunA17_Chr5g0429221, MtrunA17_Chr1g0154251, MtrunA17_Chr3g0107021, MtrunA17_Chr7g0221561, MtrunA17_Chr4g0002321) were amplified by Pfx Accuprime polymerase (Thermo Fisher; 12344024) and introduced in pENTR/ D-TOPO vector by means of TOPO cloning (Thermo Fisher; K240020) and then transferred to pK7WGF2, pK7FWG2 (<http://gateway.psb.ugent.be/>), pAM-PAT-35s::GTW:CFP or pAM-PAT-35s::CFP:GTW binary vectors.

Using pENTR/ D-TOPO:AeSSP1256, described in (Gaulin et al., 2018), AeSSP1256 was transferred by LR recombination in pAM-PAT-35s::GTW:3HA for co-immunoprecipitation and western blot experiments to create a AeSSP1256:HA construct and in pUBC-RFP-DEST (Grefen et al., 2010) to obtain a AeSSP1256:RFP construct for FRET FLIM analysis. For RNAi of MtRH10 (MtrunA17_Chr5g0429221), a 328 nucleotides sequence in the 3'UTR was amplified by PCR (see **Supplemental Table 3**), introduced in pENTR/D-TOPO vector and LR cloned in

pK7GWiwG2(II)-RedRoot binary vector (<http://gateway.psb.ugent.be/>) to obtain RNAi MtRH10 construct. This vector allows hairpin RNA expression and contains the red fluorescent marker DsRED under the constitutive *Arabidopsis* Ubiquitin10 promoter (<http://gateway.psb.ugent.be/>), to facilitate screening of transformed roots. For MtRH10 promoter expression analyses, a 1441nt region downstream of the start codon of MtRH10 gene was amplified by PCR (see **Supplemental Table 3**), fused to β -glucuronidase gene (using pICH75111 vector (Engler et al., 2014)) and inserted into pCambia2200:DsRED derivative plasmid (Fliegmann et al., 2013) by Golden Gate cloning to generate PromoterMtRH10:GUS vector.

Generation of *M. truncatula* composite plants was performed as described by (Boisson-Dernier et al., 2001) using ARQUA-1 *A. rhizogenes* strain. For leaf infiltration, GV3101 *A. tumefaciens* transformed strains were syringe-infiltrated as described by (Gaulin et al., 2002).

Cross-section sample preparation for confocal microscopy

M. truncatula A17 plants expressing GFP or AeSSP1256:GFP constructs were inoculated with *A. euteiches* zoospores 21 days after transformation as indicated previously. Roots were harvested 21 days post inoculation, embedded in 5% low-melting point agarose and cutted using a vibratome (VT1000S; Leica, Rueil-Malmaison, France) as described in (Djébali et al., 2009). Cross-sections were stained using Wheat Germ Agglutinin (WGA)-Alexa Fluor 555 conjugate (Thermo Fischer; W32464), diluted at 50 μ g/ml in PBS for 30min to label *A. euteiches*.

RNA-Seq experiments

Roots of composite *M. truncatula* A17 plants expressing GFP or AeSSP1256:GFP constructs were harvested one week later after first root emergence. Before harvest, roots were checked for GFP-fluorescence by live macroimaging (Axiozoom, Carl Zeiss Microscopy, Marly le Roi, France) and GFP-positive roots were excised from plants by scalpel and immediately frozen in liquid nitrogen. Four biological replicates per condition were performed (GFP vs AeSSP1256-expressing roots), for each biological replicate 20-40 transformed plants were used. Total RNA was extracted using E.Z.N.A.[®] total RNA kit (Omega bio-tek) and then purified using Monarch[®] RNA Cleanup Kit (NEB). cDNA library was produced using MultiScribe[™] Reverse Transcriptase kit using mix of random and poly-T primers under standard conditions for RT-PCR program.

Libraries preparation was processed in GeT-PlaGe genomic platform (<https://get.genotoul.fr/en/>; Toulouse, France) and sequenced using Illumina HiSeq3000 sequencer. The raw data was trimmed with trimgalore (version 0.6.5) (<https://github.com/FelixKrueger/TrimGalore>) with cutadapt and FastQC options, and mapped to *M. truncatula* cv. Jemalong A17 reference genome V. 5.0 (Pecrix et al., 2018) using Hisat2 (version 2.1.0) (Kim et al., 2019). Samtools (version 1.9) algorithms fixmate and markdup (Li et al., 2009) were used to clean alignments from duplicated sequences. Reads were counted by HTseq (version 0.9.1) (Anders et al., 2015) using reference GFF file. The count files were normalized and different expression were quantified using DESeq2 algorithm (Love et al., 2014), false-positive hits were filtered using HTS filter (Rau et al., 2013). GO enrichment were done using ErmineJ (Lee et al., 2005) and topGO (Alexa and Rahnenfuhrer 2020) software. RNASeq experiments on F83005.5 (F83) susceptible plants infected by *A. euteiches* and collected nine days after infection are described in (Gaulin et al., 2018).

RNA extraction and qRT-PCR

RNA was extracted using the E.Z.N.A.[®] Plant RNA kit (Omega Bio-tek). For reverse transcription, 1µg of total RNA were used and reactions were performed with the High-Capacity cDNA Reverse Transcription Kit from Applied Biosystems and cDNAs obtained were diluted 10 fold. qPCR reactions were performed as described in (Ramirez-Garcés et al., 2016) and conducted on a QuantStudio 6 (Applied Biosystems) device using the following conditions: 10min at 95°C, followed by 40 cycles of 15s at 95°C and 1min at 60°C. All reactions were conducted in triplicates.

To evaluate *A. euteiches*'s infection level, expression of *Ae* α -tubulin coding gene (*Ae_22AL7226*, (Gaulin et al., 2008)) was analyzed and histone 3-like gene and EF1 α gene of *M. truncatula* (Rey et al., 2013) were used to normalize plant abundance during infection. For *Aphanomyces* infection in plant over-expressing GFP, *AeSSP1256:GFP* or *GFP:MtRH10*, cDNAs from five biological samples were analyzed, given that a sample was a pool of 3 to 5 plants, for each time point, on three independent experiments, representing 45 to 75 transformed plants per construct. *M. truncatula* roots were harvested 7, 14 and 21 dpi. For missense *MtRH10* experiments, downregulation of *MtRH10* gene was first verified using cDNAs from five biological samples, given that a sample was a pool of 5 plants, harvested 21 days post transformation. For *A. euteiches* inoculation, three biological samples were analyzed, given

that a sample was a pool of 3 plants, for each time point, on two independent experiments, representing around 50 transformed missense MtrRH10 plants. Relative expression of *Ae* α -tubulin or MtrRH10 helicase genes were calculated using the $2^{-\Delta\Delta Ct}$ method (Livak and Schmittgen, 2001). For qPCR validation of RNAseq experiment, cDNAs from five biological replicates (pool of three plants) of AeSSP1256-expressing roots were extracted 21 days post transformation. Primers used for qPCR are listed in **Supplemental Table 3**.

Yeast Two Hybrid assays

An ULTimate Y2H™ was carried out by Hybrigenics-services (<https://www.hybrigenics-services.com>) using the native form of AeSSP1256 (20-208 aa) as bait against a library prepared from *M. truncatula* roots infected by *A. euteiches*. The library was prepared by Hybrigenics-services using a mixture of RNA isolated from uninfected *M. truncatula* F83005.5 (+/- 12%), *M. truncatula* infected with *A. euteiches* ATCC201684 harvested one day post infection (+/- 46%) and *M. truncatula* infected with *A. euteiches* harvested six days post infection (+/- 42%). This library is now available to others customers on Hybrigenics-services. For each interaction identified during the screen performed by Hybrigenics (65 millions interaction tested), a 'Predicted Biological Score (PBS)' was given which indicates the reliability of the identified interaction. The PBS ranges from A (very high confidence of the interaction) to F (experimentally proven technical artifacts). In this study we kept eight candidates with a PBS value from 'A and C' for validation.

Analysis of amino acid sequence of MtrRH10

Conserved motifs and domains of DEAD-box RNA helicase were found using ScanProsite tool on ExpASy web site (<https://prosite.expasy.org/scanprosite/>). MtrRH10 putative NLS motif was predicted by cNLS Mapper with a cut-off score of 4.0 (Kosugi et al., 2009), and the putative NES motifs were predicted by NES Finder 0.2 (<http://research.nki.nl/fornerodlab/NES-Finder.htm>) and the NetNES 1.1 Server (la Cour et al., 2004).

Immunoblot analysis

N. benthamiana leaves, infected *M. truncatula* roots or roots of *M. truncatula* composite plants were ground in GTEN buffer (10% glycerol, 25 mM Tris pH 7.5, 1 mM EDTA, 150 mM NaCl) with 0.2% NP-40, 10 mM DTT and protease inhibitor cocktail 1X (Merck; 11697498001).

Supernatants were separated by SDS-PAGE and blotted to nitrocellulose membranes. For GFP and GFP variant fusion proteins detection, anti-GFP from mouse IgG1k (clones 7.1 and 13.1) (Merck; 11814460001) were used when monoclonal Anti-HA antibodies produced in mouse (Merck; H9658) were chosen to detect HA recombinant proteins. After incubation with anti-mouse secondary antibodies coupled to horseradish peroxidase (BioRad; 170-6516), blots were revealed using ECL Clarity kit (BioRad; 170-5060).

Co-immunoprecipitation assay

Co-immunoprecipitation was performed on *N. benthamiana* infiltrated leaves expressing GFP, GFP:MtRH10 or AeSSP1256:HA tagged proteins. Total proteins were extracted with GTEN buffer and quantified by Bradford assay. 50 µg of total proteins were incubated 3H at 4°C with 30 µl of GFP-Trap Agarose beads (Chromotek; gta-20) under gentle agitation for GFP-tagged protein purification. After four washing steps with GTEN buffer containing 0,05 % Tween-20, beads were boiled in SDS loading buffer.

Confocal microscopy

Scanning was performed on a Leica TCS SP8 confocal microscope. For GFP and GFP variant recombinant proteins, excitation wavelengths were 488 nm (GFP) whereas 543 nm were used for RFP variant proteins. Images were acquired with a 40x water immersion lens or a 20x water immersion lens and correspond to Z projections of scanned tissues. All confocal images were analyzed and processed using the Image J software.

Cytological observations of transformed roots

Roots of composite plants expressing GFP, AeSSP1256:GFP, GFP:MtRH10 or RNAi MtRH10 were fixed, polymerized and cutted as described in (Ramirez-Garcés et al., 2016). NDPview2 software was used to observe longitudinal root sections of GFP or missense MtRH10 plants and to measure RAM size. Image J software was used for all others measurements. Average RAM cells size were estimated by measuring all the cells from a same layer from the quiescent center to the RAM boundary. Mean values were then calculated from more than 200 cells. In the elongation zone (EDZ) of GFP, AeSSP1256:GFP or missense MtRH10 roots, cell area and cell perimeter were measured in rectangular selection of approximately 300x600 µm (two selections per root). To obtain a normalized cell perimeter, each cell perimeter is

proportionally recalculated for a of 500 μm^2 area standard cell. To estimate cell shape differences, considering that cortical cells in EDZ of GFP control roots are mostly rectangular, we measured the perimeter bounding rectangle (PBR), which represent the smallest rectangle enclosing the cell. Then we calculated the ratio perimeter / PBR. Rectangular cells have a perimeter / PBR ratio close to 1. Three roots per construct from three independent experiments were used.

FRET / FLIM measurements

For protein-protein interactions, *N. benthamiana* agroinfiltrated leaves were analysed as described in (Tasset et al., 2010). For protein-nucleic acid interactions, samples were treated as described in (Camborde et al., 2017; Escouboué et al., 2019). Briefly, 24 h agroinfiltrated leaf discs were fixed with a 4% (w/v) paraformaldehyde solution. After a permeabilization step of 10 min at 37°C using 200 $\mu\text{g}/\text{ml}$ of proteinase K (Thermo Fisher; 25530049), nucleic acid staining was performed by vacuum-infiltrating a 5 μM of Sytox Orange (Thermo Fisher; S11368) solution. For RNase treatment, foliar discs were incubated 15 min at room temperature with 0.5 mg/ml of RNase A (Merck; R6513) before nucleic acid staining. Then fluorescence lifetime measurements were performed in time domain using a streak camera as described in (Camborde et al., 2017). For each nucleus, fluorescence lifetime of the donor (GFP recombinant protein) was experimentally measured in the presence and absence of the acceptor (Sytox Orange). FRET efficiency (E) was calculated by comparing the lifetime of the donor in the presence (τ_{DA}) or absence (τ_{D}) of the acceptor: $E=1-(\tau_{\text{DA}}) / (\tau_{\text{D}})$. Statistical comparisons between control (donor) and assay (donor + acceptor) lifetime values were performed by Student *t-test*. For each experiment, nine leaf discs collected from three agroinfiltrated leaves were used.

Accession Numbers

Transcriptomic data are available at the National Center for Biotechnology Information (NCBI), on Gene Expression Omnibus (GEO) under accession number [GEO:GSE109500] for RNAseq corresponding to *M. truncatula* roots (F83005.5 line) infected by *A. euteiches* (9 dpi) and Sequence Read Archive (SRA) under accession number PRJNA631662 for RNASeq samples corresponding to *M. truncatula* roots (A17) expressing either a GFP construct or a native AeSSP1256:GFP construct. SRA data will be release upon acceptance of the manuscript.

Supplemental Data

The following supplemental data are available:

Supplemental Figure 1: the nuclear localization of AeSSP1256 is required for biological activity in *M. truncatula* roots

Supplemental Figure 2: invasion of *M. truncatula* roots by the pathogen is unchanged in AeSSP1256 effector-expressing roots

Supplemental Figure 3: CFP:L7RP candidate and AeSSP1256:YFP are in close association

Supplemental Figure 4: AeSSP1256 drives the re-localisation of the nuclear MtRH10 RNA helicase, around the nucleolus in *N. benthamiana* cells

Supplemental Figure 5: Expression of MtRH10 is reduced in *M. truncatula* silenced-roots

Supplemental Figure 6: *M. truncatula* cell morphology is affected in RNAi MtRH10 and AeSSP1256:GFP expressing roots

Supplemental Figure 7: Western blot and confocal analyses on MtRH10-overexpressed roots infected by *A. euteiches*

Supplemental Table 1: RNASeq data of *M. truncatula* roots (A17) expressing either GFP construct or AeSSP1256:GFP construct. **ST1a.** Differentially expressed genes (DE), $p_{adj} < 0,0001$. **ST1b.** Top10 GO of DE. **ST1c.** Venn diagram. **ST1d.** qRT-PCR.

Supplemental Table 2: Yeast two-hybrid screening. **STE2a.** List of putative AeSSP1256 interactors after Y2H screening of *M. truncatula* roots infected by the pathogen. **ST2b.** FRET-FLIM validation of CFP:L7RP candidate

Supplemental Table 3: List of primers used in this study

Contributions

LC designed, performed molecular approaches on AeSSP1256 and wrote the manuscript, AK prepared and analyzed the RNAseq-experiments performed in this study and wrote the manuscript, AJ and LC performed FRET/FLIM analyses, CP and LC developed confocal studies, ALR performed cross and longitudinal sections studies and analyzed roots architecture of the different samples, MJCP prepared and analyzed yeast two hybrid assay, performed candidates cloning. BD analyzed the data and wrote the manuscript. EG conceived, designed, and analyzed the experiments, managed the collaborative work, and wrote the manuscript. All authors read and approved the final manuscript.

Conflict of Interest

The authors declare that they have no conflict of interest.

Acknowledgements

The authors would like to thank the GeT-PlaGe genomic platform (<https://get.genotoul.fr/en/>; Toulouse, France) for RNASeq studies; H. San-Clemente and M. Aguilar for statistical analysis help (LRSV, France); S. Courbier and A. Camon for their assistance in cloning steps. This work was supported by the French Laboratory of Excellence project "TULIP" (ANR-10-LABX-41; ANR-11-IDEX-0002-02) and by the European Union's Horizon 2020 Research and Innovation program under grant agreement No 766048.

References

- Alexa A and Rahnenfuhrer J** (2020). topGO: Enrichment Analysis for Gene Ontology. R package version 2.40.0. .
- Anders, S., Pyl, P.T., and Huber, W.** (2015). HTSeq--a Python framework to work with high-throughput sequencing data. *Bioinformatics* **31**: 166–169.
- Badreddine, I., Lafitte, C., Heux, L., Skandalis, N., Spanou, Z., Martinez, Y., Esquerré-Tugayé, M.T., Bulone, V., Dumas, B., and Bottin, A.** (2008). Cell wall chitosaccharides are essential components and exposed patterns of the phytopathogenic oomycete *Aphanomyces euteiches*. *Eukaryot. Cell* **7**: 1980–1993.
- Boevink, P.C., Wang, X., McLellan, H., He, Q., Naqvi, S., Armstrong, M.R., Zhang, W., Hein, I., Gilroy, E.M., Tian, Z., and Birch, P.R.J.** (2016). A *Phytophthora infestans* RXLR effector targets plant PP1c isoforms that promote late blight disease. *Nat. Commun.* **7**: 10311.
- Boisnard-Lorig, C., Colon-Carmona, a, Bauch, M., Hodge, S., Doerner, P., Bancharel, E., Dumas, C., Haseloff, J., and Berger, F.** (2001). Dynamic analyses of the expression of the HISTONE::YFP fusion protein in arabidopsis show that syncytial endosperm is divided in mitotic domains. *Plant Cell* **13**: 495–509.
- Boisson-Dernier, A., Chabaud, M., Garcia, F., Bécard, G., Rosenberg, C., and Barker, D.G.** (2001). *Agrobacterium rhizogenes*-transformed roots of *Medicago truncatula* for the study of nitrogen-fixing and endomycorrhizal symbiotic associations. *Mol. Plant-Microbe Interact.* **14**: 695–700.
- Bourgeois, B., Hutten, S., Gottschalk, B., Hofweber, M., Richter, G., Sternat, J., Abou-Ajram, C., Göbl, C., Leitinger, G., Graier, W.F., Dormann, D., and Madl, T.** (2020). Nonclassical nuclear localization signals mediate nuclear import of CIRBP. *Proc. Natl. Acad. Sci. U. S. A.* **117**: 8503–8514.
- Camborde, L., Jauneau, A., Brière, C., Deslandes, L., Dumas, B., and Gaulin, E.** (2017). Detection of nucleic acid–protein interactions in plant leaves using fluorescence lifetime imaging microscopy. *Nat. Protoc.* **12**: 1933–1950.
- Camborde, L., Raynaud, C., Dumas, B., and Gaulin, E.** (2019). DNA-Damaging Effectors: New Players in the Effector Arena. *Trends Plant Sci.* **24**: 1094–1101.
- Castello, A., Fischer, B., Eichelbaum, K., Horos, R., Beckmann, B.M., Strein, C., Davey, N.E., Humphreys, D.T., Preiss, T., Steinmetz, L.M., Krijgsveld, J., and Hentze, M.W.** (2012). Insights into RNA Biology from an Atlas of Mammalian mRNA-Binding Proteins. *Cell* **149**: 1393–1406.

- Chong, P.A., Vernon, R.M., and Forman-Kay, J.D.** (2018). RGG/RG Motif Regions in RNA Binding and Phase Separation. *J. Mol. Biol.* **430**: 4650–4665.
- la Cour, T., Kiemer, L., Mølgaard, A., Gupta, R., Skriver, K., and Brunak, S.** (2004). Analysis and prediction of leucine-rich nuclear export signals. *Protein Eng. Des. Sel.* **17**: 527–536.
- Dagdas, Y.F. et al.** (2016). An effector of the irish potato famine pathogen antagonizes a host autophagy cargo receptor. *Elife* **5**.
- Djébali, N. et al.** (2009). Partial Resistance of *Medicago truncatula* to *Aphanomyces euteiches* is associated with protection of the root stele and is controlled by a major QTL rich in proteasome-related genes. *Mol. Plant-Microbe Interact.* **22**: 1043–1055.
- Du, Y., Mpina, M.H., Birch, P.R.J., Bouwmeester, K., and Govers, F.** (2015). *Phytophthora infestans* RXLR effector AVR1 interacts with exocyst component Sec5 to manipulate plant immunity. *Plant Physiol.* **169**: 1975–1990.
- Engler, C., Youles, M., Gruetzner, R., Ehnert, T.M., Werner, S., Jones, J.D.G., Patron, N.J., and Marillonnet, S.** (2014). A Golden Gate modular cloning toolbox for plants. *ACS Synth. Biol.* **3**: 839–843.
- Escouboué, M., Camborde, L., Jauneau, A., Gaulin, E., and Deslandes, L.** (2019). Preparation of plant material for analysis of protein–Nucleic acid interactions by FRET-FLIM. In *Methods in Molecular Biology* (Humana Press Inc.), pp. 69–77.
- Fliegmann, J. et al.** (2013). Lipo-chitooligosaccharidic symbiotic signals are recognized by LysM receptor-like kinase LYR3 in the legume *Medicago truncatula*. *ACS Chem. Biol.* **8**: 1900–1906.
- Fuller-Pace, F. V** (2006). DExD/H box RNA helicases: multifunctional proteins with important roles in transcriptional regulation. *Nucleic Acids Res.* **34**: 4206–4215.
- Gao, X., Yin, C., Liu, X., Peng, J., Chen, D., He, D., Shi, W., Zhao, W., Yang, J., and Peng, Y.-L.** (2019). A glycine-rich protein MoGrp1 functions as a novel splicing factor to regulate fungal virulence and growth in *Magnaporthe oryzae*. *Phytopathol. Res.* **1**: 2.
- Gaulin, E. et al.** (2018). Genomics analysis of *Aphanomyces spp.* identifies a new class of oomycete effector associated with host adaptation. *BMC Biol.* **16**.
- Gaulin, E., Jauneau, A., Villalba, F., Rickauer, M., Esquerré-Tugayé, M.-T., and Bottin, A.** (2002). The CBEL glycoprotein of *Phytophthora parasitica* var-*nicotianae* is involved in cell wall deposition and adhesion to cellulosic substrates. *J. Cell Sci.* **115**: 4565–75.
- Gaulin, E., Madoui, M.-A., Bottin, A., Jacquet, C., Mathé, C., Couloux, A., Wincker, P., and Dumas, B.** (2008). Transcriptome of *Aphanomyces euteiches*: new oomycete putative pathogenicity factors and metabolic pathways. *PLoS One* **3**: e1723.
- Gilman, B., Tijerina, P., and Russell, R.** (2017). Distinct RNA-unwinding mechanisms of DEAD-box and DEAH-box

- RNA helicase proteins in remodeling structured RNAs and RNPs. *Biochem. Soc. Trans.* **45**: 1313–1321.
- Göhre, V., Haag, C., and Feldbrügge, M.** (2013). RNA Biology in Fungal Phytopathogens. *PLoS Pathog.* **9**: e1003617.
- Gouw, M. et al.** (2018). The eukaryotic linear motif resource - 2018 update. *Nucleic Acids Res.* **46**: D428–D434.
- Grefen, C., Donald, N., Hashimoto, K., Kudla, J., Schumacher, K., and Blatt, M.R.** (2010). A ubiquitin-10 promoter-based vector set for fluorescent protein tagging facilitates temporal stability and native protein distribution in transient and stable expression studies. *Plant J.* **64**: 355–365.
- Haas, B.J. et al.** (2009). Genome sequence and analysis of the Irish potato famine pathogen *Phytophthora infestans*. *Nature* **461**: 393–398.
- He, Q., McLellan, H., Hughes, R.K., Boevink, P.C., Armstrong, M., Lu, Y., Banfield, M.J., Tian, Z., and Birch, P.R.J.** (2019). *Phytophthora infestans* effector SFI3 targets potato UBK to suppress early immune transcriptional responses. *New Phytol.* **222**: 438–454.
- Huang, C.-K., Huang, L.-F., Huang, J.-J., Wu, S.-J., Yeh, C.-H., and Lu, C.-A.** (2010). A DEAD-Box Protein, AtRH36, is Essential for Female Gametophyte Development and is Involved in rRNA Biogenesis in *Arabidopsis*. *Plant Cell Physiol.* **51**: 694–706.
- Huang, C.-K., Shen, Y.-L., Huang, L.-F., Wu, S.-J., Yeh, C.-H., and Lu, C.-A.** (2016). The DEAD-Box RNA Helicase AtRH7/PRH75 Participates in Pre-rRNA Processing, Plant Development and Cold Tolerance in *Arabidopsis*. *Plant Cell Physiol.* **57**: 174–191.
- Jankowsky, E.** (2011). RNA helicases at work: Binding and rearranging. *Trends Biochem. Sci.* **36**: 19–29.
- Jarmoskaite, I. and Russell, R.** (2011). DEAD-box proteins as RNA helicases and chaperones. *Wiley Interdiscip. Rev. RNA* **2**: 135–52.
- Judelson, H.S.** (2017). Metabolic Diversity and Novelty in the Oomycetes. *Annu. Rev. Microbiol.* **71**: annurev-micro-090816-093609.
- Kamoun, S. et al.** (2015). The Top 10 oomycete pathogens in molecular plant pathology. *Mol. Plant Pathol.* **16**: 413–434.
- Kim, D., Paggi, J.M., Park, C., Bennett, C., and Salzberg, S.L.** (2019). Graph-based genome alignment and genotyping with HISAT2 and HISAT-genotype. *Nat. Biotechnol.* **37**: 907–915.

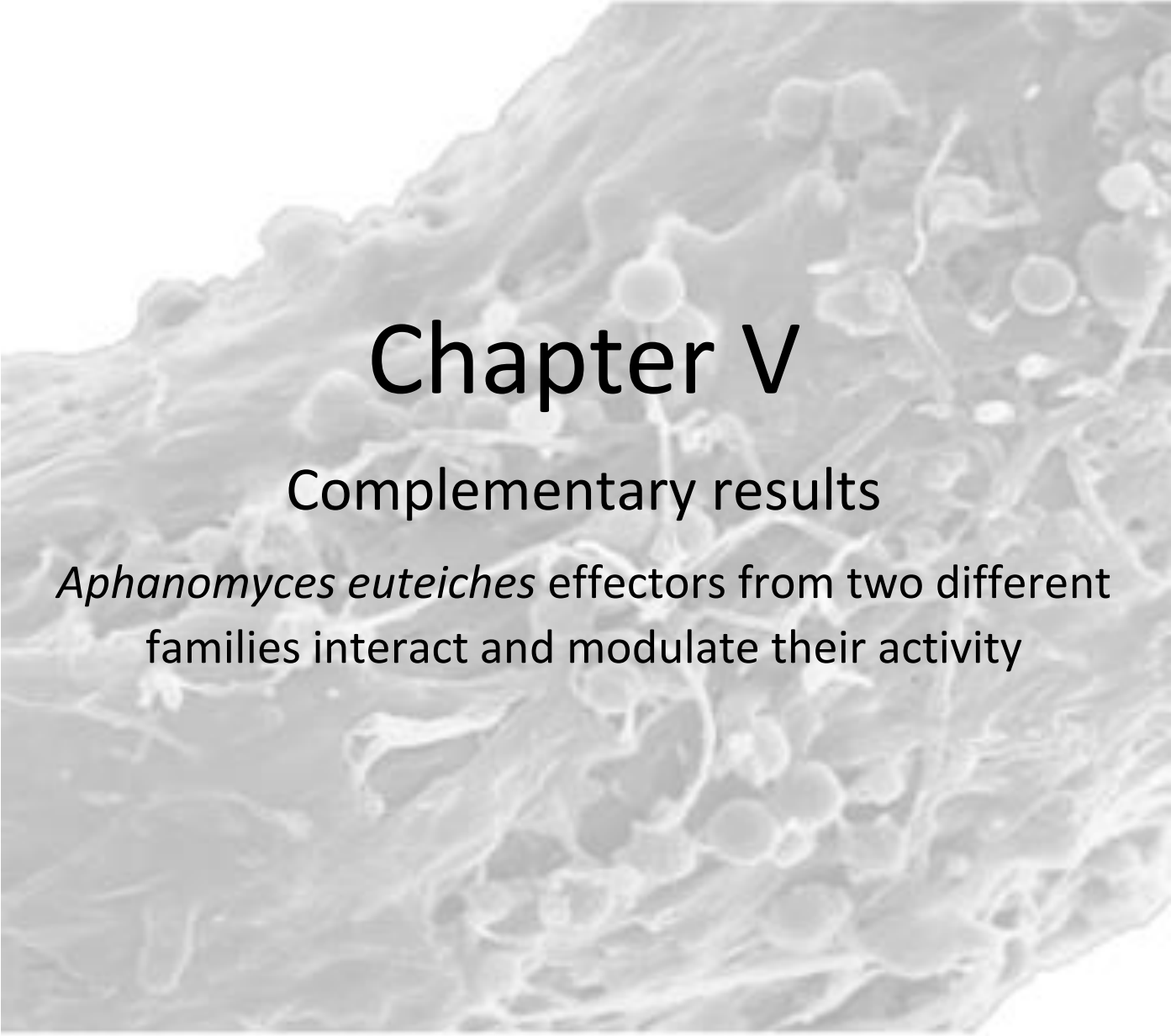
- King, S.R.F., McLellan, H., Boevink, P.C., Armstrong, M.R., Bukharova, T., Sukarta, O., Win, J., Kamoun, S., Birch, P.R.J., and Banfield, M.J.** (2014). *Phytophthora infestans* RXLR effector PexRD2 interacts with host MAPKKK ϵ to suppress plant immune signaling. *Plant Cell* **26**: 1345–59.
- Kosugi, S., Hasebe, M., Tomita, M., and Yanagawa, H.** (2009). Systematic identification of cell cycle-dependent yeast nucleocytoplasmic shuttling proteins by prediction of composite motifs. *Proc. Natl. Acad. Sci. U. S. A.* **106**: 10171–10176.
- Langin, G., Gouguet, P., and Üstün, S.** (2020). Microbial Effector Proteins – A Journey through the Proteolytic Landscape. *Trends Microbiol.*
- Lee, H.K., Braynen, W., Keshav, K., and Pavlidis, P.** (2005). ErmineJ: Tool for functional analysis of gene expression data sets. *BMC Bioinformatics* **6**: 269.
- Li, D., Liu, H., Zhang, H., Wang, X., and Song, F.** (2008). OsBIRH1, a DEAD-box RNA helicase with functions in modulating defence responses against pathogen infection and oxidative stress. *J. Exp. Bot.* **59**: 2133–2146.
- Li, H., Handsaker, B., Wysocker, A., Fennell, T., Ruan, J., Homer, N., Marth, G., Abecasis, G., and Durbin, R.** (2009). The Sequence Alignment/Map format and SAMtools. *Bioinformatics* **25**: 2078–2079.
- Liu, T. et al.** (2014). Unconventionally secreted effectors of two filamentous pathogens target plant salicylate biosynthesis. *Nat. Commun.* **5**: 4686.
- Liu, Y. and Imai, R.** (2018). Function of plant DEXD/H-Box RNA helicases associated with ribosomal RNA biogenesis. *Front. Plant Sci.* **9**.
- Livak, K.J. and Schmittgen, T.D.** (2001). Analysis of relative gene expression data using real-time quantitative PCR and the 2- $\Delta\Delta$ CT method. *Methods* **25**: 402–408.
- Love, M.I., Huber, W., and Anders, S.** (2014). Moderated estimation of fold change and dispersion for RNA-seq data with DESeq2. *Genome Biol.* **15**: 550.
- Matsumura, Y. et al.** (2016). A genetic link between epigenetic repressor AS1-AS2 and a putative small subunit processome in leaf polarity establishment of *Arabidopsis*. *Biol. Open* **5**: 942–954.
- McGowan, J. and Fitzpatrick, D.A.** (2017). Genomic, Network, and Phylogenetic Analysis of the Oomycete Effector Arsenal. *mSphere* **2**.
- McLellan, H., Boevink, P.C., Armstrong, M.R., Pritchard, L., Gomez, S., Morales, J., Whisson, S.C.,**

- Beynon, J.L., and Birch, P.R.J.** (2013). An RxLR Effector from *Phytophthora infestans* Prevents Re-localisation of Two Plant NAC Transcription Factors from the Endoplasmic Reticulum to the Nucleus. **9**.
- Nicaise, V., Joe, A., Jeong, B.R., Korneli, C., Boutrot, F., Westedt, I., Staiger, D., Alfano, J.R., and Zipfel, C.** (2013). *Pseudomonas* HopU1 modulates plant immune receptor levels by blocking the interaction of their mRNAs with GRP7. *EMBO J.* **32**: 701–712.
- O'Day, C.** (1996). 18S rRNA processing requires the RNA helicase-like protein Rrp3. *Nucleic Acids Res.* **24**: 3201–3207.
- Ohbayashi, I., Lin, C.Y., Shinohara, N., Matsumura, Y., Machida, Y., Horiguchi, G., Tsukaya, H., and Sugiyama, M.** (2017). Evidence for a role of ANAC082 as a ribosomal stress response mediator leading to growth defects and developmental alterations in *Arabidopsis*. *Plant Cell* **29**: 2644–2660.
- Ohbayashi, I. and Sugiyama, M.** (2018). Plant Nucleolar Stress Response, a New Face in the NAC-Dependent Cellular Stress Responses . *Front. Plant Sci.* **8**: 2247.
- Ohtani, M., Demura, T., and Sugiyama, M.** (2013). *Arabidopsis* ROOT INITIATION DEFECTIVE1, a DEAH-Box RNA Helicase Involved in Pre-mRNA Splicing, Is Essential for Plant Development. *Plant Cell* **25**: 2056–2069.
- Ozdilek, B.A., Thompson, V.F., Ahmed, N.S., White, C.I., Batey, R.T., and Schwartz, J.C.** (2017). Intrinsically disordered RGG/RG domains mediate degenerate specificity in RNA binding. *Nucleic Acids Res.* **45**: 7984–7996.
- Pecrix, Y. et al.** (2018). Whole-genome landscape of *Medicago truncatula* symbiotic genes. *Nat. Plants* **4**: 1017–1025.
- Pedersen, C. et al.** (2012). Structure and evolution of barley powdery mildew effector candidates. *BMC Genomics* **13**: 694.
- Pennington, H.G. et al.** (2019). The fungal ribonuclease-like effector protein CSEP0064/BEC1054 represses plant immunity and interferes with degradation of host ribosomal RNA. *PLOS Pathog.* **15**: e1007620.
- Pfister, A.S.** (2019). Emerging role of the nucleolar stress response in autophagy. *Front. Cell. Neurosci.* **13**: 156.
- Qiao, Y., Shi, J., Zhai, Y., Hou, Y., and Ma, W.** (2015). *Phytophthora* effector targets a novel component

- of small RNA pathway in plants to promote infection. *Proc. Natl. Acad. Sci. U. S. A.* **112**: 5850–5855.
- Rajyaguru, P. and Parker, R.** (2012). RGG motif proteins: Modulators of mRNA functional states. *Cell Cycle* **11**: 2594–2599.
- Ramirez-Garcés, D., Camborde, L., Pel, M.J.C., Jauneau, A., Martinez, Y., Néant, I., Leclerc, C., Moreau, M., Dumas, B., and Gaulin, E.** (2016). CRN13 candidate effectors from plant and animal eukaryotic pathogens are DNA-binding proteins which trigger host DNA damage response. *New Phytol.* **210**.
- Rau, A., Gallopin, M., Celeux, G., and Jaffrézic, F.** (2013). Data-based filtering for replicated high-throughput transcriptome sequencing experiments. *Bioinformatics* **29**: 2146–2152.
- Rey, T., Laporte, P., Bonhomme, M., Jardinaud, M.-F., Huguet, S., Balzergue, S., Dumas, B., Niebel, A., and Jacquet, C.** (2016). MtNF-YA1, A Central Transcriptional Regulator of Symbiotic Nodule Development, Is Also a Determinant of *Medicago truncatula* Susceptibility toward a Root Pathogen. *Front. Plant Sci.* **7**: 1837.
- Rey, T., Nars, A., Bonhomme, M., Bottin, A., Huguet, S., Balzergue, S., Jardinaud, M.-F., Bono, J.-J., Cullimore, J., Dumas, B., Gough, C., and Jacquet, C.** (2013). NFP, a LysM protein controlling Nod factor perception, also intervenes in *Medicago truncatula* resistance to pathogens. *New Phytol.* **198**: 875–886.
- Rodenburg, S.Y.A., de Ridder, D., Govers, F., and Seidl, M.F.** (2020). Oomycete metabolism is highly dynamic and reflects lifestyle adaptations (Cold Spring Harbor Laboratory).
- Rodríguez-Kessler, M., Baeza-Montañez, L., García-Pedrajas, M.D., Tapia-Moreno, A., Gold, S., Jiménez-Bremont, J.F., and Ruiz-Herrera, J.** (2012). Isolation of UmRrm75, a gene involved in dimorphism and virulence of *Ustilago maydis*. *Microbiol. Res.* **167**: 270–282.
- Sáez-Vásquez, J. and Delseny, M.** (2019). Ribosome biogenesis in plants: From functional 45S ribosomal DNA organization to ribosome assembly factors. *Plant Cell* **31**: 1945–1967.
- Schorneck, S., van Damme, M., Bozkurt, T.O., Cano, L.M., Smoker, M., Thines, M., Gaulin, E., Kamoun, S., and Huitema, E.** (2010). Ancient class of translocated oomycete effectors targets the host nucleus. *Proc. Natl. Acad. Sci. U. S. A.* **107**: 17421–6.
- Schütz, P. et al.** (2010). Comparative Structural Analysis of Human DEAD-Box RNA Helicases. *PLoS One* **5**: e12791.
- Sekiguchi, T., Hayano, T., Yanagida, M., Takahashi, N., and Nishimoto, T.** (2006). NOP132 is required

- for proper nucleolus localization of DEAD-box RNA helicase DDX47. *Nucleic Acids Res.* **34**: 4593–4608.
- Shaw, P. and Brown, J.** (2012). Nucleoli: Composition, function, and dynamics. *Plant Physiol.* **158**: 44–51.
- Song, T., Ma, Z., Shen, D., Li, Q., Li, W., Su, L., Ye, T., Zhang, M., Wang, Y., and Dou, D.** (2015). An Oomycete CRN Effector Reprograms Expression of Plant HSP Genes by Targeting their Promoters. *PLoS Pathog.* **11**: 1–30.
- Stam, R., Jupe, J., Howden, A.J.M., Morris, J. a., Boevink, P.C., Hedley, P.E., and Huitema, E.** (2013b). Identification and Characterisation CRN Effectors in *Phytophthora capsici* Shows Modularity and Functional Diversity. *PLoS One* **8**: e59517.
- Tabima, J.F. and Grünwald, N.J.** (2019). *effectR* : An Expandable R Package to Predict Candidate RxLR and CRN Effectors in Oomycetes Using Motif Searches. *Mol. Plant-Microbe Interact.* **32**: 1067–1076.
- Tasset, C., Bernoux, M., Jauneau, A., Pouzet, C., Brière, C., Kieffer-Jacquiod, S., Rivas, S., Marco, Y., and Deslandes, L.** (2010). Autoacetylation of the *Ralstonia solanacearum* effector PopP2 targets a lysine residue essential for RRS1-R-mediated immunity in arabidopsis. *PLoS Pathog.* **6**.
- Thandapani, P., O'Connor, T.R., Bailey, T.L., and Richard, S.** (2013). Defining the RGG/RG Motif. *Mol. Cell* **50**: 613–623.
- Wang, D., Qin, B., Li, X., Tang, D., Zhang, Y., Cheng, Z., and Xue, Y.** (2016). Nucleolar DEAD-Box RNA Helicase TOGR1 Regulates Thermotolerant Growth as a Pre-rRNA Chaperone in Rice. *PLoS Genet.* **12**.
- Wang, H., Gao, X., Huang, Y., Yang, J., and Liu, Z.R.** (2009). P68 RNA helicase is a nucleocytoplasmic shuttling protein. *Cell Res.* **19**: 1388–1400.
- Wang, S. et al.** (2019). *Phytophthora infestans* RXLR effectors act in concert at diverse subcellular locations to enhance host colonization. *J. Exp. Bot.* **70**: 343–356.
- van West, P. and Beakes, G.W.** (2014). Animal pathogenic Oomycetes. *Fungal Biol.* **118**: 525–526.
- Wieckowski, Y. and Schiefelbein, J.** (2012). Nuclear ribosome biogenesis mediated by the DIM1A rRNA dimethylase is required for organized root growth and epidermal patterning in *Arabidopsis*. *Plant Cell* **24**: 2839–2856.

- Wirthmueller, L. et al.** (2018). *Arabidopsis* downy mildew effector HaRxL106 suppresses plant immunity by binding to RADICAL-INDUCED CELL DEATH1. *New Phytol.* **220**: 232–248.
- Xiong, Q., Ye, W., Choi, D., Wong, J., Qiao, Y., Tao, K., Wang, Y., and Ma, W.** (2014). *Phytophthora* Suppressor of RNA Silencing 2 Is a Conserved RxLR Effector that Promotes Infection in Soybean and *Arabidopsis thaliana*. *Mol. Plant-Microbe Interact.* **27**: 1379–1389.
- Yang, X., Yang, M., Deng, H., and Ding, Y.** (2018). New Era of Studying RNA Secondary Structure and Its Influence on Gene Regulation in Plants. *Front. Plant Sci.* **9**: 671.
- Zamil, M.S. and Geitmann, A.** (2017). The middle lamella—more than a glue. *Phys. Biol.* **14**: 015004.
- Zhang, M., Li, Q., Liu, T., Liu, L., Shen, D., Zhu, Y., Liu, P., Zhou, J.-M., and Dou, D.** (2015). Two Cytoplasmic Effectors of *Phytophthora sojae* Regulate Plant Cell Death via Interactions with Plant Catalases. *Plant Physiol.* **167**: 164–175.

A scanning electron micrograph (SEM) showing a dense network of fungal hyphae. The hyphae are thin, thread-like structures that branch and interweave, creating a complex, porous-looking structure. The background is a light gray, and the hyphae are a slightly darker gray, highlighting their intricate morphology.

Chapter V

Complementary results

Aphanomyces euteiches effectors from two different families interact and modulate their activity

Complementary results: *Aphanomyces euteiches* effectors from two different families interact and modulate their activity.

As previously reported in Chapter V, in order to find proteins targeted by AeSSP1256, we submitted the mature form (without signal peptide) of the AeSSP1256 protein as a bait for yeast two-hybrid screening (Y2H) using a cDNA library generated from *A. euteiches* infected *Medicago* roots (see Chapter V). Results are listed in **table 1**. Eight *Medicago truncatula* genes were reported as potential protein targets and we revealed that two of them, a DEAD-box RNA helicase named MtrRH10 and a L7 ribosomal protein physically interact with AeSSP1256. We then characterized the interaction between MtrRH10 helicase and AeSSP1256 to decipher their role on plant resistance during *A. euteiches* infection (see Chapter V).

Interestingly one gene from *A. euteiches* was also found as a putative partner of AeSSP1256. Surprisingly, this gene encodes a CRN13 Crinkler effector, composed by two subdomains (known as DFA and DDC) in the C-terminal part of the protein (see Chapter I-4.3 Figure 9). All the positive clones sequenced in the Y2H screen hit with the DFA subdomain of AeCRN13. We already have functionally characterized this AeCRN13 effector (Ramirez-Garcés et al., 2016), which is known to enhance *N. benthamiana* susceptibility to *P. capsici* infection and has genotoxic effects when transiently expressed in plant cells. Even without predicted NLS, AeCRN13 accumulates in host cell nuclei, binds plant DNA thanks to an HNH-nuclease like domain (part of the DFA subdomain) when transiently expressed in *N. benthamiana* leaves. AeCRN13 triggers H2Ax phosphorylation of a marker of DNA-Damage Repair pathway (DDR), and upregulated the expression of numerous genes of the DDR pathway.

Name	Gene number	Pfam domains	Potential function
lecithin retinol acyltransferase	Medtr7g117750.1	LRAT	Involved in Vitamin A metabolism
nucleosome assembly protein	Medtr2g099940.1	NAP	acts as histone chaperones, may be involved in regulating gene expression
AT rich interactive domain protein	Medtr5g024920.1	ARID; HSP20	binds to DNA, involved in various biological processes, like gene regulation, transcriptional regulation and chromatin structure
DEAD-box ATP-dependent RNA helicase	Medtr5g069330.1	DEAD; Helicase C	possess ATP-dependent helicase activity and RNA-binding property, involved in RNA biogenesis
plant-specific B3-DNA-binding domain protein	Medtr1g021500.2	B3 (2x)	DNA binding domain, transcriptional regulation
endo/excinuclease amino terminal domain protein	Medtr3g466410.1	GIY-YIG	nucleotide excision repair endonuclease activity
carboxy-terminal domain phosphatase-like protein, putative	Medtr7g021190.1	NIF; BRCT	involved in the control of the transcription machinery by inactivation of RNA polymerase-II by dephosphorylation
thaliana 60S ribosomal protein L7	Medtr4g008160.1	Ribosomal_L30 (2x)	DNA and RNA binding domain, regulatory role in the translation machinery
CRN13-Like	Ae9AL5664	DFA	binds DNA, triggers DNA damage

Table 1: List of candidate proteins for interaction with AeSSP1256.

A Yeast-Two Hybrid screening was performed by Hybrigenics Services from cDNA library obtained with *M. truncatula* roots infected or not with *A. euteiches*. This table lists the more confident protein candidates, ranked from A to D. Two proteins have been evidenced to physically interact with AeSSP1256 and are in bold (see Chapter V). AeCRN13 is indicated in bold and red and represents the only gene from *A. euteiches* ranked as a putative partner for AeSSP1256.

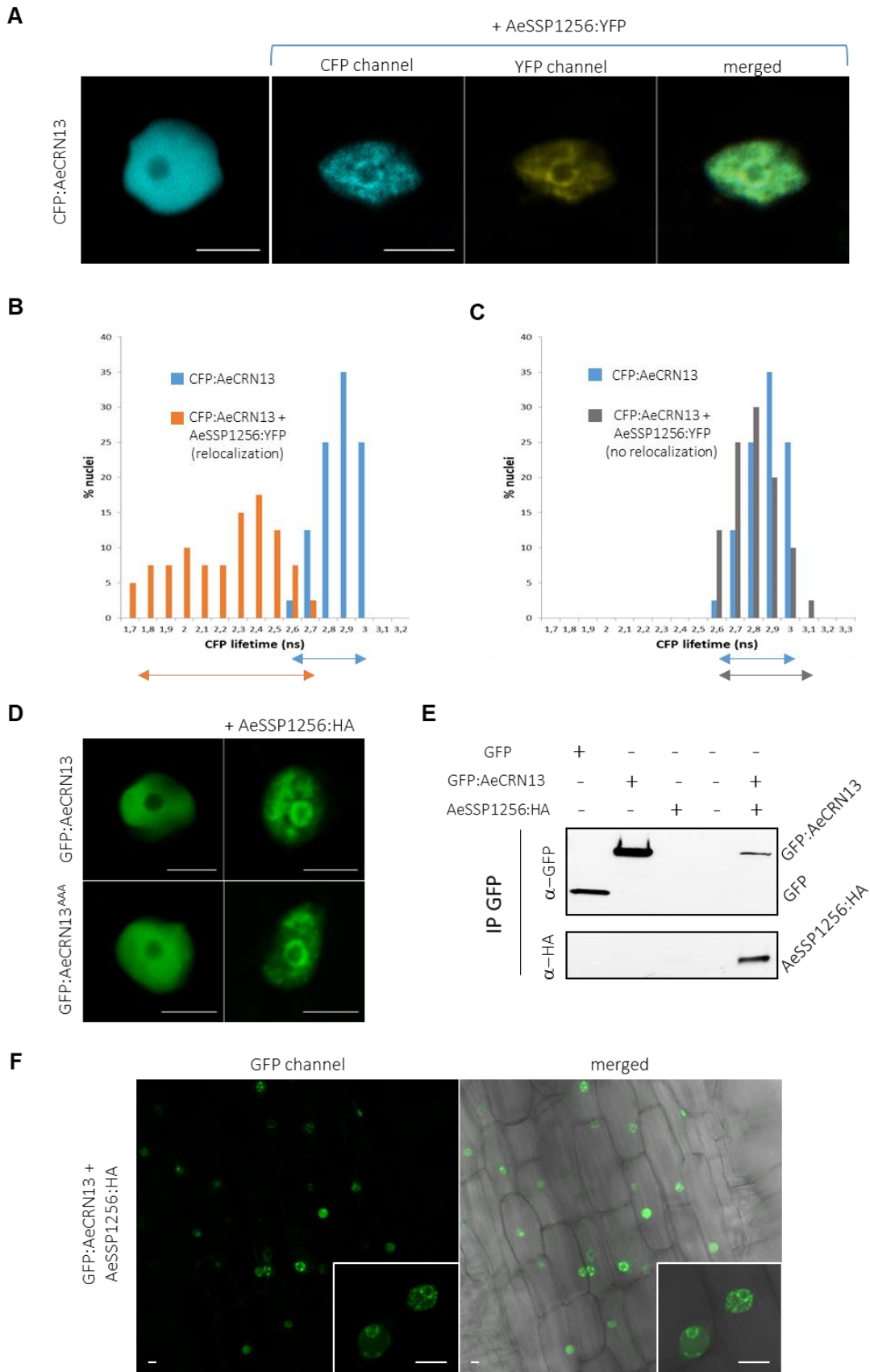


Figure 11: AeCRN13 interacts with AeSSP1256 and is relocalized by the SSP.

(A) Confocal analyses of CFP:AeCRN13 reveal homogenous nuclear localisation when expressed alone in *N. benthamiana* cells, while it is partially relocalized in presence of AeSSP1256:YFP. Pictures were taken 24h post agroinoculation. Scale bars: 10µm. (B) Histograms represent FRET-FLIM results and show the distribution of nuclei (%) according to classes of CFP:AeCRN13 lifetime in absence (blue bars) or presence (orange bars) of AeSSP1256:YFP in nuclei where CFP:AeCRN13 was relocalized. Arrows represent CFP lifetime distribution range. (C) Same experiment than in (B) but in nuclei where CFP:AeCRN13 was not relocalized by AeSSP1256:YFP. In that cases, no significant decrease in CFP lifetime is observed in presence of the acceptor AeSSP1256:YFP. (D) Confocal pictures of *N. benthamiana* leaves expressing GFP:AeCRN13 in presence or absence of AeSSP1256:HA, 24h after agroinoculation. In presence of AeSSP1256:HA, GFP:AeCRN13 is strongly relocalized around nucleolus and in subnuclear compartments. Scale bars: 10 µm. (E) Co-immunoprecipitation assay on agroinoculated *N. benthamiana* leaves expressing GFP:AeCRN13 in presence or absence of AeSSP1256:HA. GFP was used as a negative control. Total protein extract were loaded on GFP beads to trap GFP tagged proteins. After washes and elution, samples were immunoblotted against GFP and HA antibodies. HA blots reveal that AeSSP1256:HA was co-purified with GFP:AeCRN13.

Homodimers of effectors have been reported for CRN family from *Phytophthora sojae* and *Rhizophagus irregularis* (Voß et al., 2018), but the role of this process for infection is still unknown. Therefore we investigated whether AeSSP1256 makes a heterodimer with the genotoxic AeCRN13 effector, the consequence on the DNA damage activity of AeCRN13 and finally on the outcome of an infection.

First, to observe effectors subcellular localization, we co-expressed AeSSP1256:YFP and CFP:AeCRN13 tagged proteins in *N. benthamiana* leaves. One day after agroinfiltration, confocal analyses confirmed the nuclear localization of CFP:AeCRN13 when expressed alone. In contrast, the presence of AeSSP1256:YFP contributes to a partial relocalization around the nucleolus of CFP:AeCRN13, in the area where AeSSP1256 is detected, notably around the nucleolus (**Figure 11A**) in most nuclei analysed (around 65% of nuclei analysed). The partial relocalization of a protein target to the perinucleolar space where AeSS1256 is present was also observed for the MtrRH10 target. The reason why not all CFP:AeCRN13 proteins are relocalized is not known. We suspect that Fluorescent tags could disturb the interaction, or the expression level and/or timing of expression of both partners could play a role.

To confirm the protein-protein interaction we performed a FRET-FLIM assay in order to measure the fluorescence lifetime of the CFP:AeCRN13 proteins in the nucleus, in absence or in presence of AeSSP1256:YFP. In presence of AeSSP1256:YFP, analysis was conducted on nuclei where CFP:AeCRN13 was relocalized. In these nuclei, the CFP lifetime significantly decreases due to FRET effect with AeSSP1256:YFP acceptor, from 2.82 +/- 0.016 ns to 2.14 +/- 0.031 ns, indicating a close association between the two proteins (**Table 2**). The distribution of all the measurements is plotted on **Figure 11B** and clearly shows the shift into shorter CFP lifetime. Moreover, no significant difference in CFP lifetime was observed in nuclei where AeCRN13 is not relocalized in presence of AeSSP1256. Value from 2.82 +/- 0.016 ns in mean when CFP:AeCRN13 is expressed alone and 2.75 +/- 0.02 ns in presence of AeSSP1256:YFP are reported (see **Table 2**). This result is illustrate by the **Figure 11C**. Altogether, these data indicate that the relocalization of AeCRN13 is probably due to its interaction with AeSSP1256.

Donor	Acceptor	τ ^(a)	sem ^(b)	N ^(c)	E ^(d)	^(e) p-value
CFP:AeCRN13	-	2.819	0.016	40	-	-
CFP:AeCRN13	AeSSP1256:YFP	2.138	0.031	40	24	4.59E-32
CFP:AeCRN13	AeSSP1256:YFP NO relocalization	2.750	0.020	40	2.3	0.07

Table 2: FRET-FLIM measurements of CFP:AeCRN13 with or without AeSSP1256:YFP.

τ : mean life-time in nanoseconds (ns). ^(b) s.e.m.: standard error of the mean. ^(c) N: total number of measured nuclei. ^(d) E: FRET efficiency in % : $E=1-(\tau_{DA}/\tau_D)$. ^(e) p-value (Student's *t* test) of the difference between the donor lifetimes in the presence or absence of acceptor.

To confirm the results and to decipher whether the fluorescent tag could perturb the interaction, AeSSP1256 was fused to a triple HA tag, much smaller than the YFP tag (around 5 kDa for the triple HA against 27 kDa for YFP) (cloning is described in the paper from Chapter V). Similar results were obtained when CFP:AeCRN13 was coexpressed with HA-tagged version

of AeSSP1256 where approximately half of observed nuclei harbor a relocalized CFP:AeCRN13 around the nucleolus. Intriguingly, when a GFP:AeCRN13 construct is coexpressed with HA-tagged version of AeSSP1256, more than 90% of observed nuclei harbor a relocalized GFP:AeCRN13 around the nucleolus, and this relocalization appeared stronger than observed with AeSSP1256:YFP (**Figure 11D**). This could be due to different spatial organization and three-dimensional structure of GFP, CFP, YFP and HA tags.

To test whether the DNA binding ability of AeCRN13 could play a role in the interaction with AeSSP1256, we coexpressed in *N. benthamiana* a mutated version of AeCRN13, named AeCRN13^{AAA} (see Ramirez-Garcès et al. 2016), with AeSSP1256:HA. AeCRN13^{AAA} contains three alanine in place of the corresponding Histidine, Asparagine and Histidine of the HNH domain leading to a mutated protein unable to bind nucleic acids and to trigger DNA damage (see (Ramirez-Garcès et al., 2016)). Confocal analyses confirm the strong relocalization of the mutated GFP:AeCRN13^{AAA} in presence of AeSSP1256:HA, suggesting that the HNH domain of AeCRN13 is not involved in the interaction with AeSSP1256 (**Figure 11D**).

To confirm the interaction between both effectors, we performed co-immunoprecipitation (CoIP) assays using total proteins extracted from *N. benthamiana* agroinfiltrated leaves with AeSSP1256:HA and GFP:AeCRN13 constructs. As a control experiment, GFP construct was coexpressed with an AeSSP1256:HA construct. After total protein extraction 24 hours after treatment, samples were purified on GFP beads (protocol is described in the paper from Chapter V), washed, and finally loaded on polyacrylamide gels for immunoblotting. As expected, no AeSSP1256 was detected when only coexpressed with GFP, while GFP antibodies confirmed the presence of the GFP:AeCRN13 proteins (around 65 kDa) and HA antibodies revealed the presence of AeSSP1256:HA proteins (around 25 kDa) when both partners are coexpressed. This data indicates that AeSSP1256:HA was pull down with GFP:AeCRN13 and confirms their interaction (**Figure 11E**).

We then check whether AeSSP1256 and AeCRN13 effectors may also interact in host cells. The co-transformation of *M. truncatula* roots with AeSSP1256:HA and GFP:AeCRN13 constructs is poorly efficient. Nevertheless three weeks after transformation of A17-Jemalong *Medicago* roots, few roots where most nuclei displayed a GFP fluorescence in subnuclear compartments

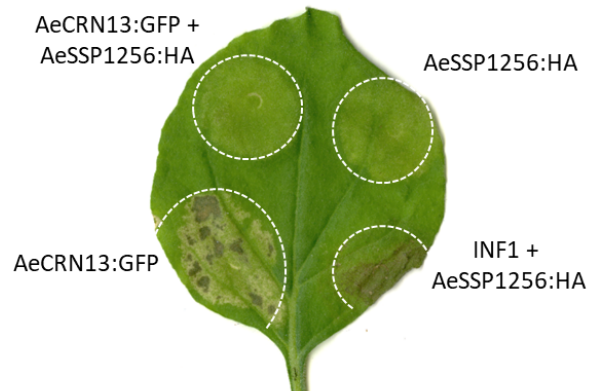
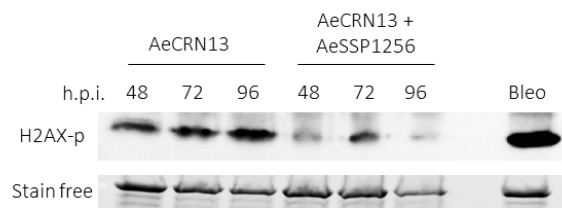
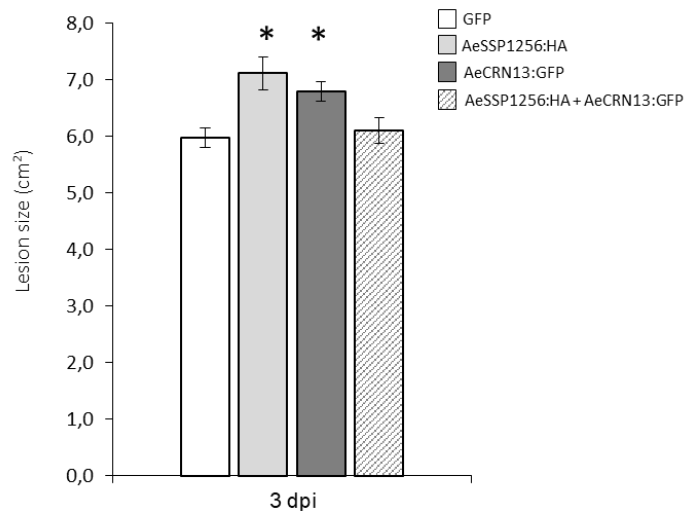
A**B****C**

Figure 12: AeSSP1256 modulates the biological activity/cell death of AeCRN13.

(A) Representative *N. benthamiana* leaf agroinfiltrated with GFP:AeCRN13 alone or in combination with AeSSP1256:HA, AeSSP1256:HA alone or in combination with INF1 (from *P. infestans*). No necrosis occur when AeSSP1256:HA is expressed alone. In contrast, necrosis appear 3 days after infiltration in cells expressing AeCRN13 or INF1+AeSSP1256:HA. Note that In presence of AeSSP1256:HA, cell death induced by AeCRN13 is strongly reduced. Pictures were taken 5 days post agroinoculation. This experiment was repeated 5 times with similar results. (B) Immunoblot showing induction of phosphorylated histone H2AX in *N. benthamiana* cells expressing GFP:AeCRN13 alone or in combination with AeSSP1256:HA at 2, 3 and 4 days post agroinoculation.

Phosphorylated H2AX is strongly reduced in samples expressing both proteins. Bleomycin is a DNA damaging agent and was used as a positive control as reported in (Ramirez-Garcés et al., 2016). Stain free stains total proteins such as Ponceau staining. (C) Histograms represent the lesion size induced by *P. capsici* infection on *N. benthamiana* agroinoculated with GFP, GFP:AeCRN13, AeSSP1256:HA, or GFP:AeCRN13 in combination with AeSSP1256:HA. When expressed alone, both effectors are able to increase *N. benthamiana* susceptibility to *P. capsici* but not when effectors are expressed together. One day post-agroinoculation, the infiltrated leaves were inoculated with *P. capsici* zoospores and symptoms were observed 3 days after infection. Asterisks represent significant differences (Student's t-test; *, $P < 0.05$). Each leaf was infiltrated with GFP on the left side, and another construct on the right side (GFP:AeCRN13, AeSSP1256:HA, or GFP:AeCRN13+AeSSP1256:HA). More than 30 leaves were used for each construct combination.

(around 75%) and showed the AeSSP1256-ring labelling around the nucleolus were detected, suggesting that AeCRN13 is relocalized (**Figure 11F**). Although more transformation events coupled with immunoblots are needed to confirm the presence of both proteins, those data suggest that AeCRN13 is relocalized into the perinucleolar space in the presence of AeSSP1256 when expressed in *Medicago* roots.

To test the impact of the interaction between both effectors, we firstly evaluate whether AeSSP1256 may modulate the genotoxic activity of AeCRN13, as reported for Crinklers effectors from *P. sojae* (Zhang et al., 2015). Agroinfiltration of *N. benthamiana* leaves indicate as we previously observed that AeSSP1256 do not induce necrosis in *N. benthamiana* leaves, even after 10 days (not shown) (**Figure 12A**). In contrast, necrotic symptoms are clearly visible 5 days after agroinfiltration of AeCRN13 C-ter domain in *Nicotiana* (Ramirez-Garcés et al., 2016). In the co-infiltration assay, AeCRN13-induced necrosis is strongly delayed or inhibited (**Figure 12A**). This inhibitory effect seems specific to AeCRN13 as necrosis induced by another necrotic oomycete effector (i.e. INF1 from *Phytophthora infestans*) is not affected by the presence of AeSSP1256 (**Figure 12A**). Then we check DNA damage activity in leaves that co-express both effector by western-blot analysis. We previously observed that AeSSP1256 do not induce the phosphorylation state of the DNA damages Histone2A marker (not shown). As shown on **Figure 12B** the phosphorylation state of the Histone2A marker due to AeCRN13 activity seems to decrease over time in presence of AeSSP1256. Even if western-blot analyses

are required to confirm the presence of both effector upon the time course, these data suggest that AeSSP1256 may affect host DNA damages triggered by AeCRN13.

Since we previously reported that both proteins independently enhance susceptibility to *P. capsici* infection when transiently expressed in *Nicotiana* leaves, we next wonder what could be the effect of the interaction of these two effectors on the plant susceptibility against this pathogen. When each protein is expressed separately in *N. benthamiana* leaves, larger lesions due to *P. capsici* infection are observed than in the infected GFP control infiltrated leaves ((Ramirez-Garcés et al., 2016; Gaulin et al., 2018) and **Figure 12C**). In contrast, when AeSSP1256 and AeCRN13 are co-expressed, lesion size induced by *P. capsici* are not significantly different than in GFP control leaves (**Figure 12C**). These data suggest that AeSSP1256 strongly reduces the biological impact of AeCRN13 in plant.

Altogether, these preliminary results reveal that two effectors from different families, Crinkler and SSPs, can physically interact when expressed *in planta*. Here, it seems that AeSSP1256 acts to reduce AeCRN13 biological effects. Such antagonism interaction was already observed in *P. infestans* with two CRNs (PsCRN63 and PsCRN115) (Zhang et al., 2015).



**General discussion
and
perspectives**

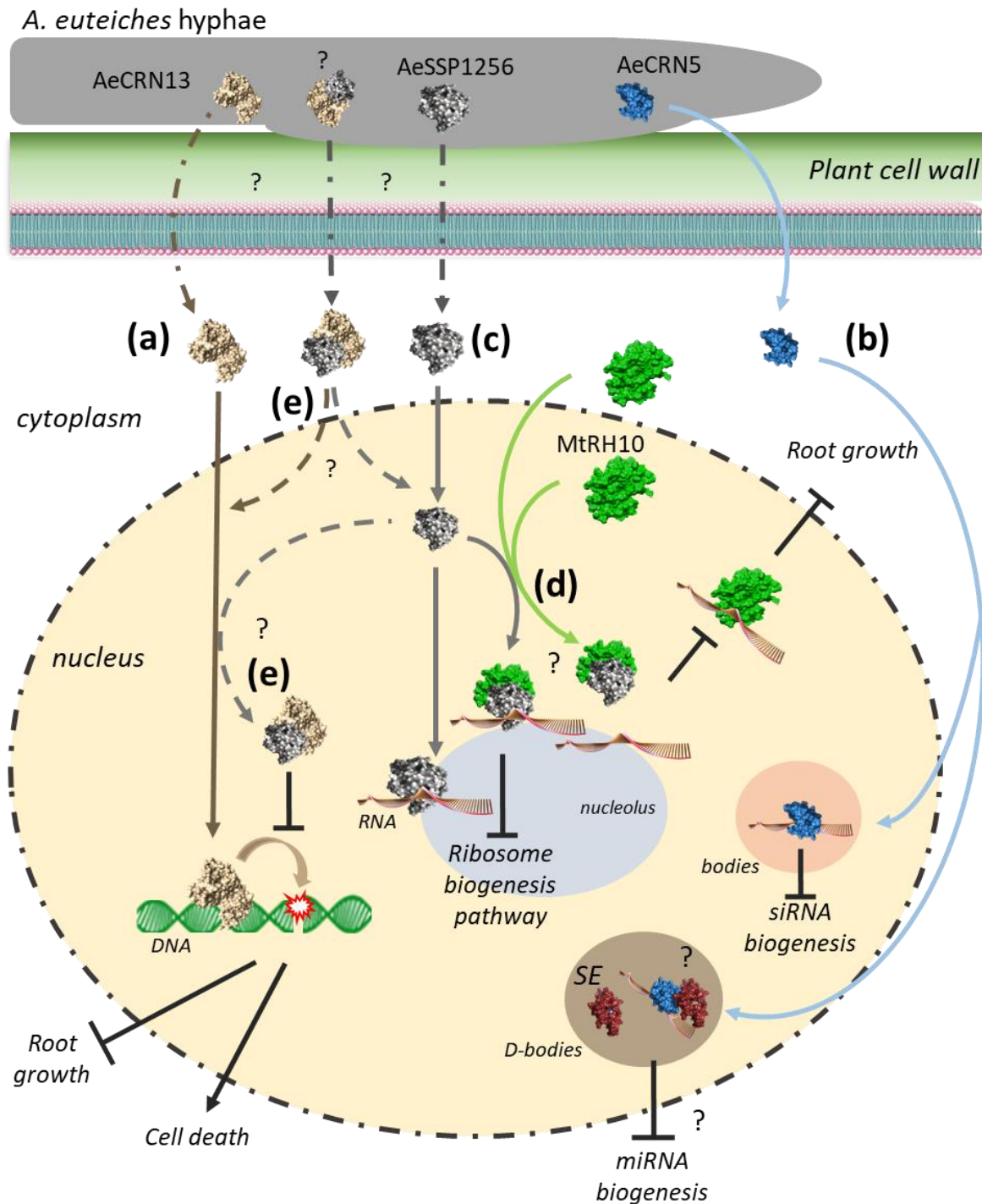


Figure 13: Main results of this PhD work.

(a) AeCRN13 is a DNA damaging effector that impacts root development and triggers cell death. **(b)** AeCRN5 has a functional translocation N-ter domain and targets RNA in nuclear bodies where it perturbs siRNA biogenesis. It could potentially interfere with SE proteins in D-bodies and deregulate miRNA biogenesis. **(c)** After secretion and translocation (unknown mechanism), AeSSP1256 targets nuclear RNA and downregulates genes involved in ribosome biogenesis pathway. **(d)** AeSSP1256 also strongly interacts with a plant RNA helicase involved in meristem development named MtrRH10. This interaction inhibits the RNA-binding activity of the helicase. **(e)** AeSSP1256 also interacts with the DNA damaging effector AeCRN13 leading to a decrease in DNA damages. It is still unclear if this interaction occurs inside the pathogen, during translocation, or inside host cells. Straight lines represent confirmed processes. Dotted lines indicate putative processes. Interrogation points indicate unknown mechanisms or hypothetical process.

General discussion and perspectives

The aim of this PhD project is to develop a better understanding of the molecular mechanisms underlying virulence and pathogenicity of the oomycete pathogen of legumes *A. euteiches* that cause root rot diseases. The study was focus on microbial secreted proteins called effectors that target host components to promote pathogen invasion. Knowing that numerous fungal and oomycetes effectors target the nuclear compartment of the host plant we firstly published in TIPS (Camborde et al., 2019) a review that reports on the activity of these eukaryotic effectors (Chapter II). Then we focused our work on AeCRN5, a crinkler effector from *A. euteiches* previously reported as a cell-death inducing protein able to target plant nucleus (Chapter III). Comparative analyses of *Aphanomyces* spp. reveal a large family of small-secreted proteins (SSPs) never reported in oomycetes in contrast to fungal pathogens (Chapter IV). Using various technology an array of SSPs was tested for their effector activity and AeSSP1256 has been selected for functional characterization. We decipher the activity of AeSSP1256 against plant targets and identify that AeSSP1256 can interact with another effector from *A. euteiches*, AeCRN13 previously reported as a DNA-damaging effector (Chapter V). This PhD work showed the biological functions of two pivotal virulence factors of *A. euteiches*. In this chapter, we reflect on the major findings of this study and discuss future strategies to pursue our work on effectors functions.

CRNs and SSPs in oomycetes

The first aim of this work was to deepen knowledge in the repertoire and the mechanisms of action of intracellular effectors from the root pathogenic oomycete *Aphanomyces euteiches*. *A. euteiches* expression data from previous work suggested a large number of CRN coding genes and in opposite the absence of RxLR protein effectors. This result was confirmed by comparative analyses of *A. euteiches*, *A. astaci* and *A. cladogamus* genomes performed during this PhD (Chapter IV). In the same time, a study using other bioinformatic criteria detected between 16 to 25 RxLR-like genes in *A. invadans* and *A. astaci* respectively (McGowan and Fitzpatrick, 2017). As expected, authors found that 87% of the predicted RxLR proteins are located in Peronosporales species (McGowan and Fitzpatrick, 2017). They also confirm the

large expansion of putative cytoplasmic genes predicted in *Phytophthora* species, with approximately 600 RxLR genes and almost 200 CRNs genes for *P. infestans*, giving a huge number of putative cytoplasmic effectors to achieve infection. In comparison, *A. euteiches* has “only” around 160 CRNs genes. This observation raises question about the arsenal of intracellular effectors secreted by *Aphanomyces* compared to other oomycetes, especially to *Phytophthora* species. Only 2% of the CRN genes were upregulated at 3 and 9 days post inoculation, and 13% upregulated in zoospores as compared to *in vitro* grown mycelium, suggesting that a subset of AeCRN is present at the early stage of *Medicago* infection and that another set of CRN genes seems to be produced at later stages. These results are in accordance with the dynamic expression of CRN genes reported in *Phytophthora* (Stam et al., 2013a), and underlines the relative low number of intracellular effector coding genes induced during host infection to sustain *A. euteiches* development. The genomic and transcriptomic analyses of *A. euteiches* also revealed a large repertoire of small-secreted protein (SSP)-encoding genes that are highly induced during plant infection and not detected in other oomycetes. SSPs are widely present in fungi and are involved in the interaction between host and mutualistic or pathogenic microorganisms (Veneault-Fourrey and Martin, 2011; Lo Presti et al., 2015). This finding paves the way to new research on this type of molecules potentially secreted by others oomycetes like *Phytophthora*.

Host nucleic acids as a target: Let's play with DNA

Despite the central role of nucleic acids in a living cell, few example of intracellular effectors able to interact with nucleic acids have been described to date in filamentous eukaryotic microorganisms. In a very recent review on intracellular effectors from filamentous phytopathogens, He and colleagues collected data from the literature describing verified targets of 41 intracellular oomycete effectors and 30 from fungi (He et al., 2020). Only three of these effectors target DNA and among them, two are Crinkler/CRNs proteins. The *Phytophthora sojae* effector CRN108 binds to heat-shock element (HSE) promoters to prevent their expression (Song et al., 2015). This CRN contains an HhH DNA binding domain, widely distributed in DNA repair or synthesis proteins and reported to have sequence-non-specific DNA-binding activity (Pavlov et al., 2002). The other CRN protein, AeCRN13, binds plant DNA thanks to its HNH motif (Ramirez-Garcés et al., 2016) found in more than 500 nucleases or in

bacterial toxins such as colicins, produced by some *E. coli* strains. AeCRN13 trigger DNA-damage of the host cell (**Figure 13a**). The third reported effector is CgEP1 from the fungus *Colletotrichum graminicola*, presented as a double-stranded DNA-binding protein that modulates transcriptional activity (Vargas et al., 2016).

DNA binding effectors from animal and plant pathogenic bacteria are also reported (see Chapter II). One of the most known example are the transcription activator-like effector (TALE) proteins. TALE proteins derived from bacteria and are built from tandem repeat units that can be linked to form a string-like structure, able to bind DNA. TALEs are unstable proteins, able to follow the shape of the double helix through a conformational heterogeneity that facilitates macromolecular assembly (Schuller et al., 2019).

Another example of DNA binding effector has been described in root pathogenic cyst nematodes. Cyst nematodes are root endoparasites that infect a wide range of crops. Then, it was reported that GLAND4, an effector secreted by *Heterodera glycines* and *H. schachtii* (parasites of soybean and sugar beet respectively), is a small DNA binding protein that represses gene expression of defense related genes. The C-terminal domain of GLAND4 possesses acidic and hydrophobic amino acids structure similar to those found in TALE proteins (Barnes et al., 2018).

Finally, in the fish oomycete pathogen *Saprolegnia parasitica*, SpHtp3 effector contains a bifunctional nuclease domain and therefore degrades RNA and DNA in host cell nuclei (Trusch et al., 2018).

Then it seems that targeting host DNA could be a common strategy shared by various animal and plant bacterial pathogens, but also nematodes and filamentous eukaryotic pathogens. The role on the pathogenesis depends on the type of DNA-effector interactions. Some DNA binding proteins, such as bacterial TALEs, CRN108 from *Phytophthora* or fungal CgEP1 protein, interfere with transcriptional activity and defense gene expression to manipulate host immunity. For DNA-damaging effectors, the consequences are less clear. Triggering DNA damage perturbs the host cell cycle and subsequently favors the colonization of the tissues. On the other hand, DNA damage can be sensed as a danger signal leading to the induction of defense responses (see Chapter II). Characterized DNA-damaging effectors are expressed at the later stage of infection (such as AeCRN13 and SpHtp3) and could correspond to the switch

to a necrophytic phase of the infection. Future studies on this type of effectors are needed to precise the role of DNA-damaging effectors in the outcome of the infection.

Host nucleic acids as a target: Let's play with RNA

Among the 71 described intracellular effectors from filamentous phytopathogens reported in He et al., 2020, six of them (8%) target RNA trafficking or RNA processing (He et al., 2020). Among them, two effectors from *Phytophthora* sp. stabilize host RNA-binding proteins to regulate mRNA biogenesis and plant immunity (Huang et al., 2017; Wang et al., 2015). Two fungal effectors have been reported to potentially interfere with mRNA processing. One is an RxLR protein from *Magnaporthe oryzae* that interacts with a nucleoporin required for accumulation of PR gene transcripts (Tang et al., 2017). The other is a candidate effector from the wheat rust fungus *Puccinia striiformis* that accumulates in processing bodies where it interacts with a protein involved in mRNA decapping (Petre et al., 2016). Finally, two RxLR effectors from *P. sojae* (PSR1 and PSR2) suppress RNA silencing by interfering with small RNA biogenesis (Qiao et al., 2015; Xiong et al., 2014; Hou et al., 2019). Based on obtained results we can include AeCRN5 and AeSSP1256 in this list.

However, none of these effectors was described to bind directly to RNA. This PhD work showed that AeCRN5 is an RNA-binding protein with modular architecture, comprising a functional translocation N-terminal domain folded as Ubiquitin family proteins, then classified as Ubi1-Header domain according to Zhang et al. (2016). The C-ter domain comprises the DN17 subdomain related to the usual classification based on *P. infestans* sequences (Haas et al., 2009). Interestingly, even if AeCRN5 was not included in the study of Zhang et al. (2016), the C-termini of the closest orthologs were described as REase5 domains, and we assumed after sequence alignment that AeCRN5 is a member of this REase5 family. AeCRN5 C-ter is nuclear localized and this localization is required to trigger necrosis in *N. benthamiana* leaves. When expressed in host cells, AeCRN5 strongly affects root development (**Figure 13b**). In addition to RNA binding ability, we found that it could interfere with PTGS mechanism, but the effect on siRNA accumulation is still unclear and requires additional experiments. This role was described in the oomycete *P. sojae*, with RxLR proteins PSR1 and PSR2. However, the mechanism and the final impact seem different since PSR1 and PSR2 were not reported to

bind RNA, but to interact with RNA binding proteins. PSR1 promotes infection by interacting with PINP1, a DEAD-box RNA helicase, to repress siRNA biogenesis in the plant hosts. PSR2 interacts with dsRNA-binding protein 4 (DRB4), which associates with Dicer-like 4 (DCL4), to inhibit secondary siRNA biogenesis to interfere with trans-kingdom RNAi (Hou et al., 2019).

In addition, we reported preliminary results about the putative localization of AeCRN5 C-ter in D-bodies, a direct or indirect interaction with the SERRATE protein, and then a perturbation in miRNA biogenesis (**Figure 13b**). As discussed in Chapter III, we still need to precise the subnuclear localization of AeCRN5 and to perform quantitative PCR on mature miR sequences to confirm the role of AeCRN5 on miRNA maturation. Additionally, we will construct mutated version of AeCRN5 C-ter domain, with substitution of the five catalytic residues conserved in REase5 domain in alanine amino acid (Zhang et al., 2016). We will then tested its RNA-binding capability, its localization in D-bodies, and expected to obtain a mutant no longer able to interfere with miRNA biogenesis. Additionally, pri-miRNA or mature miRNA analyses (using RT-qPCR) in *M. truncatula* plants infected by *A. euteiches*, or in AeCRN5 overexpressing *M.t* plants could strengthen the role of AeCRN5 on miRNA biogenesis.

Effectors with RNase-like activity and associated with Haustoria (RALPH) are largely detected in barley powdery mildew *Blumeria graminis*, and constitute the so-called RALPH effectors (Pedersen et al., 2012). This effector family contains around 120 candidate genes but few of them have been characterized, and two (BEC1011 and BEC1054) were predicted to adopt a ribonuclease structure but lack the key active amino acid sites necessary for ribonuclease activity, suggesting that these proteins are non-functional ribonucleases (Pliego et al., 2013; Spanu, 2015). Finally, a recent study evidenced the RNase-like fold of BEC1054 and reported its RNA-binding activity. Authors suggest that the role of this effector could be to protect rRNA by inhibiting the action of plant ribosome-inactivating proteins, repressing host cell death, an unviable interaction for this biotrophic fungus (Pennington et al., 2019).

Functional analysis of AeSSP1256 indicates that this SSP is also an RNA-binding protein (RBP) (**Figure 13c**). Like AeCRN5, AeSSP1256 has a subnuclear localization, but with clustered accumulation around the nucleolus, and strongly perturbs the root development of host plant. Additionally, AeSSP1256 interacts with a host ribosomal protein and a DEAD-box RNA helicase. Transcriptomic analyses also indicate a downregulation of ribosomal protein genes implicated in ribosome biogenesis pathway. Thus, ribosome biogenesis and activity seems to be a

common target for various pathogens. For example, in addition to the role of the fungal RALPH effector BEC1054 on plant ribosome-inactivating proteins, the Hs32E03 effector from the nematode *H. schachtii* manipulates host ribosomal biogenesis to promote parasitism. Hs32E03 alters acetylation of histones involved in the transcription of rRNA, a major component of ribosomes, leading to an increase in rRNA levels (Vijayapalani et al., 2018). The additional ribosome synthesis is necessary for nematode-host interaction.

In our study, we reveal that the RNA-binding protein AeSSP1256 interferes with a DEAD-box RNA helicase (named MtrRH10) by inhibiting the RNA binding ability of the helicase (**Figure 13d**). DEAD-box RNA helicases are also targeted by another oomycete effector (PSR1 from *P. sojae*) and represent a common target in mammal and plant-virus interactions, where DEAD-box helicases contribute to innate immune signalling, or can block multiple steps in the viral replication process (Taschuk and Cherry, 2020; Wu and Nagy, 2019). Although we do not know the exact function of MtrRH10 except its implication in *Medicago* roots development (Chapter V), DEAD-box RNA helicases are known to be key players in ribosome assembly and/or in ribosomal protein synthesis in eukaryotes, like in human or in plant, as well as in bacteria (Iost and Jain, 2019; Martin et al., 2013; Liu and Imai, 2018). Future studies will aim to decipher the putative link between ribosomal biogenesis pathway and MtrRH10 activity in *Medicago*. Expression level of the ribosomal genes downregulated in *M. truncatula* expressing AeSSP1256 will be evaluated in the MtrRH10 RNAi plants.

AeSSP1256 is a member of a cluster, which contains 5 other SSP encoding genes. Among them, AeSSP1251 and AeSSP1254 also harbor a NLS sequence and present the same expression profile as AeSSP1256. Hence, it could be interesting to test whether those proteins can interact together and observe their putative synergetic association. Progress in molecular cloning, especially with Golden gate technology, allows to clone longer and multiple sequences.

Target relocalization: “Come together right now over me...”

We reported in Chapter V that AeSSP1256 can strongly relocalize MtrRH10 plant helicase. Additionally, we presented complementary results about AeSSP1256, showing an interaction and relocalization with AeCRN13 (**Figure 13e**).

Target relocalization was already observed for several effectors. The fungal effector PstGSRE1 from *P. striiformis* inhibits the nuclear localization of the ROS-associated transcription factor TaLOL2 in wheat (Qi et al., 2019). In oomycetes, *P. sojae* PsAvh52 recruits a host cytoplasmic transacetylase into nuclear speckles to promote early colonization. In *P. infestans* and *Bremia lactucae*, multiple effectors have been shown to interact with and prevent the nuclear translocation of ER-associated tail-anchored transcription factors (McLellan et al., 2013; Meisrimler et al., 2019).

In *N. benthamiana* leaves, the AeSSP1256-AeCRN13 association reduces AeCRN13 biological effects. Such antagonism interaction was already observed in *P. infestans* with two CRNs (PsCRN63 and PsCRN115) (Zhang et al., 2015). In the *A. euteiches* natural infection, AeSSP1256 and AeCRN13 genes show similar expression profiles, with higher level at later stages of the infection, supporting the idea that both protein could be present at the same time in *Medicago* roots. One role of the AeSSP1256 could be to moderate the effects of AeCRN13, for instance to avoid early cell death. However, later stages of infection should correspond to the switch in a necrotrophic phase, where cell death can occur.

We can not rule out the possibility that AeSSP1256 / AeCRN13 interaction does not occur inside the host cells, but only during the secretion process, for example to avoid CRN13 toxicity against *A. euteiches* DNA. Such association is well described as Effector-Immunity pairs in bacteria (Yang et al., 2018).

AeSSP1256 contains a signal peptide that should lead the secretion outside the microorganism through the conventional pathway. In contrast, as many other CRNs, such signal peptide is absent in AeCRN13, and it is suggested that RxLR or CRNs could be secreted via unconventional secretory pathway (Wang et al., 2017; Amaro et al., 2017). One can suppose that both protein could interact within secreted microbial vesicles that are released from the pathogen and then address to the host cells. Here, both protein transit to reach the nucleus, where they can interact with other components, such as RNA for AeSSP1256, releasing free AeCRN13 that targets host DNA (**Figure 13e**). Such extracellular vesicles (EVs) have been reported in plant-microbe interactions, especially for fungi (for review see (Rizzo et al., 2020)). However, it is still an open question whether mutualistic or parasitic fungi use EVs to deliver effector molecules to plants during interaction. Since preliminary experiments using Transmission Electron Microscopy on infected roots suggest the presence of EVs during *A. euteiches* / *M.*

truncatula infection, one perspective of this study also resides in the identification of the process that allow delivery of the effectors within the plant cells.

Looking for a needle in a haystack

One of the most challenging question about effector research is how to deal with hundreds predicted genes. Although transcriptomic data help to distinguish genes induced during infection and then potentially involved in host interaction, sequence analyses often failed to detect conserved motif related to a biological function, especially for SSP genes.

In our study, AeSSP1256 putative RNA-binding motif was *in silico* identified and allowed us to confirm its affinity for nucleic acids by FRET-FLIM assays, but numerous effectors are devoid of predicted functional domain. Structure prediction of the effector can be an efficient tool to overcome this limitation. A recent study challenged the classification of CRN proteins by combining sequence analyses and structure prediction. Authors determined that most of the CRN C-ter domains displayed two architectural types: an NTPase domain coupled with a nuclease domain of the restriction endonuclease (REase) superfamily and a REase superfamily domain combined with an eukaryote-type protein kinase domain (see Chapter I Figure 4 and (Zhang et al., 2016)). Accordingly, we also predicted REase domain in the Cter of AeCRN5 and then confirm its RNA-binding capacity (Chapter III). Zhang and collaborators proposed that C-ter containing REase domains that primarily act on target cell DNA, could explain the cell-death-causing capacity reported for numerous CRNs (Zhang et al., 2016). They also suggest that some CRN with REases domain have evolved to target RNA (Zhang et al., 2016). Although experimental data are needed to support their hypothesis, future studies on CRNs should include experiments to detect nucleic acid-protein interactions.

The structural prediction of proteins, performed by dedicated server such as i-Tasser or Phyre2, are frequently included in recent studies of effectors. Such prediction analyses were successfully used on CRNs (Voß et al., 2018), RxLR proteins (Deb et al., 2018), bacterial effectors (Dhroso et al., 2018; Borah and Jha, 2019) and fungal SSPs (Zhang et al., 2017; Gong et al., 2020). In this study AeCRN5 structural prediction confirms the putative fold reported by Zhang et al., 2016 for CRNs. Furthermore, some studies using crystallography reported the conserved function of sequence-unrelated proteins. It is well illustrated with *Magnaporthe*

oryzae avirulence and ToxB-like (MAX) effectors. This effector family was identified using NMR spectroscopy to determine the three-dimensional structures of two sequence-unrelated *M. oryzae* effectors (de Guillen et al., 2015). These analyses revealed that both proteins shared highly similar six β -sandwich structures stabilized by a disulfide bridge. Finally, using structural similarity searches, authors found that another effector from *M. oryzae* and an effector of the wheat tan spot pathogen *Pyrenophora tritici-repentis*, named ToxB, harbored the same structures, leading to the identification of the MAX effectors (de Guillen et al., 2015). Recently, using crystallography experiments, structural analyses on MAX effector proteins alone or in complex with their NLRs targets (leucine-rich repeat proteins) provided detailed insights into their recognition mechanisms (Guo et al., 2018). Similarly, crystal structure of the effector AvrLm4–7 of *Leptosphaeria maculans*, the causal agent of stem canker in *Brassica napus* (oilseed rape), was resolved and validated to understand the specificity of recognition by two plant R proteins (Blondeau et al., 2015). In oomycetes, crystal structure of an RxLR effector from *P. capsici* was recently revealed (Zhao et al., 2018).

This PhD work also reveal that effector from distinct family (SSP/CRN) may interact together probably to enhance/repress their activity. Structural modeling of microbial effector will help to predict this protein-protein association that could be not detected by *in silico* data mining.

Several bioinformatics programs dedicated to effector prediction exist, such as EffectorP 2.0 (Sperschneider et al., 2018) or even more recently EffHunter, a tool for fungal effector prediction (Carreón-Anguiano et al., 2020). However, the subcellular localization of the predicted effector within the host cell is still uncertain using this software and functional studies are required. It is experimentally challenging to monitor effector trafficking but recently some studies reported the translocation of effectors from fungi or oomycetes into host cells. In *M. oryzae*, using a long-term time-lapse imaging method, the translocation of a GFP-tagged SSP from a particular infectious area, called Biotrophic Interfacial Complex (BIC), into host cells was evidenced (Nishimura et al., 2016). In oomycetes, it was evidenced by live-cell imaging that the RxLR effector Pi04314 from *P. infestans* was translocated from the haustorium into plant cells (Wang et al., 2017). In *Aphanomyces euteiches*, this kind of experiments is even more challenging since this pathogen doesn't make haustorium or BIC and is not yet transformable.

Thus, another option will be to take advantage of progress in proteomic approaches in order to detect microbial effectors inside the host cells. This approach was used successfully on wheat infected by *Fusarium graminearum* (Fabre et al., 2019). One main limitation in this approach is to distinguish plant compartments from the microorganism, nevertheless plant cytoplasm or nuclei to identify intracellular effectors can be discriminate either by labeling the compartment or by collecting samples using laser-microdissection experiments. Mass spectrometry analysis of the proteins will give a short list of putative intracellular effectors and host targets.

Concluding Remarks and Outlooks

Oomycete and fungal effectors acting as virulence factors are key players in plant-microbe interactions. While *in silico* approaches allow prediction of effector repertoire in numerous fungi and oomycetes, further investigations are required to characterize their activity during host infection. Indeed the exact function of numerous effectors and how that is related to host immunity are still unknown. This PhD study shows that the nuclear compartment of the host plant is a major target for numerous oomycete effectors. While it was recently shown that microbial effector can target different host proteins, this work also shows that effectors from different family can associate and target plant nucleus. These results reveal a new layer of complexity in the mode of action of eukaryotic effectors. More analyses to study the structural relationship between effectors and between effectors and their targets are needed to precise the consequences of these interactions.

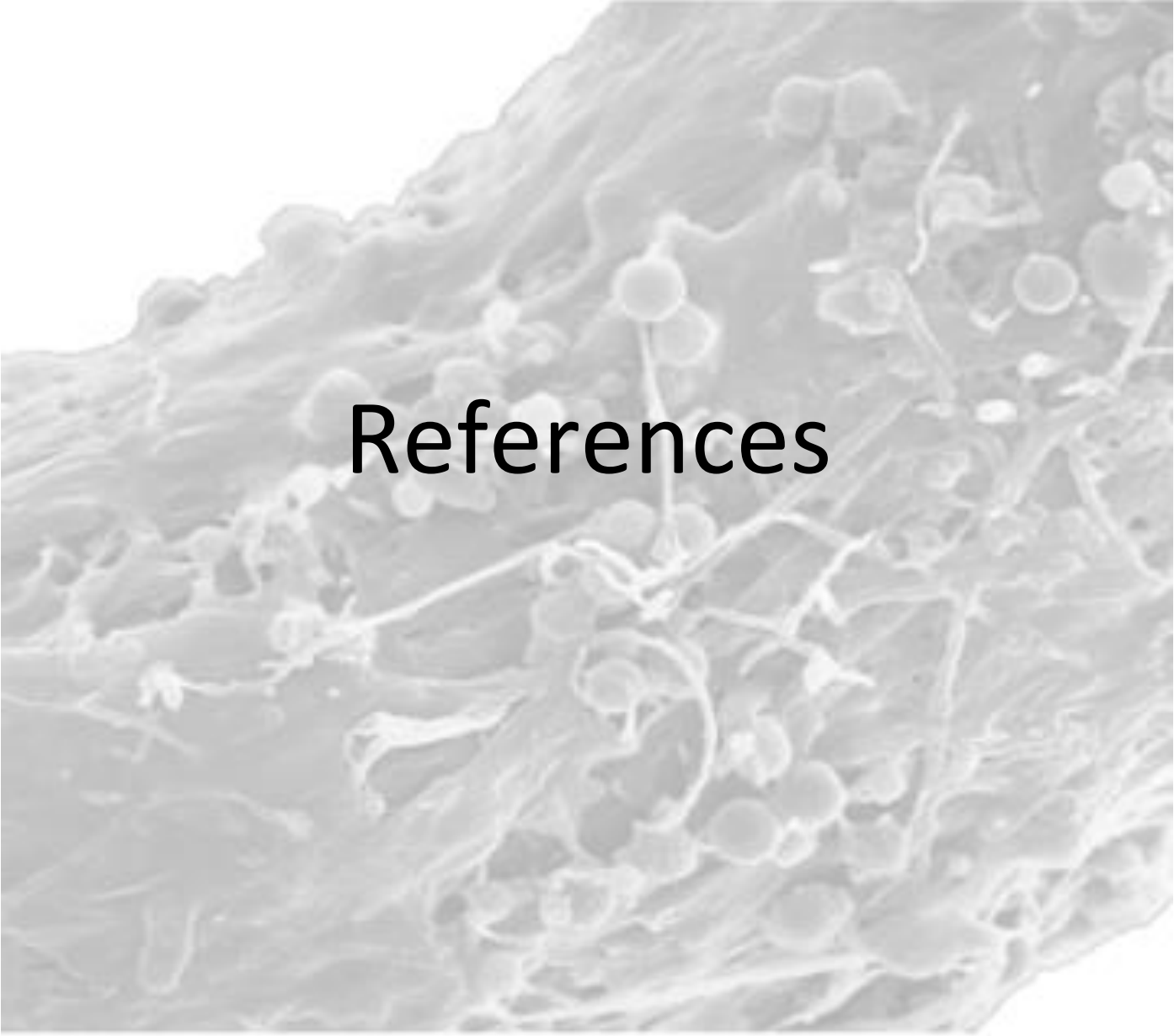
However, in the coming years, the relevance of the choice of candidate effectors for functional characterization will be crucial. Indeed, regarding the results provided by the extensive research on effectors, it seems that every biological process is targeted by one or numerous effectors. This includes sensing, signalling, defence reaction, transcription, RNA processes, DNA integrity, cell development, etc. Hence, in an objective to increase crop plant resistance, it seems difficult to block or regulate tens of molecules that target so many processes. Then, understanding the mechanisms involved in the effector delivery could lead to the development of molecules able to break the bridge between plant cells and pathogen hyphae, preventing the release of those molecules in host cells.

Another way to improve plant fitness is to understand the role and the interaction between pathogens, plants and the other microorganisms present in root close proximity, named plant microbiome (Song et al., 2020; Turner et al., 2013). This represents an emerging topic that needs to go deeper in the molecular interactions between partners.

Since relative few numbers of effector genes are expressed during plant colonisation as AeCRN or AeSSP effectors, numerous microbial effectors could play a role in other situation than host infection, especially in microbe-microbe interactions that occur in the microbiome.

To conclude, one threat resides in the emergence of new diseases due to the acquisition of a new host by an existing plant pathogen. Determining the mechanisms that govern host-specificity is crucial to understand host-switching events and variation in virulence strains. Effectors are part of the molecules involved in this host adaptation. In *Aphanomyces*, our comparative genome analyses between different strains underline variation in their SSP repertoire, suggesting that those molecules could play a role in host adaptation.

Future studies will aim to elucidate the crucial roles in pathogenicity and in microbiome interactions of *A. euteiches* effectors to improve host tolerance against the pathogen.



References

References

- Adeniyi, D.** (2019). Diversity of Cacao pathogens and impact on yield and global production. In *Theobroma Cacao - Deploying Science for Sustainability of Global Cocoa Economy* (IntechOpen).
- Adhikari, B.N., Hamilton, J.P., Zerillo, M.M., Tisserat, N., Lévesque, C.A., and Buell, C.R.** (2013). Comparative Genomics Reveals Insight into Virulence Strategies of Plant Pathogenic Oomycetes. *PLoS One* **8**.
- Allen, T.W. et al.** (2017). Soybean yield loss estimates due to diseases in the United States and Ontario, Canada, from 2010 to 2014. *Plant Heal. Prog.* **18**: 19–27.
- Almeida, F., Rodrigues, M.L., and Coelho, C.** (2019). The Still Underestimated Problem of Fungal Diseases Worldwide. *Front. Microbiol.* **10**: 214.
- Amaro, T.M.M.M., Thilliez, G.J.A., Motion, G.B., and Huitema, E.** (2017). A Perspective on CRN Proteins in the Genomics Age: Evolution, Classification, Delivery and Function Revisited. *Front. Plant Sci.* **8**: 99.
- André Lévesque, C.** (2011). Fifty years of oomycetes-from consolidation to evolutionary and genomic exploration. *Fungal Divers.* **50**: 35–46.
- Badis, Y., Bonhomme, M., Lafitte, C., Huguet, S., Balzergue, S., Dumas, B., and Jacquet, C.** (2015). Transcriptome analysis highlights preformed defences and signalling pathways controlled by the *prAe1* quantitative trait locus (QTL), conferring partial resistance to *Aphanomyces euteiches* in *Medicago truncatula*. *Mol. Plant Pathol.* **16**: 973–986.
- Badreddine, I., Lafitte, C., Heux, L., Skandalis, N., Spanou, Z., Martinez, Y., Esquerré-Tugayé, M.T., Bulone, V., Dumas, B., and Bottin, A.** (2008). Cell wall chitosaccharides are essential components and exposed patterns of the phytopathogenic oomycete *Aphanomyces euteiches*. *Eukaryot. Cell* **7**: 1980–1993.
- Bailey, B.A., Apel-Birkhold, P.C., and Luster, D.G.** (2002). Expression of NEP1 by *Fusarium oxysporum f. sp. erythroxyli* after gene replacement and overexpression using polyethylene glycol-mediated transformation. *Phytopathology* **92**.
- Baldauf, S.L., Roger, A.J., Wenk-Siefert, I., and Doolittle, W.F.** (2000). A kingdom-level phylogeny of eukaryotes based on combined protein data. *Science* (80-.). **290**: 972–977.
- Banuett, F. and Herskowitz, I.** (1996). Discrete developmental stages during teliospore formation in the corn smut fungus, *Ustilago maydis*. *Development* **122**.
- Barnes, S.N., Wram, C.L., Mitchum, M.G., and Baum, T.J.** (2018). The plant-parasitic cyst nematode effector GLAND4 is a DNA-binding protein. *Mol. Plant Pathol.* **19**: 2263–2276.
- Baxter, L. et al.** (2010). Signatures of adaptation to obligate biotrophy in the *Hyaloperonospora arabidopsidis* genome. *Science* (80-.). **330**: 1549–1551.
- Beakes, G.W., Glockling, S.L., and Sekimoto, S.** (2012). The evolutionary phylogeny of the oomycete “fungi.” *Protoplasma* **249**: 3–19.

- Beakes, G.W., Honda, D., and Thines, M.** (2014). 3 Systematics of the Straminipila: Labyrinthulomycota, Hyphochytriomycota, and Oomycota. In *Systematics and Evolution* (Springer Berlin Heidelberg), pp. 39–97.
- Belbahri, L., Calmin, G., Mauch, F., and Andersson, J.O.** (2008). Evolution of the cutinase gene family: Evidence for lateral gene transfer of a candidate *Phytophthora* virulence factor. *Gene* **408**: 1–8.
- Benhamou, N., le Floch, G., Vallance, J., Gerbore, J., Grizard, D., and Rey, P.** (2012). *Pythium oligandrum*: An example of opportunistic success. *Microbiol. (United Kingdom)* **158**: 2679–2694.
- Berg, B., McClougherty, C., Berg, B., and McClougherty, C.** (2014). Decomposer Organisms. In *Plant Litter* (Springer Berlin Heidelberg), pp. 35–52.
- Bhattacharya, S.** (2017). Deadly new wheat disease threatens Europe’s crops. *Nature* **542**: 145–146.
- Van Der Biezen, E.A. and Jones, J.D.G.** (1998). Plant disease-resistance proteins and the gene-for-gene concept. *Trends Biochem. Sci.* **23**: 454–456.
- Birch, P.R.J., Rehmany, A.P., Pritchard, L., Kamoun, S., and Beynon, J.L.** (2006). Trafficking arms: oomycete effectors enter host plant cells. *Trends Microbiol.* **14**: 8–11.
- Blondeau, K. et al.** (2015). Crystal structure of the effector AvrLm4-7 of *Leptosphaeria maculans* reveals insights into its translocation into plant cells and recognition by resistance proteins. *Plant J.* **83**.
- Bonhomme, M. et al.** (2014). High-density genome-wide association mapping implicates an F-box encoding gene in *Medicago truncatula* resistance to *Aphanomyces euteiches*. *New Phytol.* **201**: 1328–1342.
- Bonhomme, M., Fariello, M.I., Navier, H., Hajri, A., Badis, Y., Miteul, H., Samac, D.A., Dumas, B., Baranger, A., Jacquet, C., and Pilet-Nayel, M.L.** (2019). A local score approach improves GWAS resolution and detects minor QTL: application to *Medicago truncatula* quantitative disease resistance to multiple *Aphanomyces euteiches* isolates. *Heredity (Edinb).* **123**.
- Borah, S.M. and Jha, A.N.** (2019). Identification and analysis of structurally critical fragments in HopS2. *BMC Bioinformatics* **19**.
- Brunner, F., Rosahl, S., Lee, J., Rudd, J.J., Geiler, C., Kauppinen, S., Rasmussen, G., Scheel, D., and Nürnberger, T.** (2002). Pep-13, a plant defense-inducing pathogen-associated pattern from *Phytophthora* transglutaminases. *EMBO J.* **21**.
- van den Burg, H.A., Harrison, S.J., Joosten, M.H.A.J., Vervoort, J., and de Wit, P.J.G.M.** (2006). *Cladosporium fulvum* Avr4 Protects Fungal Cell Walls Against Hydrolysis by Plant Chitinases Accumulating During Infection. *Mol. Plant-Microbe Interact.* **19**: 1420–1430.
- Burki, F.** (2014). The eukaryotic tree of life from a global phylogenomic perspective. *Cold Spring Harb. Perspect. Biol.* **6**.

- Caillaud, M.C., Asai, S., Rallapalli, G., Piquerez, S., Fabro, G., and Jones, J.D.G.** (2013). A Downy Mildew Effector Attenuates Salicylic Acid-Triggered Immunity in *Arabidopsis* by Interacting with the Host Mediator Complex. *PLoS Biol.* **11**.
- Caillaud, M.C., Piquerez, S.J.M., Fabro, G., Steinbrenner, J., Ishaque, N., Beynon, J., and Jones, J.D.G.** (2012). Subcellular localization of the Hpa RxLR effector repertoire identifies a tonoplast-associated protein HaRxL17 that confers enhanced plant susceptibility. *Plant J.* **69**: 252–265.
- Camborde, L., Jauneau, A., Brière, C., Deslandes, L., Dumas, B., and Gaulin, E.** (2017). Detection of nucleic acid–protein interactions in plant leaves using fluorescence lifetime imaging microscopy. *Nat. Protoc.* **12**: 1933–1950.
- Camborde, L., Raynaud, C., Dumas, B., and Gaulin, E.** (2019). DNA-Damaging Effectors: New Players in the Effector Arena. *Trends Plant Sci.* **24**: 1094–1101.
- Carreón-Anguiano, K.G., Islas-Flores, I., Vega-Arreguín, J., Sáenz-Carbonell, L., and Canto-Canché, B.** (2020). Effhunter: A tool for prediction of effector protein candidates in fungal proteomic databases. *Biomolecules* **10**.
- Carzaniga, R., Bowyer, P., and O’Connell, R.J.** (2001). Production of extracellular matrices during development of infection structures by the downy mildew *Peronospora parasitica*. *New Phytol.* **149**: 83–93.
- Casadevall, A.** (2017). Don’t Forget the Fungi When Considering Global Catastrophic Biorisks. *Heal. Secur.* **15**: 341–342.
- Cavalier-Smith, T. and Chao, E.E.-Y.** (2006). Phylogeny and megasystematics of phagotrophic heterokonts (kingdom Chromista). *J. Mol. Evol.* **62**: 388–420.
- Chen, J.Y. et al.** (2018). Comparative genomics reveals cotton-specific virulence factors in flexible genomic regions in *Verticillium dahliae* and evidence of horizontal gene transfer from *Fusarium*. *New Phytol.* **217**.
- Chepersong, J., Motaung, T.E., Bellieny-Rabelo, D., and Moleleki, L.N.** (2020). Organize, don’t agonize: Strategic success of *Phytophthora* species. *Microorganisms* **8**: 1–21.
- Choi, Y.J., Lee, S.H., Nguyen, T.T.T., Nam, B., and Lee, H.B.** (2019). Characterization of *Achlya americana* and *A. bisexualis* (Saprolegniales, Oomycota) Isolated from Freshwater Environments in Korea. *Mycobiology* **47**.
- Cobos, R., Calvo-Peña, C., Álvarez-Pérez, J.M., Ibáñez, A., Díez-Galán, A., González-García, S., García-Angulo, P., Acebes, J.L., and Coque, J.J.R.** (2019). Necrotic and cytolytic activity on grapevine leaves produced by nep1-like proteins of *diplodia seriata*. *Front. Plant Sci.* **10**.
- Condon, B.J. et al.** (2013). Comparative genome structure, secondary metabolite, and effector coding capacity across *Cochliobolus* pathogens. *PLoS Genet.* **9**: e1003233.
- Cook, D.E., Mesarich, C.H., and Thomma, B.P.H.J.** (2015). Understanding Plant Immunity as a Surveillance System to Detect Invasion. *Annu. Rev. Phytopathol.* **53**.
- Croll, D. and McDonald, B.A.** (2012). The accessory genome as a cradle for adaptive evolution in pathogens. *PLoS Pathog.* **8**.

- Cuesta Arenas, Y., Kalkman, E.R.I.C., Schouten, A., Dieho, M., Vredenburg, P., Uwumukiza, B., Osés Ruiz, M., and van Kan, J.A.L.** (2010). Functional analysis and mode of action of phytotoxic Nep1-like proteins of *Botrytis cinerea*. *Physiol. Mol. Plant Pathol.* **74**.
- Dagdas, Y.F. et al.** (2016). An effector of the Irish potato famine pathogen antagonizes a host autophagy cargo receptor. *Elife* **5**.
- Dallery, J.F. et al.** (2017). Gapless genome assembly of *Colletotrichum higginsianum* reveals chromosome structure and association of transposable elements with secondary metabolite gene clusters. *BMC Genomics* **18**.
- Damasceno, C.M.B., Bishop, J.G., Ripoll, D.R., Win, J., Kamoun, S., and Rose, J.K.C.** (2008). Structure of the glucanase inhibitor protein (GIP) family from *Phytophthora* species suggests coevolution with plant endo- β -1,3-glucanases. *Mol. Plant-Microbe Interact.* **21**.
- Deb, D., Anderson, R.G., How-Yew-Kin, T., Tyler, B.M., and McDowell, J.M.** (2018). Conserved RxLR effectors from oomycetes *Hyaloperonospora arabidopsidis* and *Phytophthora sojae* suppress PAMP- and effector-triggered immunity in diverse plants. *Mol. Plant-Microbe Interact.* **31**: 374–385.
- Derelle, R., López-García, P., Timpano, H., and Moreira, D.** (2016). A Phylogenomic Framework to Study the Diversity and Evolution of Stramenopiles (=Heterokonts). *Mol. Biol. Evol.* **33**: 2890–2898.
- Derevnina, L. et al.** (2016a). Nine things to know about elicitors. *New Phytol.* **212**.
- Derevnina, L., Petre, B., Kellner, R., Dagdas, Y.F., Sarowar, M.N., Giannakopoulou, A., de la Concepcion, J.C., Chaparro-Garcia, A., Pennington, H.G., van West, P., and Kamoun, S.** (2016b). Emerging oomycete threats to plants and animals. *Philos. Trans. R. Soc. B Biol. Sci.* **371**.
- Desgroux, A. et al.** (2016). Genome-wide association mapping of partial resistance to *Aphanomyces euteiches* in pea. *BMC Genomics* **17**: 124.
- Dhroso, A., Eidson, S., and Korkin, D.** (2018). Genome-wide prediction of bacterial effector candidates across six secretion system types using a feature-based statistical framework. *Sci. Rep.* **8**.
- Diéguez-Urbeondo, J., García, M.A., Cerenius, L., Kozubíková, E., Ballesteros, I., Windels, C., Weiland, J., Kator, H., Söderhäll, K., and Martín, M.P.** (2009). Phylogenetic relationships among plant and animal parasites, and saprotrophs in *Aphanomyces* (Oomycetes). *Fungal Genet. Biol.* **46**: 365–76.
- Djamei, A. et al.** (2011). Metabolic priming by a secreted fungal effector. *Nature* **478**: 395–398.
- Djébali, N. et al.** (2009). Partial Resistance of *Medicago truncatula* to *Aphanomyces euteiches* is associated with protection of the root stele and is controlled by a major QTL rich in proteasome-related genes. *Mol. Plant-Microbe Interact.* **22**: 1043–1055.
- Doehlemann, G. and Hemetsberger, C.** (2013). Apoplastic immunity and its suppression by filamentous plant pathogens. *New Phytol.* **198**: 1001–1016.
- Dong, S. et al.** (2014). Effector specialization in a lineage of the Irish potato famine pathogen.

Science **343**: 552–5.

- Dong, S., Raffaele, S., and Kamoun, S.** (2015). The two-speed genomes of filamentous pathogens: waltz with plants. *Curr. Opin. Genet. Dev.* **35**: 57–65.
- Dou, D. et al.** (2008). Conserved C-Terminal Motifs Required for Avirulence and Suppression of Cell Death by *Phytophthora sojae* effector Avr1b. *Plant Cell Online* **20**: 1118–1133.
- Duplessis, S. et al.** (2011). Obligate biotrophy features unraveled by the genomic analysis of rust fungi. *Proc. Natl. Acad. Sci. U. S. A.* **108**: 9166–9171.
- Dutheil, J.Y., Mannhaupt, G., Schweizer, G., Sieber, C.M.K., Münsterkötter, M., Güldener, U., Schirawski, J., and Kahmann, R.** (2016). A tale of genome compartmentalization: The evolution of virulence clusters in smut fungi. *Genome Biol. Evol.* **8**.
- Evangelisti, E., Govetto, B., Minet-Kebdani, N., Kuhn, M.-L., Attard, A., Ponchet, M., Panabières, F., and Gourgues, M.** (2013). The *Phytophthora parasitica* RXLR effector Penetration-Specific Effector 1 favours *Arabidopsis thaliana* infection by interfering with auxin physiology. *New Phytol.* **199**: 476–489.
- Fabre, F., Bormann, J., Urbach, S., Roche, S., Langin, T., and Bonhomme, L.** (2019). Unbalanced Roles of Fungal Aggressiveness and Host Cultivars in the Establishment of the Fusarium Head Blight in Bread Wheat. *Front. Microbiol.* **10**.
- Faure, C. et al.** (2020). Long-read genome sequence of the sugar beet rhizosphere mycoparasite *Pythium oligandrum*. *G3 Genes, Genomes, Genet.* **10**: 431–436.
- Fawke, S., Doumane, M., and Schornack, S.** (2015). Oomycete Interactions with Plants: Infection Strategies and Resistance Principles. *Microbiol. Mol. Biol. Rev.* **79**: 263–280.
- Feldman, D., Yarden, O., and Hadar, Y.** (2020). Seeking the Roles for Fungal Small-Secreted Proteins in Affecting Saprophytic Lifestyles. *Front. Microbiol.* **11**: 455.
- Fellbrich, G., Romanski, A., Varet, A., Blume, B., Brunner, F., Engelhardt, S., Felix, G., Kemmerling, B., Krzymowska, M., and Nürnberger, T.** (2002). NPP1, a *Phytophthora*-associated trigger of plant defense in parsley and *Arabidopsis*. *Plant J.* **32**.
- Feng, B.-Z., Zhu, X.-P., Fu, L., Lv, R.-F., Storey, D., Tooley, P., and Zhang, X.-G.** (2014). Characterization of necrosis-inducing NLP proteins in *Phytophthora capsici*. *BMC Plant Biol.* **14**: 126.
- Fisher, M.C., Henk, D. a, Briggs, C.J., Brownstein, J.S., Madoff, L.C., McCraw, S.L., and Gurr, S.J.** (2012). Emerging fungal threats to animal, plant and ecosystem health. *Nature* **484**: 186–94.
- Fletcher, K., Gil, J., Bertier, L.D., Kenefick, A., Wood, K.J., Zhang, L., Reyes-Chin-Wo, S., Cavanaugh, K., Tsuchida, C., Wong, J., and Michelmores, R.** (2019). Genomic signatures of heterokaryosis in the oomycete pathogen *Bremia lactucae*. *Nat. Commun.* **10**.
- Frenken, T., Agha, R., Schmeller, D.S., van West, P., and Wolinska, J.** (2019). Biological Concepts for the Control of Aquatic Zoosporic Diseases. *Trends Parasitol.* **35**: 571–582.
- Friesen, T.L., Stukenbrock, E.H., Liu, Z., Meinhardt, S., Ling, H., Faris, J.D., Rasmussen, J.B., Solomon, P.S., McDonald, B.A., and Oliver, R.P.** (2006). Emergence of a new disease as

- a result of interspecific virulence gene transfer. *Nat. Genet.* **38**.
- Gan, P.H.P., Rafiqi, M., Ellis, J.G., Jones, D.A., Hardham, A.R., and Dodds, P.N.** (2010). Lipid binding activities of flax rust AvrM and AvrL567 effectors. *Plant Signal. Behav.* **5**: 1272–1275.
- Gaulin, E. et al.** (2006). Cellulose binding domains of a *Phytophthora* cell wall protein are novel pathogen-associated molecular patterns. *Plant Cell* **18**.
- Gaulin, E. et al.** (2018). Genomics analysis of *Aphanomyces spp.* identifies a new class of oomycete effector associated with host adaptation. *BMC Biol.* **16**.
- Gaulin, E., Bottin, A., and Dumas, B.** (2010). Sterol biosynthesis in oomycete pathogens. *Plant Signal. Behav.* **5**: 258–260.
- Gaulin, E., Haget, N., Khatib, M., Herbert, C., Rickauer, M., and Bottin, A.** (2007). Transgenic sequences are frequently lost in *Phytophthora parasitica* transformants without reversion of the transgene-induced silenced state. *Can. J. Microbiol.* **53**: 152–157.
- Gaulin, E., Jacquet, C., Bottin, A., and Dumas, B.** (2007). Root rot disease of legumes caused by *Aphanomyces euteiches*. *Mol. Plant Pathol.* **8**: 539–548.
- Gaulin, E., Madoui, M.-A., Bottin, A., Jacquet, C., Mathé, C., Couloux, A., Wincker, P., and Dumas, B.** (2008). Transcriptome of *Aphanomyces euteiches*: new oomycete putative pathogenicity factors and metabolic pathways. *PLoS One* **3**: e1723.
- Gijzen, M., Ishmael, C., and Shrestha, S.D.** (2014). Epigenetic control of effectors in plant pathogens. *Front. Plant Sci.* **5**.
- Gijzen, M. and Nürnberger, T.** (2006). Nep1-like proteins from plant pathogens: Recruitment and diversification of the NPP1 domain across taxa. *Phytochemistry* **67**.
- Girard, V., Dieryckx, C., Job, C., and Job, D.** (2013). Secretomes: The fungal strike force. *Proteomics* **13**: 597–608.
- Gisi, U. and Sierotzki, H.** (2015). Oomycete Fungicides: Phenylamides, Quinone Outside Inhibitors, and Carboxylic Acid Amides. In *Fungicide Resistance in Plant Pathogens* (Springer Japan), pp. 145–174.
- Gómez-Gómez, L. and Boller, T.** (2000). FLS2: An LRR receptor-like kinase involved in the perception of the bacterial elicitor flagellin in *Arabidopsis*. *Mol. Cell* **5**.
- Gong, A. dong, Jing, Z. ying, Zhang, K., Tan, Q. qun, Wang, G. liang, and Liu, W. de** (2020). Bioinformatic analysis and functional characterization of the CFEM proteins in maize anthracnose fungus *Colletotrichum graminicola*. *J. Integr. Agric.* **19**.
- de Guillen, K., Ortiz-Vallejo, D., Gracy, J., Fournier, E., Kroj, T., and Padilla, A.** (2015). Structure Analysis Uncovers a Highly Diverse but Structurally Conserved Effector Family in Phytopathogenic Fungi. *PLoS Pathog.* **11**.
- Guo, L., Cesari, S., De Guillen, K., Chalvon, V., Mammri, L., Ma, M., Meusnier, I., Bonnot, F., Padilla, A., Peng, Y.L., Liu, J., and Kroj, T.** (2018). Specific recognition of two MAX effectors by integrated HMA domains in plant immune receptors involves distinct binding surfaces. *Proc. Natl. Acad. Sci. U. S. A.* **115**: 11637–11642.

- Haas, B.J. et al.** (2009). Genome sequence and analysis of the Irish potato famine pathogen *Phytophthora infestans*. *Nature* **461**: 393–398.
- Hamon, C. et al.** (2013). QTL meta-analysis provides a comprehensive view of loci controlling partial resistance to *Aphanomyces euteiches* in four sources of resistance in pea. *BMC Plant Biol.* **13**: 45.
- Hardham, A.R. and Shan, W.** (2009). Cellular and Molecular Biology of *Phytophthora*–Plant Interactions. In *The Mycota* (Springer Berlin Heidelberg), pp. 4–27.
- Hartmann, F.E. and Croll, D.** (2017). Distinct trajectories of massive recent gene gains and losses in populations of a microbial eukaryotic pathogen. *Mol. Biol. Evol.* **34**.
- He, Q., McLellan, H., Boevink, P.C., and Birch, P.R.J.** (2020). All Roads Lead to Susceptibility: The Many Modes of Action of Fungal and Oomycete Intracellular Effectors. *Plant Commun.* **1**.
- Hou, Y. et al.** (2019). A *Phytophthora* Effector Suppresses Trans-Kingdom RNAi to Promote Disease Susceptibility. *Cell Host Microbe* **25**: 153-165.e5.
- Hu, X., Xiao, G., Zheng, P., Shang, Y., Su, Y., Zhang, X., Liu, X., Zhan, S., St. Leger, R.J., and Wang, C.** (2014). Trajectory and genomic determinants of fungal-pathogen speciation and host adaptation. *Proc. Natl. Acad. Sci. U. S. A.* **111**: 16796–16801.
- Huang, J. et al.** (2017). An oomycete plant pathogen reprograms host pre-mRNA splicing to subvert immunity. *Nat. Commun.* **8**: 2051.
- Hughes, T.J. and Grau, C.R.** (2007). *Aphanomyces* root rot or common root rot of legumes. *Plant Heal. Instr.*
- Hulvey, J.P., Padgett, D.E., and Bailey, J.C.** (2007). Species boundaries within *Saprolegnia* (Saprolegniales, Oomycota) based on morphological and DNA sequence data. *Mycologia* **99**: 421–429.
- Iberahim, N.A., Trusch, F., and van West, P.** (2018). *Aphanomyces invadans*, the causal agent of Epizootic Ulcerative Syndrome, is a global threat to wild and farmed fish. *Fungal Biol. Rev.* **32**.
- Iost, I. and Jain, C.** (2019). A DEAD-box protein regulates ribosome assembly through control of ribosomal protein synthesis. *Nucleic Acids Res.* **47**.
- Jashni, M.K., Mehrabi, R., Collemare, J., Mesarich, C.H., and de Wit, P.J.G.M.** (2015). The battle in the apoplast: Further insights into the roles of proteases and their inhibitors in plant–pathogen interactions. *Front. Plant Sci.* **6**.
- Jiang, R.H.Y. and Tyler, B.M.** (2012). Mechanisms and Evolution of Virulence in Oomycetes. *Annu. Rev. Phytopathol.* **50**: 295–318.
- Jones, J.D.G. and Dangl, J.L.** (2006). The plant immune system. *Nature* **444**: 323–329.
- Jones, K.M., Kobayashi, H., Davies, B.W., Taga, M.E., and Walker, G.C.** (2007). How rhizobial symbionts invade plants: The *Sinorhizobium* - *Medicago* model. *Nat. Rev. Microbiol.* **5**.
- Joneson, S., Stajich, J.E., Shiu, S.H., and Rosenblum, E.B.** (2011). Genomic transition to pathogenicity in chytrid fungi. *PLoS Pathog.* **7**.

- Judelson, H.S.** (2012). Dynamics and innovations within oomycete genomes: insights into biology, pathology, and evolution. *Eukaryot. Cell* **11**: 1304–12.
- Judelson, H.S.** (2017). Metabolic Diversity and Novelties in the Oomycetes. *Annu. Rev. Microbiol.* **71**: annurev-micro-090816-093609.
- Judelson, H.S. and Ah-Fong, A.M.V.** (2019). Exchanges at the plant-oomycete interface that influence disease. *Plant Physiol.* **179**: 1198–1211.
- Judelson, H.S. and Senthil, G.** (2005). Investigating the role of ABC transporters in multifungicide insensitivity in *Phytophthora infestans*. *Mol. Plant Pathol.* **7**: 17–29.
- Kale, S.D. et al.** (2010). External Lipid PI3P Mediates Entry of Eukaryotic Pathogen Effectors into Plant and Animal Host Cells. *Cell* **142**: 284–295.
- Kale, S.D. and Tyler, B.M.** (2011). Entry of oomycete and fungal effectors into plant and animal host cells. *Cell. Microbiol.* **13**: 1839–1848.
- Kamel, L., Tang, N., Malbreil, M., San Clemente, H., Le Marquer, M., Roux, C., and dit Frey, N.F.** (2017). The comparison of expressed candidate secreted proteins from two arbuscular mycorrhizal fungi unravels common and specific molecular tools to invade different host plants. *Front. Plant Sci.* **8**: 124.
- Kamoun, S. et al.** (2015). The Top 10 oomycete pathogens in molecular plant pathology. *Mol. Plant Pathol.* **16**: 413–434.
- Kamoun, S., Huitema, E., and Vleeshouwers, V.G.A.A.** (1999). Resistance to oomycetes: A general role for the hypersensitive response? *Trends Plant Sci.* **4**.
- Kang, H. et al.** (2016). Dissection of the genetic architecture of rice resistance to the blast fungus *Magnaporthe oryzae*. *Mol. Plant Pathol.* **17**: 959–972.
- Kazan, K. and Gardiner, D.M.** (2017). Targeting pathogen sterols: Defence and counterdefence? *PLoS Pathog.* **13**.
- Kemen, E., Gardiner, A., Schultz-Larsen, T., Kemen, A.C., Balmuth, A.L., Robert-Seilaniantz, A., Bailey, K., Holub, E., Studholme, D.J., MacLean, D., and Jones, J.D.G.** (2011). Gene gain and loss during evolution of obligate parasitism in the white rust pathogen of *Arabidopsis thaliana*. *PLoS Biol.* **9**.
- Khan, M., Seto, D., Subramaniam, R., and Desveaux, D.** (2018). Oh, the places they'll go! A survey of phytopathogen effectors and their host targets. *Plant J.* **93**: 651–663.
- Kim, K.-T., Jeon, J., Choi, J., Cheong, K., Song, H., Choi, G., Kang, S., and Lee, Y.-H.** (2016). Kingdom-Wide Analysis of Fungal Small Secreted Proteins (SSPs) Reveals their Potential Role in Host Association. *Front. Plant Sci.* **7**: 186.
- King, S.R.F., McLellan, H., Boevink, P.C., Armstrong, M.R., Bukharova, T., Sukarta, O., Win, J., Kamoun, S., Birch, P.R.J., and Banfield, M.J.** (2014). *Phytophthora infestans* RXLR effector PexRD2 interacts with host MAPKKK ϵ to suppress plant immune signaling. *Plant Cell* **26**: 1345–59.
- Kloppholz, S., Kuhn, H., and Requena, N.** (2011). A secreted fungal effector of *Glomus intraradices* promotes symbiotic biotrophy. *Curr. Biol.* **21**: 1204–9.

- Köhl, J., Kolnaar, R., and Ravensberg, W.J.** (2019). Mode of Action of Microbial Biological Control Agents Against Plant Diseases: Relevance Beyond Efficacy. *Front. Plant Sci.* **10**: 845.
- Kombrink, A., Rovenich, H., Shi-Kunne, X., Rojas-Padilla, E., van den Berg, G.C.M., Domazakis, E., de Jonge, R., Valkenburg, D.J., Sánchez-Vallet, A., Seidl, M.F., and Thomma, B.P.H.J.** (2017). *Verticillium dahliae* LysM effectors differentially contribute to virulence on plant hosts. *Mol. Plant Pathol.* **18**.
- Kong, L. et al.** (2017). A *Phytophthora* Effector Manipulates Host Histone Acetylation and Reprograms Defense Gene Expression to Promote Infection. *Curr. Biol.* **27**: 981–991.
- Krings, M., Taylor, T.N., and Dotzler, N.** (2011). The fossil record of the peronosporomycetes (Oomycota). *Mycologia* **103**: 445–457.
- Lamour, K. and Kamoun, S.** (2009). Oomycete Genetics and Genomics K. Lamour and S. Kamoun, eds (John Wiley & Sons, Inc.: Hoboken, NJ, USA).
- Larroque, M., Barriot, R., Bottin, A., Barre, A., Rougé, P., Dumas, B., and Gaulin, E.** (2012). The unique architecture and function of cellulose-interacting proteins in oomycetes revealed by genomic and structural analyses. *BMC Genomics* **13**.
- Latijnhouwers, M., De Wit, P.J.G.M., and Govers, F.** (2003). Oomycetes and fungi: Similar weaponry to attack plants. *Trends Microbiol.* **11**: 462–469.
- Lavaud, C., Baviere, M., Le Roy, G., Hervé, M.R., Moussart, A., Delourme, R., and Pilet-Nayel, M.-L.** (2016). Single and multiple resistance QTL delay symptom appearance and slow down root colonization by *Aphanomyces euteiches* in pea near isogenic lines. *BMC Plant Biol.* **16**: 166.
- Lévesque, C.A. et al.** (2010). Genome sequence of the necrotrophic plant pathogen *Pythium ultimum* reveals original pathogenicity mechanisms and effector repertoire. *Genome Biol.* **11**.
- Lin, K. et al.** (2014). Single Nucleus Genome Sequencing Reveals High Similarity among Nuclei of an Endomycorrhizal Fungus. *PLoS Genet.* **10**.
- Liu, D., Shi, L., Han, C., Yu, J., Li, D., and Zhang, Y.** (2012). Validation of Reference Genes for Gene Expression Studies in Virus-Infected *Nicotiana benthamiana* Using Quantitative Real-Time PCR. *PLoS One* **7**.
- Liu, J.-Z. and Whitham, S. a** (2013). Overexpression of a soybean nuclear localized type-III DnaJ domain-containing HSP40 reveals its roles in cell death and disease resistance. *Plant J.* **74**: 110–21.
- Liu, T. et al.** (2014). Unconventionally secreted effectors of two filamentous pathogens target plant salicylate biosynthesis. *Nat. Commun.* **5**: 4686.
- Liu, T., Liu, Z., Song, C., Hu, Y., Han, Z., She, J., Fan, F., Wang, J., Jin, C., Chang, J., Zhou, J.-M., and Chai, J.** (2012). Chitin-induced dimerization activates a plant immune receptor. *Science* **336**: 1160–4.
- Liu, Y. and Imai, R.** (2018). Function of plant DExD/H-Box RNA helicases associated with ribosomal RNA biogenesis. *Front. Plant Sci.* **9**.

- Lucas, J.A.** (2020). Plant Pathology and Plant Pathogens John Wiley & Sons, ed.
- Lucas, J.A., Hawkins, N.J., and Fraaije, B.A.** (2015). The Evolution of Fungicide Resistance. *Adv. Appl. Microbiol.* **90**: 29–92.
- Ma, Y. et al.** (2020). Dissecting the Genetic Architecture of *Aphanomyces* Root Rot Resistance in Lentil by QTL Mapping and Genome-Wide Association Study. *Int. J. Mol. Sci.* **21**: 2129.
- Ma, Z. et al.** (2017). A paralogous decoy protects *Phytophthora sojae* apoplastic effector PsXEG1 from a host inhibitor. *Science* (80-.). **355**.
- Malvick, D.K. and Grau, C.R.** (2001). Characteristics and frequency of *Aphanomyces euteiches* races 1 and 2 associated with alfalfa in the midwestern United States. *Plant Dis.* **85**.
- Marshall, R., Kombrink, A., Motteram, J., Loza-Reyes, E., Lucas, J., Hammond-Kosack, K.E., Thomma, B.P.H.J., and Rudd, J.J.** (2011). Analysis of Two in Planta Expressed LysM Effector Homologs from the Fungus *Mycosphaerella graminicola* Reveals Novel Functional Properties and Varying Contributions to Virulence on Wheat. *PLANT Physiol.* **156**: 756–769.
- Martin, F. and Selosse, M.A.** (2008). The *Laccaria* genome: A symbiont blueprint decoded. *New Phytol.* **180**: 296–310.
- Martin, R., Straub, A.U., Doebele, C., and Bohnsack, M.T.** (2013). DEXD/H-box RNA helicases in ribosome biogenesis. *RNA Biol.* **10**.
- Marzougui, A., Ma, Y., Zhang, C., McGee, R.J., Coyne, C.J., Main, D., and Sankaran, S.** (2019). Advanced Imaging for Quantitative Evaluation of *Aphanomyces* Root Rot Resistance in Lentil. *Front. Plant Sci.* **10**: 383.
- Matari, N.H. and Blair, J.E.** (2014). A multilocus timescale for oomycete evolution estimated under three distinct molecular clock models. *BMC Evol. Biol.* **14**: 101.
- Mattinen, L., Tshuikina, M., Mäe, A., and Pirhonen, M.** (2004). Identification and characterization of Nip, necrosis-inducing virulence protein of *Erwinia carotovora subsp. carotovora*. *Mol. Plant-Microbe Interact.* **17**.
- Mccarthy, C.G.P. and Fitzpatrick, D.A.** (2016). Systematic Search for Evidence of Interdomain Horizontal Gene Transfer from Prokaryotes to Oomycete Lineages.
- McCarthy, C.G.P. and Fitzpatrick, D.A.** (2017). Phylogenomic Reconstruction of the Oomycete Phylogeny Derived from 37 Genomes. *mSphere* **2**.
- McCotter, S.W., Horianopoulos, L.C., and Kronstad, J.W.** (2016). Regulation of the fungal secretome. *Curr. Genet.* **62**: 533–545.
- McGowan, J. and Fitzpatrick, D.A.** (2017). Genomic, Network, and Phylogenetic Analysis of the Oomycete Effector Arsenal. *mSphere* **2**.
- McGowan, J. and Fitzpatrick, D.A.** (2020). Recent advances in oomycete genomics. In *Advances in Genetics* (Academic Press Inc.), pp. 175–228.
- Mclellan, H., Boevink, P.C., Armstrong, M.R., Pritchard, L., Gomez, S., Morales, J., Whisson, S.C., Beynon, J.L., and Birch, P.R.J.** (2013). An RxLR Effector from *Phytophthora infestans* Prevents Re-localisation of Two Plant NAC Transcription Factors from the Endoplasmic

Reticulum to the Nucleus. **9**.

- Meerupati, T., Andersson, K.-M., Friman, E., Kumar, D., Tunlid, A., and Ahrén, D.** (2013). Genomic mechanisms accounting for the adaptation to parasitism in nematode-trapping fungi. *PLoS Genet.* **9**: e1003909.
- Meisrimler, C.N., Pelgrom, A.J.E., Oud, B., Out, S., and Van den Ackerveken, G.** (2019). Multiple downy mildew effectors target the stress-related NAC transcription factor LsNAC069 in lettuce. *Plant J.* **99**.
- Mentlak, T.A., Kombrink, A., Shinya, T., Ryder, L.S., Otomo, I., Saitoh, H., Terauchi, R., Nishizawa, Y., Shibuya, N., Thomma, B.P.H.J., and Talbot, N.J.** (2012). Effector-Mediated Suppression of Chitin-Triggered Immunity by *Magnaporthe oryzae* Is Necessary for Rice Blast Disease. *Plant Cell* **24**: 322–335.
- Mikes, V., Milat, M.L., Ponchet, M., Panabières, F., Ricci, P., and Blein, J.P.** (1998). Elicitins, proteinaceous elicitors of plant defense, are a new class of sterol carrier proteins. *Biochem. Biophys. Res. Commun.* **245**.
- Misner, I., Blouin, N., Leonard, G., Richards, T.A., and Lane, C.E.** (2014). The secreted proteins of *Achlya hypogyna* and *Thraustotheca clavata* identify the ancestral oomycete secretome and reveal gene acquisitions by horizontal gene transfer. *Genome Biol. Evol.* **7**.
- Mitrousia, G.K., Huang, Y.J., Qi, A., Sidique, S.N.M., and Fitt, B.D.L.** (2018). Effectiveness of Rlm7 resistance against *Leptosphaeria maculans* (phoma stem canker) in UK winter oilseed rape cultivars. *Plant Pathol.* **67**: 1339–1353.
- Morigasaki, S. and Shiozaki, K.** (2013). Phosphorelay-dependent and-independent regulation of MAPKKK by the Mcs4 response regulator in fission yeast. *Commun. Integr. Biol.* **6**.
- Nars, A. et al.** (2013). *Aphanomyces euteiches* Cell Wall Fractions Containing Novel Glucan-Chitosaccharides Induce Defense Genes and Nuclear Calcium Oscillations in the Plant Host *Medicago truncatula*. *PLoS One* **8**.
- Nicaise, V., Joe, A., Jeong, B.R., Korneli, C., Boutrot, F., Westedt, I., Staiger, D., Alfano, J.R., and Zipfel, C.** (2013). Pseudomonas HopU1 modulates plant immune receptor levels by blocking the interaction of their mRNAs with GRP7. *EMBO J.* **32**: 701–712.
- Nicaise, V., Roux, M., and Zipfel, C.** (2009). Recent Advances in PAMP-Triggered Immunity against Bacteria: Pattern Recognition Receptors Watch over and Raise the Alarm. *Plant Physiol.* **150**: 1638–1647.
- Niki, T., Mitsuhara, I., Seo, S., Ohtsubo, N., and Ohashi, Y.** (1998). Antagonistic Effect of Salicylic Acid and Jasmonic Acid on the Expression of Pathogenesis-Related (PR) Protein Genes in Wounded Mature Tobacco Leaves. *Plant Cell Physiol.* **39**: 500–507.
- Nishimura, T., Mochizuki, S., Ishii-Minami, N., Fujisawa, Y., Kawahara, Y., Yoshida, Y., Okada, K., Ando, S., Matsumura, H., Terauchi, R., Minami, E., and Nishizawa, Y.** (2016). *Magnaporthe oryzae* Glycine-Rich Secretion Protein, Rbf1 Critically Participates in Pathogenicity through the Focal Formation of the Biotrophic Interfacial Complex. *PLoS Pathog.* **12**.

- O'Brien, J.A., Daudi, A., Butt, V.S., and Paul Bolwell, G.** (2012). Reactive oxygen species and their role in plant defence and cell wall metabolism. *Planta* **236**: 765–779.
- O'Connell, R.J. et al.** (2012). Lifestyle transitions in plant pathogenic *Colletotrichum* fungi deciphered by genome and transcriptome analyses. *Nat. Genet.* **44**: 1060–1065.
- Osman, H., Mikes, V., Milat, M.L., Ponchet, M., Marion, D., Prangé, T., Maume, B.F., Vauthrin, S., and Blein, J.P.** (2001). Fatty acids bind to the fungal elicitor cryptogein and compete with sterols. *FEBS Lett.* **489**.
- Ottmann, C., Luberacki, B., Kűfner, I., Koch, W., Brunner, F., Weyand, M., Mattinen, L., Pirhonen, M., Anderluh, G., Seitz, H.U., Nürnbergger, T., and Oecking, C.** (2009). A common toxin fold mediates microbial attack and plant defense. *Proc. Natl. Acad. Sci. U. S. A.* **106**.
- Papavizas, G.C. and Ayers, W.A.** (1974). *Aphanomyces* species and their root diseases in pea and sugarbeet. *Tech. Bull. Agric. Res. Serv. United States Dep. Agric.*
- Parniske, M.** (2008). Arbuscular mycorrhiza: The mother of plant root endosymbioses. *Nat. Rev. Microbiol.* **6**.
- Patwardhan, A., Gandhe, R., Ghole, V., and Mourya, D.** (2005). Larvicidal activity of the fungus *Aphanomyces* (oomycetes: Saprolegniales) against *Culex quinquefasciatus*. *J. Commun. Dis.* **37**.
- Pavlov, A.R., Belova, G.I., Kozyavkin, S.A., and Slesarev, A.I.** (2002). Helix-hairpin-helix motifs confer salt resistance and processivity on chimeric DNA polymerases. *Proc. Natl. Acad. Sci. U. S. A.* **99**.
- Pecrix, Y., Buendia, L., Penouilh-Suzette, C., Maréchaux, M., Legrand, L., Bouchez, O., Rengel, D., Gouzy, J., Cottret, L., Vear, F., and Godiard, L.** (2019). Sunflower resistance to multiple downy mildew pathotypes revealed by recognition of conserved effectors of the oomycete *Plasmopara halstedii*. *Plant J.* **97**: 730–748.
- Pecrix, Y., Penouilh-Suzette, C., Muños, S., Vear, F., and Godiard, L.** (2018). Ten Broad Spectrum Resistances to Downy Mildew Physically Mapped on the Sunflower Genome. *Front. Plant Sci.* **9**: 1780.
- Pedersen, C. et al.** (2012). Structure and evolution of barley powdery mildew effector candidates. *BMC Genomics* **13**: 694.
- Pellegrin, C., Morin, E., Martin, F.M., and Veneault-Fourrey, C.** (2015). Comparative analysis of secretomes from ectomycorrhizal fungi with an emphasis on small-secreted proteins. *Front. Microbiol.* **6**.
- Pemberton, C.L., Whitehead, N.A., Sebaihia, M., Bell, K.S., Hyman, L.J., Harris, S.J., Matlin, A.J., Robson, N.D., Birch, P.R.J., Carr, J.P., Toth, I.K., and Salmond, G.P.C.** (2005). Novel quorum-sensing-controlled genes in *Erwinia carotovora subsp. carotovora*: Identification of a fungal elicitor homologue in a soft-rotting bacterium. *Mol. Plant-Microbe Interact.* **18**.
- Pennington, H.G. et al.** (2019). The fungal ribonuclease-like effector protein CSEP0064/BEC1054 represses plant immunity and interferes with degradation of host

ribosomal RNA. *PLOS Pathog.* **15**: e1007620.

Pennisi, E. (2010). Armed and dangerous. *Science* (80-.). **327**: 804–805.

Petrasch, S., Silva, C.J., Mesquida-Pesci, S.D., Gallegos, K., van den Abeele, C., Papin, V., Fernandez-Acero, F.J., Knapp, S.J., and Blanco-Ulate, B. (2019). Infection strategies deployed by *Botrytis cinerea*, *Fusarium acuminatum*, and *Rhizopus stolonifer* as a function of tomato fruit ripening stage. *Front. Plant Sci.* **10**: 223.

Petre, B., Saunders, D.G.O., Sklenar, J., Lorrain, C., Krasileva, K. V., Win, J., Duplessis, S., and Kamoun, S. (2016). Heterologous expression screens in *Nicotiana benthamiana* identify a candidate effector of the wheat yellow rust pathogen that associates with processing bodies. *PLoS One* **11**.

Petre, B., Saunders, D.G.O., Sklenar, J., Lorrain, C., Win, J., Duplessis, S., and Kamoun, S. (2015). Candidate Effector Proteins of the Rust Pathogen *Melampsora larici-populina* Target Diverse Plant Cell Compartments. *Mol. Plant-Microbe Interact.* **28**: 689–700.

Phillips, A.J., Anderson, V.L., Robertson, E.J., Secombes, C.J., and van West, P. (2008). New insights into animal pathogenic oomycetes. *Trends Microbiol.* **16**: 13–9.

Pilet-Nayel, M.L., Moury, B., Caffier, V., Montarry, J., Kerlan, M.C., Fournet, S., Durel, C.E., and Delourme, R. (2017). Quantitative resistance to plant pathogens in pyramiding strategies for durable crop protection. *Front. Plant Sci.* **8**: 27.

Plett, J.M., Daguerre, Y., Wittulsky, S., Vayssieres, A., Deveau, A., Melton, S.J., Kohler, A., Morrell-Falvey, J.L., Brun, A., Veneault-Fourrey, C., and Martin, F. (2014). Effector MiSSP7 of the mutualistic fungus *Laccaria bicolor* stabilizes the Populus JAZ6 protein and represses jasmonic acid (JA) responsive genes. *Proc. Natl. Acad. Sci.* **111**: 8299–8304.

Plett, J.M., Kempainen, M., Kale, S.D., Kohler, A., Legué, V., Brun, A., Tyler, B.M., Pardo, A.G., and Martin, F. (2011). A secreted effector protein of *Laccaria bicolor* is required for symbiosis development. *Curr. Biol.* **21**: 1197–203.

Pliego, C. et al. (2013). Host-induced gene silencing in barley powdery mildew reveals a class of ribonuclease-like effectors. *Mol. Plant-Microbe Interact.* **26**.

Poland, J.A., Balint-Kurti, P.J., Wisser, R.J., Pratt, R.C., and Nelson, R.J. (2009). Shades of gray: the world of quantitative disease resistance. *Trends Plant Sci.* **14**.

Prabhu, A.S., Filippi, M.C., Silva, G.B., Silva Lobo, V.L., and Morais, O.P. (2009). An Unprecedented Outbreak of Rice Blast on a Newly Released Cultivar BRS Colosso in Brazil. In *Advances in Genetics, Genomics and Control of Rice Blast Disease* (Springer Netherlands), pp. 257–266.

Lo Presti, L., Lanver, D., Schweizer, G., Tanaka, S., Liang, L., Tollot, M., Zuccaro, A., Reissmann, S., and Kahmann, R. (2015). Fungal Effectors and Plant Susceptibility. *Annu. Rev. Plant Biol.* **66**: 513–545.

Qasim, M.U., Zhao, Q., Shahid, M., Samad, R.A., Ahmar, S., Wu, J., Fan, C., and Zhou, Y. (2020). Identification of QTLs Containing Resistance Genes for *Sclerotinia* Stem Rot in *Brassica napus* Using Comparative Transcriptomic Studies. *Front. Plant Sci.* **11**: 776.

Qi, T., Guo, J., Liu, P., He, F., Wan, C., Islam, M.A., Tyler, B.M., Kang, Z., and Guo, J. (2019).

Stripe Rust Effector PstGSRE1 Disrupts Nuclear Localization of ROS-Promoting Transcription Factor TaLOL2 to Defeat ROS-Induced Defense in Wheat. *Mol. Plant* **12**.

- Qiao, Y. et al.** (2013). Oomycete pathogens encode RNA silencing suppressors. *Nat. Genet.*: 1–6.
- Qiao, Y., Shi, J., Zhai, Y., Hou, Y., and Ma, W.** (2015). *Phytophthora* effector targets a novel component of small RNA pathway in plants to promote infection. *Proc. Natl. Acad. Sci. U. S. A.* **112**: 5850–5855.
- Qutob, D. et al.** (2006). Phytotoxicity and innate immune responses induced by Nep1-like proteins. *Plant Cell* **18**.
- Qutob, D., Kamoun, S., and Gijzen, M.** (2002). Expression of a *Phytophthora sojae* necrosis-inducing protein occurs during transition from biotrophy to necrotrophy. *Plant J.* **32**.
- Qutob, D., Patrick Chapman, B., and Gijzen, M.** (2013). Transgenerational gene silencing causes gain of virulence in a plant pathogen. *Nat. Commun.* **4**.
- Raffaele, S. et al.** (2010). Genome evolution following host jumps in the Irish potato famine pathogen lineage. *Science* **330**: 1540–3.
- Raffaele, S. and Kamoun, S.** (2012). Genome evolution in filamentous plant pathogens: why bigger can be better. *Nat. Rev. Microbiol.* **10**: 417–30.
- Ramirez-Garces, D.** (2014). Analyses of CRN effectors (crinkler and necrosis) of the oomycete *Aphanomyces euteiches*. <http://www.theses.fr>.
- Ramirez-Garcés, D., Camborde, L., Pel, M.J.C., Jauneau, A., Martinez, Y., Néant, I., Leclerc, C., Moreau, M., Dumas, B., and Gaulin, E.** (2016). CRN13 candidate effectors from plant and animal eukaryotic pathogens are DNA-binding proteins which trigger host DNA damage response. *New Phytol.* **210**.
- Rehmany, A.P., Gordon, A., Rose, L.E., Allen, R.L., Armstrong, M.R., Whisson, S.C., Kamoun, S., Tyler, B.M., Birch, P.R.J., and Beynon, J.L.** (2005). Differential recognition of highly divergent downy mildew avirulence gene alleles by RPP1 resistance genes from two *Arabidopsis* lines. *Plant Cell* **17**: 1839–1850.
- Richards, J.K., Stukenbrock, E.H., Carpenter, J., Liu, Z., Cowger, C., Faris, J.D., and Friesen, T.L.** (2019). Local adaptation drives the diversification of effectors in the fungal wheat pathogen *Parastagonospora nodorum* in the United States. *PLOS Genet.* **15**: e1008223.
- Richards, T.A., Soanes, D.M., Jones, M.D.M., Vasieva, O., Leonard, G., Paszkiewicz, K., Foster, P.G., Hall, N., and Talbot, N.J.** (2011). Horizontal gene transfer facilitated the evolution of plant parasitic mechanisms in the oomycetes. *Proc. Natl. Acad. Sci. U. S. A.* **108**.
- Rizzo, J., Rodrigues, M.L., and Janbon, G.** (2020). Extracellular Vesicles in Fungi: Past, Present, and Future Perspectives. *Front. Cell. Infect. Microbiol.* **10**.
- Robin, G.P., Kleemann, J., Neumann, U., Cabre, L., Dallery, J.-F., Lapalu, N., and O’Connell, R.J.** (2018). Subcellular Localization Screening of *Colletotrichum higginsianum* Effector Candidates Identifies Fungal Proteins Targeted to Plant Peroxisomes, Golgi Bodies, and Microtubules. *Front. Plant Sci.* **9**: 562.

- Rocafort, M., Fudal, I., and Mesarich, C.H.** (2020). Apoplastic effector proteins of plant-associated fungi and oomycetes. *Curr. Opin. Plant Biol.* **56**: 9–19.
- Romero-Contreras, Y.J., Ramírez-Valdespino, C.A., Guzmán-Guzmán, P., Macías-Segoviano, J.I., Villagómez-Castro, J.C., and Olmedo-Monfil, V.** (2019). Tal6 From *Trichoderma atroviride* Is a LysM Effector Involved in Mycoparasitism and Plant Association. *Front. Microbiol.* **10**.
- Rose, J.K.C.** (2002). Molecular Cloning and Characterization of Glucanase Inhibitor Proteins: Coevolution of a Counterdefense Mechanism by Plant Pathogens. *Plant Cell Online* **14**: 1329–1345.
- Royo, F., Andersson, G., Bangyeekhun, E., Múzquiz, J.L., Söderhäll, K., and Cerenius, L.** (2004). Physiological and genetic characterisation of some new *Aphanomyces* strains isolated from freshwater crayfish. *Vet. Microbiol.* **104**.
- Sakihama, Y., Shimai, T., Sakasai, M., Ito, T., Fukushi, Y., Hashidoko, Y., and Tahara, S.** (2004). A photoaffinity probe designed for host-specific signal flavonoid receptors in phytopathogenic Peronosporomycete zoospores of *Aphanomyces cochlioides*. *Arch. Biochem. Biophys.* **432**.
- Sánchez-Vallet, A. et al.** (2020). A secreted LysM effector protects fungal hyphae through chitin-dependent homodimer polymerization. *PLOS Pathog.* **16**: e1008652.
- Sánchez-Vallet, A., Fouché, S., Fudal, I., Hartmann, F.E., Soyer, J.L., Tellier, A., and Croll, D.** (2018). The Genome Biology of Effector Gene Evolution in Filamentous Plant Pathogens. *Annu. Rev. Phytopathol.* **56**: annurev-phyto-080516-035303.
- Sánchez-Vallet, A., Saleem-Batcha, R., Kombrink, A., Hansen, G., Valkenburg, D.J., Thomma, B.P.H.J., and Mesters, J.R.** (2013). Fungal effector Ecp6 outcompetes host immune receptor for chitin binding through intrachain LysM dimerization. *Elife* **2013**.
- Sarowar, M.N., Hossain, M.J., Nasrin, T., Naznin, T., Hossain, Z., and Rahman, M.M.** (2019). Molecular identification of oomycete species affecting aquaculture in Bangladesh. *Aquac. Fish.* **4**.
- Saunders, D.G.O., Pretorius, Z.A., and Hovmøller, M.S.** (2019). Tackling the re-emergence of wheat stem rust in Western Europe. *Commun. Biol.* **2**: 1–3.
- Savory, F., Leonard, G., and Richards, T.A.** (2015). The Role of Horizontal Gene Transfer in the Evolution of the Oomycetes. *PLOS Pathog.* **11**: e1004805.
- Scheele, B.C. et al.** (2019). Amphibian fungal panzootic causes catastrophic and ongoing loss of biodiversity. *Science (80-.)*. **363**: 1459–1463.
- Schmidt, S.M., Kuhn, H., Micali, C., Liller, C., Kwaaitaal, M., and Panstruga, R.** (2014). Interaction of a *Blumeria graminis* f. sp. *hordei* effector candidate with a barley ARF-GAP suggests that host vesicle trafficking is a fungal pathogenicity target. *Mol. Plant Pathol.* **15**: 535–549.
- Schornack, S., van Damme, M., Bozkurt, T.O., Cano, L.M., Smoker, M., Thines, M., Gaulin, E., Kamoun, S., and Huitema, E.** (2010). Ancient class of translocated oomycete effectors targets the host nucleus. *Proc. Natl. Acad. Sci. U. S. A.* **107**: 17421–6.

- Schuller, K.G., Mitra, J., Ha, T., and Barrick, D.** (2019). Functional instability allows access to DNA in longer transcription activator-like effector (Tale) arrays. *Elife* **8**.
- Sello, M.M. et al.** (2015). Diversity and evolution of cytochrome P450 monooxygenases in Oomycetes. *Sci. Rep.* **5**: 1–13.
- Shindo, T. et al.** (2016). Screen of Non-annotated Small Secreted Proteins of *Pseudomonas syringae* Reveals a Virulence Factor That Inhibits Tomato Immune Proteases. *PLOS Pathog.* **12**: e1005874.
- Snelders, N.C., Kettles, G.J., Rudd, J.J., and Thomma, B.P.H.J.** (2018). Plant pathogen effector proteins as manipulators of host microbiomes? *Mol. Plant Pathol.* **19**.
- Soanes, D.M., Alam, I., Cornell, M., Wong, H.M., Hedeler, C., Paton, N.W., Rattray, M., Hubbard, S.J., Oliver, S.G., and Talbot, N.J.** (2008). Comparative genome analysis of filamentous fungi reveals gene family expansions associated with fungal pathogenesis. *PLoS One* **3**.
- Song, C., Zhu, F., Carrión, V.J., and Cordovez, V.** (2020). Beyond Plant Microbiome Composition: Exploiting Microbial Functions and Plant Traits via Integrated Approaches. *Front. Bioeng. Biotechnol.* **8**: 896.
- Song, J. and Bent, A.F.** (2014). Microbial Pathogens Trigger Host DNA Double-Strand Breaks Whose Abundance Is Reduced by Plant Defense Responses. *PLoS Pathog.* **10**: e1004030.
- Song, T., Ma, Z., Shen, D., Li, Q., Li, W., Su, L., Ye, T., Zhang, M., Wang, Y., and Dou, D.** (2015). An Oomycete CRN Effector Reprograms Expression of Plant HSP Genes by Targeting their Promoters. *PLoS Pathog.* **11**: 1–30.
- Spanu, P.D.** (2015). RNA-protein interactions in plant disease: hackers at the dinner table. *New Phytol.* **207**: 991–995.
- Sperschneider, J., Catanzariti, A.M., Deboer, K., Petre, B., Gardiner, D.M., Singh, K.B., Dodds, P.N., and Taylor, J.M.** (2017). LOCALIZER: Subcellular localization prediction of both plant and effector proteins in the plant cell. *Sci. Rep.* **7**.
- Sperschneider, J., Dodds, P.N., Gardiner, D.M., Singh, K.B., and Taylor, J.M.** (2018). Improved prediction of fungal effector proteins from secretomes with EffectorP 2.0. *Mol. Plant Pathol.* **19**.
- Spies, C.F.J., Grooters, A.M., Lévesque, C.A., Rintoul, T.L., Redhead, S.A., Glockling, S.L., Chen, C. yu, and de Cock, A.W.A.M.** (2016). Molecular phylogeny and taxonomy of *Lagenidium*-like oomycetes pathogenic to mammals. *Fungal Biol.* **120**.
- Sprague, S.J., Balesdent, M.H., Brun, H., Hayden, H.L., Marcroft, S.J., Pinochet, X., Rouxel, T., and Howlett, B.J.** (2006). Major gene resistance in *Brassica napus* (oilseed rape) is overcome by changes in virulence of populations of *Leptosphaeria maculans* in France and Australia. In *European Journal of Plant Pathology* (Springer), pp. 33–40.
- Stam, R., Howden, A.J.M., Delgado-Cerezo, M., Amaro, T.M.M.M., Motion, G.B., Pham, J., and Huitema, E.** (2013a). Characterization of cell death inducing *Phytophthora capsici* CRN effectors suggests diverse activities in the host nucleus. *Front. Plant Sci.* **4**.
- Stam, R., Jupe, J., Howden, A.J.M., Morris, J. a., Boevink, P.C., Hedley, P.E., and Huitema, E.**

- (2013b). Identification and Characterisation CRN Effectors in *Phytophthora capsici* Shows Modularity and Functional Diversity. PLoS One **8**: e59517.
- Stanton-Geddes, J. et al.** (2013). Candidate Genes and Genetic Architecture of Symbiotic and Agronomic Traits Revealed by Whole-Genome, Sequence-Based Association Genetics in *Medicago truncatula*. PLoS One **8**: e65688.
- Strullu-Derrien, C., Kenrick, P., Rioult, J.P., and Strullu, D.G.** (2011). Evidence of parasitic Oomycetes (Peronosporomycetes) infecting the stem cortex of the Carboniferous seed fern *Lyginopteris oldhamia*. Proc. R. Soc. B Biol. Sci. **278**: 675–680.
- Stuthman, D.D., Leonard, K.J., and Miller-Garvin, J.** (2007). Breeding Crops for Durable Resistance to Disease. Adv. Agron. **95**: 319–367.
- Sun, G., Yang, Z., Kosch, T., Summers, K., and Huang, J.** (2011). Evidence for acquisition of virulence effectors in pathogenic chytrids. BMC Evol. Biol. **11**: 195.
- Takahara, H. et al.** (2016). *Colletotrichum higginsianum* extracellular LysM proteins play dual roles in appressorial function and suppression of chitin-triggered plant immunity. New Phytol. **211**.
- Tanaka, S., Brefort, T., Neidig, N., Djamei, A., Kahnt, J., Vermerris, W., Koenig, S., Feussner, K., Feussner, I., and Kahmann, R.** (2014). A secreted *Ustilago maydis* effector promotes virulence by targeting anthocyanin biosynthesis in maize. Elife **3**: e01355.
- Tang, M., Ning, Y., Shu, X., Dong, B., Zhang, H., Wu, D., Wang, H., Wang, G.-L., and Zhou, B.** (2017). The Nup98 Homolog APIP12 Targeted by the Effector AvrPiz-t is Involved in Rice Basal Resistance Against *Magnaporthe oryzae*. Rice **10**: 5.
- Taschuk, F. and Cherry, S.** (2020). DEAD-box helicases: Sensors, regulators, and effectors for antiviral defense. Viruses **12**.
- Thines, M.** (2018). Oomycetes. Curr. Biol. **28**: R812–R813.
- Thomas, S.W., Rasmussen, S.W., Glaring, M.A., Rouster, J.A., Christiansen, S.K., and Oliver, R.P.** (2001). Gene identification in the obligate fungal pathogen *Blumeria graminis* by expressed sequence tag analysis. Fungal Genet. Biol. **33**.
- Torto, T.A., Li, S., Styer, A., Huitema, E., Testa, A., Gow, N.A.R., van West, P., and Kamoun, S.** (2003). EST mining and functional expression assays identify extracellular effector proteins from the plant pathogen *Phytophthora*. Genome Res. **13**: 1675–1685.
- Trusch, F. et al.** (2018). Cell entry of a host-targeting protein of oomycetes requires gp96. Nat. Commun. **9**: 1–12.
- Turner, T.R., James, E.K., and Poole, P.S.** (2013). The plant microbiome. Genome Biol. **14**: 209.
- Tyler, B.M.** (2002). Molecular Basis of Recognition Between *Phytophthora* Pathogens and their Hosts. Annu. Rev. Phytopathol **40**: 137–67.
- Tyler, B.M. et al.** (2006). *Phytophthora* Genome Sequences Uncover Evolutionary Origins and Mechanisms of Pathogenesis. Science (80-.). **313**: 1261–1266.
- Vallet, M., Baumeister, T.U.H., Kaftan, F., Grabe, V., Buaya, A., Thines, M., Svatoš, A., and Pohnert, G.** (2019). The oomycete *Lagenisma coscinodisci* hijacks host alkaloid synthesis

- during infection of a marine diatom. *Nat. Commun.* **10**: 1–8.
- Vance, V.** (2001). RNA Silencing in Plants--Defense and Counterdefense. *Science* (80-). **292**: 2277–2280.
- Vargas, W.A., Sanz-Martín, J.M., Rech, G.E., Armijos-Jaramillo, V.D., Rivera, L.P., Echeverria, M.M., Díaz-Mínguez, J.M., Thon, M.R., and Sukno, S.A.** (2016). A Fungal Effector With Host Nuclear Localization and DNA-Binding Properties Is Required for Maize Anthracnose Development. *Mol. Plant-Microbe Interact.* **29**: 83–95.
- Veit, S., Wörle, J.M., Nürnberger, T., Koch, W., and Seitz, H.U.** (2001). A novel protein elicitor (PaNie) from *Pythium aphanidermatum* induces multiple defense responses in carrot, *Arabidopsis*, and tobacco. *Plant Physiol.* **127**.
- Veneault-Fourrey, C. and Martin, F.** (2011). Mutualistic interactions on a knife-edge between saprotrophy and pathogenesis. *Curr. Opin. Plant Biol.* **14**.
- Vijayapalani, P., Hewezi, T., Pontvianne, F., and Baum, T.J.** (2018). An Effector from the Cyst Nematode *Heterodera schachtii* Derepresses Host rRNA Genes by Altering Histone Acetylation. *Plant Cell* **30**: 2795–2812.
- Vivek-Ananth, R.P., Mohanraj, K., Vandanashree, M., Jhingran, A., Craig, J.P., and Samal, A.** (2018). Comparative systems analysis of the secretome of the opportunistic pathogen *Aspergillus fumigatus* and other *Aspergillus* species. *Sci. Rep.* **8**: 6617.
- Voß, S., Betz, R., Heidt, S., Corradi, N., and Requena, N.** (2018). RiCRN1, a Crinkler Effector From the Arbuscular Mycorrhizal Fungus *Rhizophagus irregularis*, Functions in Arbuscule Development. *Front. Microbiol.* **9**: 1–18.
- Walker, C.A. and van West, P.** (2007). Zoospore development in the oomycetes. *Fungal Biol. Rev.* **21**.
- Wang, S., Boevink, P.C., Welsh, L., Zhang, R., Whisson, S.C., and Birch, P.R.J.** (2017). Delivery of cytoplasmic and apoplastic effectors from *Phytophthora infestans* haustoria by distinct secretion pathways. *New Phytol.*: 205–215.
- Wang, X., Boevink, P., McLellan, H., Armstrong, M., Bukharova, T., Qin, Z., and Birch, P.R.J.** (2015). A host KH RNA binding protein is a susceptibility factor targeted by an RXLR effector to promote late blight disease. *Mol. Plant.*
- Wang, Y., Tyler, B.M., and Wang, Y.** (2019). Defense and Counterdefense During Plant-Pathogenic Oomycete Infection. *Annu. Rev. Microbiol.* **73**.
- Warburton, A.J. and Deacon, J.W.** (1998). Transmembrane Ca²⁺ fluxes associated with zoospore encystment and cyst germination by the phytopathogen *Phytophthora parasitica*. *Fungal Genet. Biol.* **25**.
- Wawra, S., Agacan, M., Boddey, J.A., Davidson, I., Gachon, C.M.M., Zanda, M., Grouffaud, S., Whisson, S.C., Birch, P.R.J., Porter, A.J., and Van West, P.** (2012). Avirulence protein 3a (AVR3a) from the potato pathogen *Phytophthora infestans* forms homodimers through its predicted translocation region and does not specifically bind phospholipids. *J. Biol. Chem.* **287**: 38101–38109.
- Wawra, S., Djamei, A., Albert, I., Nürnberger, T., Kahmann, R., and Van West, P.** (2013). In

in vitro translocation experiments with RxLR-reporter fusion proteins of *avr1b* from *Phytophthora sojae* and AVR3a from *Phytophthora infestans* fail to demonstrate specific autonomous uptake in plant and animal cells. *Mol. Plant-Microbe Interact.* **26**.

Wawra, S., Trusch, F., Matena, A., Apostolakis, K., Linne, U., Zhukov, I., Stanek, J., Koźmiński, W., Davidson, I., Secombes, C.J., Bayer, P., and van West, P. (2017). The RxLR Motif of the Host Targeting Effector AVR3a of *Phytophthora infestans* Is Cleaved before Secretion. *Plant Cell* **29**: 1184–1195.

van West, P. (2006). *Saprolegnia parasitica*, an oomycete pathogen with a fishy appetite: new challenges for an old problem. *Mycologist* **20**: 99–104.

Whisson, S.C. et al. (2007). A translocation signal for delivery of oomycete effector proteins into host plant cells. *Nature* **450**: 115–118.

Whisson, S.C., Vetukuri, R.R., Avrova, A.O., and Dixelius, C. (2012). Can silencing of transposons contribute to variation in effector gene expression in *Phytophthora infestans*? *Mob. Genet. Elements* **2**.

Wicker, E., Hullé, M., and Rouxel, F. (2001). Pathogenic characteristics of isolates of *Aphanomyces euteiches* from pea in France. *Plant Pathol.* **50**.

Wu, C.Y. and Nagy, P.D. (2019). Blocking tombusvirus replication through the antiviral functions of DDX17-like RH30 DEAD-box helicase. *PLoS Pathog.* **15**: e1007771.

Wu, J., Cai, G., Tu, J., Li, L., Liu, S., Luo, X., Zhou, L., Fan, C., and Zhou, Y. (2013). Identification of QTLs for Resistance to *Sclerotinia* Stem Rot and BnaC.IGMT5.a as a Candidate Gene of the Major Resistant QTL SRC6 in *Brassica napus*. *PLoS One* **8**.

Wu, L., Chang, K.F., Conner, R.L., Strelkov, S., Fredua-Agyeman, R., Hwang, S.F., and Feindel, D. (2018). *Aphanomyces euteiches*: A Threat to Canadian Field Pea Production. *Engineering* **4**: 542–551.

Xiong, Q., Ye, W., Choi, D., Wong, J., Qiao, Y., Tao, K., Wang, Y., and Ma, W. (2014). *Phytophthora* Suppressor of RNA Silencing 2 Is a Conserved RxLR Effector that Promotes Infection in Soybean and *Arabidopsis thaliana*. *Mol. Plant-Microbe Interact.* **27**: 1379–1389.

Yaeno, T. and Shirasu, K. (2013). The RXLR motif of oomycete effectors is not a sufficient element for binding to phosphatidylinositol monophosphates. *Plant Signal. Behav.* **8**.

Yang, X., Long, M., and Shen, X. (2018). Effector–immunity pairs provide the T6SS nanomachine its offensive and defensive capabilities. *Molecules* **23**.

Yu, P.L., Chen, L.H., and Chung, K.R. (2016). How the pathogenic fungus *Alternaria alternata* copes with stress via the response regulators SSK1 and SHO1. *PLoS One* **11**.

Zeng, T., Rodriguez-Moreno, L., Mansurkhodzhaev, A., Wang, P., van den Berg, W., Gascioli, V., Cottaz, S., Fort, S., Thomma, B.P.H.J., Bono, J.J., Bisseling, T., and Limpens, E. (2020). A lysin motif effector subverts chitin-triggered immunity to facilitate arbuscular mycorrhizal symbiosis. *New Phytol.* **225**.

Zhang, D., Burroughs, A.M., Vidal, N.D., Iyer, L.M., and Aravind, L. (2016). Transposons to toxins: the provenance, architecture and diversification of a widespread class of

eukaryotic effectors. *Nucleic Acids Res.*: gkw221.

Zhang, M., Li, Q., Liu, T., Liu, L., Shen, D., Zhu, Y., Liu, P., Zhou, J.-M., and Dou, D. (2015a). Two Cytoplasmic Effectors of *Phytophthora sojae* Regulate Plant Cell Death via Interactions with Plant Catalases. *Plant Physiol.* **167**: 164–175.

Zhang, X., Nguyen, N., Breen, S., Outram, M.A., Dodds, P.N., Kobe, B., Solomon, P.S., and Williams, S.J. (2017). Production of small cysteine-rich effector proteins in *Escherichia coli* for structural and functional studies. *Mol. Plant Pathol.* **18**.

Zhao, L., Zhang, X., Zhang, X., Song, W., Li, X., Feng, R., Yang, C., Huang, Z., and Zhu, C. (2018). Crystal structure of the RxLR effector PcRxLR12 from *Phytophthora capsici*. *Biochem. Biophys. Res. Commun.* **503**.

Zhou, E., Jia, Y., Singh, P., Correll, J.C., and Lee, F.N. (2007). Instability of the *Magnaporthe oryzae* avirulence gene AVR-Pita alters virulence. *Fungal Genet. Biol.* **44**: 1024–1034.

Zuccaro, A. et al. (2011). Endophytic life strategies decoded by genome and transcriptome analyses of the mutualistic root symbiont *Piriformospora indica*. *PLoS Pathog.* **7**.

Résumé

Les oomycètes sont des microorganismes eucaryotes capables d'infecter des plantes ou des animaux. Lors de l'interaction avec leur hôte, les oomycètes produisent des molécules, appelées effecteurs, capables d'interagir avec des composants moléculaires des cellules de l'hôte afin de perturber les réponses de défense et ainsi favoriser le développement du microorganisme. Les Crinklers (CRNs) et les protéines à domaine RxLR représentent les deux grandes familles d'effecteurs cytoplasmiques décrites chez les oomycètes. La grande majorité de ces effecteurs ont cependant un mode d'action encore inconnu. Chez l'oomycète parasite racinaire des légumineuses *Aphanomyces euteiches*, il apparaît que seuls les CRNs sont présents. En se basant sur des travaux précédemment publiés par notre équipe, nous proposons une revue sur le rôle de certains effecteurs engendrant des dommages sur l'ADN des cellules hôtes. De précédents travaux portant sur le Crinkler AeCRN5 ont démontré que cet effecteur possédait un domaine fonctionnel de translocation dans la cellule végétale et impactait fortement la croissance racinaire. Mes travaux révèlent que cet effecteur se lie à l'ARN de la cellule hôte et perturbe la biogenèse de petits ARN impliqués dans la défense ou dans la croissance de la plante. De plus, nous avons pu mettre en évidence une nouvelle classe d'effecteurs potentiels composée de petites protéines sécrétées appelées SSP, spécifiques d'*Aphanomyces euteiches*. Les premières analyses sur ces SSP ont montré que AeSSP1256 augmente la sensibilité de la plante hôte. L'analyse fonctionnelle de cet effecteur a révélé que AeSSP1256 est capable de se lier à l'ARN ainsi qu'à une RNA hélicase de la plante, perturbant son activité et engendrant un stress nucléolaire, perturbant la biogénèse des ribosomes.

Ces travaux mettent en évidence que les acides nucléiques peuvent être la cible de différents types d'effecteurs et démontrent que deux effecteurs de familles différentes sont capables de se lier aux ARN afin de perturber des mécanismes de défense et de croissance de la plante, favorisant le développement du microorganisme.

Abstract

Oomycetes are eukaryote pathogens able to infect plants and animals. During host interaction, oomycetes secrete various molecules, named effectors, to counteract plant defence and modulate plant immunity. Crinklers (CRNs) and RxLR proteins represent the two main classes of cytoplasmic effectors described in oomycetes to date. Most of these effectors have not been yet characterized.

In the root rot pathogen of legumes *Aphanomyces euteiches*, only the CRNs are present. Based on a previous study reported by our research group, we published an opinion paper focused on the emergence of DNA damaging effectors and their role during infection.

Previous experiments indicated that one of these Crinklers, AeCRN5, harboured a functional translocation domain and dramatically disturbed root development. Here we reveal that AeCRN5 binds to RNA and interferes with biogenesis of various small RNAs, implicated in defence mechanisms or plant development. Additionally, comparative genetic analyses revealed a new class of putative effectors specific to *Aphanomyces euteiches*, composed by a large repertoire of small-secreted protein coding genes (SSP). Preliminary results on these SSPs point out that AeSSP1256 enhances host susceptibility. Functional characterisation of AeSSP1256 evidenced that this effector binds to RNA, relocalizes a plant RNA helicase and interferes with its activity, causing stress on plant ribosome biogenesis.

This work highlights that various effector target nucleic acids and reveals that two effectors from distinct family are able to interact with plant RNA in order to interfere with RNA related defence mechanisms and plant development to promote pathogen infection.